Numerical Investigation of Heat Transfer Performance in Cylindrical Pipes using Wall Grooves and Nanofluids

BIRMINGHAM CITY
University

Ajay Gunti

Numerical Investigation of Heat Transfer Performance in Cylindrical Pipes using Wall Grooves and Nanofluids

A thesis submitted for the degree of Doctor of Philosophy

in the

College of Engineering

of the

Birmingham City University

By

Ajay Gunti

PGCert, M.Sc. & B.Tech.

September 2024

Faculty of Computing, Engineering, and the Built Environment

College of Engineering

Birmingham City University

Birmingham, UK

Supervised by

Associate Professor Noel Perera

Dr Olusegun Ilori

Dr Dominic Flynn

Associate Professor Reaz Hasan

Copyright and Intellectual Property Rights Statement

Abstract

Optimising heat exchangers by enhancing heat transfer, reducing heat transfer time, and improving fluid thermal properties is essential for maximising energy efficiency. While grooves and nanofluids are promising solutions, their combined effects introduce challenges, such as increased pumping power requirements and inconsistent numerical modelling results. This study addresses these issues by numerically analysing a single-tube heat exchanger under turbulent forced convection by incorporating grooves and nanofluids. This numerical investigation uses single and multiphase models alongside the Realizable k-ε and SST k-ω turbulence models to capture the thermal and hydrodynamic behaviour of the single-tube heat exchanger. Initial validation with experimental data for a smooth tube and a smooth tube with circular grooves using water at Re = 10,000 to 60,000 with an average error of less than 8% confirmed the reliability of the models.

This study assessed different groove shapes such as circular, triangular, rectangular, trapezoidal, and hybrid combinations to enhance heat transfer in corrugated tubes. The trapezoidal grooves achieved the highest Nusselt number, with a 37.92% improvement compared to a smooth tube, for Reynolds numbers ranging from 10×10^3 to 60×10^3. However, triangular grooves exhibited the maximum thermal performance factor (PEC) due to the lower pressure drop compared to other groove shapes and hybrid combinations. Additionally, optimising rectangular grooves by adding curvature reduced pressure drop by 10.76% and improved the heat transfer coefficient of the single-tube heat exchanger by 13.4%, although triangular grooves remained superior.

This study evaluated the impact of turbulent models on nanofluid simulations, revealing significant variations in the Nusselt number, friction factor, turbulent kinetic energy, and wall shear stress. The single-phase model with the Realizable k-ε turbulence model showed an average error under 5% in predicting the Nusselt number and was closer to experimental data, outperforming the two-phase models (Eulerian and Mixture). In addition, the Al_2O_3-based hybrid nanofluids demonstrated up to 83.8% enhancement in heat transfer compared to pure water in a smooth tube at Re = 60,000. Finally, the combination of efficient triangular grooves with a 1% Al_2O_3-CuO/Water-EG hybrid nanofluid enhanced heat transfer rates by a factor of 2.14 in PEC values.

Declaration

I hereby confirm that all the findings contained in this thesis are my own work. Any ideas or approaches taken from previously published works have been appropriately cited using the BCU reference guidelines.

Ajay Gunti

September 2024

Acknowledgements

I wish to express my gratitude to my supervisor, Dr. Dominic Flynn. I received lots of support and assistance throughout my PhD from him, and his experience has been invaluable in support, feedback, constructive criticism, and guidance. You have always been a big supporter and have always been happy to assist me. I want to express my appreciation to my other supervisors, Associate Professor Noel Perera, Dr. Olusegun Ilori, and Associate Professor Reaz Hasan, for their continuous support and encouragement in the preparation of this PhD project. I benefited from their numerous valuable comments and helpful discussions.

I would also like to thank Professor Peter Larkham for his advice. You provided me with the encouragement I needed to make the best decisions during my PhD. I'd also like to show my gratitude to Associate Professor Karunamurthy K. (VIT University) for sharing his thoughts and suggestions to help me improve my PhD project. I would also like to convey my gratitude to Birmingham City University's administration, notably the CEBE department, for offering several resources for my research. I'd like to convey my sincere thanks to my parents for their unconditional support. You're always there for me. Finally, I say a big thank you to everyone who are incredibly supportive when it comes to discussing ideas and outcomes.

Table of Contents

List of Figures

List of Tables

List of Symbols

C_p – Specific heat (J/kgk)

d – Tube diameter (m)

e – Groove depth (m)

f – Friction factor (-)

h – Convective heat transfer coefficient (W/m^2K)

H – Tube height (m)

k – Turbulent kinetic energy (m^2/s^2)

K – Thermal conductivity (W/mk)

N – Number of grooves

N_x – Axial direction

N_y – Radial direction

Nu – Nusselt Number (-)

p – Groove pitch (m)

Pe – Peclet number (-)

Pr – Prandtl number (-)

R – Tube radius (m)

r_1 – Radius at the top edge of the groove (m)

r_2 – Radius at the base edge of the groove (m)

Re – Reynolds number (-)

T_w – Wall temperature (K)

v – Velocity (m/s)

W – Water

w – Groove width (m)

Greek letters

ρ – Density (Kg/m^3)

μ – Viscosity of fluid $(Pa\ s)$

τ – Shear stress (kg/m^2)

ε – Turbulent dissipate rate (m^2/s^3)

ω – Turbulent dissipate rate (m^2/s^3)

$\emptyset$ – Shape factor of Nano particle

φ – Volume concentration of Nano particle

Ratios

B/H – Aspect ratio of width (-)

e/d – Aspect ratio of depth (-)

s/d – Aspect ratio of pitch (-)

Subscripts

r – Radius of the groove (m)

g – Actual rectangular groove

o – Inlet of the tube

w – tube's wall

b – bulk

w – wall

p – nanoparticle

0 – base fluid (water)

t – turbulence

Acronyms

nk – Normalised Turbulent Kinetic Energy (m^2/s^2)

PEC – Performance Evaluation Criteria (-)

SPM- Single phase model

TPM- Two phase model

RKE – Realizable k-ε model

SST- Shear stress Transport k- ω model

TKE - Turbulent kinetic energy (m^2/s^2)

GNP – Graphene nanoplatelets

Chapter 1: Introduction

This chapter outlines the importance of convective heat transfer in various engineering applications in terms of heating and cooling systems related to heat exchangers. It provides the significance of optimising the heat transfer mechanisms, which results in substantial power savings along with other benefits. The background and motivation of this research were mentioned by emphasising the challenges associated with enhancing the heat transfer efficiency of cylindrical tubes used in heat exchangers. This chapter also discusses the potential solutions (e.g., internal corrugation, nanofluids, etc.) for enhancing heat transfer from the literature review and the problems associated with them. Additionally, this chapter defines the aim and objectives of this research, listing out the specific goals of numerically investigating combined geometrical and fluid effects. Finally, the overview of the thesis construction details each chapter that systematically relates to the objectives.

1.1 Background and Motivation

Convective heat transfer is essential in various small to large scale industrial processes, mainly heating and cooling systems. Some convective heat transfer applications in industries are oil and gas engineering, power generation, chemical processing, space engineering, gas pipelines, etc. [1-4]. Efficient heat transfer mechanisms are important to optimise performance, reduce energy consumption, and minimise the operational costs of the thermal system. This benefits the environment by reducing greenhouse gas (GHG) emissions, individual household bills, and reliance on non-renewable energy sources. In engineering fluid flow applications, many researchers have introduced different heat transfer augmentation techniques to achieve reliable and efficient thermal systems while reducing the size, cost, weight, etc. of the heat transfer equipment. One of these is the passive technique, which focusses on modifying flow geometry, operating conditions, and the thermophysical properties of the working fluid (e.g., thermal conductivity, etc.) without requiring the direct application of external power [5].

Cylindrical tubes are the most common heat transfer equipment and have widespread industrial applications involving fluid transport and heat exchange processes. These tubes are integral parts of various heat exchangers and are mainly preferred for their structural integrity, ease of installation, and effective handling of fluids. However, one of the challenges in utilising cylindrical tubes is optimising heat transfer efficiency, which is often constrained by material properties and fluid dynamics within the tube. To overcome this problem, internal corrugation in tubes is utilised, which is one of the most promising methods of energy savings using a passive heat transfer technique [5, 6]. This is because adding the grooves to the tube increases turbulence, which then disrupts the flow direction and boundary layer. Thereby increasing the convection. These internal corrugated tubes, as mentioned in Figure 1. 1 are used in various applications like evaporators, steam condensers, solar air heaters, heat exchangers, nuclear reactors, gas turbine blades, etc. [7].

Figure 1. 1: Cylindrical tubes with repeated ring type grooves at different pitch ratios [8]

Many researchers made various surface modifications by implementing the different grooves or ribs in a cylindrical pipe and various other heat exchanger applications to enhance convective heat transfer [9-11]. For instance, Selvaraj, et al. [12] numerically investigated the impact of different internal groove shapes (circular, square, and trapezoidal) on a cylindrical tube under constant heat flux using water. The results showed a significant increase in Nusselt number of up to 42% and a pressure drop of 78% compared to the plain tube in a turbulent flow (Re = 5000 to 13,500). Similarly, Zontul, et al. [13] investigated the rectangular grooved channels to understand the

convective heat transfer and flow characteristics experimentally and numerically under a turbulent flow (Re = 20,000–65,000). The results indicated that the heat transfer coefficient was 1.9 to 2.4 times larger than the straight channels, along with a 3 to 3.5 times increment in the pressure drop. In addition, Xu, et al. [14] numerically investigated the helically coiled spiral grooved tube heat exchanger to study the various effects of grooving methods and groove parameters in a turbulent flow. Their findings indicated a significant increase in the Nusselt number and pumping power, with increments ranging from 20 to 45% increment compared to a tube without corrugation.

Similar research studies [15-17] based on corrugation have also shown significant improvement in heat transfer results; however, it came with the cost of an increase in pumping power and pressure drop. This can be a potential drawback to the overall energy efficiency of the heat exchanger. This means that despite the grooves are better at increasing convection, there are still challenges to improving overall heat transfer efficiency. Balancing the trade-off between increased heat transfer efficiency and pressure drop is one of the key challenges in all thermal systems. Therefore, to address this challenge, this study focuses on exploring the different strategies to reduce the pumping power and pressure drop while maximising heat transfer.

Rectangular, triangular, trapezoidal, and circular groove shapes were selected for this study due to their straightforward geometries, which simplify their integration into conventional cylindrical tubes [18, 19]. These designs are advantageous for their cost-effectiveness and adaptability to standard manufacturing processes (turning, milling, drilling, rolling, extrusion, welding, etc.) [20, 21]. Moreover, they effectively improve convective heat transfer while keeping friction coefficient increases within acceptable limits, making them practical for industrial heat exchanger applications [22].

On the other hand, the working fluid is also an important parameter in the forced convection process of heat exchangers, particularly in passive technique. The selection of appropriate working fluid is critical to optimising the efficiency of any thermal system. Traditional fluids such as water, methanol, and ethylene glycol failed to meet today's rigorous requirements for heat removal due to their limited temperature range [23]. In contrast, various research studies have shown that nanofluids (solid-liquid mixtures) exhibited a better enhancement in thermal properties such as thermal conductivity and heat transfer coefficients over the past two decades [24, 25]. These

attributes have made nanofluids one of the most promising ways for energy savings and efficiency improvements in various applications, including heat exchangers, nuclear reactors, evaporators, steam condensers, solar air heaters, gas turbine blades, etc. [7].

Nanofluids have been widely used in recent years. The importance was given due to their enhanced thermal properties, which can potentially improve convective heat transfer. For example, Maïga, et al. [26] studied the thermal and hydrodynamic behaviour of Al_2O_3 nanoparticles dispersed in water at different volume concentrations in a circular tube. Their numerical results showed that the heat transfer coefficient increased from 3.5% to 47% as the nanoparticle volume concentration increased from 1% to 10%, respectively, at Re = 10,000. Similarly, even at low nanoparticle volume concentrations of Al_2O_3 nanoparticles, such as 0.02%, there was still a 0.5% increment in the Nusselt number [27]. Further studies [28-30] have reported similar heat transfer enhancements using Al_2O_3-water and TiO_2-ethylene glycol nanofluids. These studies found that both the Nusselt number and pressure drop increased with Reynolds numbers.

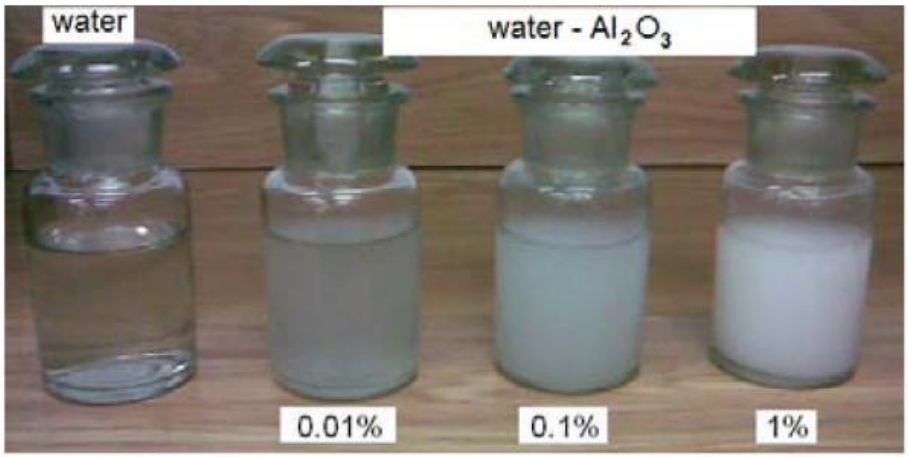

Figure 1. 2: Al_2O_3-water nanofluid at 0.01%, 0.1% and 1% volume concentrations [31]

Figure 1. 2 shows an example of Al_2O_3-water nanofluid at different nanoparticle volume concentrations. This study focuses on considering only Al_2O_3-based nanofluids because of their superior thermal properties, cost-effectiveness, chemical stability, and widespread use [32, 33]. Al_2O_3 nanoparticles are known for their high thermal conductivity, which significantly enhances the base fluid's heat transfer performance [34, 35]. These attributes, combined with their proven

performance in various industrial heat transfer applications, make Al_2O_3-based nanofluids an ideal focus for this research.

Additionally, hybrid nanofluids are also similar to nanofluids but consist of a combination of two or more types of nanoparticles added to the base fluid. These hybrid nanofluids are used in various heat transfer applications and can be more effective than standard nanofluids because the addition of multiple nanoparticles often results in better heat transfer performance[36]. For instance, Ba, et al. [37] investigated the heat transfer performance in a cylindrical tube using SiO_2-TiO_2 hybrid nanofluid with constant heat flux and wall temperature in a turbulent flow (Re = 5000 to 17,000). Their CFD results showed a significant improvement in overall convection with increasing volume concentration (φ = 0.5% to 1.5%). Similarly, Takabi and Shokouhmand [38] numerically examined the characteristics of heat transfer using Al_2O_3-Cu/water hybrid nanofluid (φ = 0-2%) in a uniformly heated circular tube. Their results showed that the Al_2O_3-Cu/water hybrid nanofluid increased the Nusselt number by 32.07% compared to pure water at Re = 10,000 to 100,000, while the Al_2O_3-water nanofluid exhibited an increase of only 13.68%.

To avoid the complexity and costs associated with experimental work, this research focuses on numerical modelling approaches. Both single-phase and multi-phase numerical models are employed to model nanofluids and hybrid nanofluids. These numerical models capture the complex dynamics of the fluid in terms of convective heat transfer. The single-phase model treats any number of phases as one phase; hence, it is easy to model. However, the multiphase model treats the number of phases as different individual phases, thereby introducing complexity in the governing equations, which need to include different fluid effects such as dispersion and Brownian effects, etc. The common multiphase models are Eulerian-Eulerian and Eulerian-Lagrangian. This research is constrained to Eulerian-Eulerian models (Eulerian and Mixture models to avoid the intricacy of the numerical simulation.

The differences between single and multiphase model heat transfer results in various heat exchanger applications under turbulent flow were compared by a limited number of research studies. According to Akbari, et al. [39], the single-phase model was more accurate and closer to the experimental data than the two-phase model using Al_2O_3-water and Cu-water nanofluids. Conversely, Peng, et al. [40] and Kalteh, et al. [41] indicated that the Eulerian model provided a

more accurate representation of nanofluid behaviour compared to the single-phase model using TiO_2-water and Al_2O_3-water. Moreover, Behzadmehr, et al. [42], Hejazian and Moraveji [43] and Beheshti, et al. [44] have all demonstrated that the mixture model was more effective than other models for modelling multiphase flows involving nanofluids, including Cu-water, TiO_2-water, and Al_2O_3-water nanofluids. Many other researchers also reported conflicting results based on the use of different nanofluids, volume concentrations, temperature ranges, flow conditions, or other factors. Therefore, the most suitable numerical model for Al_2O_3-based nanofluids remains uncertain, which impacts the accuracy of numerical simulations. This study addresses this challenge to enhance the reliability of numerical simulations and provide clear guidance for future research and heat transfer applications.

In addition, very few researchers combined the concept of grooves and nanofluids to achieve maximum heat transfer. One such study by Karami, et al. [45] investigated the effect of rectangular grooves in a cylinder using CuO-water nanofluid at Reynolds numbers ranging from 10,000 to 17,500. This research showed a significant improvement in heat transfer, with a 1.1 to 1.6 times increase in the Nusselt number for low depth groove ratios. Similarly, Salman [46] numerically examined different groove configurations (rectangular, triangular, and trapezoidal) on heat transfer, friction factor, and thermal performance in turbulent nanofluid (Al_2O_3, CuO, SiO_2, and ZnO) flows. Their results indicated that SiO_2 at a 4% volume fraction and 30 nm particle size in triangular ribs, achieved the highest Nusselt number at Re = 30,000.

Many of the research studies reviewed have demonstrated significant improvements in convective heat transfer through the combination of grooves and nanofluids. However, these approaches also introduced challenges, as previously discussed. Despite these advancements, the optimisation of groove geometries for energy efficiency and the accuracy of nanofluid models remain unresolved. This raises uncertainties about achieving the maximum heat transfer with high precision in numerical simulations. Therefore, this PhD research focuses on addressing these gaps with the main intention of contributing to various heat transfer engineering applications.

1.2 Research Aim and Objectives

This numerical research aims to investigate the enhancement of convective heat transfer performance by combining the wall grooves and nanofluids in a cylindrical tube under turbulent flow.

The objectives of this study are as follows:

- To conduct a comprehensive literature review assessing the geometric effects of grooves and the impact of nanofluids and hybrid nanofluids on convective heat transfer, as well as multiphase studies in various heat exchanger applications.

- To numerically investigate the combined effects of four groove shapes (rectangular, triangular, circular, and trapezoidal) on heat transfer efficiency in cylindrical tubes under turbulent forced convection.

- To develop and implement optimisation strategies to minimise pumping power while simultaneously improving heat transfer in a corrugated tube with a specific groove shape that results in the maximum pressure drop.

- To evaluate the accuracy of nanofluid numerical models, specifically the Single-Phase Model (SPM) and Two-Phase Model (TPM), using different RANS turbulence models (Realizable k-ε and Shear Stress Transport (SST) k-ω models).

- To investigate the thermal and hydrodynamic behaviour of Al_2O_3-based hybrid nanofluids on convective heat transfer using the most accurate nanofluid numerical model identified in the previous objective.

- To examine the combined effects of grooved geometries with different volume concentrations of Al_2O_3-based nanofluids and hybrid nanofluids, focusing on potential improvements in overall thermal efficiency.

1.3 Research contributions

- This study enhances the understanding of geometric effects by investigating various groove shapes and design optimisation strategies to improve the convective heat transfer rate of heat exchangers. Additionally, it explores innovative hybrid groove case studies and their impact on power consumption.

- This study emphasises the significance of selecting single-phase and multiphase models for simulating nanofluids and hybrid nanofluids. It provides a quantitative foundation for model selection based on key variables such as temperature, volume concentration, and nanoparticle properties. The research explores these models using RANS turbulence models, focusing on their impact on heat transfer accuracy.

- This numerical study advances convective heat transfer performance through efficient heat exchanger designs and the use of nanofluids and hybrid nanofluids. The research findings contribute to understanding the trade-off between heat transfer enhancement and increased pressure drop, offering valuable insights for practical applications in industrial heat transfer systems.

1.4 Thesis Construction

Chapter 1

This chapter introduces surface corrugation in heat exchangers, as well as nanofluids and hybrid nanofluids, and explores their impact on convective heat transfer performance in various engineering applications. Additionally, it outlines the research aim, objectives, and structure of the thesis.

Chapter 2

This chapter explores a thorough literature review on grooves, nanofluids, and hybrid nanofluids, including multiphase studies in turbulent flows. In addition, the combination of grooves with nanofluids and hybrid nanofluids in previous research studies is also critically reviewed. Finally, the research gaps are addressed in detail along with the numerical simulation approach.

Chapter 3

This chapter provides the heat transfer governing equations for the Single-Phase Model (SPM) and Two-Phase Models (namely the Mixture and Eulerian models) for incompressible fluid flow in a cylindrical tube. For the closure of the equations, two different turbulence models (the Realizable k-ε model and the Shear Stress Transport (SST) k-ω model) are also presented. In addition, the thermal properties of nanofluids and hybrid nanofluids, along with the relevant heat transfer formulas, are mentioned.

Chapter 4

This chapter studies the impact of various groove shapes (rectangular, circular, trapezoidal, and triangular) on a cylindrical tube to evaluate the Performance Evaluation Criteria (PEC) for convective heat transfer using water. In addition, hybrid grooves in six different cases are also investigated under a forced convection turbulent regime.

Chapter 5

This chapter investigates the rectangular groove shape discussed in Chapter 4 to further reduce pumping power or pressure drop and enhance the efficiency of the heat exchanger using design optimisation techniques. The heat transfer analysis is carried out with different groove parameter combinations.

Chapter 6

This chapter explores the single- and two-phase behaviour of the Al_2O_3-water nanofluid in a cylindrical tube under turbulent flow. It evaluates the compatibility of the Single-Phase Model (SPM) and Two-Phase Model (TPM) with the RANS turbulence models (Realizable k-ε model and

Shear Stress Transport (SST) k-ω model) to assess the accuracy and reliability of the numerical solution.

Chapter 7

This chapter investigates the thermal and hydrodynamic behaviour of various combinations of Al_2O_3-based hybrid nanofluids in a cylindrical tube under turbulent flow. It also explores the impact of the hybrid nanocomposite mixture ratio and the types of nanoparticles on heat transfer. Additionally, the accuracy of classical models is assessed.

Chapter 8

This chapter reports the maximum and most efficient heat transfer results achieved through the combined effects of optimised groove geometry with Al_2O_3-water nanofluids and Al_2O_3-based hybrid nanofluids.

Chapter 9

This chapter highlights the important findings of this research along with future recommendations.

1.5 Summary

This chapter establishes the foundation for the research by addressing the problem statement and the challenges associated with combining grooves and nanofluids to enhance convective heat transfer. The motivation for this study arises from the need to improve thermal systems and reduce energy costs in various practical applications. Therefore, the research aims to systematically investigate the combined effects of grooves and nanofluids on heat transfer efficiency, while overcoming challenges related to optimising groove geometry designs and accurately modelling nanofluids.

Chapter 2: Literature Review

This chapter covers a comprehensive literature review on grooves, nanofluids, and hybrid nanofluids that affect convective heat transfer. Several experimental and numerical research works were thoroughly reviewed. Initially, this chapter explores the importance of the groove geometrical effects (section 2.1.1) on cylindrical tubes and various heat exchanger applications. This includes the impact of geometrical parameters (e.g., groove depth to diameter ratio (e/D), groove width to diameter ratio (w/D), and groove pitch to diameter ratio (P/D)) on convection. Secondly, this chapter focuses on the fluid effects, which are nanofluids (section 2.2.1) and hybrid nanofluids (section 2.2.2) studies. This contains a detailed analysis of heat transfer parameters such as shape, type, size, volume fractions, material properties, volume concentration, etc. It also covers multiphase studies comparing single-phase models and two-phase models (Eulerian-Eulerian and Eulerian-mixture models). Furthermore, the combined effects of grooves with nanofluids and hybrid nanofluids are also reviewed in sections 2.3.1 and 2.3.2. Finally, the chapter concludes by identifying gaps in the current research and discussing the flowchart of the conducted numerical approach in detail.

2.1 Geometrical effects on heat transfer

2.1.1 Grooves

Many researchers have experimentally and numerically investigated the impact of adding grooves to the various heat exchangers to improve convective heat transfer in a turbulent flow [47-50]. These studies have explored different groove parameters such as shape, size, angle, type, etc. and examined their effects on thermal performance factor, Nusselt number, friction factor, pressure drop, wall shear stress, etc. The addition of wall grooves to heat exchangers has shown a significant enhancement in overall heat transfer due to the improvement in turbulence, disruption in boundary layer formation, and increment in surface area [45, 51-53]. The flexibility of

implementing different groove designs in various applications makes them one of the most efficient passive techniques for enhancing heat transfer.

In particular, Kaood, et al. [19] numerically investigated the effects of various groove geometries on heat transfer in a transverse grooved tube under a turbulent regime. Four different groove shapes (trapezoidal, rectangular, circular, and triangular) were implemented to perform the tests at Reynolds numbers ranging between 5,000 and 61,000 using water. Their results confirmed that all groove shapes significantly improved heat transfer. Additionally, inward grooves were found to be most efficient in obtaining the highest turbulent kinetic energy than the outward grooves. Similarly, Dhaidan and Abbas [54] numerically examined the hydrodynamic and thermal behaviours of tubes with inward-outward, inward, and outward groove arrangements under turbulent flow, as shown in Figure 2. 1. Their results revealed that inward corrugated grooves (rectangular, trapezoidal, and semicircular shapes) achieved a maximum increment in heat transfer by an average of 23.2%, compared to the smooth tube at Re = 60,000. In addition, the inward-outward groove arrangement resulted in a lower pressure drop of 27.2% compared to the inward groove combinations. In another study, the outward transverse grooves showed the lowest heat transfer performance (PEC) of 1.18, whereas the helical grooved tube achieved a PEC of 1.23, higher than that of the smooth tube, in turbulent flow at Re = 18,800 [55].

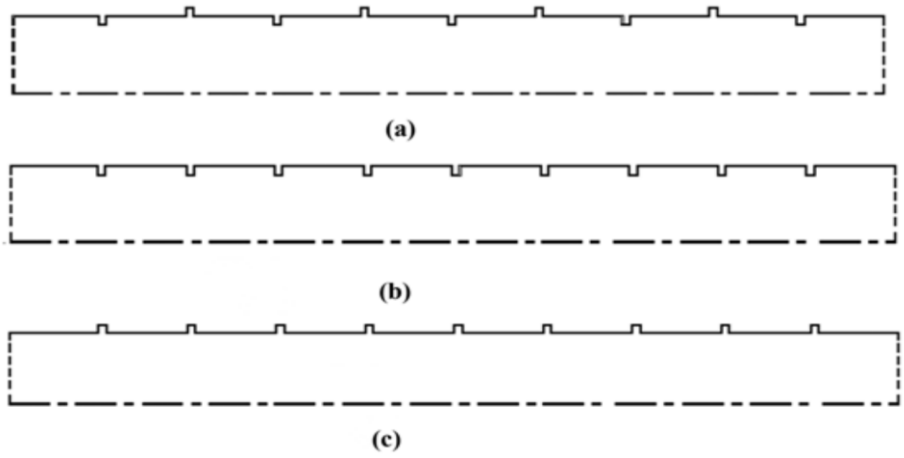

Figure 2. 1: Corrugated tubes distribution of rectangular grooves (a – Inward-Outward, b – inward, c- outward arrangement) [54]

From the above findings, it can be noted that while the inward-outward groove arrangement results in a lower pressure drop, its manufacturing complexity makes it unsuitable for real-world applications. Therefore, this study focuses on inward corrugated tubes.

The impact of various groove shapes on heat transfer has been explored in a limited number of studies. For example, Bilen, et al. [22] experimentally investigated the air flow of various groove shapes (rectangular, circular, and trapezoidal) in a circular tube for different Reynolds numbers ranging from 10,000 to 38,000. Their results indicated that the circular grooves were efficient with a 63% increment in heat transfer coefficient compared to the smooth tube due to less flow recirculation. In contrast, the rectangular grooves exhibited the least heat transfer performance. Additionally, the variation of the friction coefficient of all corrugated tubes tends to be closer to each other, with no fluctuations in the friction factor at higher Re. In a related study, Abed, et al. [56] investigated three groove shapes (triangular, trapezoidal, and semi-trapezoidal) over a rectangular ribbed channel in a turbulent flow using air and water. Results showed that triangular grooves had better thermal efficiency, with a 59% increase in heat transfer compared to smooth tubes.

Similarly, the convective heat transfer of internally grooved tubes with different rib shapes (rectangular, trapezoidal, and semi-circular) was numerically investigated by Mohebbi, et al. [57] using an Al_2O_3-water nanofluid (φ = 0–5%) under a constant heat flux boundary condition. Their numerical simulations demonstrated that the trapezoidal grooves exhibited the highest Nusselt number than other groove shapes with fixed groove depth ratios in a turbulent regime (Re = 10,000 to 35,000). In addition, Selvaraj, et al. [12] also concluded that the trapezoidal grooved tubes exhibited the highest heat transfer with an efficient turbulent intensity for a Reynolds number range of between 5000 and 13,500 respectively, under a constant heat flux condition as shown in Figure 2. 2.

Based on these studies, it is evident that there is no optimal shape for predicting higher heat transfer. This is because results change significantly with the groove dimensions, tube length, and tube diameter. Hence, the optimal groove shape differs across the studies, indicating the dependency of groove parameters (e/d, w/d, and p/d) on the smooth tube dimensions.

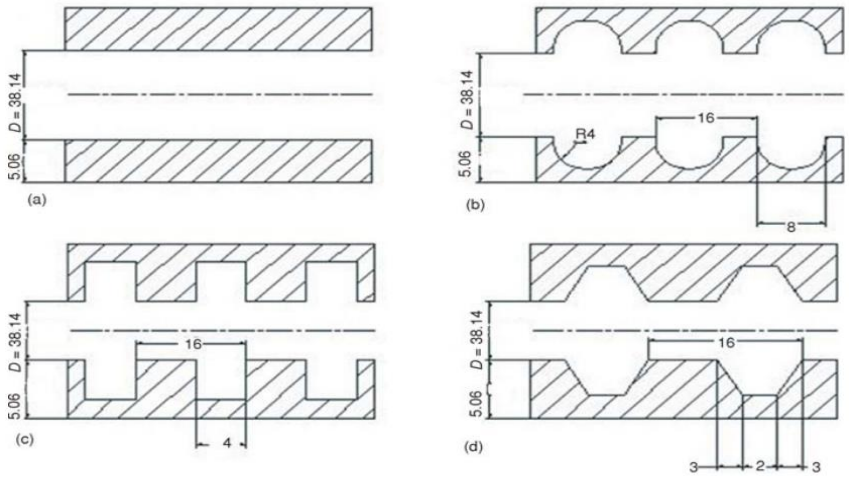

Figure 2. 2: Example of different groove shapes in a corrugated tube (a) Plain, (b) circular, (c) rectangular, (d) trapezoidal) [12]

The effects of groove depth (d), width (w), and pitch (p) ratios on convection have been highlighted in different studies. Specifically, Mohammed, et al. [18] studied the effects of different groove geometrical parameters through nineteen corrugated tubes on flow and thermal fields under constant heat flux boundary condition (Re = 5,000 to 60,000) as shown in Figure 2.3. These simulation tests were conducted by changing the rectangular groove depth to the tube diameter ratio (e/d) in the range of 0.025–1, the groove width to the tube diameter (w/d) in the range of 0.05–2, and the groove pitch to the tube diameter (p/d) in the range of 0.5–1.5. The results showed that the maximum PEC was achieved with e/d = 0.025, w/d = 0.2, and p/d = 0.5. This suggests that the lower groove depth and pitch ratios lead to maximum heat transfer. Additionally, the friction factor decreases as the groove width increases for a fixed groove depth and pitch ratios.

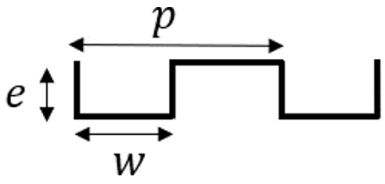

Figure 2. 3: Example of Rectangular Groove parameters (e- depth, w- width, and p- pitch) [18]

In a similar study, Ramadhan and Al Anii [58] numerically investigated two aspect ratios of depth (e/d = 0.1 and 0.2) with four different groove shapes (triangular, trapezoidal, circular, and rectangular) in a cylindrical tube under turbulent flow (Re = 10,000–20,000). They found that the

optimal value was obtained at e/d = 0.1 with a 64.4% increment in heat transfer over a smooth tube. The maximum thermal performance of 1.52 was obtained for a triangular groove in an air flow. Furthermore, the influence of grooves on the friction factor at high Reynolds numbers was negligible. This is because, at higher velocities, the turbulence dominates the flow, negating the groove effect.

The relationship between e/d (0.025–0.069) and p/d (0.29–5.8) with the variation of air, water, and ethylene glycol was experimentally investigated by Huang, et al. [8] using ring-type ribs in a circular tube. Results indicated that effective heat transfer was obtained for $e/d \leq 0.043$ when p/d was smaller than 4.35 at Re = 3,601 to 26,025. Similarly, the combination of $e/d \geq 0.069$ with a p/d value higher than 1.45 avoids a large pressure drop. This means that the Nusselt number increases with the e/d value and decreases with an increase in the p/d value. In a related study, Wang, et al. [59] numerically investigated the effect of various depth (e/d = 0.1, 0.15, and 0.2) and pitch (p/d = 1, 1.5, and 2) ratios in helically corrugated tubes in turbulent flow at Re = 25,500. The results revealed that increased groove depth (e/d) contributed to strengthening both swirl intensity and flow rotation, thereby increasing the Nusselt number. Furthermore, ratios of the friction factor and Nusselt number both increased with e/d when e/d was less than 0.1. However, the increase in pitch (p/d) enhanced the flow rotation but weakened the swirl flow, which led to a decrease in turbulent kinetic energy levels and heat transfer. The optimum combination was also provided at $e/d<0.1$ and $p/d<2$, where the heat transfer coefficient growth rate is greater than the flow resistance coefficient (friction factor).

It can, therefore, be interpreted from the above studies that the groove parameters of depth, width, and ratio of pitch are mutually interrelated with each other, having a large influence on tube diameter to achieve better heat transfer. The interpretations by the different authors contradict each other, so making a direct comparison between studies can be challenging. Consequently, there cannot be a universal optimal range or combination of groove parameters, as the effectiveness depends on the groove shape, dimensions, and different applications of various heat exchangers.

The impact of the groove angle also plays an important role in obtaining effective convective heat transfer. In this context, Pourfattah, et al. [60] numerically investigated the effect of the angle of attack (30, 60, 90, 120, and 150 degrees) of the rectangular groove, as shown in Figure 2. 4 at

different Reynolds numbers ranging from 24,000 to 60,000 using an Al_2O_3-water nanofluid (φ = 0-4%). Their results indicated that maximum heat transfer was obtained at 90^0, which created large gradients behind the grooves in terms of efficient mixing and a significant improvement in the pressure drop. While the ratio of the Nusselt number to the applied pressure drop of the fluid-thermal performance indicated maximum values at $\theta = 60^0$. However, it can also be pointed out that production complexity, time, and cost increased with an increase or decrease in angles of attack accordingly [61]. In a related study conducted by Mohammed, et al. [18], the rectangular groove obtained a maximum performance evaluation criterion (PEC) at $\theta = 90^0$ for a range of Reynolds numbers between 5,000 and 60,000.

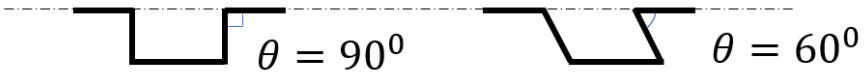

Figure 2. 4: Rectangular groove angle of attack at $\theta = 90^0$ and 60^0 [60]

Similarly, Zheng, et al. [62] studied a novel discrete inclined grooved tube at θ = 15, 30, and 45 degrees under fully developed turbulent flow condition (Re = 6,780 to 20,340). The findings showed that the grooved tubes generated longitudinal swirl flows with numerous vortices, which were directly correlated with the number of grooves. This resulted in an increase in thermohydraulic performance from 1.04 to 1.52, with the maximum heat transfer coefficient observed at an angle of 30 degrees and the lowest Re. In addition, Firoozeh, et al. [63] experimentally investigated spiral grooves in a double tube heat exchanger under a turbulent regime (Re = 9,000 to 18,000) with a focus on inner tube groove angle variations (θ = 0, 15, and 45 degrees) for both counter and parallel flows. Their results showed that highest Nu/Nu_s and f/f_s were obtained at $\theta = 15^0$ with an increment of around 40 to 50%. This indicates that a lower angle of inclination for the spiral groove, or a more vertical groove, enhances turbulence and improves fluid mixing in the boundary layer. Based on previous studies, the impact of groove angle on convection appears to be significant. Therefore, for simple shapes such as circular, rectangular, triangular, and trapezoidal, an angle of inclination of 90^0 seems to be more effective in obtaining the maximum convective heat transfer performance.

Apart from simple groove shapes such as circular, rectangular, and triangular, more complex groove structures can significantly impact the performance of thermal systems. According to Vicente, et al. [64], the influence of ten different spiral grooves on convective heat transfer was experimentally investigated using water and ethylene glycol (Pr = 2.5 to 100) at Re = 2,000 to 90,000 under constant heat flux on the wall of a circular tube. The results revealed that the Nusselt number increased by up to 250%, and the friction factor showed enhancements ranging from 20% to 300%, with e/d values from 0.02 to 0.06 and p/d values from 0.6 to 1.2 compared to a smooth tube. Additionally, the severity index ($\emptyset = e^2/pd$), which characterises the roughness influence on the flow, has also been employed, and it was suggested that most effective tubes have high severity index values.

In terms of the variation in helical grooves, Mogaji, et al. [65] studied the heat transfer augmentation in an internal helical grooved tube for different pitch sizes at Re = 12,000 to 22,000 as shown in Figure 2.5. The results suggested that increasing the pitch from 19 mm to 95 mm significantly enhanced convection. However, this increase in pitch was associated with a substantial increase in the Nusselt number, but also resulted in a significant penalty on the pressure drop, approximately 5.31 times higher than that of a smooth tube. Consequently, this phenomenon increased resistance, rendering the helically corrugated tube less efficient. To overcome this problem, Miansari, et al. [66] numerically compared helically grooved tubes (HGT) and helically coiled tubes (HCT) under turbulent flow conditions for forced convection. Their results indicated that the HCT demonstrated better thermal performance than the HGTs in a 3D simulation. Furthermore, Xu, et al. [14] introduced the helically coiled spiral groove tube (HCSGT), which exhibited a PEC 25% higher than HCT's.

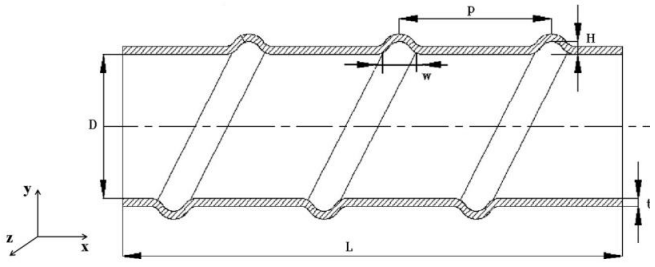

Figure 2. 5: 2D structure of helical groove [59]

Another complex groove structure is the conical tube, a novel type of heat exchange tube that offers high efficiency but has been studied less extensively. Wu, et al. [67] found that conical tubes have lower axial elastic stiffness, higher ultimate strength, and higher yield strength compared to smooth tubes. Furthermore, their results concluded that conically corrugated tubes provide a higher heat transfer coefficient than spiral grooved tubes, convergent diverging tubes, and smooth tubes, by 15%, 17%, and 115%. Similarly, Meng, et al. [68] experimentally investigated an innovative structure known as the alternating elliptical axis tube. This study focused on heat transfer and flow resistance across Reynolds numbers ranging from 500 to 50,000. The experiments revealed that the Nusselt number ratio was significantly improved, accompanied by reduced flow resistance. This enhancement in heat transfer performance was attributed to the multi-longitudinal vortices generated by the cross-sectional changes in the elliptical axis tubes.

Additionally, Dizaji, et al. [69] experimentally investigated sinusoidal (wavy) corrugated tubes with convex (outward) and concave (inward) grooves in a double tube heat exchanger under a turbulent regime (Re = 3,500–18,000). Their results revealed that maximum NTU – effectiveness ($\varepsilon/\varepsilon_s$) was obtained in concave outer tubes for both parallel and counter flows, with a range of increments of about 28% to 55%. On the other hand, Xu and Zhang [70] compared different corrugated groove structures such as arc line, circular, and convergent–divergent variations and concluded that the highest friction factor was obtained for an arc-line grooved tube and maximum energy efficiency with the best anti-fouling performance (particle deposition) was achieved for a circular grooved tube. From the above studies, Figure 2. 6 compares the different structures of inward corrugated tubes.

This study avoids complex groove structures due to the intricacies of manufacturing limitations and the complexity of numerical simulations. Instead, it focuses on simpler groove shapes, such as circular, rectangular, triangular, and trapezoidal grooves, to effectively capture the dynamics and heat transfer of fluid flow.

a. Rectangular grooved tube [71]

b. Helically corrugated tube [72]

c. Conically corrugated tube [67]

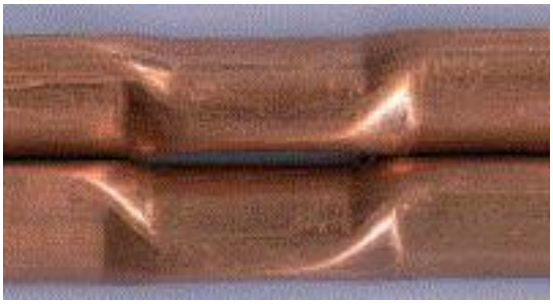

d. Elliptical axis tube [68]

e. Sinusoidal corrugated tube [69]

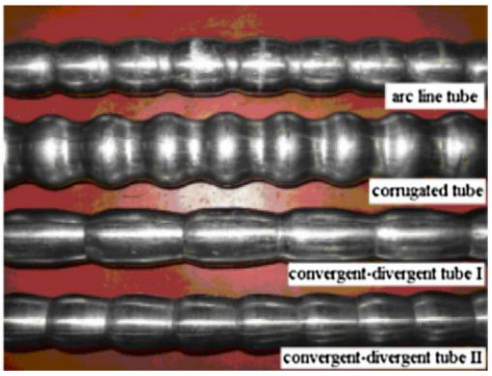

f. Other corrugated tubes [70]

Figure 2. 6: Different types of Inward grooves structures

Many researchers rely on empirical correlations or data to validate their numerical research, thereby avoiding the complexity of conducting experiments. These empirical correlations are used to calculate the Nusselt number or the friction factor, which are essential for predicting the thermal and fluid dynamic performance of heat exchangers. The data derived from these correlations depend on geometrical parameters and flow conditions, which directly impact heat transfer and pressure drop characteristics. Moreover, this data can be used to refine numerical models, enhancing their predictive accuracy. In recent years, several studies have explored the effects of corrugation on heat exchanger tubes experimentally to develop these correlations and improve heat transfer in turbulent flows. However, it is crucial for any numerical model to be validated against a smooth tube before introducing surface grooves in a heat exchanger, as discussed below.

The smooth tube (without corrugation) has been experimentally examined in various experimental studies [73-76] under forced convection turbulent flow with a constant heat flux ($q = 50\, w/cm^2$) and a wall temperature (300K) using water. These studies provided baseline heat transfer results for thermally and hydraulically developing flow, which are crucial for validating numerical models in circular tubes across Reynolds numbers ranging from 10×10^3 to 60×10^3 with a Prandtl number of 5.83 at 300 K. The proposed empirical correlations for the Nusselt number and friction factor are valid only within specific ranges of Reynolds numbers. The Nusselt number correlations are given by the Petukhov [73], Notter and Sleicher [74] and Gnielinski [75] models. Similarly, the Darcy friction factor is represented using the Blasius [76] and Petukhov [73] models. These correlations are as follows:

Blasius equation: [76]

$$f = \frac{0.316}{Re^{0.25}}, 3000 \leq Re \leq 10^5 \tag{2.1}$$

Petukhov equation: [73]

$$f = (0.79 \ln Re - 1.64)^{-2} \tag{2.2}$$

$$Nu = \frac{\frac{f}{8} Re\, Pr}{1.07 + 12.7 \left(\frac{f}{8}\right)^{0.5} \left(Pr^{\frac{2}{3}} - 1\right)}, (0.5 \leq Pr \leq 2000; 10^4 \leq Re \leq 5 \times 10^6) \tag{2.3}$$

Notter-Rouse equation: [74]

$$Nu = 5.0 + 0.015\, Re^{0.856}\, pr^{0.347} \tag{2.4}$$

Gnielinski equation: [75]

$$Nu = \frac{\frac{f}{8} (Re - 1000) Pr}{1.0 + 12.7 \left(\frac{f}{8}\right)^{0.5} \left(Pr^{\frac{2}{3}} - 1\right)}, (0.5 \leq Pr \leq 2000; 3000 \leq Re \leq 5 \times 10^6) \tag{2.5}$$

where *Nu, f, Re*, and *Pr* represent the Nusselt number, friction factor, Reynolds number and Prandtl number.

The smooth tube with corrugation was experimentally investigated by Huang, et al. [8] using repeated ring or circular type grooves in thirteen different corrugated tubes. These tubes varied in depth (e/d = 0.025-0.069) and pitch (p/d = 0.29-5.8) ratios using three different working fluids (air, water, and ethylene glycol) in a turbulent flow as illustrated in Figure 1. 1 in chapter 1. Their results concluded that the Nu enhancement index (Nu/Nu_0) and mechanical energy index (PEC) increase with e/d values and decrease with p/d values across different Reynolds numbers. They also suggested that to achieve maximum heat transfer, the e/d value should be less than or equal

to 0.043 with smaller p/d values. Additionally, they proposed empirical correlations for calculating the Nusselt number and friction factor as follows:

$$Nu = 0.34Re^{\left[-0.0222\left(\frac{p}{d}\right)+0.746\right]\left(\frac{e}{d}\right)^{-0.1}} e^{0.177\left(\frac{p}{d}\right)} \left(\frac{e}{d}\right)^{1.29} Pr^{0.45} \left(\frac{\mu_b}{\mu_w}\right)^{0.14} \quad (2.6)$$

where *Nu, Re*, *Pr,* $\frac{e}{d}$, $\frac{p}{d}$, μ_b, and μ_w represent the Nusselt number, Reynolds number, Prandtl number, groove depth ratio, groove pitch ratio, bulk fluid viscosity and mean fluid viscosity at the wall. The above equation is valid for $0.025 \leq \frac{e}{d} \leq 0.069$, $0.29 \leq \frac{p}{d} \leq 5.8$, $3601 \leq Re \leq 26025$, and $0.7 \leq Pr \leq 15.6$ with 19% error.

$$f = 0.48Re^{\left[0.00263\left(\frac{p}{d}\right)^2-0.0401\left(\frac{p}{d}\right)-0.169\right]} e^{0.025\left(\frac{p}{d}\right)} \left[5.946\left(\frac{e}{d}\right)+0.85\right]^{4.65} \quad (2.7)$$

where *f is* the friction factor. The above equation is valid for $0.025 \leq \frac{e}{d} \leq 0.069$, $0.29 \leq \frac{p}{d} \leq 5.8$, and $3967 \leq Re \leq 17850$ with the error of 22.6%.

In a similar numerical study, the effect of rectangular groove parameters (depth, width, and pitch ratios) of a circular tube on thermal and fluid flow was examined under a constant heat flux ($50\ w/cm^2$) in a turbulent flow (Re = 5,000 to 60,000) [18]. The results suggested that the heat transfer was greatly impacted by altering the groove parameters. This signifies that the Nusselt number increases with the groove depth, width, and Reynolds number while it decreases with the roughness pitch values. In addition, the maximum heat transfer performance (PEC) was achieved for the effective groove combination e/d = 0.025, w/d = 0.2 and p/d = 0.5.

Among different applications, corrugated tubes are the most commonly employed. For instance, Wang, et al. [77] numerically investigated a multi-tube heat exchanger (MTHX) with an outward helically corrugated tube (HCTs) using three different groove shapes (square, circular, and triangular) and pitch ratios (1.25, 1.375, 1.5, and 1.625) to test the mechanism of heat transfer in

a turbulent flow (Re = 8,000 to 89,400). Their results show that the addition of HCTs improved thermal performance. It was reported that the secondary flow increases the heat transfer coefficient due to the strong spiral cortex effect. While rotational flow slightly weakens the PEC because of the strong overlay effect in the opposite direction.

According to Zontul, et al. [13], the impact of the rectangular groove channel on hydrodynamic flow was studied both numerically and experimentally, with Re ranging from 20,000 to 65,000 respectively. Comparing the Nusselt number to the straight channel, the results implied that it was improved by 1.9 to 2.4 times. Conversely, adding grooves reduces the thermal coefficient of performance by increasing the pressure drop. This is because higher corrugation leads to larger energetic swirls, which together improve flow instabilities [78]. Another study on nanochannels by Chakraborty, et al. [79] showed that uniform and randomly distributed grooves or ribs significantly improved the heat distribution between the liquid and the wall. This demonstrated that surface topology and material selection were important factors in heat dissipation. In addition, the numerical study conducted by Zhang and Che [80] on cross-corrugated plates in a turbulent flow also showed significant improvements in pressure drop and heat transfer. Therefore, it can be concluded that employing corrugation in any application can significantly enhance the overall convection of the thermal system.

2.2 Fluid Effects on heat transfer

2.2.1 Nanofluids

Nanofluids, which are colloidal suspensions of nanoparticles in the base fluid, have received significant attention in recent years due to their superior thermal properties. These nanoparticles typically consist of metals (Ag, Cu, Au), oxides (Al_2O_3, CuO), carbides (SiC, TiC), carbon nanotubes, etc. mixed with base fluids such as water, ethylene glycol, oil, etc. [81]. Nanofluids are primarily used in heating and cooling purposes, which is another passive technique used for enhancing heat transfer. Several experimental and numerical studies have demonstrated the potential of

nanofluids, specifically depending on their heat transfer parameters such as nanoparticle shape, size, type, volume fraction, etc., which impact energy efficiency [82].

Several nanofluids have been utilised to examine the influence of heat transfer parameters in forced convection under both turbulent and laminar flows. The results reveal that adding nanoparticles to the base fluid increases the overall convective heat transfer performance and pumping power. This enhancement was due to the strong influence of the thermophysical properties of nanoparticles (e.g., specific heat, viscosity, thermal conductivity, etc.) [32, 83]. Following this, Saha and Paul [84] carried out a numerical study to investigate the effects of different types of nanoparticles (Al_2O_3 and TiO_2) on fluid flow and heat transfer under turbulent forced convection in a circular tube. Their findings showed that the addition of Al_2O_3 and TiO_2 nanoparticles (φ=4% to 6%) into water improved the fluid flow, temperature distribution, pressure drop, and heat transfer coefficient at different Reynolds numbers (Re=10,000 to 100,000). Moreover, Al_2O_3–water nanofluid exhibited a higher heat transfer rate than TiO_2-water nanofluid due to its high thermal conductivity. A similar experimental investigation conducted by Sajadi, et al. [85] concluded that the inclusion of ZnO nanoparticles dispersed in water increased the heat transfer coefficient by 11% to 18% at volume concentrations (φ = 1% to 2%) and also elevated wall shear stress for Reynolds numbers ranging from 5,000 to 30,000.

On the other hand, some researchers have highlighted the importance of using base fluids other than water, which can affect heat transfer. For instance, Ebrahimnia-Bajestan, et al. [86] numerically investigated Al_2O_3, carbon nanotubes (CNT), CuO, and titanate nanotubes (TNT) dispersed in an ethylene glycol/water mixture and water (0–6 vol%) to study the pressure drop and heat transfer characteristics in a cylindrical tube under laminar flow. Their results pointed out that the Nusselt number and friction factor were strongly influenced by base fluids, where the water-based nanofluid combination exhibited the highest heat transfer.

Volume concentration is one of the important parameters in nanofluids and is defined as the ratio of the volume of nanoparticles to the volume of the base fluid. Based on previous studies, it is quite evident that the nanoparticles have a higher thermal conductivity than the base fluid. Therefore, as the nanoparticle's dispersion percentage increases, the total thermal conductivity of the nanofluid also increases. Many experimental and numerical studies confirmed that heat transfer

coefficients were improved by at least 20% for nanoparticle volume concentrations less than 5% [82].

According to Maïga, et al. [26], the heat transfer performance was studied using γ-Al_2O_3 nanoparticles (φ=1% - 10%)) dispersed in water under a turbulent regime (Re=10,000 to 500,000) in a cylindrical tube's forced convection. Their results found that the increase in Al_2O_3 nanoparticle volume concentration from 1% to 10% in the base fluid improved the average heat transfer coefficient from 1.035 to 1.47. In a related study, Kumar and Ganesan [27] investigated the thermal and hydrodynamic behaviour of Al_2O_3-water nanofluid at low volume concentrations ((i.e., 0.02%, 0.1, and 0.5%) in a circular tube. Their numerical results suggested that Nusselt number increased by 0.5% even at 0.02 vol% compared to the water. In addition, it was also observed that the Nusselt number increased by up to 10%, 40%, and 60% for volume concentrations of 1%, 4%, and 6%. Therefore, it was apparent that the variation in the nanoparticle volume concentration demonstrated a significant impact on convective heat transfer.

The shape of nanoparticles can also alter the thermal conductivity and dynamic viscosity of the resulting nanofluid. Most of the numerical investigations have focused on spherical-shaped nanoparticles due to the dependency on the Maxwell model [87], a fundamental model for calculating the thermal conductivity of nanofluids. This model, which is limited to spherical particles, has been widely cited and forms the basis of existing research areas. According to Meriläinen, et al. [88], a numerical investigation was conducted using various nanoparticle shapes, with Al_2O_3, MgO, and SiO_2 nanoparticles in an annular tube with a constant wall temperature for Reynolds numbers ranging from 3000 to 10,000. Their findings indicated that SiO2-based nanofluid containing smooth spherical particles (average size 6.5 ± 1.8 nm) demonstrated a significant increase in heat transfer at concentrations ranging from 0.5 to 2 vol%. Similarly, studies conducted by various Tiwari and Das [89], Oztop and Abu-Nada [90], Ho, et al. [91] and Aminossadati and Ghasemi [92] have also shown that spherical-shaped nanoparticles are effective in achieving reliable heat transfer results, with numerical simulations closely matching experimental data. Therefore, this study considers the spherical shape due to its widespread use for the proper validity and accuracy of the numerical results.

The non-uniform nanoparticle shapes have been explored by a few researchers. For instance, Timofeeva, et al. [93] experimentally examined the effects of various nanoparticle shapes (brick, cylindrical, platelet, blade, and spherical) on heat transfer using alumina-water/ethylene glycol nanofluids. It was found that cylindrical shapes have high thermal conductivity, and spherical shapes have the lowest dynamic viscosity or pumping power. Furthermore, Murshed, et al. [94] revealed that cylindrical nanoparticles were better at improving the thermal conductivity of the TiO_2-water nanofluid due to their large surface area's aspect ratio and elongated particles.

Nanoparticle size is another effective parameter that contributes to the hydraulic and thermal behaviour of the nanofluids. Theoretical evidence [95] suggests that the effective thermal conductivity increased with the decrease in the nanoparticle size. To illustrate, Saha and Paul [84] numerically investigated different nanoparticle sizes (10, 20, 30, and 40 nm) using the Al_2O_3-water nanofluid under uniform heat flux wall boundary conditions in a circular tube. The results revealed that smaller nanoparticles (10 nm) with Brownian motion exhibit the highest average Nusselt number, shear stress ratio, and thermal performance factor. For example, the average shear stress ratio of the nanofluid increased from 2 to 3.58 times higher than the base fluid when the nanoparticle diameter was reduced from 40 nm to 10 nm at Re = 20,000. Similarly, an experimental study found that SiO_2 nanoparticles with a size of 15 nm obtained the highest heat transfer coefficient and performance evaluation criteria (PEC) compared to nanoparticles sized at 30 nm and 80 nm [96]. Additionally, studies conducted by Davarnejad, et al. [97] and Anoop, et al. [98] support the observation that the heat transfer coefficient improves with decreasing nanoparticle size. Furthermore, nanoparticle sizes smaller than 100 nm are essential for optimising the effective fluid's thermal conductivity; variations in nanoparticle size below this threshold have negligible effects on heat transfer [99]. Hence, it is evident that nanoparticle diameter significantly impacts heat transfer performance.

In terms of nanoparticle effects, the buoyancy forces in nanofluids are often regarded as negligible due to the extremely small size of nanoparticles. These particles contribute minimally to the density variations typically caused by temperature differences, rendering buoyant forces insignificant. Additionally, in forced convection, where pumps or similar mechanisms drive the flow, the influence of buoyancy is diminished by the momentum of the forced flow at high Reynolds

numbers. This is particularly evident at high Reynolds numbers, where inertial and viscous forces dominate. Research studies conducted by Dukhan [100] and Chakraborty and Panigrahi [101], supports the notion that buoyancy plays a minimal role under these conditions, allowing for its exclusion from heat transfer models without impacting their accuracy.

To validate this numerical research on Al_2O_3-based nanofluids, several studies have proposed empirical correlations. For instance, Pak and Cho [102] conducted an experimental investigation on the heat transfer behaviour of Al_2O_3- and TiO_2-water nanofluids (with particle diameters of 13 nm and 27 nm) in a circular tube under constant heat flux conditions and turbulent flow. Their results showed a significant improvement in heat transfer coefficient and friction factor at both volume concentrations (φ=1.34% and 2.78%) of Al_2O_3 -water nanofluid compared to conventional base fluid for a fixed Reynolds number. In addition, they proposed a correlation for calculating the Nusselt number specifically depending on the Reynolds number and Prandtl numbers. It is important to note that this correlation does not depend on the diameter or volume concentration of the nanoparticle.

$$Nu = 0.021\, Re^{0.8}\, Pr^{0.5} \tag{2.22}$$

The above equation is valid for the volume concentration $\varphi = 0\ to\ 3\%$, Reynolds number $Re = 10^4\ to\ 10^5$ and Prandtl number $Pr = 6.54\ to\ 12.3$.

Similarly, Maïga, et al. [26] numerically investigated the thermal and hydrodynamic behaviour of Al_2O_3-water nanofluid under uniform heat flux conditions in turbulent flow using a cylindrical tube's forced convection. Their numerical results revealed an augmentation in convective heat transfer and wall shear stress with increasing nanoparticle volume concentration. For instance, the wall shear stress increased from 728 Pa at φ = 0% to 4,960 Pa at φ = 10%. In addition, they developed a new correlation for calculating the Nusselt number of Al_2O_3-water nanofluid for a wide range of volume concentrations.

$$Nu = 0.085\ Re^{0.71}\ Pr^{0.35} \tag{2.23}$$

This above equation is based on the single-phase model, and it is valid for the range of Reynolds number $Re = 10^4\ to\ 5 \times 10^5$; Prandtl number $Pr = 6.6\ to\ 13.9$ and volume concentration $\varphi = 0\ to\ 10\%$.

2.2.1.1 Impact of Thermo-physical properties correlations

Thermo-physical properties are crucial for numerical modelling of heat transfer, as they enable the calculation of effective fluid parameters such as specific heat, density, viscosity, and thermal conductivity of a nanofluid under specific operating conditions. These parameters are often determined using empirical correlations, which are essential for the accuracy of numerical heat transfer predictions. Despite the availability of numerous correlations, calculating thermal conductivity and viscosity, especially for Al_2O_3-water nanofluids, remains challenging. This difficulty arises from uncertainties in the experimental preparation of nanofluids, which can lead to nanoparticle agglomeration, sedimentation, and aggregation, thereby affecting the accuracy of the measured values. Moreover, while these correlations can be effective within a limited range, they often lack accuracy under varying conditions. This limitation is due to the fact that many of these correlations do not account for factors such as temperature or particle size, focusing primarily on the volume concentration of nanoparticles.

Below are equations representing different correlations proposed by various researchers for calculating the thermal conductivity and viscosity of Al_2O_3-water nanofluids with volume fractions ranging from 1% to 5% at 300K.

Pak and Cho model [102]

$$k_{nf} = k_w(1 + 7.47\varphi) \tag{2.8}$$

$$\mu_{nf} = \mu_w(1 + 39.11\varphi + 533.9\varphi^2) \tag{2.9}$$

Maiga et al. model [103]

$$k_{nf} = k_w(1 + 2.72\varphi + 4.97\varphi^2) \tag{2.10}$$

$$\mu_{nf} = \mu_w(1 + 7.3\varphi + 123\varphi^2) \tag{2.11}$$

Chen et al. model [104]

$$k_{nf} = k_w(1 + 1.72\varphi) \tag{2.12}$$

$$\mu_{nf} = \mu_w e^{14.8\varphi} \tag{2.13}$$

Ho et al. model [105]

$$k_{nf} = k_w(1 + 2.944\varphi + 19.672\varphi^2) \tag{2.14}$$

$$\mu_{nf} = \mu_w(1 + 4.93\varphi + 222.4\varphi^2) \tag{2.15}$$

Rea et al. model [106]

$$k_{nf} = k_w(1 + 4.5503\varphi) \tag{2.16}$$

$$\mu_{nf} = \mu_w \, e^{\frac{4.91\varphi}{0.2092-\varphi}} \tag{2.17}$$

Azmi et al. model [107]

$$k_{nf} = k_w 0.8938 \left(1 + \frac{\varphi}{100}\right)^{1.37} \left(1 + \frac{T_{nf}}{70}\right)^{0.2777} \left(1 + \frac{d_p}{150}\right)^{-0.0336} \left(\frac{\alpha_p}{\alpha_w}\right)^{0.01737} \tag{2.18}$$

$$\mu_{nf} = \mu_w \left(1 + \frac{\varphi}{100}\right)^{11.3} \left(1 + \frac{T_{nf}}{70}\right)^{-0.038} \left(1 + \frac{d_p}{170}\right)^{-0.061} \tag{2.19}$$

Maxwell - Brinkman model [87, 108]

$$k_{nf} = k_w \frac{\left(k_s + 2k_w - 2\varphi(k_w - k_s)\right)}{\left(k_s + 2k_w + \varphi(k_w - k_s)\right)} \tag{2.20}$$

$$\mu_{nf} = \mu_w \frac{1}{(1-\varphi)^{0.25}} \tag{2.21}$$

where φ, k_{nf}, k_w, $\mu_{nf}, and\ \mu_w$ represent the volume concentration of nanoparticles, thermal conductivity of nanofluid, thermal conductivity of water, dynamic viscosity of nanofluid, and dynamic viscosity of the water.

It can be noted that the Prandtl number (Pr) is greatly influenced by nanofluid thermal conductivity and viscosity correlations. To evaluate these correlations, the Prandtl number (Pr) was used as a reference. Table 4.2 compares the calculated ratios of thermal conductivity, viscosity, and Prandtl number for different empirical correlations for Al_2O_3-water nanofluids (φ = 1.34% and 2.78%). The Pak and Cho model [102] values are used as a reference because they closely align with experimental values and exhibit the highest Prandtl number ratio, indicating a high heat transfer rate. For Al_2O_3 volume concentrations of 1.34% and 2.78%, the Prandtl number ratio increased by 46% to 110%, which corresponds to an overall improvement in convective heat transfer performance of 16% to 30%. In contrast, the Chen et al. model [104] shows a Prandtl number ratio ranging from 1.179 to 1.407, with an associated increase in the average heat transfer coefficient of approximately 5% to 10%. These differences highlight the significant impact that varying correlations can have on heat transfer results under the same operating conditions, affecting the accuracy of numerical predictions.

Conversely, the Maxwell-Brinkman model [87, 108] indicates a Pr ratio below 1, suggesting a reduction in heat transfer. However, this contradicts practical observations, as adding nanoparticles to the base fluid typically enhances the performance of heating or cooling systems [109, 110]. Additionally, the Azmi correlation [107], which accounts for nanoparticle diameter, temperature, and volume concentration, shows only a slight increment of less than 1% to 5% for volume concentrations of 1.34% to 2.78%.

Table 2. 1: Impact of different thermo-physical properties model correlations of Al_2O_3-water at 300K

Model	Volume concentration φ (%)	Thermal conductivity ratio k_{nf}/k_w	Viscosity ratio μ_{nf}/μ_w	Prandtl number ratio Pr_{nf}/Pr_w
Pak and Cho model [102]	1.34	1.1012	1.6245	1.459
	2.78	1.2153	2.6304	2.115
Maiga et al. model [103]	1.34	1.037	1.119	1.067
	2.78	1.079	1.297	1.175
Chen et al. model [104]	1.34	1.023	1.219	1.179
	2.78	1.047	1.508	1.407
Ho et al. model [105]	1.34	1.043	1.106	1.048
	2.78	1.097	1.308	1.165
Rea et al. model [106]	1.34	1.061	1.398	1.304
	2.78	1.126	2.122	1.841
Azmi et al. model [107]	1.34	1.067	1.135	1.012
	2.78	1.088	1.221	1.194
Maxwell - Brinkman model [87, 108]	1.34	1.038	1.003	0.955
	2.78	1.082	1.007	0.911

where φ, k_{nf}/k_w, μ_{nf}/μ_w and $\mathrm{Pr_{nf}}/Pr_w$ represent the volume concentration of nanoparticles, the ratio of thermal conductivity of nanofluid to the water, the ratio of dynamic viscosity of nanofluid to the water, and the ratio of Prandtl number of nanofluid to the water.

From Table 2.1 it is evident that the Prandtl number (Pr) ratio has a significant impact on heat transfer performance. The results indicate that different correlations produce different Pr ratios, which leads to more fluctuations in nanofluid thermo-physical properties that greatly impact the heat transfer coefficients. This suggests that there is no universal correlation in predicting the nanofluid properties accurately. Consequently, it is challenging for researchers to use or develop a

correlation that considers nanoparticle interactions such as operating conditions, particle diameter, Brownian motion, diffusion effects, etc. Therefore, this research considers the correlations proposed by the Pak and Cho [102] model.

2.2.1.2 Single and Multiphase studies

For modelling nanofluids numerically, the single- and two-phase models are used under forced convection heat transfer. The single-phase model considers the nanoparticle and base fluid to be single-phase, whereas the two-phase model treats them separately with different governing equations. The two-phase approach is characterised by two main models: Eulerian-Eulerian (VOF, Mixture, and Eulerian) and Eulerian-Lagrangian (Discrete Phase Model - DPM).

In the Eulerian-Eulerian model, the solid and liquid phases are numerically solved using the Eulerian approach. These include Mixture and Eulerian models, which are widely used and cited in various nanofluid studies. On the other hand, the volume of fluid (VOF) model was used mainly for immiscible flows where the interface of fluid phases is captured accordingly and was not suitable for nanofluid applications [111]. Therefore, studies related to VOF were avoided. On the contrary, the Eulerian-Lagrangian model solves the solid phase using a Lagrangian approach and the liquid phase using an Eulerian approach. The numerical results obtained from this model were accurate, close to experimental data, and computationally expensive [112, 113]. Therefore, studies related to Eulerian-Lagrangian model, such as the Discrete Phase model (DPM) were also excluded.

Due to the lower computational cost and complexity, the single-phase model (SPM) attracted a lot of researchers considering different conditions and applications. Studies using this model have investigated forced convection in laminar and turbulent flows, primarily focused on circular pipes [114], square cavities [115], wavy channels [116], macro and micro channels [117], flat surfaces [118], and corrugated double pipe [119], etc. These studies consistently found that the single-phase model effectively predicts heat transfer.

Akbari, et al. [39] numerically investigated single- and two-phase models using Al_2O_3-water and CuO-water nanofluids under turbulent forced convection in a horizontal tube with constant heat flux. They concluded that both models have the same hydrodynamic fields for Reynolds numbers

ranging from 11,300 to 17,670. However, single phase model was closer to the experimental data in terms of the thermal field. It was also pointed that the thermal predictions by two phase models were sensitive to nanoparticle volume concentration (φ=0.001 and 0.02). In a later study, Akbari, et al. [120] found that single phase model exhibited more precise results only at higher Reynolds numbers compared to two phase models using a counter flow double tube heat exchanger with TiO_2-water nanofluid. For instance, the heat transfer coefficient and Nusselt number were accurately predicted for a 0.2% volume concentration at Reynolds number greater than 8,000.

In a related study, Hussein, et al. [121] investigated heat transfer and friction factor using the single phase model in different straight tubes (circular, elliptical, and flat) with TiO_2-water nanofluid (φ = 1, 1.5, 2, and 2.5) in a turbulent regime (Re = 5000–20,000). Their results indicated that the friction factor and the heat transfer coefficient showed an average deviation between 4% and 6%, compared to the empirical data. Additionally, elliptical and flat tubes predicted the lowest friction factor. Similarly, Akhtari, et al. [122] found that the relative average error between single phase CFD predictions and experimental data was 15.6% and 11.2% for a shell and tube heat exchanger and a double pipe heat exchanger. Based on these studies, the single-phase model has proven to accurately predict heat transfer results.

In contrast, Akbari, et al. [39] conducted investigations into the limitations of single-phase models, emphasising oversimplification of the nanofluid behaviour and raising the issue of non-uniform particle dispersion and particle clustering, which were challenging to handle effectively in predicting heat transfer. Similarly, Amani, et al. [123] pointed out that this non-uniform particle distribution was caused by Brownian motion, shear-induced migration, viscosity gradient, and thermophoretic migration, which significantly affected the hydrodynamic flow and performance of heat transfer. Therefore, nanoparticle distribution inside the based fluid is critical, which has been disregarded or neglected in the single-phase method.

The mixture model is widely used in several studies [124, 125] to model the two phase behaviour of nanofluids in various heat exchanger applications. The two-phase mixture model was first implemented by Behzadmehr, et al. [42] to investigate the turbulent convective heat transfer using 1% Cu-water nanofluid through a circular tube (Re = 10,515 to 22,540). By comparing their numerical results (Nu) with the experimental data of Xuan and Li [126], they concluded that the

mixture model was more precise than the single phase model. Results showed that adding 1 vol.% of Cu to the water increased the Nusselt number by 15%, while it had no effect on skin friction and turbulent kinetic energy. The same theory was applied by Mirmasoumi and Behzadmehr [127]. They concluded that as volume concentration increased, the secondary flow was enhanced, resulting in a higher Nusselt number. They also observed that particle concentration was higher near the wall region and that nanoparticles tended to accumulate more at the bottom of the tube. In addition, increasing the particle diameter enhances the axial velocity and skin friction while reducing the secondary flow, temperature, and Nusselt number [128]. It was also noted that increasing the nanoparticle diameter does not alter the flow behaviour.

In another comparative study conducted by Hejazian and Moraveji [43], the single- and two-phase approaches were evaluated in a circular tube under a turbulent regime (Re = 4,800 to 30,500) with saturated steam on the wall. The accuracy of the single-phase and mixture models was compared against experimental data, revealing maximum deviations of 10.85% for the single-phase model and 9.36% for the mixture model at φ = 0.05 to 0.25%. Similarly, Lotfi, et al. [129] also concluded that the mixture model showed a good agreement in predicting heat transfer coefficients and wall temperature with empirical data, while the single-phase and Eulerian models underestimated the convective heat transfer using Al_2O_3-water nanofluid. In addition, various other studies performed by Moghadassi, et al. [130], Beg, et al. [131], and Hazeri-Mahmel, et al. [132] have also suggested that the mixture model was highly accurate in predicting heat transfer, particularly well-suited for applications involving nanofluids.

However, Al Mahmud, et al. [133] pointed out that while the mixture model was useful in some scenarios, it failed to capture the intricate interphase interactions and phase distribution observed in nanofluid flows. Similarly, Amani, et al. [123] highlighted another significant challenge with the mixture model: the reliance on a single set of velocity components in the mixture momentum equation, which leads to inaccurate predictions of the heat transfer coefficient. Additionally, both the mixture and single-phase models did not show any changes in the friction coefficient with varying concentrations, whereas the Eulerian model exhibited some degree of variation [134]. Furthermore, El-Batsh, et al. [135] suggested that a mixture model with temperature-dependent thermophysical properties does not accurately predict the heat transfer values. Based on these

studies, even though the mixture model can accurately predict heat transfer, there are still complications associated with it.

The Eulerian model has emerged as a superior choice compared to single-phase and mixture models in various studies. For example, Peng, et al. [40] investigated the hydrodynamic flow characteristics of TiO_2-water nanofluid (φ = 0.5–1.5%) using single, mixture, and Eulerian models inside a circular tube under turbulent conditions (Re = 6180–14,137). It was noted that the Eulerian-Eulerian approach offered superior predictions of heat transfer coefficients, with empirical deviations ranging from 1.36% to 4.87%, while the single-phase model exhibited a higher pressure drop compared to the two-phase models. Additionally, the study explored the importance of using different viscosity models. Similarly, Rezaei Gorjaei and Rahmani [136] demonstrated a more precise representation of nanofluid behaviour by considering particle interactions, non-uniform concentration profiles, and enhanced thermal properties, all of which are essential for accurate predictions in various nanofluid applications.

The difference between the mixture and the Eulerian model was numerically compared by Hejazian, et al. [137], using Al_2O_3-water nanofluid ($d_p = 40nm$) in a horizontal circular tube under forced convection with saturated steam on the wall. They found that the heat transfer coefficient with 2% volume concentration increased by 25% compared to the base fluid at Reynolds number Re = 4000. In addition, their results suggest that the mixture model was slightly more accurate than the Eulerian model in predicting the Nusselt number, with a maximum error of 9.91% compared to the experimental results. It was also reported that the pressure drop increased only slightly with increasing volume concentration. Furthermore, Vanaki, et al. [81] suggested that this model is particularly suitable for higher volume concentrations of nanoparticles and can also be used at lower nanoparticle concentrations. However, Behroyan, et al. [138] showed that the Eulerian model can accurately predict flow only at low concentrations, such as 0.5% Cu/water nanofluid in a tube.

Overall, the most significant advantage of the Eulerian model over single-phase homogeneous modelling is the elimination of the necessity of using appropriate thermophysical models for calculating nanofluid properties [139]. However, studies conducted by Beheshti, et al. [44] and

Lotfi, et al. [129] suggest that this assumption may not always provide precise results compared to the mixture model. Most of the researchers concluded that the two-phase model (TPM) offers a better prediction of convective heat transfer compared to the single-phase model (SPM) because it captures particle-particle interactions [140-142]. However, it is unclear which model is better among the researchers because of their conflicting results.

The importance of turbulent models such as RANS, LES, and DES in nanofluid numerical simulations has been highlighted by a few studies. This is because convective heat transfer results are strongly affected by different turbulent models in single- and two-phase flows. One such study by Beheshti, et al. [44] conducted a numerical investigation of Al_2O_3–water and TiO_2–water nanofluids flowing through a 2D rectangular channel using single- and two-phase models (mixture and Eulerian) with Realizable k–ε turbulence model (enhanced wall function). The study applied heated wall boundary conditions with Reynolds numbers ranging from 3500 to 11,500. They found that the maximum errors predicted by the Eulerian–Eulerian model were 9.94% for Al_2O_3-water and 10.61% for TiO_2-water nanofluids (at 1 and 1.5 vol.%), indicating its effectiveness. In another study related to the single phase model, Saha and Paul [84] investigated the circular tube and found that the Realizable k-ε model better captures the intricacies of heat transfer, including near-wall effects and boundary layer behaviour, by incorporating a more realistic and physically consistent representation of the turbulent kinetic energy dissipation rate compared to standard and Renormalisation Group (RNG) k-ε models. In contrast, Shynybayeva and Rojas-Solórzano [143] pointed out the limitations of k-ε models, particularly unfavourable pressure gradients and additional deformations that led to inaccurate results.

On the other hand, Sekrani, et al. [144] revealed that the SST k-ω model performed better compared to eight other turbulent models when using the single and two phase models in a uniformly heated tube with Al_2O_3–water nanofluid. It was also suggested that the SST k-omega model with low Re formulation offers higher accuracy for free shear flows, boundary layers, and separated flows. A similar study conducted by Isman [145], also showed that the SST k-ω model using a two phase approach was close to the experimental results in turbulent flows. Based on the above studies, RANS models such as the realizable k-ε model and the SST k-ω model appear

effective in predicting convective heat transfer in single- and two-phase flows. However, the effect of using different RANS turbulence models has not been widely explored in multiphase models.

Furthermore, this research excluded the advanced turbulent models such as Large Eddy Simulation (LES), Detached Eddy Simulation (DES), and Direct Numerical Simulation (DNS) due to the widespread use and reliability of RANS turbulent models. This exclusion is attributed to several factors, which are

(1) limited availability of literature on these advanced turbulent models with nanofluid applications.
(2) Increased complexity and computational demands of modelling two-phase approaches with these turbulent models.
(3) Significant resources are required for their implementation.

The RANS models are generally preferred because they provide a good balance between accuracy and computational efficiency. They are well-validated for a wide range of turbulent flows and supported by extensive empirical data. Additionally, RANS models can handle complex boundary conditions and large-scale simulations more feasibly. Consequently, studies involving LES, DES, and DNS were omitted.

2.2.2 Hybrid Nanofluids

From the previous section, it is clear that nanofluids, also known as mono nanofluids, have a significant impact on convective heat transfer performance. Mono nanofluids contain only a single type of nanoparticle, either metallic or non-metallic, suspended in the base fluid. The characteristics of mono nanofluids can be adjusted by altering the nanoparticle concentration, with higher concentrations generally indicating a higher heat transfer coefficient. However, higher nanoparticle concentrations tend to cause agglomeration or particle clustering, thereby limiting the potential benefits of the nanofluids. To address this issue, hybrid nanofluids have been developed in recent years. These hybrid nanofluids, which combine different types of

nanoparticles, aim to enhance the thermophysical properties and heat transfer characteristics of the base fluid, overcoming the limitations associated with mono nanofluids.

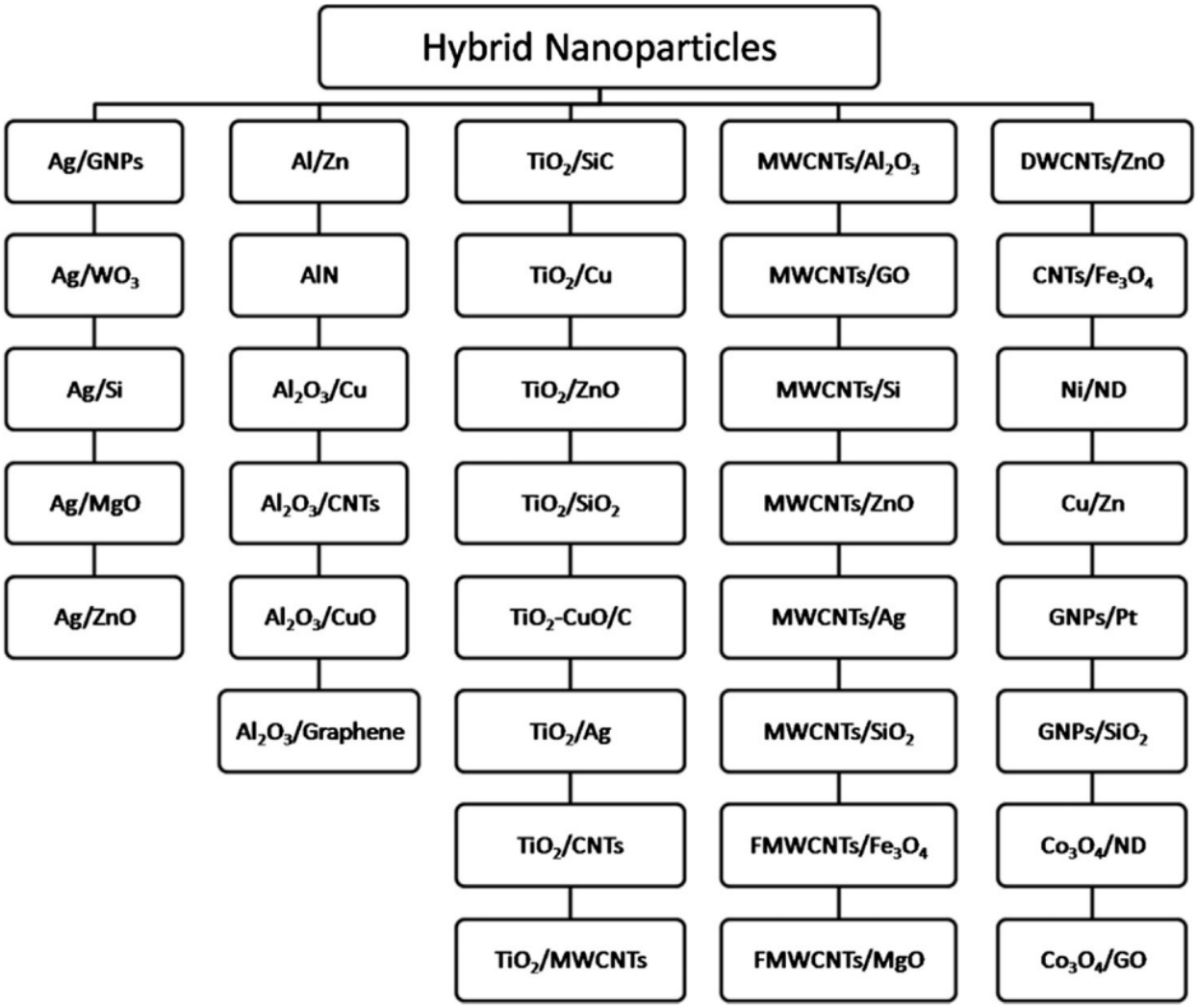

Figure 2. 7: Different hybrid nanoparticles used in experiments by various researchers [146]

Hybrid nanofluids represent an advanced category of nanofluids, combining two or more types of nanoparticles with the base fluid. These suspensions of multiple nanoparticles in the base fluid can be either in composite or mixture form, which are synthesised experimentally. Many studies conducted by various researchers indicated that the hybrid nanofluid replaces the mono nanofluids because it provides more heat transfer enhancement (advantage) along with the pressure drop or viscosity increment (trade-off) in different applications such as electro-mechanical, automotive, HVAC, manufacturing processes, and solar energy [147].

Hybrid nanofluids are a relatively new concept that has attracted greater attention lately. As a result, limited studies have been reported so far in various heat exchanger applications. Most of the research conducted focused on the experimental synthesis and preparation methods of hybrid nanofluids by varying the different combinations of nanoparticles. This research avoided studies related to experimental preparation techniques of hybrid nanofluids because the focus of this research is on the numerical simulations. In addition, studies on laminar flows were also disregarded because the main emphasis of this research is related to turbulent flows. Therefore, this section only covers the experimental studies on turbulent flows using various hybrid nanofluids, which impacted the heat transfer results.

Ramadhan, et al. [148] conducted both experimentally and numerically investigations into the thermal behaviour of TiO_2-SiO_2 dispersed in water and ethylene glycol under a constant heat flux in a cylindrical tube. Their results indicated that hybrid nanofluids exhibited higher heat transfer coefficients and friction factors compared to water. As the volume concentration increased from 1% to 3%, the Nusselt number also augmented across different Reynolds numbers (Re = 2900 to 11,200). The average deviation of the Nusselt number between experimental and numerical results was found to be 8.8%, 8.9%, and 7.9% for 1%, 2%, and 3 vol.% concentrations. Similarly, Nabil, et al. [149] investigated the thermal and hydrodynamic characteristics of TiO_2/SiO_2 nanoparticles dispersed in a 60:40 volume ratio of water and ethylene glycol mixture in a heat transfer circular tube under turbulent flow conditions. Their study revealed that the heat transfer coefficient increased by 29.4%, 33.2%, and 45.9% at volume concentrations of 1%, 2%, and 3%, respectively, compared to the base fluid. Additionally, the friction factor also improved with increasing volume concentration.

Several researchers have explored the impact of hybrid nanofluid properties on heat transfer. Zareie and Akbari [150] studied the flow and deformation characteristics (rheological behaviour) of MgO-MWCNT nanoparticles dispersed in an EG-water mixture at different volume concentrations (φ = 0.025–0.8%) and temperatures (25–60 °C). Their experimental results indicated that all hybrid nanofluid samples exhibited Newtonian behaviour. Additionally, the density, viscosity, and thermal conductivity increased with the rise in nanoparticle volume concentration. In a similar study conducted by Soltani and Akbari [151], the relative dynamic

viscosity of MgO/MWCNT-ethylene glycol hybrid nanofluid increased up to 168% from 0.1 to 1% nanoparticle volume concentration for temperatures ranging from 30 °C to 60 °C. This suggests a significant potential to improve the convective heat transfer as viscosity directly impacts the pressure drop.

Bellos and Tzivanidis [152] investigated the thermal behaviour of Al_2O_3/TiO2-oil hybrid nanofluid with a 1.5% nanoparticle concentration over a temperature range from 300 K to 600 K. They observed that, with increasing temperature, the density, thermal conductivity, and viscosity decreased, while the specific heat capacity increased. In contrast, a study conducted by Yarmand, et al. [153] pointed out that with the increment in temperature from 20 to 40 °C, the density decreased, but the thermal conductivity of the GNP/Ag-water hybrid nanofluid increased for a specific volume concentration range (0–0.1 vol.%). Based on the studies conducted by Bellos and Tzivanidis [152] and Yarmand, et al. [153], it was quite significant that the impact of temperature on base fluid altered the thermal properties (e.g., thermal conductivity) of hybrid nanofluid, affecting the heat transfer results.

The mixture ratio of hybrid nanoparticle composites is a crucial parameter in the preparation and modelling of hybrid nanofluids, as it directly impacts their thermal conductivity. Hamid, et al. [154] studied the heat transfer characteristics of TiO_2/SiO_2 nanoparticles at different mixture ratios (TiO_2: SiO_2= 20:80, 40:60, 50:50, 60:40, and 80:20) dispersed in water and ethylene glycol mixture in a heat tube (30 °C, 50 °C, and 70 °C) under turbulent regime. Their study found that the maximum heat transfer performance was obtained with a 40:60 mixture ratio at 70 °C with an enhancement of 35.32% for a constant volume concentration of 1%. Conversely, the lowest Nusselt number and friction factor were observed with a 50:50 mixture ratio at 30 °C. The study concluded by suggesting that 20:80 and 40:60 mixture ratios were effective in obtaining better PEC values using TiO_2/SiO_2 hybrid nanofluids.

In a similar study conducted by Wanatasanappan, et al. [155], the highest thermal conductivity of Al_2O_3/CuO- water/EG hybrid nanofluid was obtained for a 60:40 mixture ratio with an enhancement of 12.33% compared to the based fluid. This indicates that the heat transfer coefficient exhibited an increment in the thermal performance. Furthermore, they revealed that the 50:50 mixture of Al_2O_3-CuO hybrid sample has moderate dispersion stability. It is important to

note that these experimental tests were conducted with different nanoparticle sizes due to the high cost and experimental complexity. This can also affect the results, as the preparation of hybrid nanocomposites may introduce uncertainties in the experimental values. Therefore, it can be summarised that the influence of hybrid nanofluid on heat transfer had the potential to obtain higher heat transfer rates compared to the convection base fluids.

Several numerical studies have explored Al_2O_3-based and other hybrid nanofluids using both single-phase and multiphase models, though research in turbulent flow conditions remains limited. Tekir, et al. [156] conducted a numerical study to investigate the forced convection inside a square duct with Al_2O_3/Cu-water hybrid nanofluid (φ = 0–2%) under a constant heat flux in a turbulent regime (Re = 10,000 to 100,000) using a single-phase model. Their results showed a heat transfer coefficient increment of up to 53% at 2% volume concentration compared to water. It was also pointed out that an increase in nanoparticle volume concentration does not influence the friction factor.

Similarly, Zhang, et al. [112] conducted a numerical and experimental study to investigate heat transfer and flow performance of Al_2O_3/CuO-water (φ = 1–3%) in a circular tube under a turbulent regime using different multiphase models (mixture, Eulerian, DPM). It was found that the average Nusselt number was increased by 35% with a significant rise in pressure drop of 12% compared to the water. This translated to a thermal performance factor ranging from 1.01 to 1.29 for Reynolds numbers between 18,000 and 64,000. Moreover, the Eulerian model predicted values closer to experimental values with an 8.1% deviation compared to mixture (10.2%) and DPM (12.5%).

Takabi and Shokouhmand [38] studied the hydrodynamic and heat transfer performance of Al_2O_3-water nanofluid and Al_2O_3/Cu-water hybrid nanofluid through a uniform heat tube under a forced convection turbulent flow numerically using single-phase model. The volume concentration of nanoparticles was varied from 0 to 2% for a wide range of Reynolds numbers (Re = 10,000 to 100,000). Results revealed that the hybrid nanofluid has superior heat transfer results compared to the mono nanofluid. For instance, the average increment in heat transfer coefficient for Al_2O_3/Cu-water and Al_2O_3-water at Re = 20,000 was 32.07% and 13.6%, respectively, at 1% volume concentration compared to water. However, the impact of the friction factor seems to be significant and reasonable because Al_2O_3/cu-water has an increment of 13.76%, and Al_2O_3-water

has an increment of 10.45%. This shows that even though the friction coefficient is higher for hybrid nanofluid by a small margin, it clearly produced better heat transfer results.

Similarly, Wong and Tiong [157] conducted a numerical study to investigate the thermal performance factor of Al_2O_3/Cu-water nanofluid (φ =0.001 to 0.02) by comparing circular, rectangular, and square ducts for Reynolds numbers ranging from 10,000 to 100,000 under a constant heat flux condition. Using a single-phase model (SPM), they found that the average increase in convective heat transfer was 58.6%, while the pressure drop rose significantly, by 4.79 times compared to water at Re = 10,000 (φ = 2%). This rapid pressure increase was attributed to the rise in viscosity, which was influenced by the thermo-physical property correlations used. The study emphasised the importance of considering the geometrical parameters of the tube, such as diameter and length, along with accurate empirical data or correlations for fluid properties, as avoiding these factors can result in higher energy consumption or pumping costs.

Bhattad, et al. [158] conducted a numerical study to examine the pressure drop and heat transfer characteristics of Al_2O_3/MWCNT-water hybrid nanofluid (φ = 0.01–0.03%) at different operating temperatures (15 to 30 °C) in a counter flow plate heat exchanger. Their results indicated that the single-phase homogenous model was less accurate than the discrete phase model (DPM). It was found that Al_2O_3/MWCNT-water hybrid nanofluid exhibited higher heat transfer performance compared to Al_2O_3-water nanofluid.

From the open literature, there are very limited multiphase studies conducted in hybrid nanofluids. Hence, mono-nanofluids were used as a reference using the Prandtl numbers to compare the hybrid nanofluids.

2.2.2.1 Thermo-physical properties overview

To quantify the thermal and hydraulic performance of the system, the determination of fluid thermophysical properties such as viscosity, density, thermal conductivity, specific heat, etc. is extremely important. This is because they control the stability, heat transfer performance, and pumping power of the fluid. This section covers a few thermal property correlations using hybrid nanofluids.

Table 2. 2: Different correlations to calculate the thermal properties of different hybrid nanofluids

Nanofluid	Range	Correlations
Al_2O_3-Cu (50–50)/EG [159]	$0.125 \leq \varphi \leq 2\%$ $25 \leq T \leq 50°C$	$\frac{K_{nf}}{K_{bf}} = \frac{(9.6128 + \varphi)}{9.3885 - 0.00010759T^2} - \frac{0.0041099}{\varphi}$
ZnO-TiO2/EG [160]	$25 \leq T \leq 50°C$ $0.1 \leq \varphi \leq 3.5\%$	$\frac{K_{nf}}{K_{bf}} = 1 + 0.004503\varphi^{0.8717}T^{0.7972}$
SiO2-TiO2(60:40)/water and EG (60:40) [161]	$0 \leq \varphi \leq 3\%$ $30 \leq T \leq 70°C$	$K_r = \frac{K_{nf}}{K_{bf}} = \left(1 + \frac{\varphi}{100}\right)^{5.25}\left(1 + \frac{T}{70}\right)^{0.076}$
SiO2-TiO2/water and EG (60:40) [162]	$20:80 \leq VR \leq 80:20$ $30 \leq T \leq 80°C$	$K_{eff} = \frac{K_{nf}}{K_{bf}} = 1.17(1 + R)^{-0.1151}\left(\frac{T}{80}\right)^{0.0437}$
ZnO-Ag/water [163]	$0.125 \leq \varphi \leq 2\%$ $25 \leq T \leq 50°C$	$\frac{K_{nf}}{K_{bf}} = 1 + 0.0008794\varphi^{0.5899}T^{1.345}$
TiO2-CuO-C/EG [164]	$0.5 \leq \varphi \leq 2\%$	$\frac{K_{nf}}{K_{bf}} = 1 + 6.2299\left(\frac{\varphi}{100}\right)^{0.9371}\left(\frac{T}{333}\right)^{10.2685}$

MgO-MWCNTs/EG [165]	$0.05 \leq \varphi \leq 0.6\%$ $25 \leq T \leq 50°C$	$\frac{K_{nf}}{K_{bf}} = 0.9787 + exp(0.3081\varphi^{0.3097} - 0.002T)$
MgO-MWCNT/EG [151]	$0 \leq \varphi \leq 1\%$ $30 \leq T \leq 60°C$	$\frac{\mu_{hnf}}{\mu_{bf}} = [0.191\varphi + 0.240(T^{-0.342}\varphi^{-0.473})]$ $\exp[1.45T^{0.120}\varphi^{0.158}]$
Ag–MgO/water [166]	$0 \leq \varphi \leq 2\%$	$\mu_{nf} = (1 + 32.795\varphi_p - 7214\varphi_p^2 + 714600\varphi_p^3 - 0.1941 \times 10^8\varphi_p^4)\mu_f$
TiO2-SiO2/water-EG [167]	$0.5 \leq \varphi \leq 3\%$ $30 \leq T \leq 70°C$	$\frac{\mu_{nf}}{\mu_{bf}} = 37\left(0.1 + \frac{\varphi}{100}\right)^{1.59}\left(0.1 + \frac{T}{80}\right)^{0.31}$
SiO2-TiO2/water and EG (R=mixture ratio 20:80) [162]	$20{:}80 \leq VR \leq 80{:}20$ $30 \leq T \leq 80°C$	$\frac{\mu_{nf}}{\mu_{bf}} = 1.42 + (1 + R)^{-0.1063}\left(\frac{T}{80}\right)^{0.2321}$
SiO2-graphite/water [168]	$0.1 \leq \varphi \leq 2\%$ $15 \leq T \leq 60°C$	$\frac{\mu_{nf}}{\mu_{bf}} = 1.00527 \times (T^{0.00035}) \times (1 + \varphi)^{9.36265} \times \left(\frac{w_G}{w_{SiO_2}}\right)^{-0.028935}$
SiO2-CuO/C-G/EG [169]	$0.05 \leq \varphi \leq 1\%$ $50 \leq T \leq 80°C$	$\frac{\mu_{nf}}{\mu_{bf}} = 0.9894\left[1 + \frac{\varphi}{100}\right]^{6.6301} \times \left[\frac{T_{nf}}{T_o}\right]^{0.064}$

where φ, T, K_{nf}, K_{bf}, μ_{nf} and μ_{bf} are the volume concentration, temperature, thermal conductivity of the nanofluid, thermal conductivity of the base fluid, viscosity of the nanofluid, and viscosity of the base fluid.

Based on the empirical thermal conductivity and viscosity correlations as mentioned in Table 2.2, most of the equations solely rely on temperature and nanoparticle volume concentration. However, the other fluid parameters shape, size range, etc., are excluded due to the complexity of measuring experimental values. Empirical data of hybrid nanofluids is essential for validating this numerical research, thereby enhancing the reliability of the results. As previously discussed, this research is directed towards Al_2O_3-based nanofluids. Due to the limited literature available on empirical correlations or data related to Al_2O_3 based hybrid nanofluids in turbulent flows, studies on other nanofluids were also reviewed.

Suresh, et al. [170] experimentally investigated the convective heat transfer and pressure drop characteristics of an Al_2O_3/Cu-water hybrid nanofluid using a heated circular tube. The Al_2O_3-Cu composite nano powder is dispersed in water, forming a stable hybrid nanofluid with a 0.1% volume concentration. Results show the average enhancement in heat transfer and friction factor was 8.02% and 10.48% at 0.1 vol.%, which was greater than that of pure water in a fully developed turbulent regime (Re = 2300 to 13000). In addition, it was pointed out that the experimental friction factor is higher than the numerical one. They also proposed correlations for calculating the Nusselt number and friction factor, which agreed well with the empirical data.

$$\mathrm{Nu} = 0.000264(\mathrm{Re}\ \mathrm{Pr})^{1.166}(1+\varphi)^{77.56} \tag{2.24}$$

$$\mathrm{f} = 0.366(\mathrm{Re})^{-0.26}(1+\varphi)^{129.58} \tag{2.25}$$

The average correlation deviations from the experimental data for the Nusselt number were ±5%, and the friction factor was around ±8%, respectively. These above equations are valid for a 0.1% volume concentration of Al_2O_3/Cu-water hybrid nanofluid for Reynolds numbers ranging from 2300 to 13000.

Similarly, Sundar, et al. [171] conducted an experimental study to investigate heat transfer and flow performance of MWCNT/Fe_3O_4-water hybrid nanofluid (φ =0.1 to 0.3%) in a uniformly heated tube under a turbulent regime. The results reveal a maximum improvement of 31.1% in the Nusselt number along with an increase in pumping power of 18% for 0.3 vol.% compared to the base fluid at Re = 22,000. In addition, the empirical correlations were also proposed to calculate the Nusselt number and the friction factor.

$$\mathrm{Nu} = 0.0215\ \mathrm{Re}^{0.8}\ Pr^{0.5}(1+\varphi)^{0.78} \tag{2.26}$$

$$f = 0.3108\ \mathrm{Re}^{-0.245}\ (1+\varphi)^{0.42} \tag{2.27}$$

The above equations are valid for 3.72 < Pr < 6.37, 0 < φ < 0.6% and 3000 < Re < 22000.

Another experimental investigation of graphene nanoplatelets (GNP/Ag-water hybrid nanofluid) using a heated circular tube in a fully developed turbulent regime was conducted by Yarmand, et al. [153]. The results provided a significant enhancement in convective heat transfer due to the improvement in the fluid's thermal conductivity by 22.22% and viscosity by 30% in comparison to the base fluid. This enhancement of heat transfer efficiency was a function of the volume concentration of nanoparticles (0.1%) and temperature for a specific volume concentration at Re = 17,500. In addition, empirical correlations were suggested to predict the Nusselt number and friction factor.

$$\mathrm{Nu} = 0.0017066\ \mathrm{Re}^{0.9253}\ P^{1.29001} \tag{2.28}$$

$$\mathrm{f} = 0.567322\ Re^{-0.285869}\ \varphi^{0.0271605} \tag{2.29}$$

The above equations are valid for 0 < φ < 0.1% and 5000 < Re < 17,500.

Over many years, nanofluids and hybrid nanofluids have covered a wide range of practical applications for improving the efficiency of thermal systems. Some examples are covered below.

- Heat Exchangers: To improve energy efficiency and thermal performance [172].
- Cooling of Electronics: To enhance heat dissipation in high-performance electronics (CPU's and GPU's) [173].
- Solar Water Heating: To increase the thermal efficiency of solar water heaters (converting solar energy into usable heat) [174].
- Nuclear Reactor Cooling: To enhance cooling processes and improve safety margins [175].
- Domestic Refrigerators: To improve heat transfer rates in the refrigeration cycle [176].
- Engine Cooling or Vehicle Thermal Management: To improve cooling performance and fuel efficiency in automotive engines [177].
- Cooling and Heating in Buildings: To increase efficiency in HVAC systems for residential and commercial buildings to reduce energy consumption and cost [178].
- Cooling of Diesel Electric Generators: To ensure efficient operation and longevity of generators [179].
- Diesel Combustion: To improve combustion efficiency and reduce emissions [180].
- Biomedical Applications: Used in drug delivery, cancer treatment, and medical imaging [181].
- Fuel Cells: To enhance the efficiency and performance of fuel cells in the overall energy conversion process [182].
- New Sensors for Improving Exploration: To improve the accuracy and efficiency of exploration sensors [81].
- Boiler Flue Gas Temperature Reduction: To reduce the temperature of boiler flue gases for efficiency [140].

Hence, nanofluids and hybrid nanofluids have a lot of scope for improving future thermal related technologies.

2.3 Geometrical and Fluid effects on heat transfer

2.3.1 Grooves and Nanofluids

The combination of grooves and nanofluids in forced convection can be a feasible technique to improve convective heat transfer efficiency. For instance, Salman [46] numerically investigated the thermal characteristics of different nanofluids of SiO_2, Al_2O_3, ZnO and CuO (1%-4%) using triangular, trapezoidal, and rectangular ribs on a heated circular tube under turbulent flows (Re = 10,000–30,000). The results indicated that SiO_2 nanoparticles (30 nm) combined with triangular grooves exhibited the highest heat transfer coefficient, up to a 66% increment, compared to the smooth tube without corrugation using water at Re = 30,000. This was due to the increase in friction coefficient and pressure drop. In addition, the maximum thermal performance factor was achieved at a Reynolds number of 10,000. In a related study conducted by Vatani and Mohammed [183] to investigate the heat transfer behaviour in channels using different groove shapes (arc, square, and triangular) with Al_2O_3, ZnO, CuO, and SiO2-water based nanofluids. The constant heat flux boundary condition was implemented with Reynolds numbers ranging from 30,000 to 50,000. Results indicated that the rectangular groove combination with SiO_2-water (φ = 4%) exhibited the maximum performance evaluation criterion (PEC). This signifies the maximum increment in Nusselt number with negligible increase in friction coefficient.

The groove-nanofluid variations also impacted various applications of heating and cooling systems. Akbari, et al. [184] numerically investigated the forced convection heat transfer in a microchannel with a semi-attached rectangular groove using a CuO-water nanofluid (φ = 0-4%) under a turbulent regime (Re = 10,000 to 60,000). They concluded that the impact of a higher tooth ratio (R/W) was significant in improving convective heat transfer. This indicates that lower groove width values produced stronger vortices that caused better turbulence and improved the Nusselt number. They also suggested a reasonable tooth ratio ($0<R/W \leq 0.325$) for predicting efficient pressure drop conditions while maximising the PEC. In contrast, a numerical study conducted by Gravndyan, et al. [185] pointed out that the pressure drop or friction factor was completely independent of the groove aspect ratio of pitch (p/d), and was solely dependent on nanoparticle

volume concentration of TiO_2-water nanofluid in a laminar flow condition. However, the studies reviewed have proven the impact of aspect ratio on heat transfer and pressure drop in turbulent flows. In another study, Khoshvaght-Aliabadi, et al. [186] investigated the hydrothermal performance for a specific aspect ratio (waviness AR=0.1mm and w=0.3mm) of the wavy heat sink with the addition of rectangular grooves using Al_2O_3-water nanofluid. Their results showed that pressure drop, and heat transfer coefficient were 1.85 and 1.28 times higher than the smooth heat sink with water. This led to an enhancement in thermal performance factor ranging from 0.93 to 1.75.

2.3.2 Grooves and Hybrid Nanofluids

The impact of hybrid nanofluids combined with surface corrugation on convection has been investigated in a few studies. However, the use of hybrid nanofluids in simple grooved tubes remains limited. This section explores various passive techniques to enhance heat transfer.

According to Syam Sundar, et al. [187], the hydrothermal characteristics of a CNT/Fe_3O_4-water hybrid nanofluid with a combination of twisted tape inserts inside a tube were investigated experimentally. The constant heat flux boundary condition was implanted under a turbulent flow. The results indicated that the addition of a hybrid nanofluid to a straight tube increased the Nusselt number by 31.1% with a pumping power penalty of 1.18 times the base fluid at a 0.3% volume concentration. These empirical results are similar to those of MWCNT/Fe_3O_4-water (0.3 vol.%) conducted by Sundar, et al. [171]. This implies that the thermo-fluid performance of CNT/Fe_3O_4-water and the results of MWCNT/Fe_3O_4-water at 0.3% volume concentration were almost identical. Additionally, due to the insertion of twisted tapes (e/d = 5), the Nusselt number was further increased to 42.51% at a Reynolds number of 22,000, respectively. They also proposed a correlation for predicting the Nusselt number and friction factor for a specific range of values, as mentioned below.

$$\mathrm{Nu} = 0.0223\ \mathrm{Re}^{0.8}\ Pr^{0.5}\ (1+\varphi)^{0.58}(1+e/d)^{0.036} \tag{2.28}$$

$$f = 0.31\,\mathrm{Re}^{-0.245}\,(1+\varphi)^{0.473}(1+e/d)^{0.013} \quad (2.29)$$

These equations are valid for Reynolds number Re= 3000 to 22,000, volume concentration φ = 0 to 3% and groove depth ratio e/d = 0 to 15 respectively.

In another experimental study, the effect of Al_2O_3/Cu-water with V-cut twisted tape inserts in a heated straight tube was studied by investigating the pressure drop and heat transfer characteristics by Arunachalam and Edwin [188]. They found that the heat transfer coefficient increased from 2.5% to 20.8% for 0.1 to 0.4% volume concentrations using a straight tube with Al_2O_3-water nanofluid. With tape inserts, the heat transfer was further enhanced by 13.6% to 35.9% in a turbulent flow. Furthermore, with the addition of a hybrid nanofluid (0.01% Cu + 0.4% Al_2O_3) to V-cut inserts, the maximum Nusselt number was observed to be 42% higher than the plain tube with water. Similarly, Togun, et al. [189] numerically investigated the thermal efficiency of Al_2O_3/Cu-water (φ = 0.33 to 2%) hybrid nanofluid flowing in a 2D channel with semi-circular grooves for the Reynolds number ranging between 10,000 and 25,000. Results revealed a pressure coefficient increased with an increase in Reynolds number and nanoparticle volume concentration, which enhanced the Nusselt number. In addition, the recirculation's near the groove edges also significantly impacted velocity and temperature profiles.

Based on the above studies, it can be summarised that the impact of combining the nanofluid or hybrid nanofluid with groove insertions had a significant impact on the convective heat transfer performance.

2.4 Research Gaps

From the review of geometrical and fluid effects on heat transfer discussed in the previous section, the research gaps in this study are outlined as follows:

- Different groove geometries (rectangular, circular, triangular, and trapezoidal) have not been extensively studied to improve thermal performance, and the potential of hybrid grooves (combinations of multiple groove shapes) remains unexplored. This study aims to address this gap to further enhance convective heat transfer through hybrid grooves.

- Many studies have identified that grooves significantly increase pressure drop and pumping power, negatively affecting thermal performance (PEC). Despite attempts to optimise parameters such as depth, width, and pitch ratio, these challenges persist. This research introduces novel groove designs intended at mitigating these negative effects while enhancing heat transfer performance.

- There are mixed results in the literature regarding the use of single- and two-phase models (SPM & TPM) for nanofluids and hybrid nanofluids in turbulent flows. The choice of turbulent model significantly impacts the accuracy of numerical results. This study aims to assess the accuracy and reliability of combining SPM and TPM with two RANS turbulent models (Realizable k-ε and SST k-ω), investigating their sensitivity and compatibility to improve the accuracy of multiphase models.

- Despite significant advancements in the study of nanofluids, there are limited numerical studies conducted on Al_2O_3-based hybrid nanofluids and their impact on overall convective heat transfer performance. This is because of the limited availability of experimental data on hybrid nanofluids. In addition, balancing the trade-off between the heat transfer enhancement and pressure drop for different mixture ratios and different hybrid nanoparticles has not been fully explored.

2.5 Research Methodology

Figure 2. 8 illustrates the research methodology developed to address the research gaps identified in this PhD. The numerical approach is systematically divided into three phases. Phase 1 focuses

on analysing the geometrical effects, beginning with the validation of circular grooves and exploring different mono-groove shapes. The purpose is to identify the groove shape that offers the lowest pressure drop while maximising heat transfer, or PEC, which then serves as the basis for hybrid groove combinations. This strategic investigation of these hybrid grooves aims to manipulate flow behaviour for enhanced heat transfer. Their effectiveness is compared to mono-grooves, and optimisation strategies are implemented to reduce pressure drop or pumping power, thereby improving the overall efficiency of the single tube heat exchanger.

In Phase 2, the research shifts to fluid effects, starting with the validation of Al_2O_3-water nanofluid. The accuracy of nanofluid numerical models, including Single-Phase Model (SPM) and Two-Phase Model (TPM), using different turbulence models (Realizable k-ε and SST k-ω) is evaluated and compared against experimental data. The validated models are then used to investigate hybrid nanofluids, assessing their thermal and hydrodynamic behaviour in a smooth tube, ultimately identifying the optimal hybrid nanofluid combination.

Finally, Phase 3 integrates the optimal groove and hybrid nanofluid combinations to achieve maximum heat transfer efficiency.

2.6 Summary

This chapter reviewed studies on grooves, nanofluids, and hybrid nanofluids, focusing on their impact on convective heat transfer in turbulent flows. It highlighted the extensive research conducted on surface corrugation and its potential to improve convection. Similarly, fluid effects were also reviewed, showing the ability of nanofluids and hybrid nanofluids despite needing more empirical data for calculating the Nusselt number and friction factor. In addition, critical research gaps were identified, particularly in optimising groove geometries and improving multiphase model accuracy. Finally, this research aims to enhance convective heat transfer and reduce pumping power to improve overall thermal efficiency (PEC).

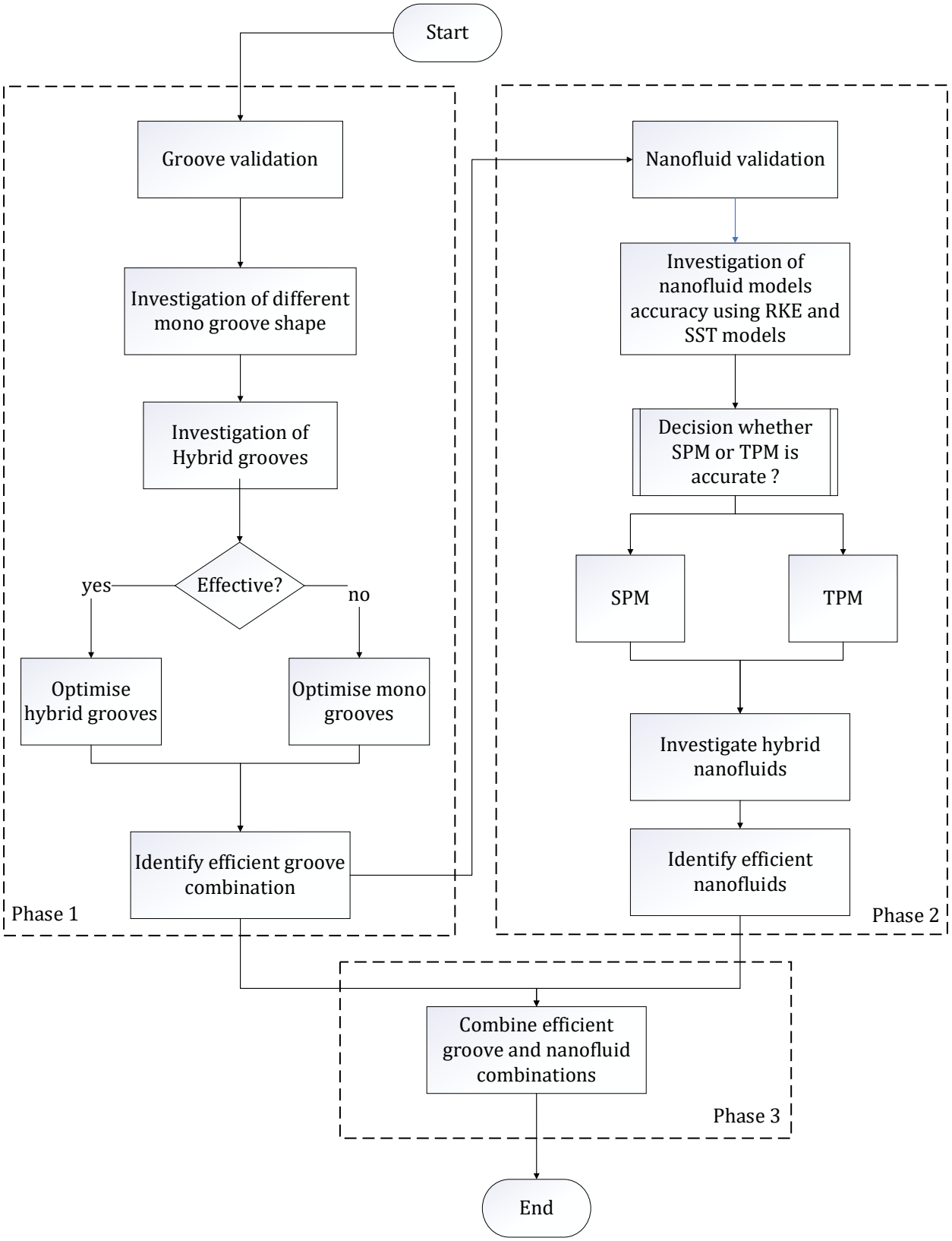

Figure 2. 8: Flowchart of the Numerical Simulation Approach in the Present Study

Chapter 3: Numerical Modelling

Computational Fluid Dynamics (CFD) is the natural choice for fluid flow analysis due to its robust capability for solving complex flow problems. CFD involves the use of numerical methods and algorithms to analyse and solve problems involving fluid flows. This research is directed towards forced convection fluid flows within a cylindrical pipe subjected to constant wall heat flux under a turbulent regime, with nanofluids used as the working fluid. The Finite Volume Method (FVM) is employed to effectively model these flows, which is widely recognised for its accuracy and efficiency in handling complex geometries and boundary conditions. This method discretizes the fluid domain into control volumes, ensuring the conservation of mass, momentum, and energy within each volume, making it ideal for CFD simulations in this research.

Given the nature of turbulent flows in this study, Reynolds-Averaged Navier-Stokes (RANS) turbulent models, specifically the Realizable k-ε model and the Shear Stress Transport (SST) k-ω model, are utilized, which are well-suited for high Reynolds number flows. For modelling nanofluids and hybrid nanofluids, both single-phase and multiphase approaches (Eulerian-Eulerian and Eulerian-Mixture models) are employed to capture the complex interactions between nanoparticles and the base fluid. This chapter comprehensively covers the numerical methods used, detailing the governing equations for mass, momentum, and energy. The simulations are conducted using ANSYS Fluent 2023 software [190]. The chapter includes the thermophysical properties of nanoparticles and base fluids, providing the necessary correlations. Relevant heat transfer formulas used in the calculations are also mentioned, ensuring a thorough understanding of the numerical modelling approaches adopted in this research.

3.1 Governing equations

The thermal and fluid dynamic behaviour of the nanofluid and hybrid nanofluids were examined using the single-phase and multiphase models.

3.1.1 Single Phase Model (SPM)

The single-phase model treats the nanofluid as a homogenous mixture which assumes the nanoparticles are uniformly distributed within the base fluid. This means that the base fluid and nanoparticles have the same velocity field and temperature with negligible slip between them. Any interphase forces and momentum exchange between solid and fluid are neglected, thereby simplifying the calculations [191]. This simplification allows the model to use averaged properties for thermal conductivity, viscosity, specific heat, and density, making the model less complex and time effective. Therefore, Navier-Stokes equations of mass, momentum and energy are solved for a Newtonian fluid with effective nanofluid properties (a function of temperature and volume concentration) [134].

These effective fluid thermal properties are constant in this homogeneous model and are obtained from the empirical correlations or data. It is extremely important to use appropriate empirical correlations as they directly affect the heat transfer results as discussed in Section 2.2.1.

The assumptions of the single-phase model are as follows: [111, 124]

- The physical properties of the nanofluid (e.g., density, viscosity, thermal conductivity) are assumed to be constant.
- The model assumes that the addition of nanoparticles alters the base fluid's properties predictably, without considering nanoparticle interactions.
- The nanofluid is treated as a continuum fluid, neglecting the discrete nature of nanoparticles.

The limitations of the single-phase model are as follows: [39, 111]

- High nanoparticle concentration makes the homogeneous mixture assumption less valid, leading to agglomeration and sedimentation.

- The model neglects particle interactions, neglecting effects such as changes in effective viscosity or nanoparticle clustering.

The steady-state differential equations are written as follows [81]:

Continuity equation:

$$\nabla.\left(\rho_{nf}\vec{v}\right) = 0 \tag{3.1}$$

where ∇ is the divergence operator, representing the net flow out of a small control volume, ρ_{nf} is the density of the nanofluid, and $\vec{v}$ is the velocity vector of the nanofluid.

Momentum equation:

$$\nabla.\left(\rho_{nf}\vec{v}\,\vec{v}\right) = -\nabla P + \nabla.\left(\mu_{\mathrm{nf}}\nabla\vec{v}\right) \tag{3.2}$$

where $\rho_{nf}\vec{v}\,\vec{v}$ represents the momentum flux (transport of momentum by the flow), ∇P is the pressure gradient force, which drives the fluid flow, μ_{nf} is the dynamic viscosity of the nanofluid, and $\nabla.\left(\mu_{\mathrm{nf}}\nabla\vec{v}\right)$ is the viscous term, representing the diffusion of momentum due to viscosity.

Energy equation:

$$\nabla.\left(\rho_{nf}\vec{v}\,C_pT\right) = \nabla.\left(K_{nf}\nabla.T\right) \tag{3.3}$$

from the above equation, $\rho_{nf}\vec{v}\,C_pT$ represents the convective heat transport, where C_p and T are the specific heat capacity and temperature of the nanofluid. In addition, $\nabla.\left(K_{nf}\nabla.T\right)$ represents the heat conduction term, representing heat diffusion within the fluid, where K_{nf} is the thermal conductivity of the nanofluid.

3.1.2 Multiphase Models

Many researchers have explored the Eulerian-Eulerian and Eulerian-mixture models for modelling the multiphase behaviour of various nanofluids. This is because these models capture the intricate dynamics between the nanoparticles and the base fluid, which significantly affects the thermal performance factor. The following section discusses the governing equations, and the assumptions associated with them.

3.1.2.1 Mixture Model

The mixture model is a simplified multiphase model because it considers the combination of continuous (fluid) and dispersed (solid) particles to be a single fluid mixture. This makes it computationally more efficient. The particles in this model closely follow the flow due to the strong coupling between the dispersed and continuous phases. In this model, only one set of velocity quantities are solved for mixture momentum conservation equation. The secondary phase's velocity is extracted from the algebraic formulations. It is also assumed that all phases are interpenetrating with each other. Each phase has a separate velocity vector field, which is represented by its own volume concentration. The primary and secondary phases each have a volume fraction. The primary phase influences the secondary phase through turbulence and drag, and the primary phase is affected by the secondary phase's turbulence and mean momentum loss.

The assumptions of the mixture model are as follows: [111, 125]

- The model treats both the base fluid and nanoparticles as continuous phases with their own properties, sharing a common velocity field.
- There is no relative velocity between the solid and fluid phases, indicating the nanoparticles move with the same velocity as the fluid.
- The volume fraction of nanoparticles in the nanofluid is assumed to be constant during flow, with no sedimentation or dispersion changes.

- The flow is assumed to be homogeneous at the macroscopic level, with the mixture behaving as a single-phase fluid.

- Nanofluid properties, like thermal conductivity and viscosity, are considered effective properties dependent on nanoparticle volume fraction.

- The model includes interphase momentum transfer, considering drag forces between the nanoparticles and the base fluid.

The limitations of the mixture model are as follows: [111, 125]

- The model neglects interactions between nanoparticles, which can influence nanofluid behaviour, especially at higher concentrations.

- Agglomeration or clustering of nanoparticles is not accounted for, assuming perfect dispersion.

- The model simplifies the interphase drag force calculations, which may not fully capture complex interactions.

- The effects of Brownian motion on nanoparticle dispersion and stability are not considered.

The mixture model applies to a wide variety of particle sizes, velocity differences, and density ratios, but it is most effective for small particles. The mixture model governing equations are expressed similarly to the single-phase homogenous model [24].

Continuity equation:

$$\nabla . (\rho_m \overrightarrow{v_m}) = 0 \tag{3.4}$$

Where, ρ_m and $\overrightarrow{v_m}$ are the mass averaged density and velocity of the nanofluid's mixture.

Momentum equation:

$$\nabla.(\rho_m \overrightarrow{v_m}\,\overrightarrow{v_m}) = -\nabla P + \nabla.(\mu_m \nabla \overrightarrow{v_m}) + \nabla.\left(\sum_{k=1}^{n} \varphi_k \rho_k \overrightarrow{v_{dr,k}}\,\overrightarrow{v_{dr,k}}\right) \tag{3.5}$$

where ∇P and μ_m are the pressure and dynamic viscosity of the mixture. In addition, $\nabla.\left(\sum_{k=1}^{n} \varphi_k \rho_k \overrightarrow{v_{dr,k}}\,\overrightarrow{v_{dr,k}}\right)$ represents the drift term, where φ_k, ρ_k, and $v_{dr,k}$ are the volume fraction, density, and drift velocity of phase k in the mixture. Also, n is the total number of phases in the mixture.

Energy equation:

$$\nabla.\sum_{k=1}^{n}(\varphi_k \overrightarrow{v_k}(\rho_k H_k + P_m)) = \nabla.(K\nabla \mathrm{T}) \tag{3.6}$$

where, φ_k, H_k represent volume concentration and enthalpy of the k phase and P_m and K are pressure and thermal conductivity of the mixture.

and the volume fraction equation can be written as

$$\nabla.\left(\varphi_p \rho_p \overrightarrow{v_m}\right) = \nabla.\left(\varphi_p \rho_p \overrightarrow{v_{dr,p}}\right) \tag{3.7}$$

where, mixture velocity ($\overrightarrow{v_m}$), mixture density (ρ_m), mixture dynamic viscosity (μ_m) and enthalpy of phase k (H_k) are expressed as

$$\vec{V}_m = \frac{\sum_{k=1}^{n} \varphi_k \rho_k V_k}{\rho_m} \tag{3.8}$$

$$\rho_m = \sum_{k=1}^{n} \varphi_k \rho_k \tag{3.9}$$

$$\mu_m = \sum_{k=1}^{n} \varphi_k \mu_k \tag{3.10}$$

$$H_k = h_k - \frac{P}{\rho_k} + \frac{v_k^2}{2} \tag{3.11}$$

where h_k represents the internal energy per unit mass of phase k.

In the momentum equation (3.5) $V_{dr,k}$ is the drift velocity for the nanoparticles and defined as:

$$\vec{V}_{dr,k} = \vec{V}_k - \vec{V}_m \tag{3.12}$$

where $\vec{V}_k$ is the velocity of phase k and $\vec{V}_m$ is the velocity of the mixture.

The particle phase's velocity (p) with respect to the fluid phase's velocity (f) is known as the relative velocity or slip velocity:

$$\vec{V}_{pf} = \vec{V}_p - \vec{V}_f \tag{3.13}$$

where $\vec{V}_p$ is the velocity of phase p (nanoparticles) and $\vec{V}_f$ is the velocity of the fluid phase.

The drift velocity ($\vec{V}_{dr,p}$) and the relative velocity ($\vec{V}_{pf}$) are related as follows:

$$\vec{V}_{dr,p} = \vec{V}_{pf} - \sum_{k=1}^{n} \frac{\phi_k \rho_k}{\rho_m} \vec{V}_{fk} \tag{3.14}$$

where $\vec{V}_{fk}$ is the velocity of the fluid phase k.

The relative velocity ($\vec{V}_{pf}$) in Eq. (25) proposed by Manninen, et al. [125] is defined as:

$$\vec{V}_{pf} = \frac{\rho_p d_p^2}{18\mu_m f_{\text{drag}}} \frac{(\rho_p - \rho_m)}{\rho_p} \vec{a} \tag{3.15}$$

where the f_{drag}, d_p, and $\vec{a}$ are the drag function, diameter of the particle and acceleration vector.

The drag function is determined by Schiller [192]:

$$f_{\text{drag}} = \begin{cases} 1 + 0.15\text{Re}_p^{0.687} & Re_{\text{p}} \leqslant 1000 \\ 0.0183 Re_p & Re_{\text{p}} \geqslant 1000 \end{cases} \tag{3.16}$$

where Re_p is the Reynolds number for particles.

The acceleration ($\vec{a}$) in Eq. (26) can be expressed as:

$$\vec{a} = \vec{g} - (\vec{V}_m \cdot \nabla)\vec{V}_m \tag{3.17}$$

where $\vec{g}$ is the gravitational acceleration vector.

3.1.2.2 Eulerian Model

The Eulerian-Eulerian model resolves "n" sets of continuity and momentum equations for each phase in multi-phase flows. The interactions between phases are characterised by additional terms that represent the exchange of momentum and heat between them [193]. The pressure is shared by all phases. The strong coupling between the phases is achieved by the exchange and pressure coefficients. The coupling manner completely depends on the phases involved, e.g., solid-fluid and fluid-fluid. In addition, nanoparticles and base fluids are assumed to be continuous. For different phases (continuous and discrete), the Navier-Stokes equations (continuity, momentum, and energy) are employed separately. By integrating the volume fraction of each phase across the domain, the volume of each phase is calculated. Also, the volume fraction's sum for both phases equal to one.

The assumptions of the Eulerian model are as follows: [111, 194]

- The phases share the same velocity field, but each phase has its own velocity, and interphase momentum transfer is considered.
- The model accounts for particle-particle interactions and particle clustering, allowing more accurate predictions of nanofluid behaviour.
- The volume fraction of each phase is treated as a variable, which can change locally due to particle dispersion, sedimentation, or agglomeration.
- The interphase momentum transfer is described by drag models, considering both the solid and liquid phase dynamics.

The limitations of the Eulerian model are as follows: [39, 111, 195]

- The model assumes that the phases are well-mixed, which may not be true in certain flow regimes where separation occurs.

- The model is computationally more expensive due to the need to solve separate equations for each phase.

- It can be difficult to obtain accurate models for interphase drag and particle-pair interactions, leading to potential inaccuracies.

The governing equations are as follows [194]:

Continuity equation:

$$\nabla.\left(\varphi_q \rho_q \overrightarrow{v_q}\right) = 0 \tag{3.18}$$

where φ_q, ρ_q and $\overrightarrow{v_q}$ are the volume fraction, density, and velocity of the qth phase. The velocity of the q phase, defined as $\overrightarrow{v_q} = \int \varphi_q dv$ and $\sum_{q=1}^{n} \varphi_q = 1$ where q is the index of phase.

Momentum equation: (qth Phase)

$$\nabla.\left(\varphi_q \rho_q \vec{v}\,\vec{v}\right) = -\varphi_q \nabla P + \varphi_q \nabla.\left(\mu_q \nabla \vec{v}\right) + \varphi_q \rho_q \vec{g} + \sum_{p=1}^{n} \overrightarrow{R_{pq}} + \overrightarrow{F_{lift,q}} \tag{3.19}$$

where $\varphi_q \nabla.\left(\mu_q \nabla \vec{v}\right)$ represents the shear stress due to viscosity of the phase q, $\varphi_q \rho_q \vec{g}$ relates to the body force acting due to gravity, $\overrightarrow{F_{lift,q}}$ signifies the lift force of the phase q and $\overrightarrow{R_{pq}}$ represents the interaction forces between the phases, and defined as $\sum_{q=1}^{n} \overrightarrow{R_{pq}} = \sum_{q=1}^{n} S_{pq}(\overrightarrow{v_p} - \overrightarrow{v_q})$, where $S_{pq} = (\varphi_q\ \varphi_p\ \varphi_q\ f)/\tau_p$ denotes the coefficient for interaction forces, $\tau_p = \frac{\rho_p\, d_p^2}{18\ \mu_q}$ is the relaxation time for phase p and f, $\vec{g}$ indicates the gravitational acceleration vector and drag friction.

The drag friction (f) can determined according to syamlal-obrien [196] as:

$$f = \frac{C_D \, Re\varphi_q}{24 \, v_{r,s}^2} \tag{3.20}$$

Where $v_{r,s}$ is the relative velocity between the solid-fluid phases, Re is the Reynolds number and C_D represents the drag coefficient and defined as

$$C_D = \left(0.63 + \frac{4.8}{\sqrt{\frac{Re_p}{v_{r,s}}}} \right)^2 \tag{3.21}$$

$$v_{r,s} = 0.5(A - 0.06Re_p + \sqrt{(0.06Re_p)^2 + 0.12Re_p(2B - A) = A^2}) \tag{3.22}$$

where, Re_p is the Reynolds number of the particle and A and B are model constants.

$$A = \varphi_q^{4.14}$$

$$B = 0.8\varphi_q^{1.28} \; for \; \varphi \leq 0.85$$

$$B = \varphi_q^{2.65} \; for \; \varphi > 0.85$$

$$Re_p = \frac{\rho_q \, d_p \, |\overrightarrow{v_p} - \overrightarrow{v_q}|}{\mu_p} \tag{3.23}$$

The lift force is computed as follows [197]:

$$\overrightarrow{F_{lift,q}} = -0.5\rho_p\varphi_p(\overrightarrow{v_p} - \overrightarrow{v_q}) \times (\nabla \times \overrightarrow{v_q}) \tag{3.24}$$

Energy equation:

$$\nabla.\left(\varphi_q\rho_q\overrightarrow{v_p}H_q\right) = -\nabla.\left(K_q\nabla.T_q\right) - \tau_q:\nabla\vec{V}_q + \sum_{p=1}^{n}\overrightarrow{Q_{pq}} \tag{3.25}$$

Where H_q is enthalpy, T_q is temperature at q^{th} phase, and τ_q is stress strain tensor, $\overrightarrow{Q_{pq}} = h(\overrightarrow{v_p} - \overrightarrow{v_q})$ is the coefficient of heat exchange, and h is the heat transfer coefficient and defined as $h = (6K_q\varphi_p\varphi_q Nu_p)/(d_p^2)$, and Nu_p is the Nusselt number of the particle and can be computed from the Ranz and Marshal model [198].

$$Nu_p = 2 + 0.6Re^{0.5}\,Pr_q^{0.333} \tag{3.26}$$

where, Pr_q is the Prandtl number of the phase q and can be represented as

$$Pr_q = (C_{pq}\mu_q)/K_q \tag{3.27}$$

and K_q is the thermal conductivity of the phase q defined as

$$K_{pq} = \frac{3\varphi_p\varphi_q\rho_q}{4v_{r,p}^2 d_p}\,C_D\left(\frac{Re_p}{v_{r,p}}\right)|\overrightarrow{v_p} - \overrightarrow{v_q}| \tag{3.28}$$

Where p and q are solid phase and liquid phase.

3.2 Turbulence Modelling

Turbulence phenomena is considered for the closure of the thermal and fluid dynamic governing equations.

3.2.1 Realizable k- ε Model

The Realizable k- ε model proposed by Shih, et al. [199] includes a new dissipation rate transport equation and a new formulation for the eddy viscosity that varies from the standard and RNG k-ε models. This dissipation rate model transport equation is based on mean square vorticity fluctuation. The new formulation of the eddy viscosity was derived from the constraints of realizability, which are the modulus of normal (diagonal) Reynolds stresses and turbulent shear (off-diagonal) Reynolds stresses of Schwarz's inequality.

The RKE model introduces two transport equations, one for kinetic energy k and one for dissipation rate ε. The transport equation for kinetic energy in the Realizable k-ε model is same as in the RNG k-ε model. In terms of dissipation rate ε, two modifications were made: replacing the model constant and eliminating the last term on the ε equation.

The assumptions of the Realizable k- ε model are as follows: [84, 199, 200]

- The model assumes turbulence is isotropic at high Reynolds numbers.
- It applies the Boussinesq hypothesis, assuming the Reynolds stress tensor is proportional to the mean velocity gradients.
- Near-wall behaviour is modelled using wall functions.

The limitations of the Realizable k- ε model are as follows: [84, 143, 199, 200]

- The model requires fine meshing for accurate results in complex geometries.

- The model is less accurate for compressible flows or flows with significant density variations.

- The model struggles to accurately predict turbulence near the wall at low Reynolds numbers.

The following is a representation of these transport equations: [199].

$$div(\rho k\vec{v}) = div\left\{\left(\mu + \frac{\mu_t}{\sigma_k}\right) grad\ k\right\} + G_k - \rho\varepsilon \tag{3.29}$$

$$div(\rho\varepsilon\vec{v}) = div\left\{\left(\mu + \frac{\mu_t}{\sigma_\varepsilon}\right) grad\ k\right\} + \rho C_1 S_\varepsilon - \rho C_2 \frac{\varepsilon^2}{k + \sqrt{v\varepsilon}} \tag{3.30}$$

In these above equations, ρ, k, ε, $\vec{v}$, μ, μ_t, σ_k, σ_ε, and G_k represents the density, turbulent kinetic energy, dissipation rate of turbulent kinetic energy, velocity vector, dynamic viscosity, turbulent viscosity, turbulent Prandtl number for k ($\sigma_k = 1.0$), turbulent Prandtl number for ε ($\sigma_\varepsilon = 1.2$) and turbulent kinetic energy generation due to mean velocity gradients. In addition, C_1 and C_2 determine the coefficient for the turbulent production term and the coefficient for the dissipation term ($C_2 = 1.9$) and defined as $C_1 = \max\left[0.43, \frac{\eta}{\eta+5}\right]$, and dimensionless ratio $\eta = \frac{k}{\varepsilon}\sqrt{2\,S_{ij}\,S_{ij}}$, where S is the modulus of the mean rate of strain tensor (source term).

The turbulent molecular viscosity μ_t is

$$\mu_t = \frac{\rho k^2}{\varepsilon}\left(A_0 + A_s \frac{kU^*}{\varepsilon}\right)^{-1} \tag{3.31}$$

where $A_0 = 4.04$ and $A_s = \sqrt{6cos\emptyset}$ respectively with $\emptyset = \left(3\cos^{-1}\sqrt{6W}\right)^{-1}$ and U^* and W are the velocity scale parameter and a dimensionless parameter which depends on the angular velocity.

3.2.2 SST k-ω Model

The Shear Stress Transport (SST) k-ω turbulence model combines the two different elements of the existing models, where it utilises the original Wilcox k-ω formulation in the boundary layer's inner region and k- ε model for the outer region in open shear regimes. The model incorporates blending functions that ensure a smooth transition between the k-ω model near the wall and the k-ε model in the free stream. In addition, a modification to the eddy viscosity was made to consider the transportation of principal turbulent stress [201]. The SST k-ω model is particularly well-suited for flows involving strong adverse pressure gradients, separation, and high turbulence intensity.

The assumptions of the SST k-ω model are as follows: [201-203]

- The model assumes turbulence is partially isotropic, combining k-ε and k-ω models for better accuracy.
- It uses the Boussinesq hypothesis to relate Reynolds stresses to velocity gradients.
- The model assumes wall-adapting functions for near-wall turbulence resolution.

The limitations of the SST k-ω model are as follows: [201-203]

- The model can be sensitive to the choice of boundary conditions, mesh resolution, and compressible flows.
- It can overestimate turbulence in free-shear flows due to near-wall assumptions.
- The blending function can lead to inaccuracies in transitional flow regimes.

The equations governing the transport of turbulent kinetic energy (k) and specific dissipation rate (ω) are as follows:

$$div(\rho k\vec{v}) = div\left\{\left(\mu + \frac{\mu_t}{\sigma_k}\right) grad\ k\right\} + G_k - \rho k\omega\beta_1 \tag{3.32}$$

$$div(\rho\omega\vec{v}) = div\left\{\left(\mu + \frac{\mu_t}{\sigma_\omega}\right) grad\ \omega\right\} + G_\omega - \rho\omega^2\beta_2 + 2(1 - F_1)\,\rho\,\sigma_{\omega,2}\frac{grad\ \omega\ grad\ k}{\omega} \tag{3.33}$$

where, k, ω, G_k, G_ω, σ_k, σ_ω, $\beta_{1,2}$, and F_1 are the turbulent kinetic energy, specific dissipation rate, production of turbulent kinetic energy, production of specific dissipation rate, effective Prandtl number for k, , effective Prandtl number for ω, model constants and blending function.

The turbulent viscosity (μ_t) is defined as:

$$\mu_t = \frac{\rho k}{\omega}\frac{1}{\max\left(\frac{1}{\alpha^*}, \frac{SF_2}{\alpha_1\omega}\right)} \tag{3.34}$$

where, S is the strain rate value, α^* and α_1 are model constants and F_2 is the blending function. In equations (3.35) and (3.36), σ_k and σ_ω are the effective Prandtl numbers of kinetic energy and dissipations respectively, which are defined as follows.

$$\sigma_k = \frac{1}{\frac{F_1}{\sigma_{k,1}} + \frac{(1 - F_1)}{\sigma_{k,2}}} \tag{3.35}$$

$$\sigma_\omega = \frac{1}{\frac{F_1}{\sigma_{\omega,1}} + \frac{(1 - F_1)}{\sigma_{\omega,2}}} \tag{3.36}$$

The blending functions are calculated as,

$$F_1 = \tanh\left(\emptyset_1^4\right) \tag{3.37}$$

$$F_2 = \tanh\left(\emptyset_2^4\right) \tag{3.38}$$

where,

$$\emptyset = \min\left[\max\left(\frac{\sqrt{k}}{0.09\omega y}, \frac{500\mu}{\rho y^2 \omega}\right), \frac{4\rho k}{\sigma_{\omega,2} D_\omega^+ y^2}\right],$$

$$D_\omega^+ = \max\left[2\rho \frac{1}{\sigma_{\omega,2}\omega} \frac{\partial k}{\partial x_j} \frac{\partial \omega}{\partial x_j}\ 10^{-20}\right],$$

$$\emptyset_2 = \min\left[\left(\frac{2\sqrt{k}}{0.09\omega y}, \frac{500\mu}{\rho y^2 \omega}\right)\right]$$

Where y is the wall distance and D_ω^+ is the cross-diffusion term's positive portion. The model constants are $\sigma_{k,1} = 1.176$, $\sigma_{k,2} = 1$, $\sigma_{\omega,1} = 2$, $\sigma_{\omega,2} = 1.168$, $\beta_1 = 0.075$, $\beta_2 = 0.0828$, and $\alpha_1 = 0.31$.

3.3 Thermo-physical properties

The estimation of the nanofluid thermophysical properties is the most difficult part of the numerical simulation, particularly thermal conductivity, and viscosity. This is due to the experimental uncertainty that affects the accuracy of results from a wide range of classical equations. This section discusses the various thermo-physical property correlations used to calculate nanofluid and hybrid nanofluid values.

3.3.1 Nanofluids

The nanofluid thermo-physical property correlations are drawn from the experimental data. It's critical to use the appropriate correlations to get accurate results. Nevertheless, no universal correlation exists that can reliably predict the characteristics of nanofluids. This is because the dependency on many variables (e.g., nanoparticle diameter, temperature, volume concentration, Brownian motion, etc.) cannot be implemented practically. The correlations used here have been selected because they align more closely with experimental data and have demonstrated better predictive accuracy in CFD results.

To evaluate the Al_2O_3-water nanofluid, the following equations are considered, as mentioned below:

The density of the nanofluid is defined as: [81]

$$\rho_{nf} = (1 - \varphi)\rho_{bf} + \varphi\rho_{np} \tag{3.39}$$

where, ρ_{bf} and ρ_p are the densities of base fluid and nanoparticles.

The specific heat capacity of the nanofluid can be expressed as: [204]

$$(c_p)_{nf} = (1 - \varphi)\left(C_p\right)_{bf} + \varphi\left(C_p\right)_{np} \tag{3.40}$$

where, $\left(C_p\right)_{bf}$ and $\left(C_p\right)_{np}$ are the specific heat capacities of base fluid and nanoparticles.

The thermal conductivity for Al_2O_3-water nanofluid can be represented as: [102]

$$k = k_{bf}(1 + 7.47\varphi) \tag{3.41}$$

where, k_{bf} is the thermal conductivity of the base fluid.

The viscosity for Al_2O_3-water nanofluid can be calculated as: [102]

$$\mu = \mu_w(1 + 39.11\varphi + 533.9\varphi^2) \tag{3.42}$$

where, μ_w is the dynamic viscosity of the base fluid (water).

The above equations (3.41 and 3.42) are valid for a range of volume concentration $\varphi = 0\ to\ 3\%$, fluid temperature T=300K, and nanoparticle diameter $d_{np} = 13\ and\ 27mm$.

The equations (3.39) and (3.40) are based on the classical theory of two-phase mixture models. For the mixture under consideration, the thermal conductivity and viscosity formulations (eq. 3.41 and 3.42) are derived by fitting the available experimental data to a least squares curve.

3.3.2 Hybrid nanofluids

To calculate the thermo-physical properties of hybrid nanofluids, the following equations are utilised.

The density of the hybrid nanofluid is defined as: [205]

$$\rho_{hnf} = (1 - \varphi)\rho_{bf} + \varphi_{np1}\rho_{np1} + \varphi_{np2}\rho_{pn2} \tag{3.43}$$

where, φ_{np1} and φ_{np2} are volume concentrations of nanoparticle 1 and 2, and φ is the total volume concentration and represented as $\varphi = \varphi_{np1} + \varphi_{np2}$. In addition, ρ_{bf}, ρ_{np1}, ρ_{np2} are the densities of base fluid, nanoparticle 1 and 2.

The specific heat capacity of the hybrid nanofluid can be expressed as: [205]

$$\left(c_p\right)_{hnf} = (1-\varphi)\left(C_p\right)_{bf} + \varphi_{p1}\left(C_p\right)_{np1} + \varphi_{p2}\left(C_p\right)_{np2} \tag{3.44}$$

where, $\left(C_p\right)_{bf}$, $\left(C_p\right)_{np1}$ and $\left(C_p\right)_{np2}$ are the specific heat capacities of base fluid, nanoparticle 1 and nanoparticle 2.

According to the Maxwell model [87], the thermal conductivity of the nanofluid is defined as:

$$k = k_w \frac{\left(k_{np} + 2k_{bf} - 2\varphi\left(k_{bf} - k_{np}\right)\right)}{\left(k_{np} + 2k_{bf} + \varphi\left(k_{bf} - k_{np}\right)\right)} \tag{3.45}$$

Based on the equation (Eq. 3.45), the thermal conductivity of hybrid nanofluid can be represented as: [38]

$$k_{hnf} = k_{bf} \frac{\frac{\left(k_{np1}\varphi_{np1} + k_{np2}\varphi_{np2}\right)}{\varphi} + 2k_{bf} + 2\left(k_{np1}\varphi_{np1} + k_{np2}\varphi_{np2}\right) - 2k_{bf}\varphi}{\frac{\left(k_{np1}\varphi_{np1} + k_{np2}\varphi_{np2}\right)}{\varphi} + 2k_{bf} - 2\left(k_{np1}\varphi_{np1} + k_{np2}\varphi_{np2}\right) + k_{bf}\varphi} \tag{3.46}$$

where, k_{bf} , k_{np1} and k_{np2} are the thermal conductivities of base fluid, nanoparticle 1 and nanoparticle 2.

Another thermal conductivity model was developed by Timofeeva, et al. [206] and expressed as:

$$K = K_{bf}(1 + 3\varphi) \tag{3.47}$$

the above equation can be further represented as:

$$K = K_{bf}(1 + 3(\varphi_{np1} + \varphi_{np2})) \tag{3.48}$$

From the Brinkman model [108], the viscosity of nanofluid is

$$\mu = \mu_{bf} \frac{1}{(1-\varphi)^{0.25}} \tag{3.49}$$

where, μ_{bf} is the dynamic viscosity of the base fluid.

Based on the equation (Eq. 3.47), the viscosity of hybrid nanofluid can be expressed as: [38]

$$\mu = \mu_{bf} \frac{1}{\left(1 - (\varphi_{np1} + \varphi_{np2})\right)^{2.5}} \tag{3.50}$$

where, $\varphi_{np1}$and φ_{np2} are volume concentrations of nanoparticle 1 and 2.

The viscosity equation, according to the Einstein [207] model, is

$$\mu = \mu_{bf}(1 + 2.5\varphi) \tag{3.51}$$

The above equation (eq. 3.51) can be expressed in terms of hybrid nanofluid's viscosity as mentioned below

$$\mu = \mu_{bf}(1 + 2.5(\varphi_{np1} + \varphi_{np2}) \tag{3.52}$$

In addition, also Batchelor [208] proposed a viscosity model, which is represented as

$$\mu = \mu_{bf}(1 + 2.5\varphi + 6\varphi^2) \tag{3.53}$$

From the above equation (eq. 3.53), the hybrid nanofluid viscosity can be expressed as below.

$$\mu = \mu_{bf}(1 + 2.5(\varphi_{np1} + \varphi_{np2}) + 6(\varphi_{np1} + \varphi_{np2})^2) \tag{3.54}$$

3.3.3 Base fluid and Nanoparticles

The properties of the base fluid and different nanoparticles are mentioned in Table 3. 1.

Table 3. 1: Physical properties of water and different nanoparticles of average size less than 40 nm at room temperature

Material	$\boldsymbol{\rho[kg/m^3]}$	$\boldsymbol{c_p[J/kgK]}$	$\boldsymbol{k}$ $\boldsymbol{[w/mK]}$	$\boldsymbol{\mu}$ $\boldsymbol{[Kg/m\,s]}$
water [23]	997.01	4179	0.613	0.855×10^{-3}
Al_2O_3 [102]	3880	773	36	-
Cu [157]	8940	390	400	-
CuO [155]	6930	550	32	-
TiO2 [209]	3700	686	11.8	-
GO [210]	2700	710	0.3	-
Ag [166]	10490	235	429	-
MgO [166]	3580	940	45	-
SiO2 [167]	2220	703	1.4	-

Table 3. 2 shows the experimental thermo-physical properties values of Al_2O_3/Cu-water hybrid nanofluid. The weight percent of the Al_2O_3-Cu hybrid nanoparticle used was 9:1.

Table 3. 2: Thermo-physical properties of Al_2O_3/Cu-water hybrid nanofluids at 300K [157]

φ [%]	$\rho[kg/m^3]$	$c_p[J/kgK]$	$k\ [w/mK]$	$\mu\ [Kg/m\ s]$
0.1	998.91	4163.53	0.619	0.9×10^{-3}
0.5	1011.74	4106.58	0.633	1.2×10^{-3}
1	1027.78	4037.40	0.652	1.602×10^{-3}
2	1059.86	3905.30	0.685	1.935×10^{-3}

3.4 Relevant heat transfer formulas

The average Nusselt number of a corrugated tube is defined as [102]

$$Nu = \frac{hd_h}{k} \tag{3.55}$$

Where, h, d_h,and k are the heat transfer coefficient, hydraulic diameter, and thermal conductivity of the working fluid.

The heat transfer coefficient for a constant heat flux boundary condition is defined as: [102]

$$h_{avg} = \frac{q}{T_w - T_b} \tag{3.56}$$

where, q, T_w *and* T_b are heat flux, wall and bulk temperatures.

The Reynolds number, Re is defined as [211]

$$Re = \frac{\rho v d_h}{\mu} \tag{3.57}$$

where, ρ, μ, and v are the density, dynamic viscosity, and mean velocity of the fluid.

The Darcy friction factor f for turbulent flows is defined as [211]

$$f = \frac{\Delta p}{\frac{1}{2}\frac{L}{D}\,\rho\, v^2} \tag{3.58}$$

where, Δp is the pressure drop between the inlet and the outlet.

The Performance Evaluation Criteria (PEC) can be calculated using the predicted f and Nu as follows: [212]

$$PEC = \frac{Nu/Nu_s}{(f/f_s)^{1/3}} \tag{3.59}$$

3.5 Summary

This chapter covered the fundamental numerical methods for modelling nanofluids and turbulent flows. Additionally, the thermo-physical property correlations were explored for calculating the properties of nanofluids and hybrid nanofluids. The chapter also included relevant heat transfer formulas.

Chapter 4: Geometrical Effects - The Impact of various Groove Shapes on the Heat Transfer

This chapter explores the numerical investigation of the thermal and hydraulic behaviour of cylindrical tubes with different groove shapes (rectangular, triangular, circular, and trapezoidal) to improve convective heat transfer under forced convection. This study aligns with Objective 2 outlined in Section 1.2 of Chapter 1. The chapter begins with the validation of the numerical model by comparing the cylindrical tubes with and without corrugation (circular and rectangular grooves) using water as the working fluid under a turbulent regime. The validation employs two RANS turbulence models: the realizable k-ε model and the SST k-ω model.

Initially, both two-dimensional and three-dimensional results are compared to empirical data to identify the model that most closely aligns with experimental findings. Following this, various corrugated groove shapes, with fixed parameters such as width, depth, and pitch, are numerically simulated and analysed. The chapter also investigates hybrid groove designs, strategically altering the groove configurations to assess their impact on flow patterns and heat transfer performance. Finally, the results are presented in terms of mean velocity, temperature, turbulent kinetic energy, Nusselt number, and other relevant metrics. This comprehensive numerical analysis aims to deepen the understanding of geometrical modifications and their impact on heat exchanger performance, ultimately contributing to more efficient thermal systems.

4.1 Model Description

In this chapter, the numerical simulations are performed for the two-dimensional axisymmetric model with a hydraulic diameter $d_h = 0.01\ m$, and length $L = 0.4\ m$. A schematic representation of the 2D model with different groove shapes (e.g., rectangular, triangular, circular, and trapezoidal) is shown in Figure 4. 1. In similar studies, the effect of 3D vortex instabilities was neglected. Thus, the 3D model was simplified into an axisymmetric 2D model, significantly reducing the cost and time of computing resources [18, 19, 58, 213]. The circular tube consists of 2 sections, with the test

section placed after the hydrodynamic entry length of 0.3 m to achieve a fully developed flow and capture the maximum groove effect. In addition, this study also considered the assumption of neglecting conduction to adjacent pipe surfaces. This assumption holds true when the pipe wall is subjected to a constant heat flux boundary condition, ensuring that axial or radial conduction has minimal impact on convective heat transfer [214]. This implies that localised thermal gradients have little effect on the overall thermal and flow profiles, as they do not significantly alter the convective behaviour of the system.

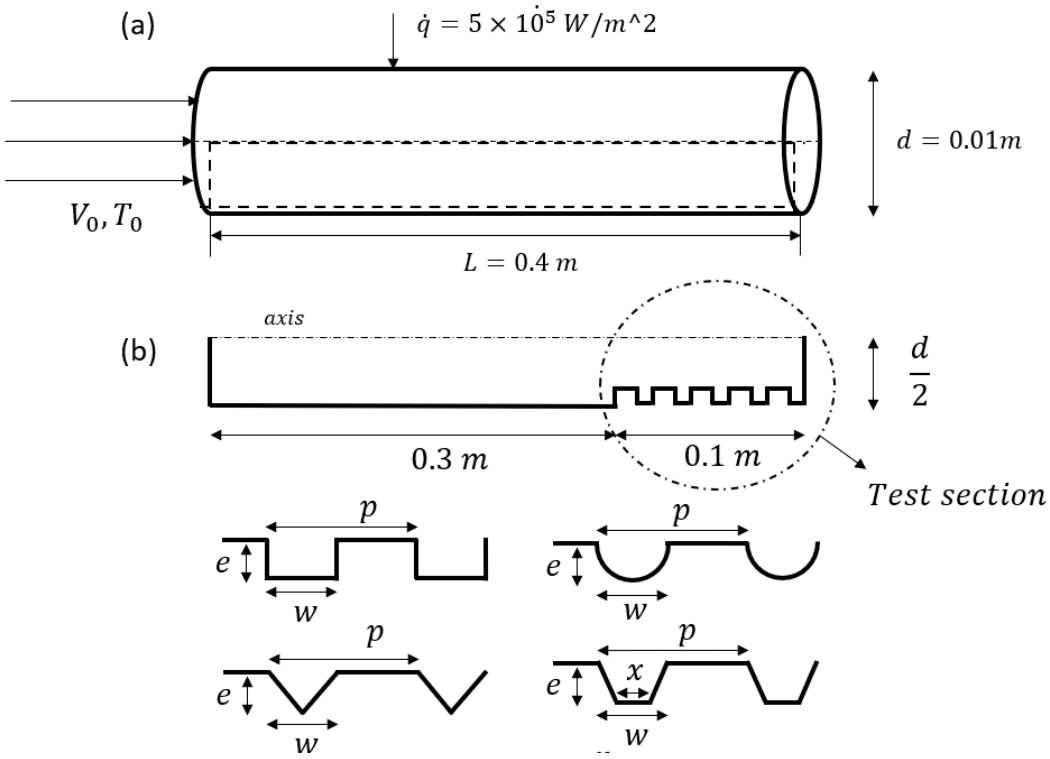

Figure 4. 1: 2D Cylindrical tube with different groove shapes

The inward grooves were selected due to their superior heat transfer coefficients compared to the outward grooves [19]. The dimensionless roughness parameters of the grooves were expressed as follows: the ratio of the groove depth to the tube diameter (e/d = 0.025); the ratio of the groove width to the tube diameter (w/d = 0.2); and the groove pitch to the tube diameter (p/d = 0.5) were considered for this study. These values were identified as optimal for achieving high convective

heat transfer performance among the nineteen groove combinations [18]. In addition, the tube material was assumed to be isotropic and homogeneous. Also, the tube wall's thermal conductivity was constant and unaffected by temperature. Furthermore, hybrid grooves were also considered, combining two different groove shapes repeatedly added to the tube's wall. Table 4. 1 shows the six different cases of hybrid groove combinations used in this study.

Table 4. 1: Different variations of hybrid groove combinations

Cases	Combinations
Case 1	Triangular - Rectangular
Case 2	Triangular - Trapezoidal
Case 3	Triangular - Circular
Case 4	Circular - Rectangular
Case 5	Circular - Trapezoidal
Case 6	Trapezoidal - Rectangular

4.1.1 Boundary conditions

The set of partial differential equations is coupled, non-linear, and subjected to boundary conditions to investigate the complex fluid flow with gravity in a circular tube using FLUENT [2023]. The constant fluid (water) temperature at the inlet $T_{in} = 300K$ was specified at different Reynolds numbers ($Re = 10{,}000$ to $60{,}000$). The turbulent intensity of 5% was imposed. The steady-state realizable k-ε model and the SST k-ω model with enhanced wall treatment were implemented to capture the hydrodynamic flow field with y+ less than 1 near the viscous boundary layer. To prevent any potential turbulence kinetic energy overproduction in regions of diminished flow velocity zones, a production limiter was applied when it was available. Additionally, the effective velocity distribution near the tube's wall was also resolved, taking into account pressure gradients and thermal effects. As mentioned in Figure 4. 1, a constant heat flux of $5 \times 10^5\ W/m^2$ and a no-slip condition were introduced on the tube's wall. At the outlet, the gauge pressure

$P_{guage} = 0$ was stated. The flow and thermal fields were axisymmetric to the horizontal plane. The second-order upwind schemes for energy, momentum, and equations were also employed to achieve the highest accuracy. All these governing equations were solved iteratively and sequentially until the convergence of 10^{-6} was achieved. Finally, the flow was thermally and hydrodynamically fully developed at the end of the tube.

4.1.2 Mesh sensitivity test

The reliability and consistency of the numerical results in a cylindrical tube of *Nu* and *f* at a fully developed flow of cylindrical tube for the resolution of the grid were examined using the mesh independence tests. Figure 4. 2 displays the two-dimensional mesh of a cylindrical tube. Various mesh sizes ($N_x \times N_y$) were evaluated at $Re = 10 \times 10^3$.

a. b.

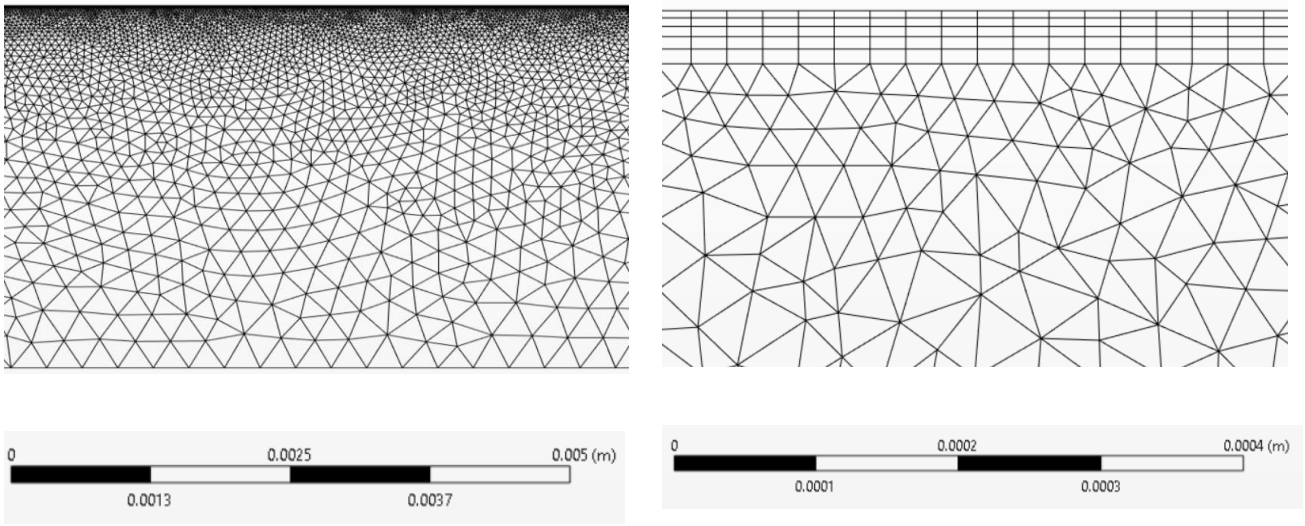

Figure 4. 2: Visualisation of the 2D Mesh of a Cylindrical Tube (a) Full Geometry (b) Near Wall

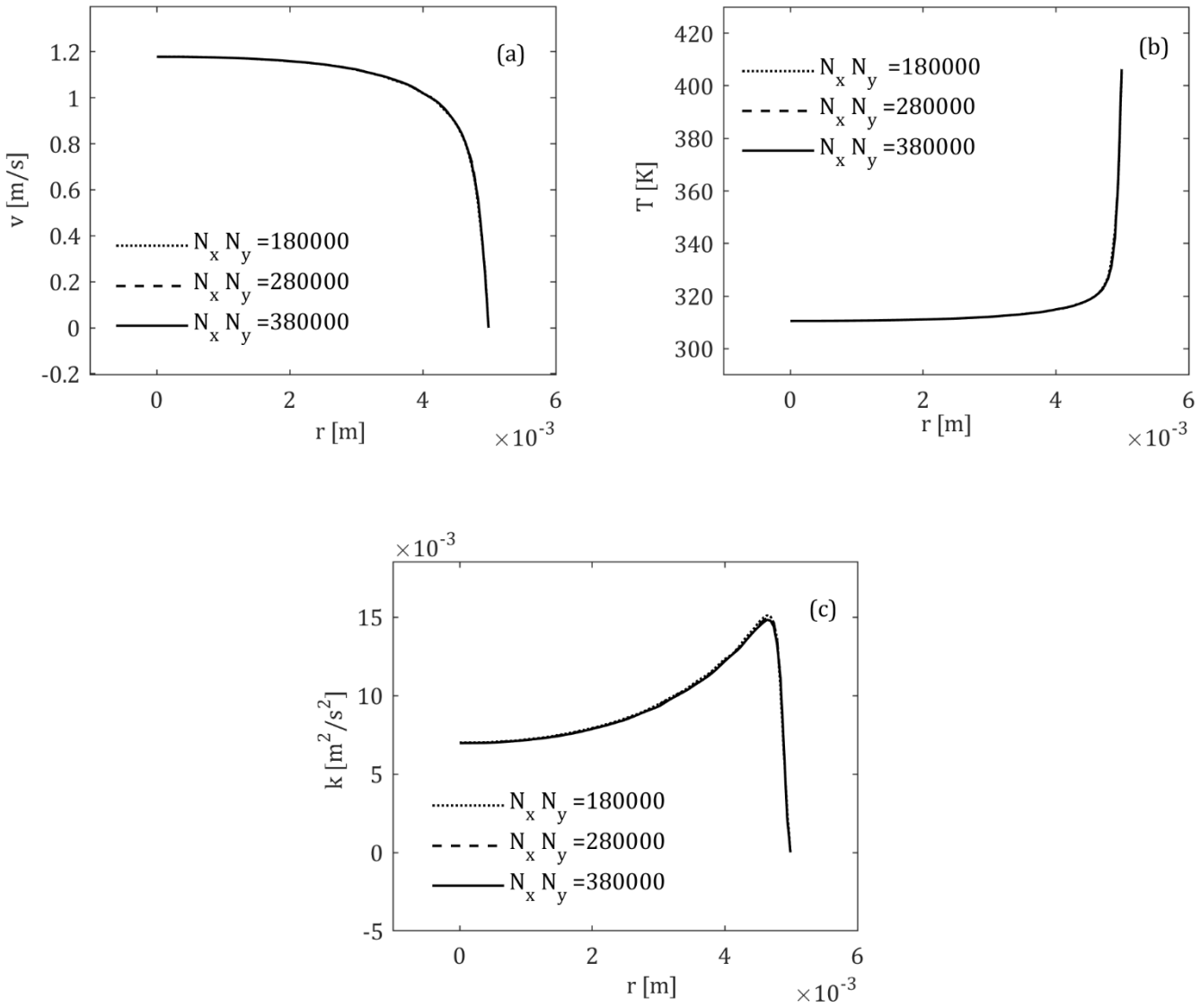

Figure 4. 3: Variation of radial (a) velocity (b) temperature (c) turbulent kinetic energy at a fully developed region near the outlet at Re = 10,000.

Results indicated that non-uniform-grid 3 (380,000) was more satisfactory to ensure the precision of the numerical solution where the radial temperature, velocity, and turbulent kinetic energy components were also checked as shown in Figure 4. 3. The mesh-independence findings showed the average error percentage was less than 0.1%, were displayed in Table 4. 2. This ensured that the grid resolution was sufficient to capture the intricate flow features without adding excessive computational cost. Thus, grid 3 was selected as optimal for further simulations.

Table 4. 2: Mesh Independence test at Re=10,000 using water at 300K

S. no	Cells ($\boldsymbol{N_x \times N_y}$)	Nu	Nu % Difference	f	f % Difference
1	80000	85.55741	1.94	0.03491	0.36
2	180000	87.25108	1.29	0.03479	0.23
3	280000	88.39197	0.62	0.03471	0.21
4	380000	88.94041	0.01	0.03463	0.04
5	480000	88.94962	-	0.03462	-

4.1.3 Validation

To assess the accuracy of the numerical simulations, the validity of the numerical model results of a fully developed flow is ensured by comparing the results with the existing literature results.

4.1.3.1 Cylindrical tube without corrugation

The computational model of the cylindrical tube has been validated against experimental correlations reported in equations (2.1) – (2.5) for hydraulically and thermally developing flow under constant heat flux using water. Figure 4. 4 presents a comparison of the Nusselt number (Nu) and friction factor (f) obtained from numerical simulations using the RKE and SST turbulence models with the empirical correlations. Figure 4. 4a shows the RKE model's results for the average Nusselt number compared to the correlations by Petukhov [73], Gnielinski [75], and Notter and Sleicher [74], with average deviations of 8%, 7%, and 9%, respectively. In contrast, the SST model results exhibited deviations of 3.4%, 2.2%, and 4.5% from the same correlations. Both RKE and SST results showed good agreement with correlations and replicated their trend effectively. The observed deviations ranged from a maximum of 13% to a minimum of 1% across Reynolds numbers from 10×10^3 to 60×10^3.

The results of the Darcy friction factor vary at various Reynolds numbers, as shown in Figure 4. 4b. When compared to the Blasius and Petukhov equations, the RKE model's average deviation from

the present study was approximately 3% for both equations, whereas the SST model showed deviations of 9% and 8%, respectively. The observed maximum and minimum variances were around 8% and 1%. These discrepancies could be attributed to the high pressure drop obtained at various Reynolds numbers. Overall, the RKE model seems to closely replicate the experimental data in terms of convective heat transfer and friction factor.

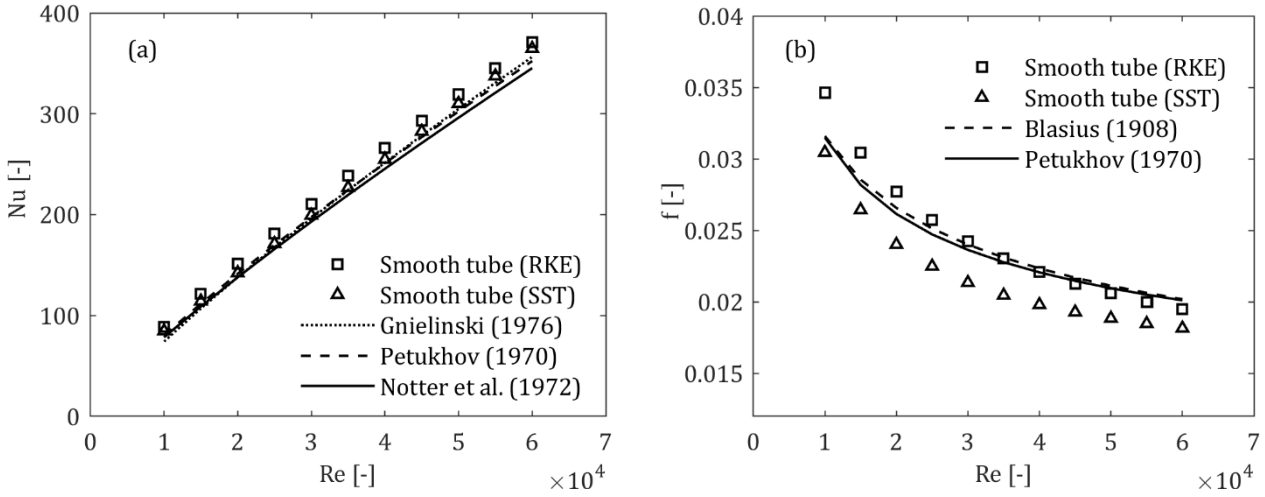

Figure 4. 4: Comparison of simulated (a) Nusselt number (b) friction factor from the present study with the selected correlations over a range of Re using two turbulent models.

4.1.3.2 Cylindrical tube with corrugation

The impact of circular grooves on a cylindrical tube is depicted in Figure 4. 5. It shows the simulated results of the Nusselt number at different Reynolds numbers, $Re = 4 \times 10^3$ to 16×10^3 using the RKE. The simulated results were compared to the experimental data of Huang, et al. [8], with an average deviation of 6.4%, respectively, demonstrating good agreement. The observed deviations ranged from a maximum of 8.6% to a minimum of -3.4%. The positive and negative signs indicate that the simulated data overestimates and underestimates the referred data.

The effect of friction factor at different Reynolds numbers is shown in Figure 4. 5b. It can be seen that the simulated data trend of the friction factor closely aligns with the experimental data of Huang, et al. [8] with an average error percentage of around 6.3%, respectively. The maximum and minimum deviations were -13.4% and 4.6%, respectively. These results were acceptable because

observed deviations fall within the acceptable error range of correlation of 22.6% as mentioned in eq. (35).

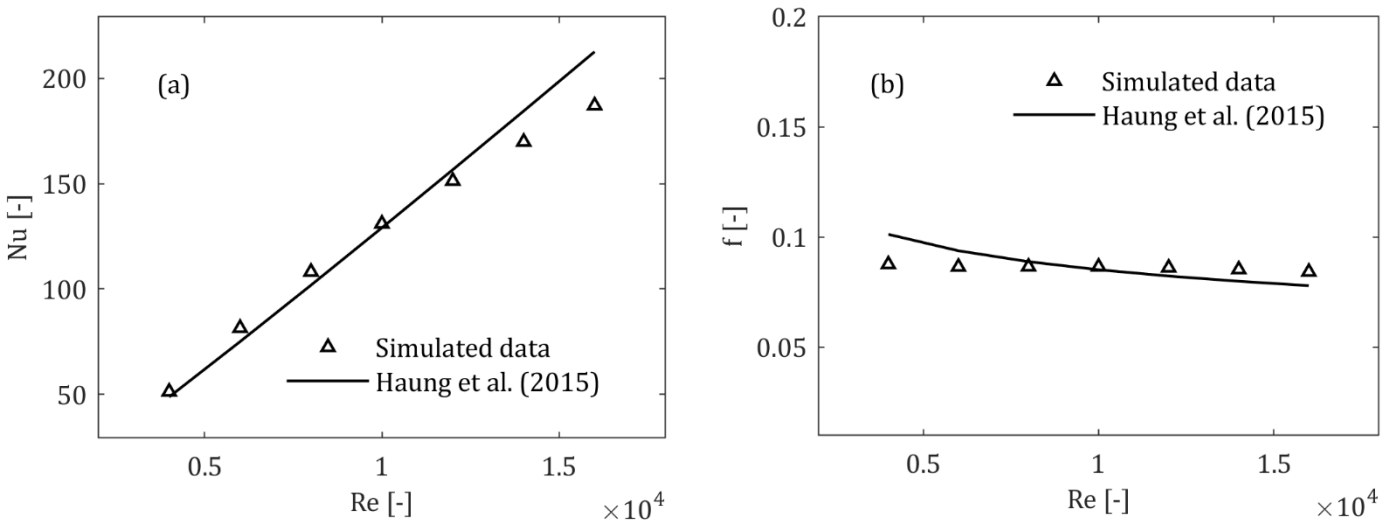

Figure 4. 5: Comparison of simulated (a) Nusselt number (b) friction factor with published data using a circular grooved tube with e/d=0.025, w/d=0.2 and p/d=0.5

The experimental data presented by Huang, et al. [8] has several limitations. The study focused on a limited Reynolds number range (3,601 to 26,025), which did not cover the full range of behaviour at both low and high Reynolds numbers, important for industrial applications. Additionally, measurement uncertainties related to temperature, flow rate, and pressure drop could impact the accuracy and validation of the results. Additionally, improper manufacturing techniques of corrugated tubes can also impose uncertainties in heat transfer results. Moreover, the experiments were conducted with specific rib configurations (e/d and p/d ratios), limiting the applicability of the findings to other geometric shapes or materials.

4.2 Results and Discussion

4.2.1 Comparison of 2D vs 3D model

This section covers the numerical accuracy of the 2D model and 3D model results in a cylindrical tube using the RKE turbulence model. Figure 4. 6a shows the relationship between the heat transfer coefficient and the Reynolds numbers for both 2D and 3D cylindrical tube simulations, compared to the empirical data of Gnielinski [75], Petukhov [73], and Notter and Sleicher [74]. The heat transfer coefficient directly relates to the convective heat transfer rate inside a cylindrical tube. It can be noted that the heat transfer coefficient increased almost linearly with an increase in the Reynolds number (Re) ranging from 10,000 to 60,000. This is because as the Re increases, the flow rate, or the level of turbulence, increases. Thereby disrupting the thermal boundary layer, which enhances fluid mixing from the wall to the centre of the tube and therefore improves convection.

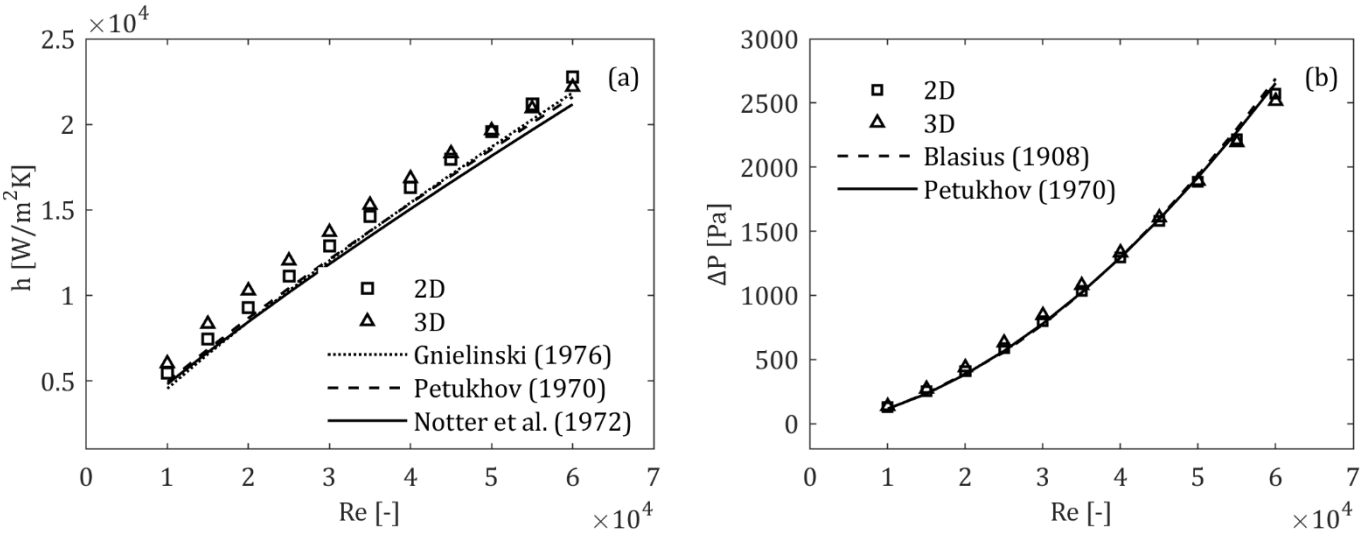

Figure 4. 6: Comparison of simulated (a) h (b) P results with the published data over a given range of Re for 2D and 3D models

In addition, it can be seen that both 2D and 3D simulation results of heat transfer coefficient closely follow the trends predicted by empirical correlations reported in equations (2.1) – (2.5). For instance, the average deviation of the 2D heat transfer coefficient was 8%, 7%, and 9%, respectively, compared to the Gnielinski [75], Petukhov [73], and Notter and Sleicher [74] values. In contrast, the 3D model predicted relatively higher values with deviations of 13%, 12%, and 15%, respectively.

The effect of the pressure drop with the variation in Reynolds number for both 2D and 3D simulations is shown in Figure 4. 6b. It can be shown that pressure drop increases exponentially with an increase in Reynolds number due to the enhancement in the flow resistance. This behaviour occurred as higher Reynolds numbers correspond to greater flow velocities and instabilities, thereby increasing frictional losses within the tube. Furthermore, the 2D simulation results showed minimal deviations from empirical data, with average deviations of 2% and 2% when compared to Blasius [76] and Petukhov [73] correlations. Similarly, the 3D simulations indicated slightly larger deviations, averaging 5.6% and 5.9% compared to the same empirical correlations. However, at higher Reynolds numbers, particularly beyond Re=45,000, the 3D model demonstrates a closer alignment than the 2D model.

Figure 4. 7 illustrates the comparison of flow characteristics such as mid-axial line velocity, temperature, pressure, and turbulent kinetic energy for both 2D and 3D models in a cylindrical tube at the fully developed region with Re=10,000. It can be seen that both 2D and 3D simulations show a nearly constant velocity profile along the length of the pipe. The 3D model shows slightly higher velocity gradients and shear forces compared to the 2D model due to high turbulence intensity and a more stable flow. This indicates that more energy is transferred from the mean flow to the turbulent eddies, thereby increasing the turbulent kinetic energy.

In addition, the axial temperature increases linearly along the tube's length for both computational models. This is because of the constant heat addition ($50\ W/cm^2$) along the tube's wall. The temperature profiles are almost identical for 2D and 3D models, suggesting that both models can accurately predict the thermal behaviour of the flow. Also, the fluid pressure decreases along the length of the tube. This constant decrease in pressure drop indicates the steady resistance of the

fluid flow. The pressure drop is higher for the 3D model compared to the 2D model. This can be due to the complex flow dynamics and interactions that are captured in a 3D simulation.

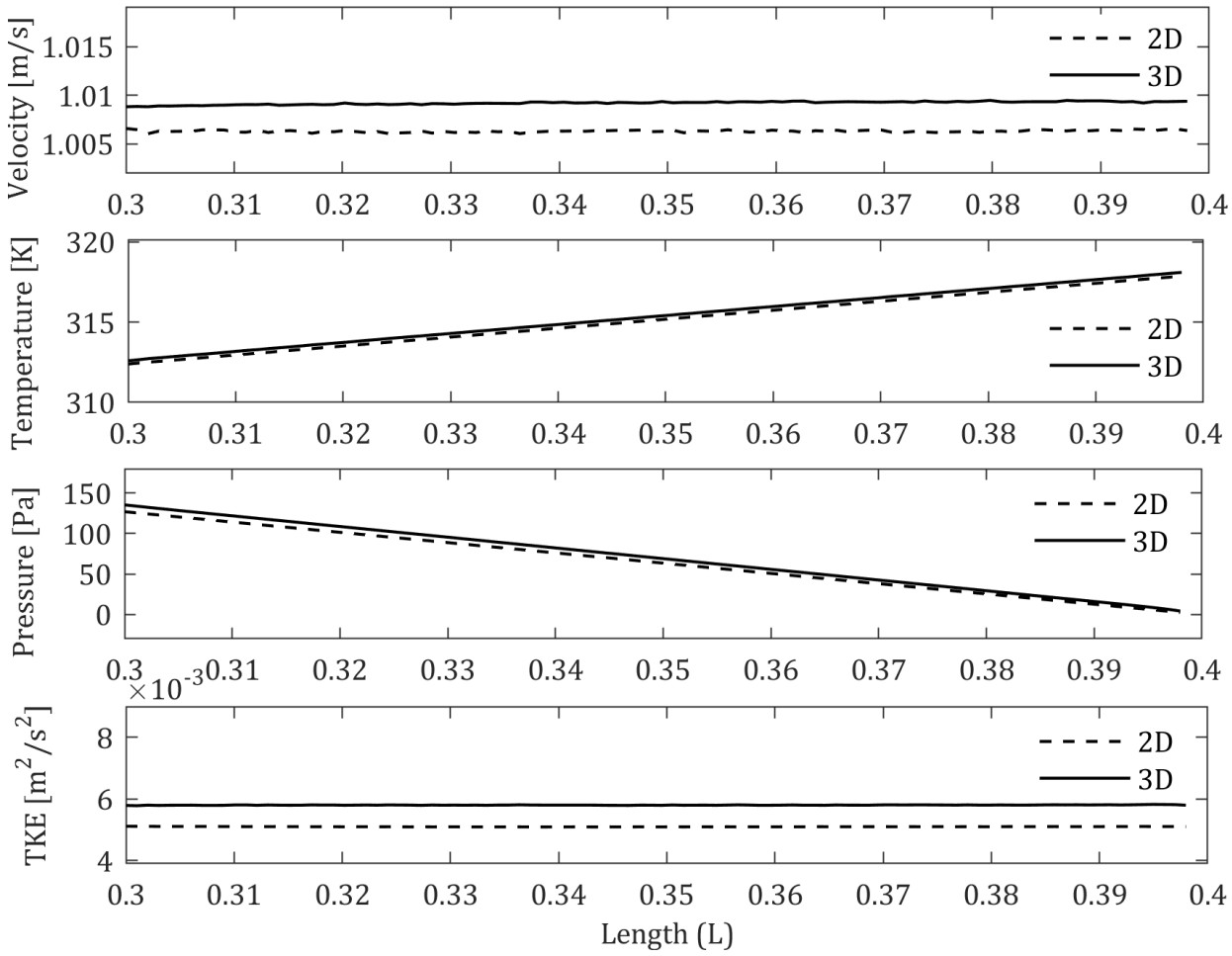

Figure 4. 7: Comparison of 2D and 3D Mid-Axial Line Velocity, Temperature, Pressure, and TKE at Re=10,000

Overall, the deviations of a 2D model are relatively small and closely align with the empirical data compared to the 3D model. This suggests that 2D simulations were more accurate and reliable in predicting heat transfer and pressure drop. Additionally, the 2D model significantly reduces computational power, cost, and time. Therefore, this research primarily utilises the 2D model for numerical simulations.

4.2.2 Impact of different grooves shapes

Figure 4. 8a compares the Nusselt number for different groove shapes (circular, rectangular, triangular, and trapezoidal) in a corrugated tube compared to a smooth tube without corrugation. It can be observed that all grooved tubes exhibited higher Nusselt numbers compared to the smooth tube at different Reynolds numbers (10×10^3 to 60×10^3). This is due to the addition of wall grooves to the cylindrical pipe, which leads to higher flow instabilities enhancing convection. The Nusselt number increase is more pronounced in trapezoidal grooves, followed by triangular, circular, and rectangular grooves. This is because trapezoidal grooves have a high surface area, which is beneficial for efficient energy and mass transfer between the fluid and the surface. In addition, the average convective heat transfer coefficients of trapezoidal, triangular, circular, and rectangular grooves were 37.92%, 34.49%, 34.37%, and 34.26% higher, respectively, than those of the smooth tube.

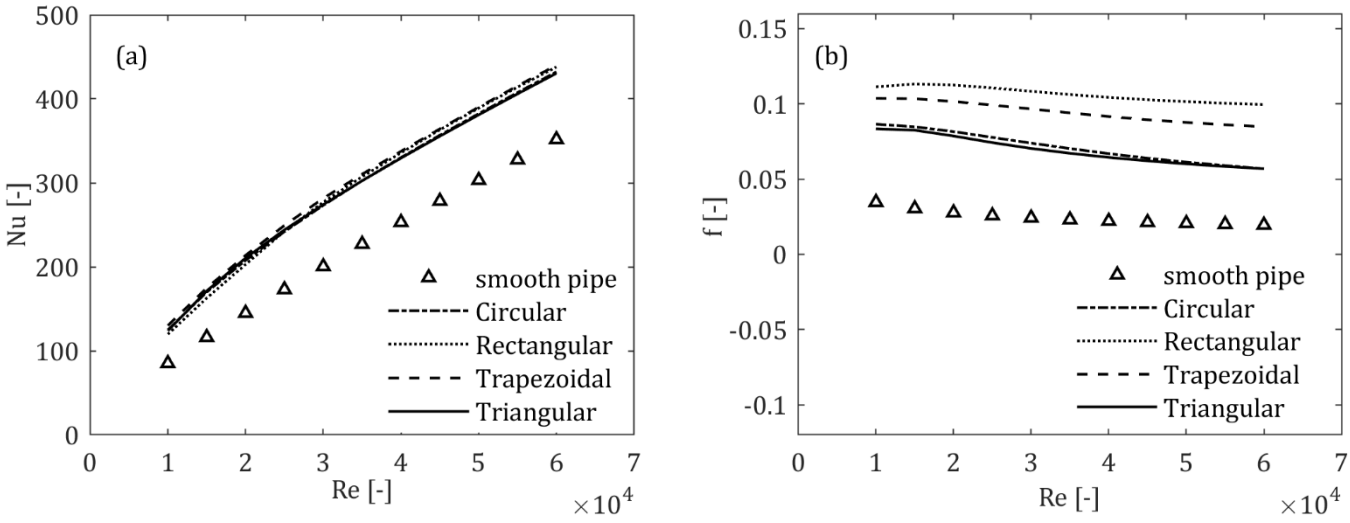

Figure 4. 8: Variation of (a) Nusselt number and (b) friction factor at different Reynolds numbers

It was also noted from Figure 4. 8a that the heat transfer coefficient difference between the different groove shapes ranges from 1 to 9%, respectively, for Reynolds number Re=10×10^3 to 35×10^3. After that, the difference seems to be less than 1%. This indicates that the effect of the groove shape is negligible at higher velocities. This is because the dominance of the turbulent flow minimises the effect of surface irregularities such as grooves. In other words, laminar flow can have

a greater impact on groove shape. As a result, the convective heat transfer coefficient was influenced by overall flow conditions.

As shown in Figure 4. 8b, the investigation of the friction factor is based on two-dimensional flow phenomena and separation using different groove shapes in a turbulent regime (Re $= 10 \times 10^3$ to 60×10^3). It can be stated that the friction factors are significantly higher in grooved tubes than in smooth tubes at different Reynolds numbers. As the Reynolds number increases, the friction factor tends to decrease due to friction losses, but grooved tubes still maintain higher friction factors compared to the smooth pipe. The average increment of friction factor in terms of pressure drop for trapezoidal, triangular, circular, and rectangular groove shapes were 293%, 184%, 193%, and 346%, respectively, compared to the tube without corrugation. This indicates that triangular grooves are effective in exhibiting the lowest pressure drop or pumping power while balancing the enhancement of heat transfer. In addition, the average incremental difference in pumping power of all groove shapes was around 200% at $Re = 10 \times 10^3$ and it almost increased to 400% at Re $= 60 \times 10^3$, compared to the normal tube. This suggests that the heat transfer results at higher velocities consume significantly higher pumping power, which can affect the performance of the single tube heat exchanger.

When fluid flows over grooved surfaces, the local heat transfer coefficient of the wall can vary significantly, and certain regions experience higher heat transfer rates than others. Figure 4. 9 shows the different fluctuations of various groove-shaped heat transfer coefficients across the length of the cylindrical tube. When compared to the other grooves, the rectangular grooves show the highest peaks in the localised enhancement in heat transfer coefficient, specifically at the sharp edges. This is because the groove's sharp edges disrupt the flow chaotically and lead to a high pressure drop and turbulence production, which produced higher heat transfer than other groove shapes.

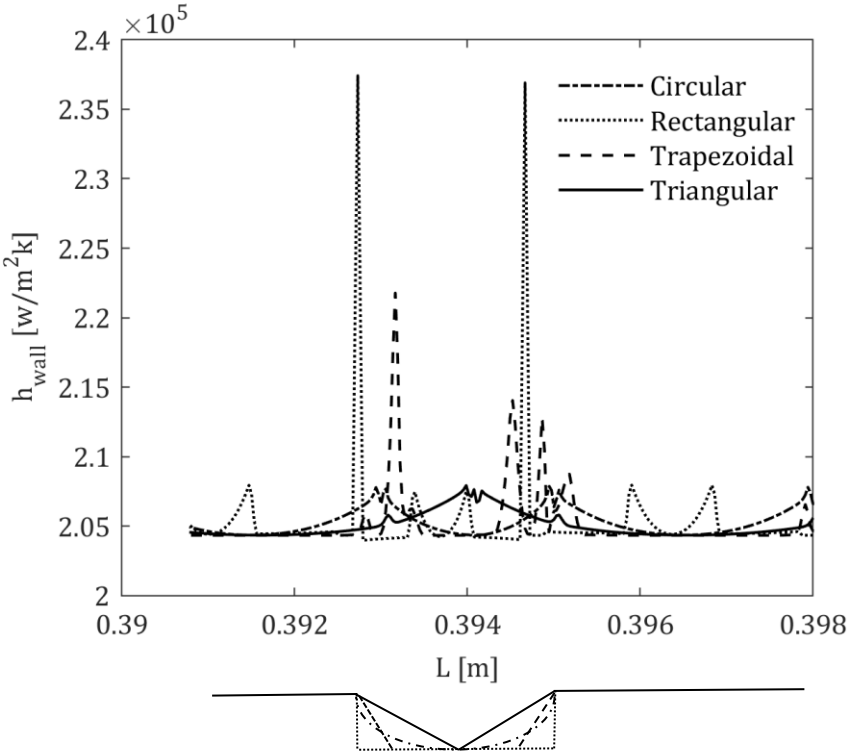

Figure 4. 9: Effect of wall heat transfer coefficient at Re=10,000

However, in this case, the rectangular grooves sharp edges created more recirculation near the wall groove, which negatively affected the performance of the thermal system, as shown in Figure 4. 10. Therefore, rectangular grooves exhibited the least heat transfer enhancement ratio.

The circular and triangular grooves show relatively smaller peaks, indicating a more uniform distribution of heat transfer enhancement but with less turbulent intensity compared to rectangular and trapezoidal grooves. This directly reflects the lowest pressure drop or friction factor obtained. In addition, the trapezoidal grooves also exhibit noticeable peaks of heat transfer coefficient, although they are slightly lower than those of the rectangular grooves. However, trapezoidal grooves have achieved the maximum Nusselt number values compared to the other groove shapes. This is because of the combined effect of rectangular and triangular grooves, which together create a trapezoidal groove shape that generates better vortices and promotes fluid mixing, reducing backflow and potentially improving heat transfer performance, as shown in Figure 4. 10.

As shown below, corrugated tubes provide high values and homogeneity of velocity distribution near the wall region along the length of the tube. The fluid's recirculation for the first groove after the hydrodynamic entrance length is shown in Figure 4. 10 to understand the differences between the various groove shapes in terms of velocity streamlines. It can be seen that the velocity near the wall's recirculation was almost close to zero due to frictional forces and the impact of the groove shape. While the velocity towards the centre of the tube increased to one.

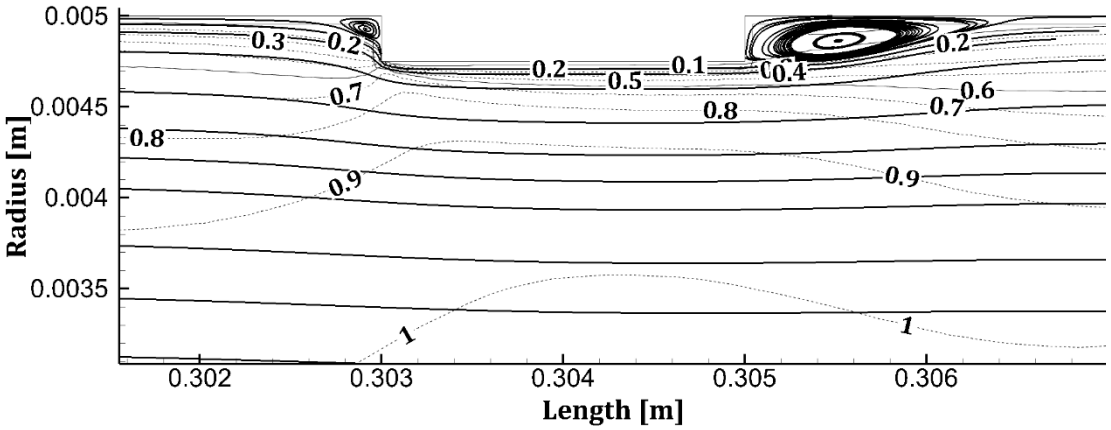

(a)

Rectangular grooves

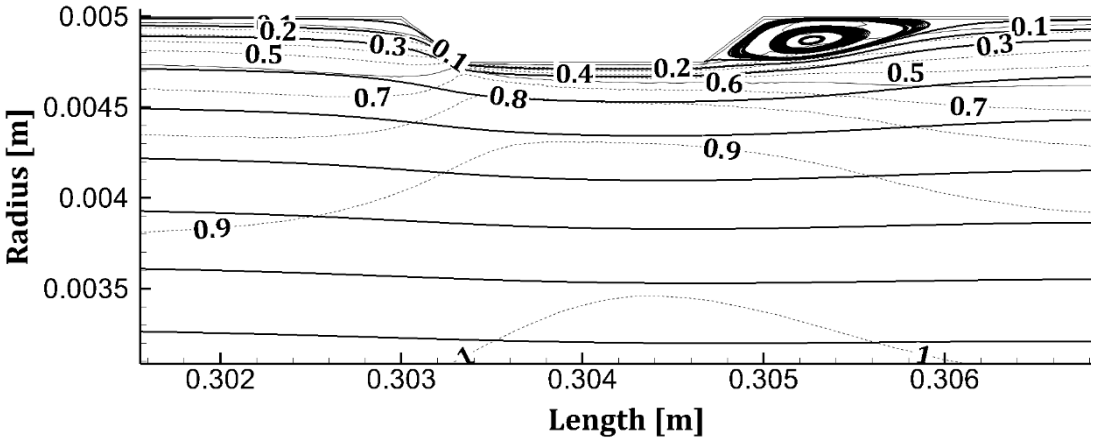

(b)

Trapezoidal grooves

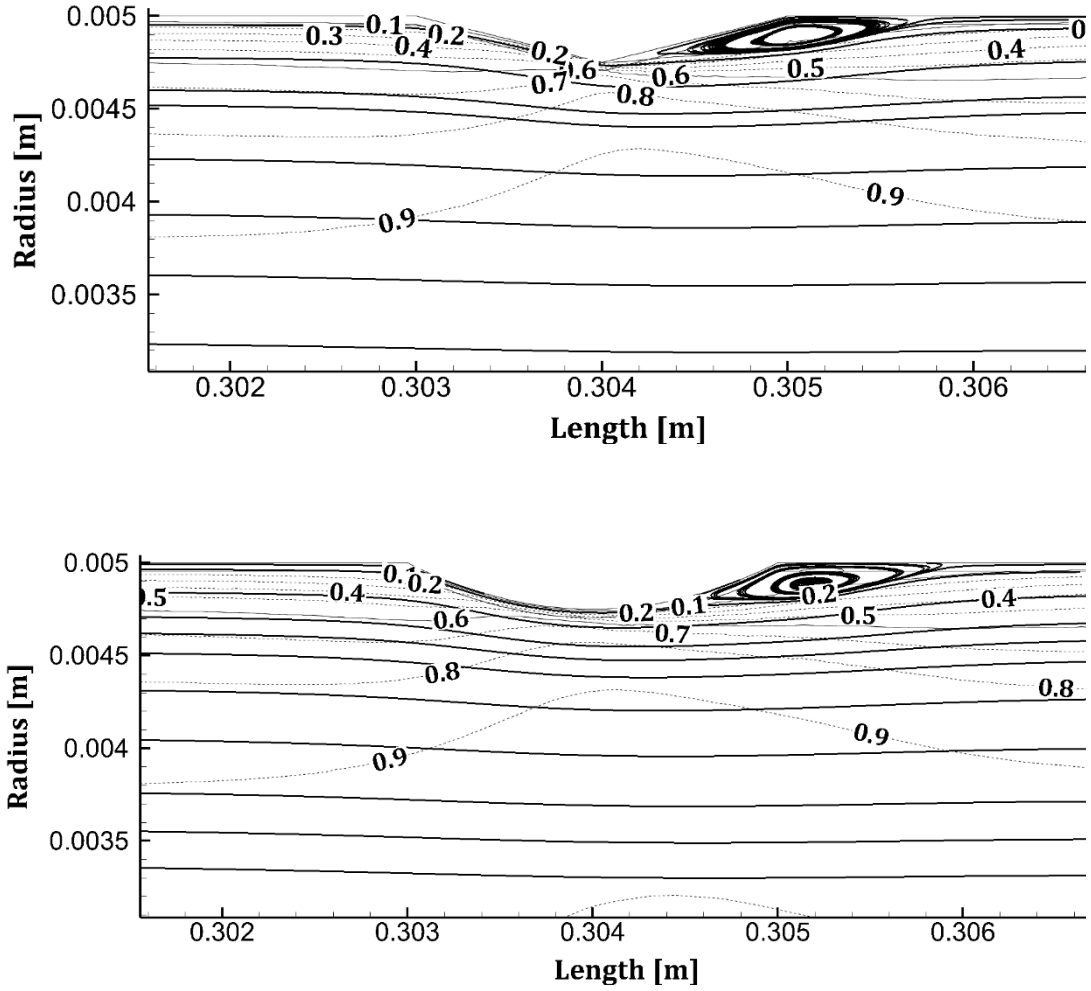

Figure 4. 10: Velocity Streamlines for Various Groove Shapes at Re=10,000

To provide more insight into energy distribution and transfer within the flow field, the turbulent kinetic energy of various groove contours is compared for the first two grooves as shown in Figure 4. 11. These two grooves are placed after the tube's inlet (L = 0.3 m) at a Reynolds number of 10,000. The red region represents the high magnitude TKE along the fluid flow. The magnitude of TKE was higher near the wall region for all grooves. This indicates strong flow mixing and high

convective heat transfer from the wall region to the centre of the tube's axis. It can be observed that the rectangular grooves exhibited the highest turbulent kinetic energy compared to other groove shapes. The trapezoidal grooves also have maximum reflection of turbulent intensity and have relatively reasonable TKE values of the flow, which led to enhanced heat transfer. This is because the base shape width (w/d) is smaller, which means it acts as a converging and diverging section, thereby increasing the fluid's velocity magnitude and reducing the pressure drop simultaneously, which improves convection. In addition, it was also found that TKE increases along the test section length, which clearly indicates an increment in convection.

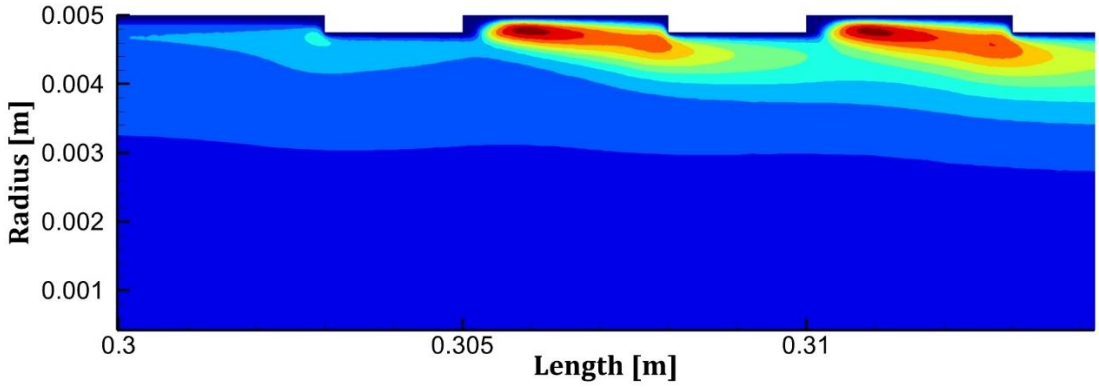

(a)

Rectangular grooves

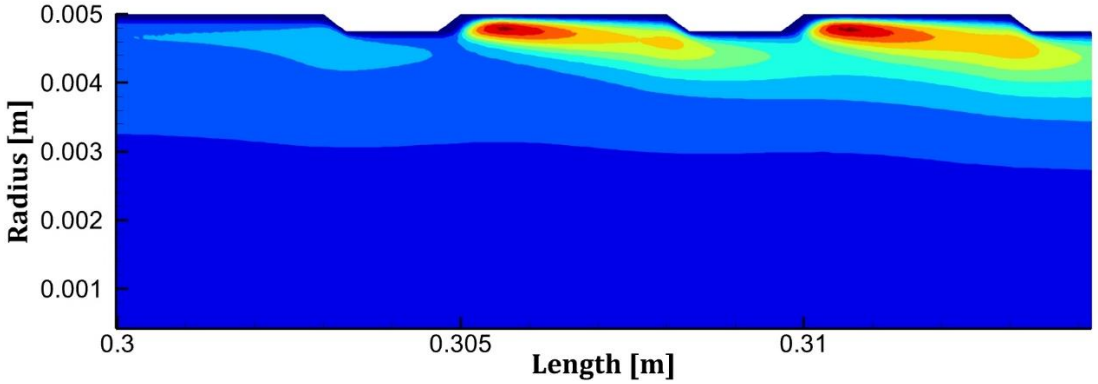

(b)

Trapezoidal grooves

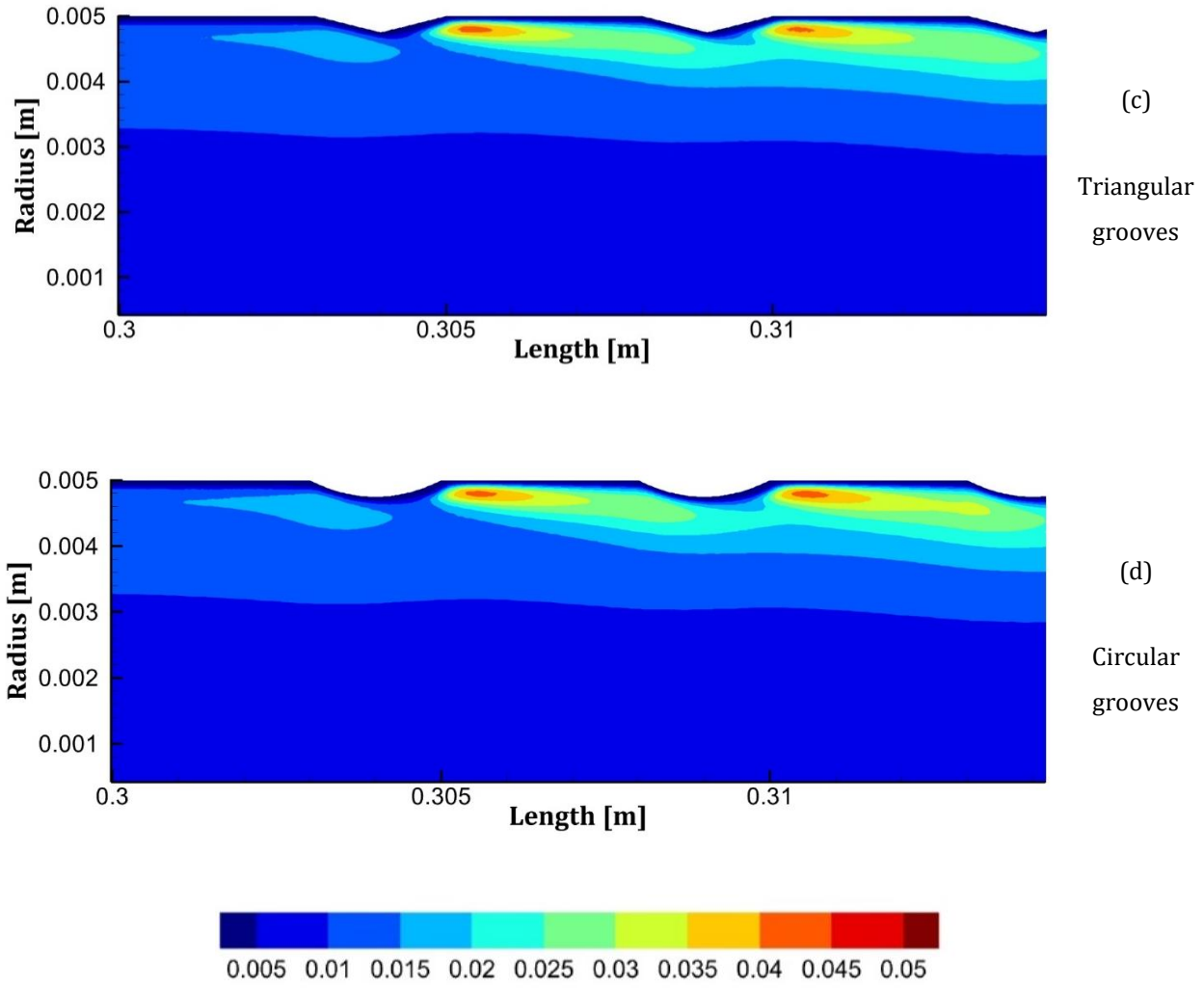

Figure 4. 11: Normalized Turbulent kinetic energy (TKE/u^2) distribution of various groove shapes at Re = 10,000

In Figure 4. 12, the effect of turbulent kinetic energy of different transverse inward groove shapes was compared at different Reynolds numbers ranging from 10,000 to 60,000. For all cases, the turbulent kinetic energy increases with the increase in Reynolds number, indicating the impact of turbulence. The grooved tubes have obtained a drastic enhancement in TKE values compared to the smooth tube. It can also be shown that the rectangular grooves have the highest TKE, causing more flow disruption, even though they do not obtain maximum heat transfer compared to other groove shapes. This indicates that the Nusselt number not only considers turbulence characteristics but is also influenced by various other heat transfer parameters specifically related

to the geometry and flow conditions. In addition, the circular grooves induced the lowest TKE levels.

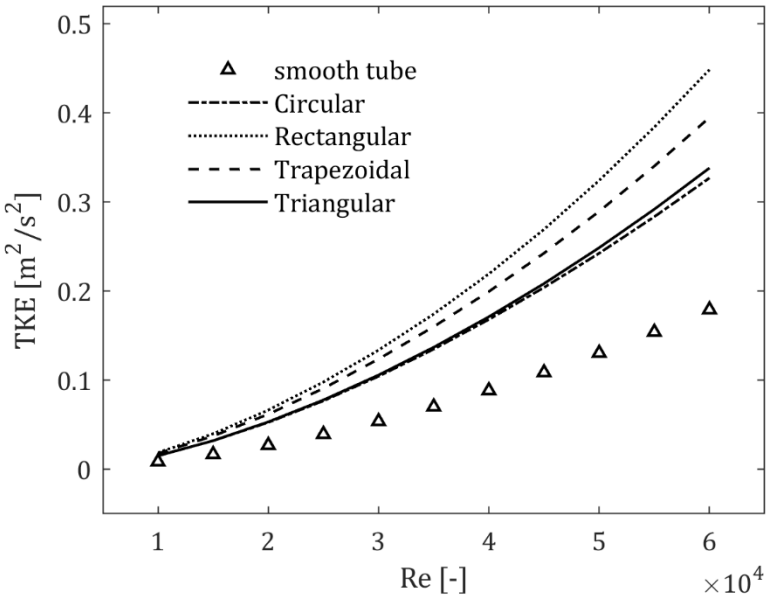

Figure 4. 12: Effect of average turbulent kinetic energy of different groove shapes at Re ranging from 10,000 to 60,000

The variation of wall shear stress (τ) was compared for different grooves with Reynolds numbers ranging from 10,000 to 60,000 in Figure 4. 13. For all cases (both grooved and smooth tubes), shear stress increases as the Reynolds number increases. This is expected because higher Reynolds numbers indicate more unstable flow, which results in higher shear stress. This indicates that higher values of shear stress mean higher flow disruption. However, a peculiar behavior of wall shear stress has been observed for rectangular and trapezoidal grooves, which showed lower shear stress values compared to smooth tubes. For instance, the average shear stress values of rectangular and trapezoidal grooves were 32.6% and 10.78% and were less than the smooth tube without corrugation. This can be due to large flow separations or recirculation occurring near the sharp groove edges. In contrast, triangular and circular grooves have a larger shear stress because the smooth streamlines lead to more momentum transfer and less swirling, which enhances the flow pattern. Therefore, a different groove shape has a different impact on the flow velocity near the surface of the wall, which can act as a barrier by reducing the shear stress values.

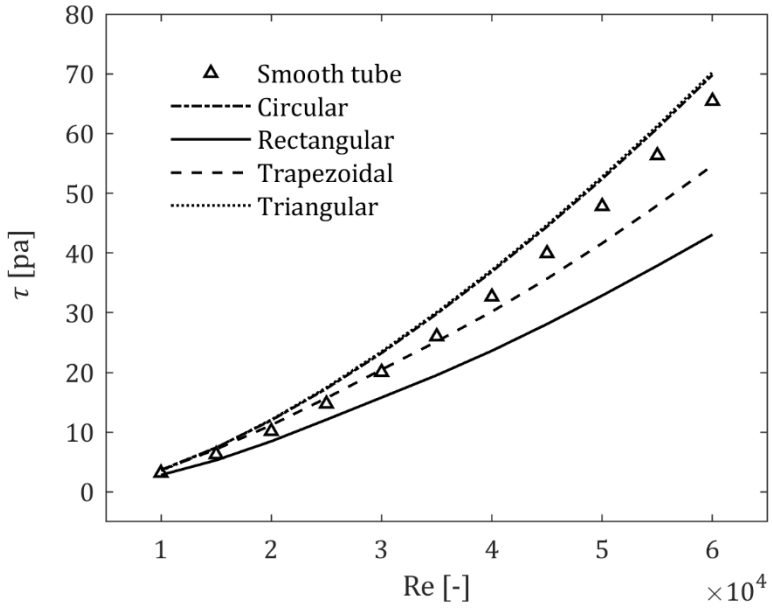

Figure 4. 13: Average wall shear stress distribution at different Reynolds numbers

Figure 4. 14 represents the variance of Nusselt number ratio (groove to smooth tube), friction factor ratio (groove to smooth tube), and PEC for different groove shapes at various Reynolds numbers to better understand the heat transfer and flow resistance. Figure 4. 14a indicates that the ratio of the Nusselt number decreases by increasing the Reynolds number. This suggests that the relative enhancement in heat transfer due to corrugation becomes less significant at higher Reynolds numbers. In addition, the maximum values of Nu_g/Nu_s were obtained for trapezoidal grooves with a heat transfer enhancement of 53.3%, respectively, at Reynolds number 10,000. In contrast, the ratio of f_g/f_s values shown in Figure 4. 14b was significantly less for all groove shapes at Re = 10,000. This is a clear indication of less or minimal pumping power utilised at Re = 10,000. Furthermore, the triangular grooves exhibited the lowest values of friction factor for a wider Reynolds number, ranging from 10,000 to 60,000. The relative increment in f_g/f_s ratio with Re can be due to the increase in the pressure drop or friction resulting from the grooves, which becomes more pronounced at higher Reynolds numbers.

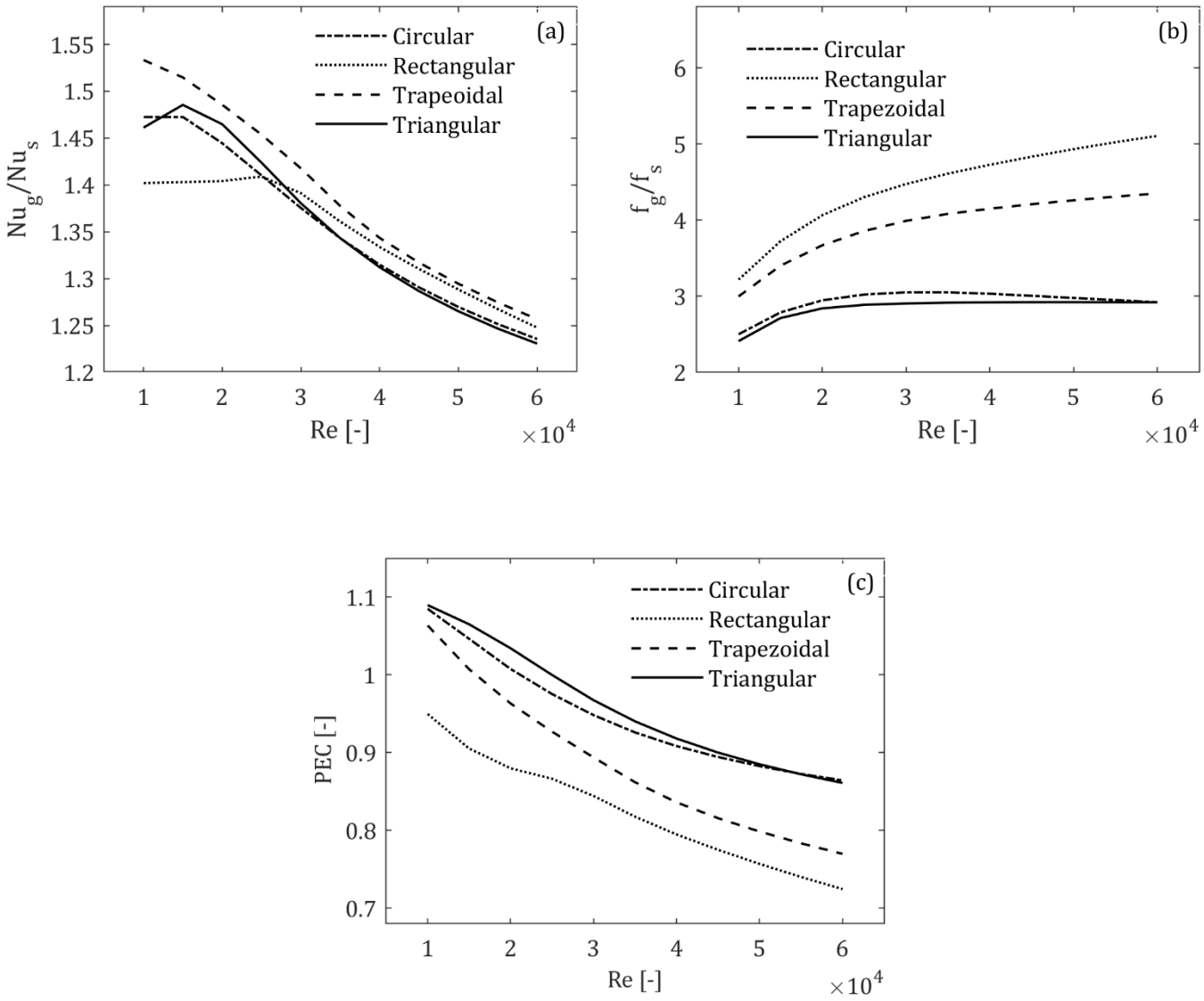

Figure 4. 14: Effect of (a) Nusselt number ratio (b) friction factor ratio (c) PEC of groove shapes at different Reynolds numbers

The enhancement of convective heat transfer performance (PEC) is measured by the ratio of the Nusselt number of the groove to the smooth tube (Nu_g/Nu_s) and the ratio of the friction factor of the groove to the smooth tube (f_g/f_s). Figure 4. 14c shows the PEC decreases with increasing Reynolds number. This suggests that at higher flow rates, the relative enhancement in heat transfer does not compensate for the increased frictional losses as effectively. In addition, the triangular grooves exhibited the highest PEC values compared to other groove shapes. For instance, the maximum increment in the PEC value of triangular grooves was 1.089 times higher than the

smooth tube at Re = 10,000 using water. The optimum Re corresponds to the maximum PEC value in terms of energy savings, making the fluid flow efficient and more suitable for practical applications. It is always better to see the PEC > 1, which represents the enhancement in heat transfer.

4.2.3 Impact of hybrid grooves

This section covers the effect of hybrid groove variations on the convective heat transfer performance. Table 4. 1 covers the six test cases of hybrid grooves as mentioned in Section 4.2. It can be found that in cases 1 to 6, the reason for keeping the circular and triangular groove as the first groove was because these grooves had the least pumping or pressure drop as mentioned in Section 4.2.2. Therefore, the new concept of hybrid groove combinations focuses on contributing to the convective heat transfer improvement without increasing the impact of the pumping power or the pressure drop. This reflects on the intention of strategically modifying the flow patterns that affect the convective heat transfer.

Figure 4. 15 illustrates the performance evaluation criterion (PEC) as a function of the Reynolds number for different hybrid groove combinations compared with the triangular grooves. The triangular grooves were taken as a reference because they exhibited the maximum PEC compared to the groove shapes (rectangular, trapezoidal, and circular) as mentioned in Figure 4. 14. It can be observed that mono-triangular grooves obtained the highest PEC values compared to the hybrid groove test cases for different Reynolds numbers ranging from 10,000 to 60,000, respectively. Case 2 (triangular- trapezoidal) and Case 5 (circular - trapezoidal) also showed relatively high PEC values but slightly lower for Case 3, suggesting good performance but not as optimal as the triangular-circular configuration. It was evident that maximum values of PEC were obtained at Re = 10,000. For example, the average PEC enhancements of case 3 (triangular - circular) and triangular grooves are 8.16% and 8.97%, respectively, compared to the smooth tube at Re = 10,000. In contrast, case 1 (triangular-rectangular), case 4 (circular - rectangular), and case 6 (trapezoidal - rectangular) combinations were not efficient because their PEC values were less than 1, indicating a loss in heat transfer rate. Since the triangular and case 3 (triangular - circular) grooves exhibited

the maximum heat transfer rates at Re = 10,000. It was important to study the thermal and flow behaviour of these grooves compared to the smooth tube without corrugation at Re = 10,000.

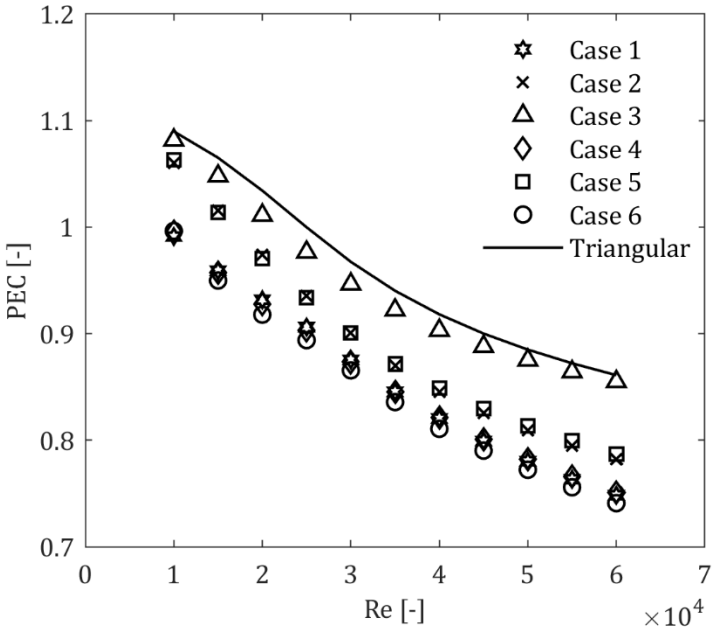

Figure 4. 15: Effect of hybrid groove combinations on PEC

To closely monitor the behaviour of the grooves, the flow and thermal characteristics were examined using an axial line placed 0.0045 m away from the tube's wall for case 3 (triangular-circular) grooves, triangular grooves, and a smooth tube without corrugation, as shown in Figure 4. 16. Figure 4. 16a shows significant fluctuations in local Nusselt number values for the grooved tubes compared to the smooth tube. These peaks indicate regions where heat transfer is highly enhanced due to the presence of grooves, which generate higher turbulence. The spikes in the Nusselt number correspond to the increases in local turbulent kinetic energy shown in Figure 4. 16b, indicating the impact of rapid boundary layer disruption, increased flow instabilities, and mixing that enhance heat transfer coefficients.

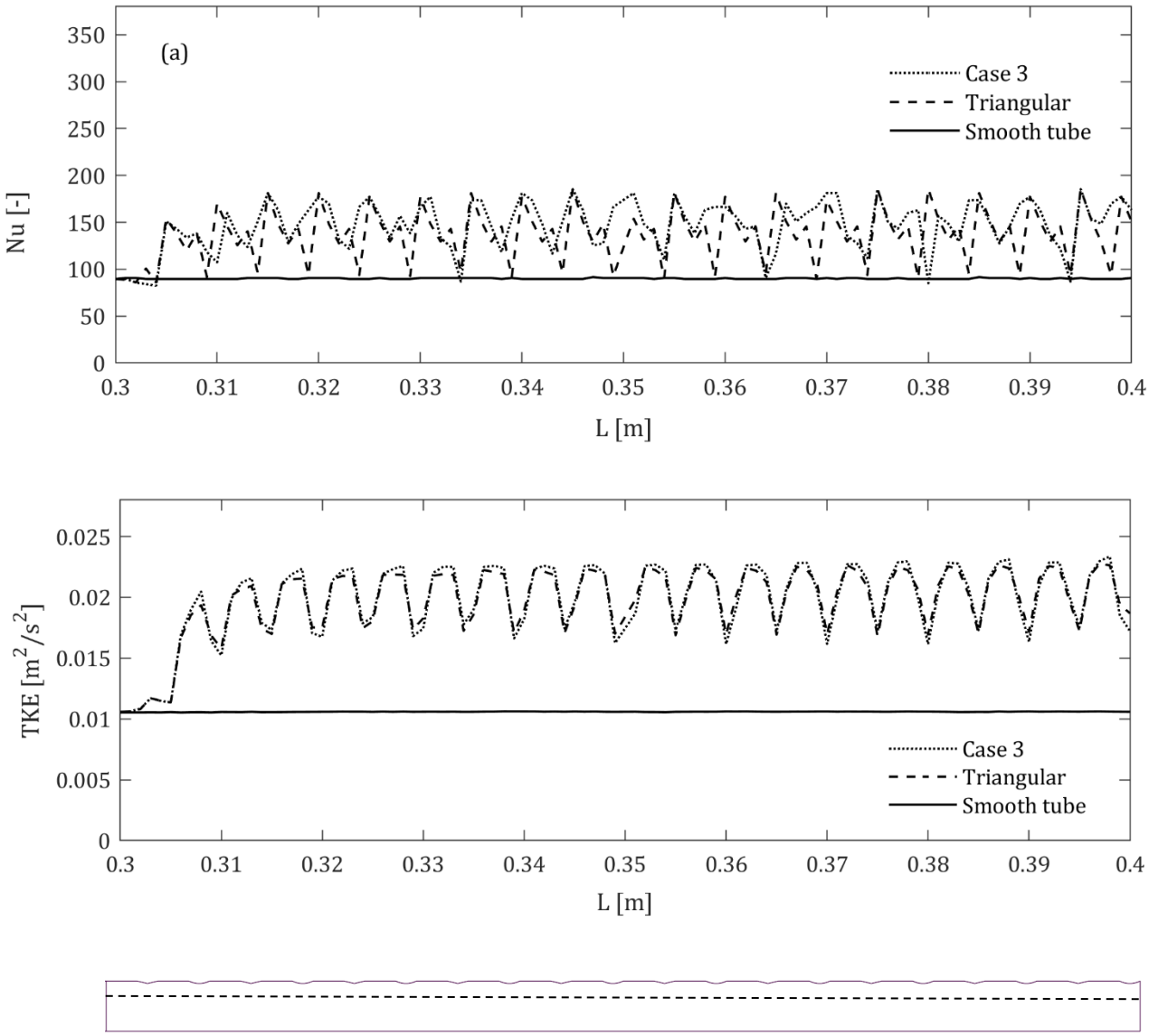

Figure 4. 16: Variation of (a) local Nusselt number and (b) TKE of an axial line placed 0.0045 m away from wall across the tube's length at Re = 10,000

For instance, the average Nusselt number for case 3 (triangular-circular) grooves was 62.4% higher than that of the smooth tube and 10.7% higher than that of the triangular grooves. This improvement is attributed to the larger values of TKE achieved for the case 3 grooves. The maximum values of turbulent kinetic energy were observed at the sharp edges of the grooves, as shown in the contours of Figure 4. 19. It can be observed that near the wall, the values of turbulent

kinetic energy were significantly lower due to the effects of the minimal velocity gradient. In contrast, the smooth tube exhibited relatively constant, lower Nusselt number and turbulent kinetic energy values, indicating less heat transfer enhancement.

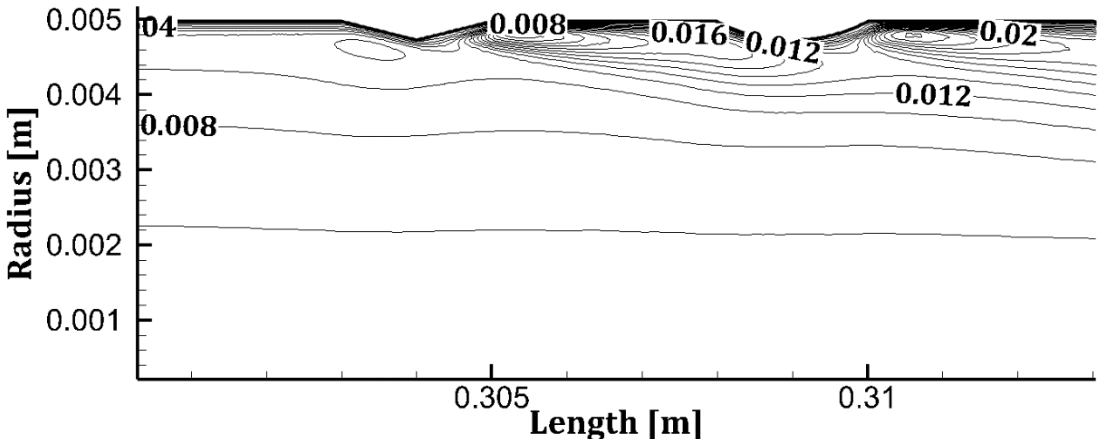

(a)

Case 3 grooves

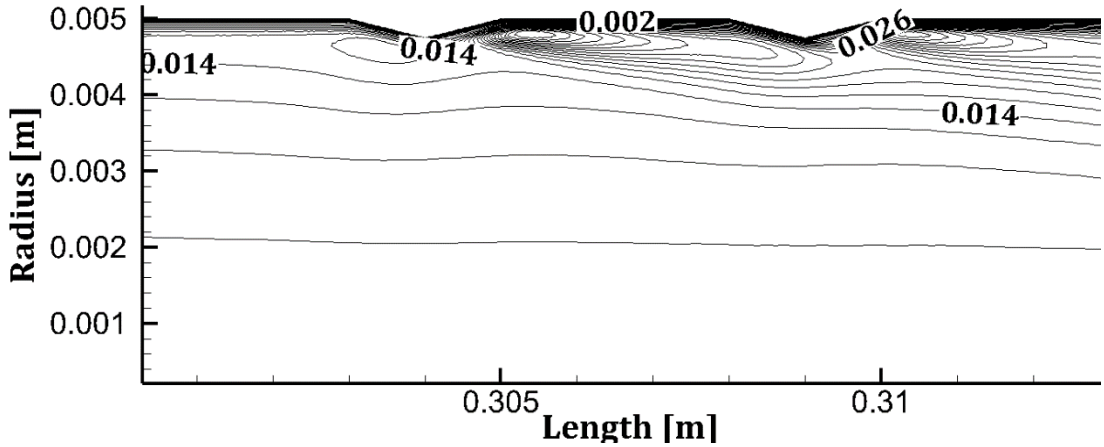

(b)

Triangular grooves

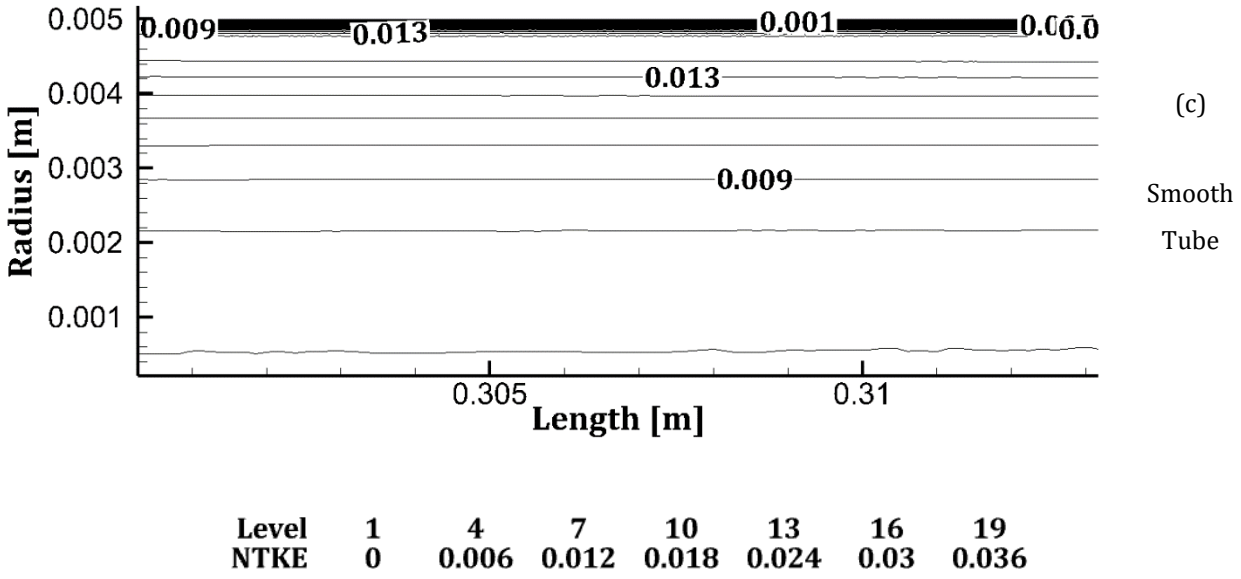

Figure 4. 17: Comparison of Normalized TKE distribution for the first two grooves at Re=10,000

Figure 4. 18 illustrates the variation of the pressure coefficient (cp) along the length of the tube for different configurations such as a smooth tube, triangular grooved tube, and case 3 (triangular-circular) grooved tube of an axial line placed 0.0045 m away from the wall. It can be observed that the pressure coefficient decreases along the tube length for all configurations, indicating a pressure loss along the flow direction at Re = 10,000. The cp values of case 3 (triangular-circular) grooves are consistently higher than those for the triangular grooves and smooth tube. Specifically, the average c_p of case 3 grooves was 9.9% higher than triangular grooves.

In case 3, the presence of sharp edges in triangular grooves and the curvature in circular grooves enhance local flow separation and reattachment, leading to peaks in the cp distribution. This indicates a substantial increase in local pressure drops due to the chaotic flow caused by these geometric features. Therefore, the impact of the groove shape is further reflected in the maximum cp values generated near the groove edges, as shown in the contours of Figure 4. 19, which significantly affect the turbulent kinetic energy.

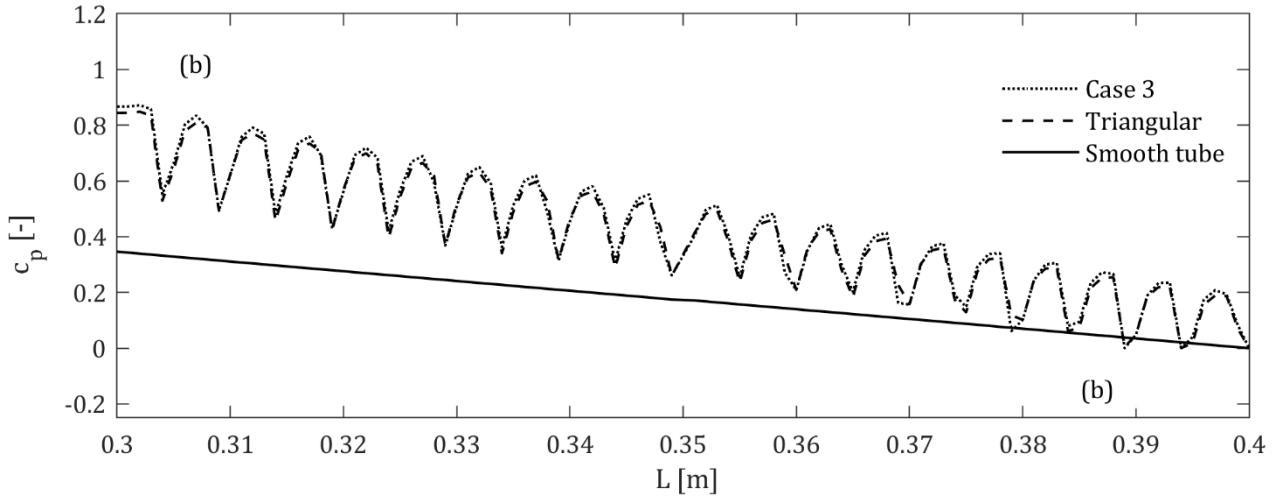

Figure 4. 18: Variation of Pressure coefficient of an axial line placed 0.0045 m away from wall across the tube's length at Re = 10,000

Consequently, the performance evaluation criterion (PEC) for case 3 grooves was lower than triangular grooves. This is because the increased pressure drop, indicated by higher cp values, negatively impacts the overall efficiency of the heat transfer process despite the enhanced heat transfer rates as shown in Figure 4. 15. In contrast, the smooth tube maintained a relatively uniform and lower c_p values, demonstrating less frictional effects compared to the grooved tubes. Additionally, the average variation of pressure drop values for the smooth tube, case 3 grooved tube and triangular grooved tube, at different Reynolds numbers were mentioned in Table 4. 3, indicating the superiority of case 3 grooves.

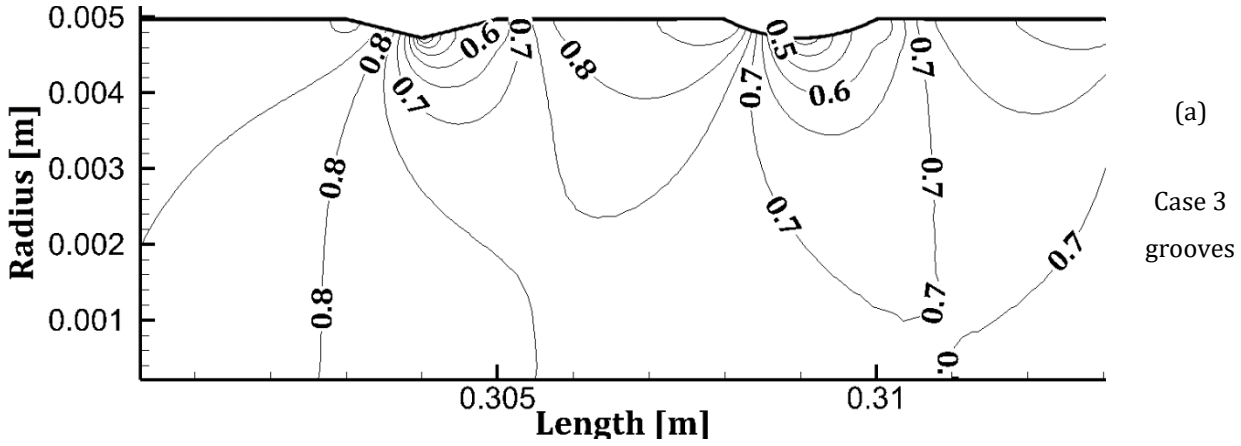

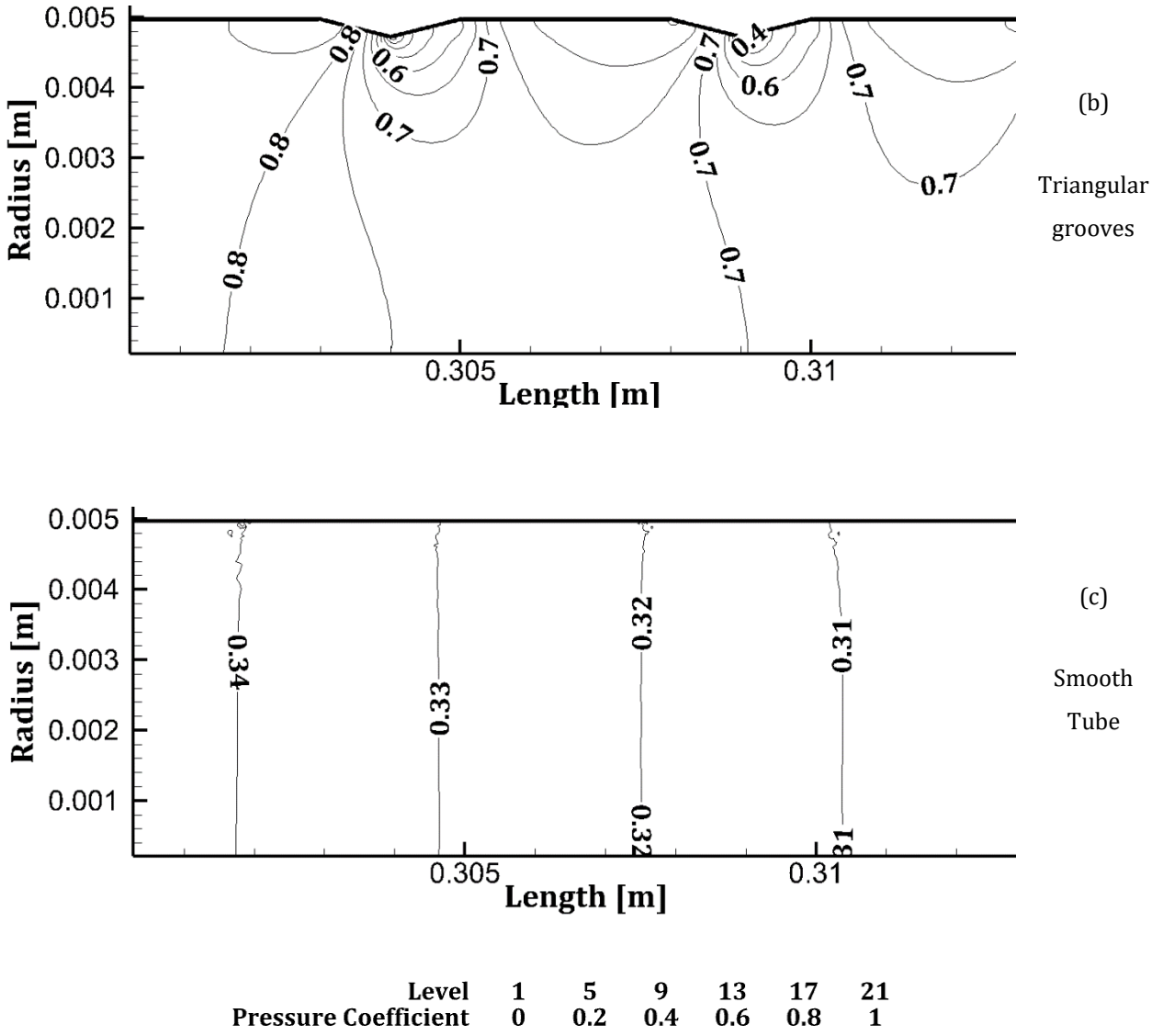

Figure 4. 19: Comparison of pressure coefficient distribution for the first two grooves at Re=10,000

Table 4. 3: Variation of Pressure drop at different Reynolds numbers

	Case 3	**Triangular**	**Smooth tube**
Re	**ΔP (Pa)**	**ΔP (Pa)**	**ΔP (Pa)**
10000	314.2005	305.9005	126.9053
15000	311.2493	302.4954	111.5077
20000	300.6906	288.3388	101.4927
25000	287.3339	272.2212	94.29138
30000	273.6899	258.0085	88.80838
35000	260.7731	246.2114	84.4637
40000	249.0578	236.1785	80.9164
45000	238.6512	227.7113	77.952
50000	229.7635	220.4172	75.44623
55000	222.0996	214.0778	73.30487
60000	215.1289	208.611	71.4447

The effect of fluid temperature along the axial line for a smooth tube, triangular grooves, and case 3 (triangular-circular) grooves at Reynolds numbers of 10,000 was shown in Figure 4. 20. It can be seen that the temperature of the fluid increases along the tube in all cases due to the applied constant heat flux boundary condition. The fluid temperature of corrugated tubes was significantly higher for the smooth tube for tube lengths ranging between 0.3 m and 0.35 m. This can be attributed to the frictional forces generated due to the addition of wall grooves that promoted better heat transfer while effectively dissipating heat. These temperature fluctuations were more pronounced in case 3 than in triangular grooves.

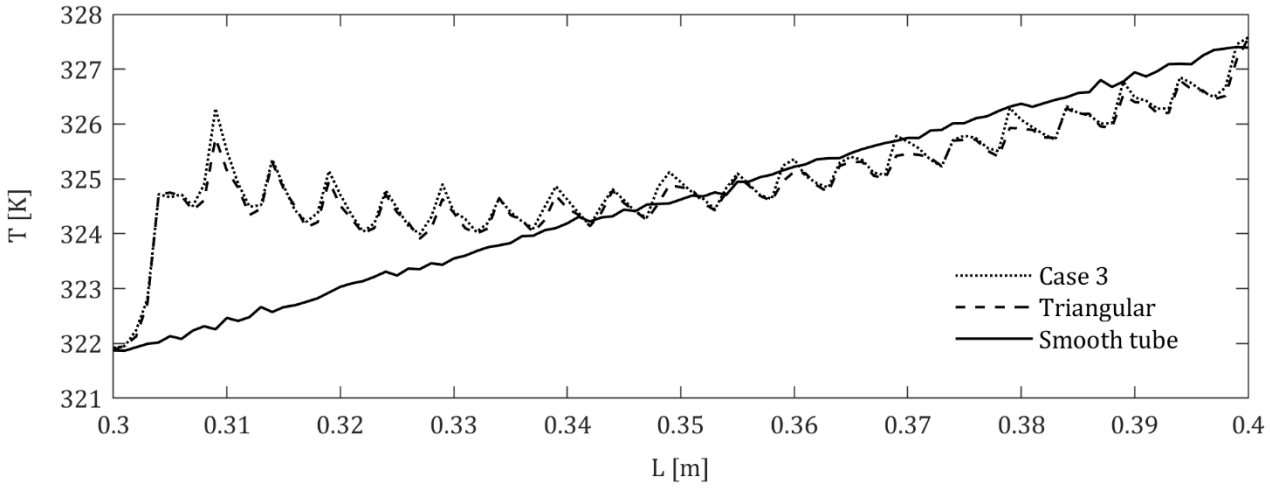

Figure 4. 20: Variation of fluid temperature of an axial line placed 0.0045 m away from wall across the tube's length at Re = 10,000

In contrast, an interesting observation is that the fluid temperature of the smooth tube was consistently higher near the tube's wall compared to the grooved configurations, especially towards the end of the tube. This suggests that the impact of the grooves towards the end of the tube was less effective due to the produced recirculation. However, the average increment in fluid temperature of case 3 and the triangular grooves were 0.13% and 0.1% higher than the smooth tube along the flow direction, suggesting an overall increment in Nusselt number.

Table 4. 4 presents the wall shear stress (τ) values for case 3 (triangular-circular grooves), triangular grooves, and a smooth tube across various Reynolds numbers (Re) ranging from 10,000 to 60,000. It can be observed that the wall shear stress is higher for case 3 grooves, similar to the pressure drop compared to the other combinations at Re = 10,000. The average increment in wall shear stress values of case 3 grooves and triangular grooves were 13.9% and 11.9% higher than a smooth tube. This indicates that the circular component in case 3 significantly altered the shear stress. However, the average shear stress of triangular grooves was slightly larger than case 3 grooves for a specific range of Reynolds numbers (10,000 to 60,000).

Table 4. 4: Variation of wall shear stress at different Reynolds numbers

	Case 3	**Triangular**	**Smooth tube**
Re	**τ (Pa)**	**τ (Pa)**	**τ (Pa)**
10000	3.609636	3.547671	3.168857
15000	7.390477	7.389037	6.265159
20000	12.00836	12.07566	10.1412
25000	17.34022	17.47583	14.74301
30000	23.31582	23.50001	20.04415
35000	29.86806	30.07636	26.0219
40000	36.93173	37.1566	32.65408
45000	44.47667	44.71728	39.92155
50000	52.49947	52.77173	47.81534
55000	61.00303	61.28846	56.32704
60000	69.9825	70.27152	65.44042

Based on the above results, it can be concluded that hybrid grooves were less effective than the mono-grooves because they exhibited lower thermal performance factor values.

4.3 Summary

In this chapter, the heat transfer effects of different grooved tubes (rectangular, circular, triangular, and trapezoidal grooves) along with a straight tube were studied with water at $Re = 10 \times 10^3 - 60 \times 10^3$ under a forced convection. In addition, the effects of hybrid grooves were further investigated to assess the thermo-hydraulic performance of the single tube heat exchanger.

The following conclusions are summarised:

- The numerical models, validated against empirical data, provide reliable predictions of heat transfer and pressure drop for smooth and grooved tube configurations. The 2D simulation results align closely with the experimental data, demonstrating a reliable balance of accuracy, cost-effectiveness, and computational efficiency. Additionally, the RKE turbulence model outperformed the SST model, though the SST model still provided useful Nusselt number predictions despite its inability to accurately predict pressure drop at high Reynolds numbers.

- The convective heat transfer coefficient and friction factor of grooved tubes were observed to be higher compared to smooth tubes, with variations depending on groove shapes. Among these, trapezoidal grooves appeared to exhibit the highest Nusselt number, while triangular grooves showed better heat transfer performance (PEC), primarily due to their lower friction factor. The grooved tubes also influenced wall shear stress and turbulent kinetic energy.

- The introduction of hybrid grooves offers a potential approach for enhancing convective heat transfer by altering flow patterns. The findings suggest that Case 3 (triangular-circular) grooves provided better heat transfer performance compared to six different configurations. However, the mono-triangular grooves outperformed the hybrid grooves, indicating that the increased complexity of hybrid grooves may not always lead to better performance.

Hence, the addition of grooves to the cylindrical tube simply operated as a micro vortex generator that enhanced convection.

Chapter 5: Geometrical Effects - Optimisation of the Rectangular Groove

The aim of this chapter is to investigate the corrugated tube with rectangular grooves using the optimisation strategies (design constraint) to further reduce pressure drop conditions. This aligns with Objective 3 outlined in Section 1.2 of Chapter 1. The rationale for selecting rectangular grooves for design optimization, compared to other grooves, was that they exhibited the highest friction factor and pumping power, as mentioned in Chapter 4. This provides a scope to reduce maximum values of pressure drop while maintaining an effective convection rate, making it suitable for real-world heat transfer applications.

The novelty of this chapter lies in the energy optimisation achieved by replacing the sharp edges of the rectangular grooves with curved edges within the corrugated tube. The study examined fifteen transversely corrugated tubes containing different groove radii under a 2D turbulent forced convection using water. To better understand the flow and thermal field distribution, the effects of convective heat transfer coefficient, pressure reductions, thermal performance factor, wall shear stress, and turbulent kinetic energy were reported for different combinations of groove radii. Additionally, the impact of velocity streamlines and turbulent kinetic energy contours on heat transfer was also highlighted for Reynolds numbers ranging between 10,000 and 60,000.

5.1 Model description

This numerical study investigates the thermal and hydraulic characteristics of the corrugated tubes with different transversely distributed groove configurations for different radii r_1 and r_2 under a constant heat flux condition. A schematic representation of the 2D model is shown in Figure 5. 1. The dimensionless roughness parameters of the rectangular grooves were expressed as: the ratio of the groove depth to the tube diameter (e/d = 0.025); the ratio of the groove width to the tube diameter (w/d = 0.2); and the groove pitch to the tube diameter (p/d = 0.5) were considered for this study. These were optimal for achieving high convective heat transfer performance among the

nineteen groove combinations [18]. In addition, the tube material was assumed to be isotropic and homogeneous. Additionally, the tube wall's thermal conductivity was constant and unaffected by temperature.

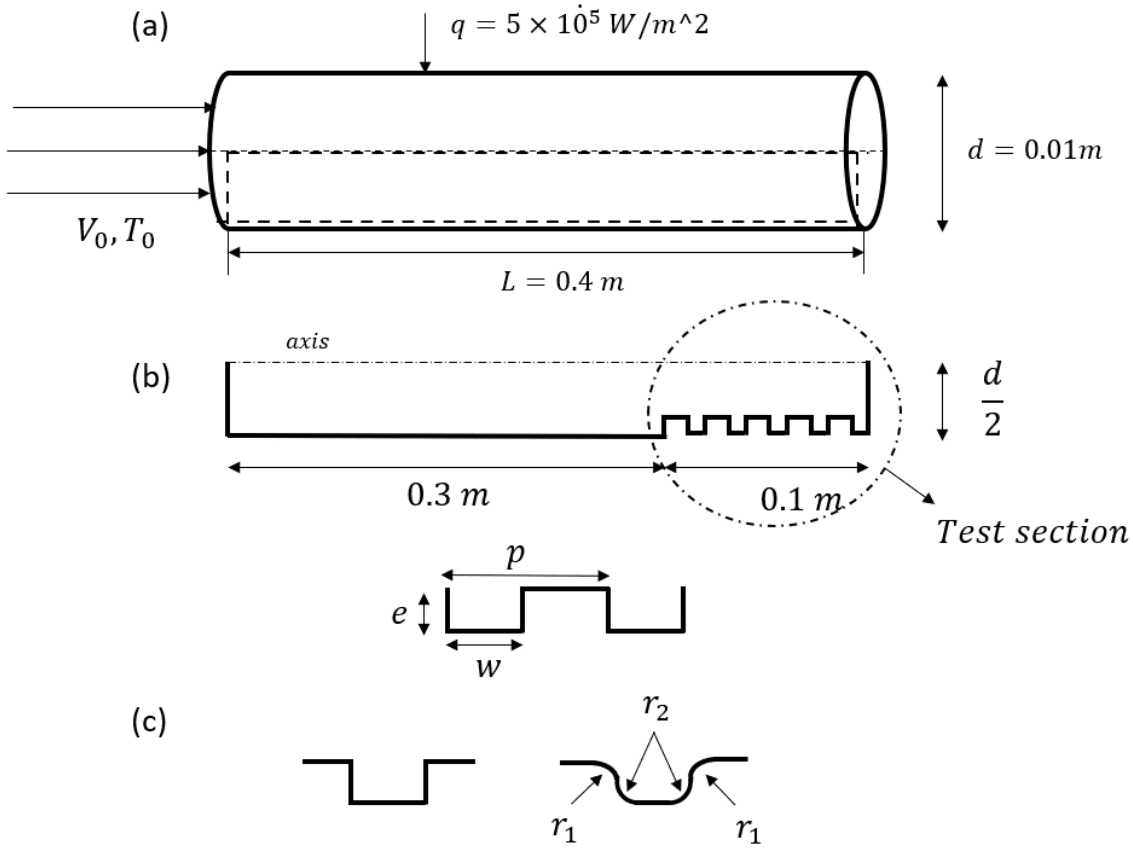

Figure 5. 1: Computational models a.) Cylindrical tube b.) Cylindrical tube with rectangular grooves (e/d=0.025, w/d=0.2, p/d=0.5, N=20 grooves) c.) Rectangular groove radii r_1 and r_2

The circular tube's rectangular groove radii r_1 and r_2 were also varied to investigate the effective combination of pressure drop and convective heat transfer. These two radii were divided into various combinations consisting of sharp edges (r_1=0 or r_2=0), equal radii (r_1=r_2), and different radii (r_1>r_2 or r_1<r_2). Table 5. 1 lists the range of radius parameters used in this CFD-based analysis. It should be noted that the maximum groove radius is half of the groove depth ($r_{1,2} \leq \frac{1}{2}e$). This is because the radii of the grooves were determined by the depth of the rectangular grooves, which was constrained to 0.25 mm. By dividing the groove's depth equally, the top half groove edge

contributes to r_1 and the bottom half to r_2, resulting in fifteen combinations. This approach allows for a comprehensive examination of groove configurations while maintaining structural integrity.

Table 5. 1: Rectangular Groove Radii Combinations

Combination	**Radius r_1 (mm)**	**Radius r_2 (mm)**
Sharp Edges ($\boldsymbol{r_1}$=0 or $\boldsymbol{r_2}$=0)	0.045	0
	0.085	0
	0.125	0
	0	0.045
	0	0.085
	0	0.125
Equal Radii ($\boldsymbol{r_1}$=$\boldsymbol{r_2}$)	0.045	0.045
	0.085	0.085
	0.125	0.125
Different Radii ($\boldsymbol{r_1}$>$\boldsymbol{r_2}$ or $\boldsymbol{r_1}$<$\boldsymbol{r_2}$)	0.045	0.085
	0.045	0.125
	0.085	0.045
	0.085	0.125
	0.125	0.045
	0.125	0.085

5.1.1 Boundary conditions

The boundary conditions used in the numerical simulations are the same as those in Section 4.1 of Chapter 4. Also, a constant heat flux ($5 \times 10^5\ W/m^2$) and a no-slip condition were introduced on the tube's wall. At the outlet, the gauge pressure $P_{guage} = 0$ was stated. The flow and thermal fields were axisymmetric to the horizontal plane, with a specified hydraulic diameter of $d_h = 0.01m$ and a length of $L = 0.4\ m$ at varying Reynolds numbers. The inlet temperature was maintained at $T_{in} = 300K$, and a medium turbulent intensity of 5% was imposed. Finally, the flow was thermally and hydrodynamically fully developed at the tube's end.

5.1.2 Mesh Sensitivity test

Extensive computational simulations were conducted for the rectangular grooves mesh as shown in Figure 5.2 to identify the optimal grid density, ensuring the accuracy and consistency of the numerical results. Table 5. 2 displays the numerical results for the Nusselt number and friction factor for fully developed flow inside a corrugated tube with rectangular grooves at a Reynolds number of 10,000. The number of mesh cells is rounded to the nearest hundred for accurate comparison. As the mesh cell count ($N_x \times N_y$) increases, the differences in the Nusselt number (Nu) and friction factor (f) decrease. This indicates that the results are converging, and further increasing the grid density does not significantly affect the results. The grid with 380,000 cells shows a minimal percentage difference of 0.02% for Nu and 0.05% for f compared to the grid with 480,000 cells, which is considered the reference. This suggests that the 380,000-cell grid is sufficiently dense to produce accurate and reliable results without further refinement. Additionally, the simulations maintained a y+ value of less than one to capture effects near the wall region. The components of radial temperature, velocity, and turbulent kinetic energy were also checked for the non-uniform grid with 380,000 cells.

a. b.

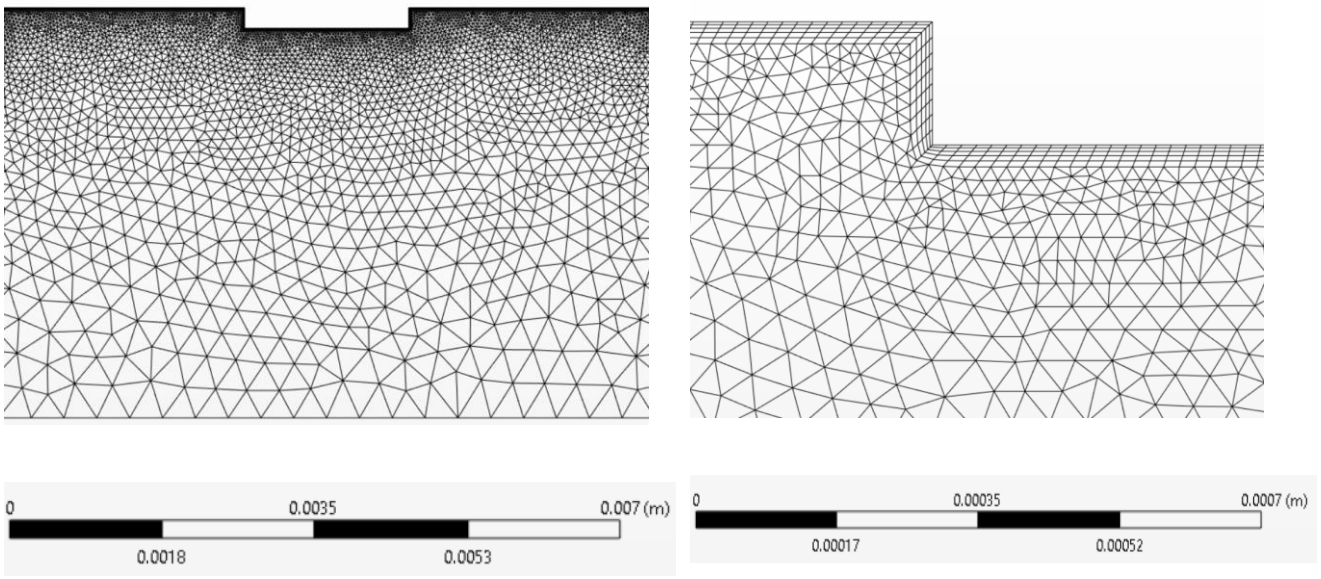

Figure 5. 2: Visualisation of the 2D Mesh of a Rectangular-Grooved Cylindrical Tube. (a) Full Geometry, (b) Near Wall

Table 5. 2: Mesh Independence test of the rectangular grooved tube at Re=10,000 using water at 300K

S. no	Cells ($N_x \times N_y$)	Nu	Nu % Difference	f	f % Difference
1	80000	124.2152	2.14	0.119681	4.51
2	180000	124.4816	1.43	0.114522	1.93
3	280000	124.6599	0.59	0.112346	0.87
4	380000	124.73351	0.02	0.111372	0.05
5	480000	124.7584	-	0.110817	-

5.1.3 Validation

Figure 5. 3 presents a comparison of rectangular grooves inside a corrugated tube with groove parameters of e/d = 0.025, w/d = 0.2, and p/d = 0.5 against published data. The simulated Nusselt number results for Reynolds numbers ranging from Re = 10,000 to 60,000, using the RKE model, are compared with published data from Kaood, et al. [19] and Mohammed, et al. [18], with an average difference of -6% and -4%, respectively, demonstrating good agreement. The observed deviations range from a maximum of -9% to a minimum of -2%, with the negative sign reflecting an underestimation of the simulated data compared to the referenced studies. The effect of friction factor at different Reynolds numbers is shown in Figure 5. 3b. The average error percentage of the present study was around 4% and -4% when compared to Kaood, et al. [19] and Mohammed, et al. [18]. The maximum and minimum deviations were -11% and 2%, respectively. Therefore, the comparison of all simulated results with published data indicates minimal deviations, demonstrating the high reliability of the present research findings.

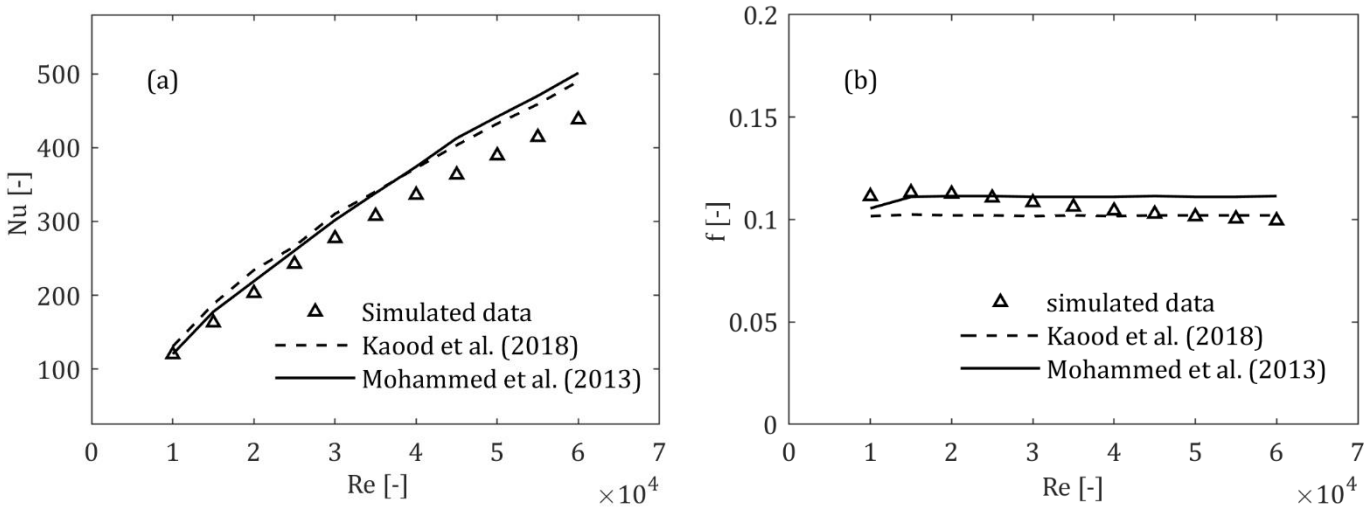

Figure 5. 3: Comparison of simulated (a) Nu (b) f results with the published data using a rectangular grooved tube with e/d=0.025, w/d=0.2 and p/d=0.5

In addition, an exceptional case was observed in Figure 5. 3b. The friction factor tends to increase between Re = 10,000 and 20,000. After that, the flow profile exhibits a decreasing trend. This was due to the impact of high turbulent intensity generated by the rectangular grooves. The average friction factor of the rectangular groove was 3.46 times greater than that of the smooth tube, with a 34.26% enhancement in heat transfer from $Re = 10 \times 10^3$ to 60×10^3. In addition, the maximum increment in Nu of 40.66% was found at Re = 10,000. This showed that the rectangular groove shape has a more significant impact on heat transfer at low Reynolds numbers.

5.2 Results and Discussion

This section covers the effects of different groove radii r_1 and r_2 variations, on the convective heat transfer parameters. This means the impact of heat transfer coefficient, friction factor, and thermal enhancement factor were thoroughly discussed to understand the impact of the pressure drop variation on convection.

Figure 5. 4 represents the heat transfer coefficient distribution with various Reynolds numbers for groove combinations of sharp edges, different radii, and equal radii compared with the actual rectangular groove. Results reveal that the heat transfer coefficient was sensitive to the groove radius. For almost all instances, the heat transfer coefficient of radii to the actual rectangular groove ratio, h_r/h_g values, were greater than 1, which represents the dominance of groove curvature, indicating enhancement in convective heat transfer. The purpose of utilising the ratios of heat transfer coefficients rather than absolute values was to ensure the normalisation of the data, enabling comparisons at various scales and conditions. This method minimises the influence of specific parameters, enabling a broader applicability of results and promoting the development of generalised models. Such an approach enhances the overall comprehension of convective heat transfer phenomena.

In Figure 5. 4a, it was found that varying the radius r_1 while keeping r_2 at 0 mm resulted in more effective heat transfer than the reverse configuration. This was because most of the recirculation occurred near r_1. Increasing r_1 significantly reduced reverse flow, as shown in the velocity streamlines in Figure 5. 6[a-c], thus enhancing overall convection. Conversely, the average heat transfer coefficient did not increase with a larger r_2. This indicates that the primary cause of

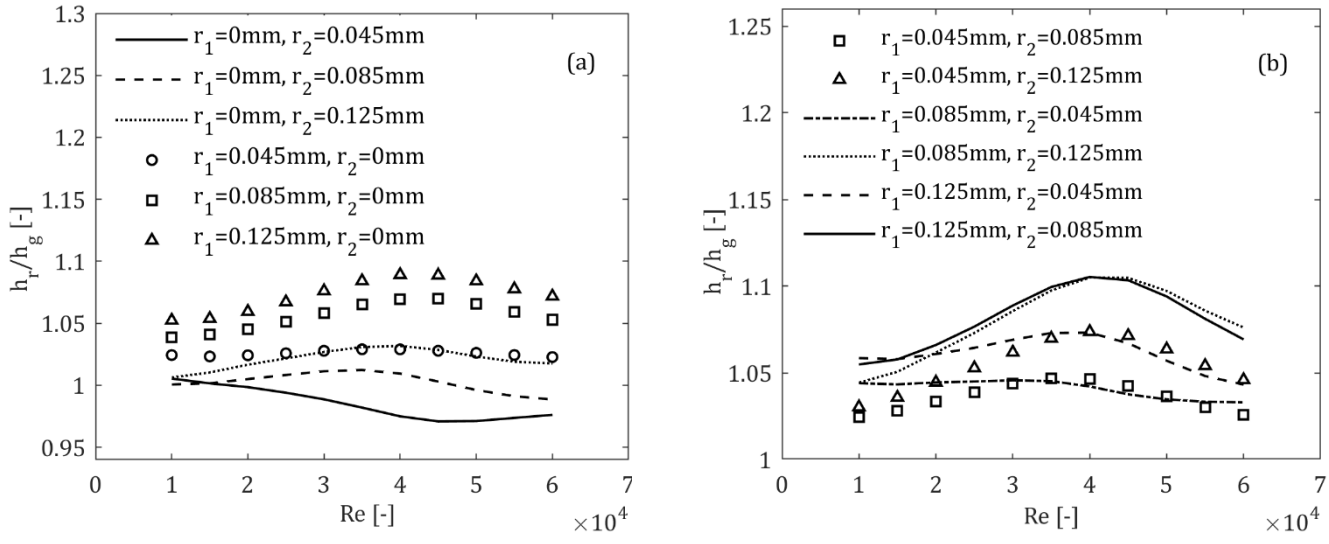

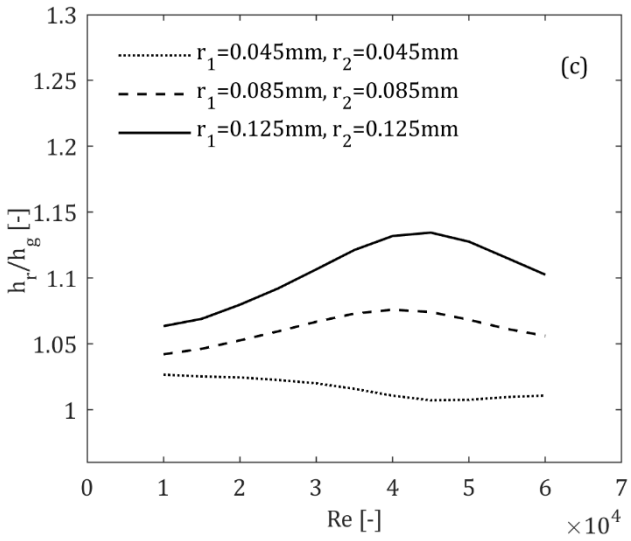

Figure 5. 4: Variation of heat transfer coefficient ratio for different groove combinations (a) sharp edges (b) different radii (c) equal radii.

reduced heat transfer efficiency was the diminished surface area at the base of the rectangular groove. This means that the radii at the base of the rectangular groove did not contribute significantly to heat transfer enhancement. Nonetheless, combinations of varying the radius r_2 while keeping r_1 at 0 mm are not entirely ineffective. In fact, at larger r_2 radii, results showed a 2% increase in heat transfer compared to the original rectangular groove. However, at smaller radii of r_2 = 0.045 mm, 0.085 mm, the heat transfer improvements were minimal. Therefore, the findings suggest that r_1 is the primary contributor in enhancing heat transfer and reducing recirculation, while the impact of r_2 was less significant.

Similarly, Figure 5. 4b depicts the combined effects of different radii r_1 and r_2. The groove configurations with larger radii (r_1 = 0.085 mm with r_2 = 0.125 mm and r_1 = 0.125 mm with r_2 = 0.085 mm) demonstrated significant performance improvements, showing heat transfer enhancements of 8% and 8.2%, respectively, compared to the actual rectangular grooved tube. In contrast, a smaller r_2 of 0.045 mm had a minor impact on heat transfer enhancement. Furthermore, equal groove radii of r_1 = r_2 = 0.125 mm exhibited the highest average heat transfer increment of 10.4% among all configurations, as shown in Figure 5. 4c. In fact, maximum heat transfer was obtained at Re=45,000 with a 13.4% heat transfer enhancement. Therefore, the addition of groove curvature had a significant impact on convection.

The influence of geometrical parameters on the pressure drop for various radii combinations is presented in Figure 5. 5. It is evident that the pressure drop decreases with the increase in groove radii at different Reynolds numbers. Specifically, the pressure drop reduced with the increments in r_2 while maintaining r_1 at 0 mm. For example, the average pressure drop decreased from 1.30% to 10.76% as r_2 increased from 0.045 mm to 0.125 mm for Reynolds numbers ranging from 10,000 to 60,000, respectively. This reduction was due to the addition of the groove curvature at the base of the rectangular groove, which minimised turbulence and reduced the fluid intensity around the corner as shown in velocity streamlines in Figure 5. 6[e-f]. As r_2 increased, the major vortex became more stable, moving the core fluid away from the wall. This stabilisation near the inner wall's surface promoted a more efficient flow, reduced pressure drop, and enhanced convection even at high velocities. Thus, optimising r_2 is essential for saving pumping power and improving system efficiency.

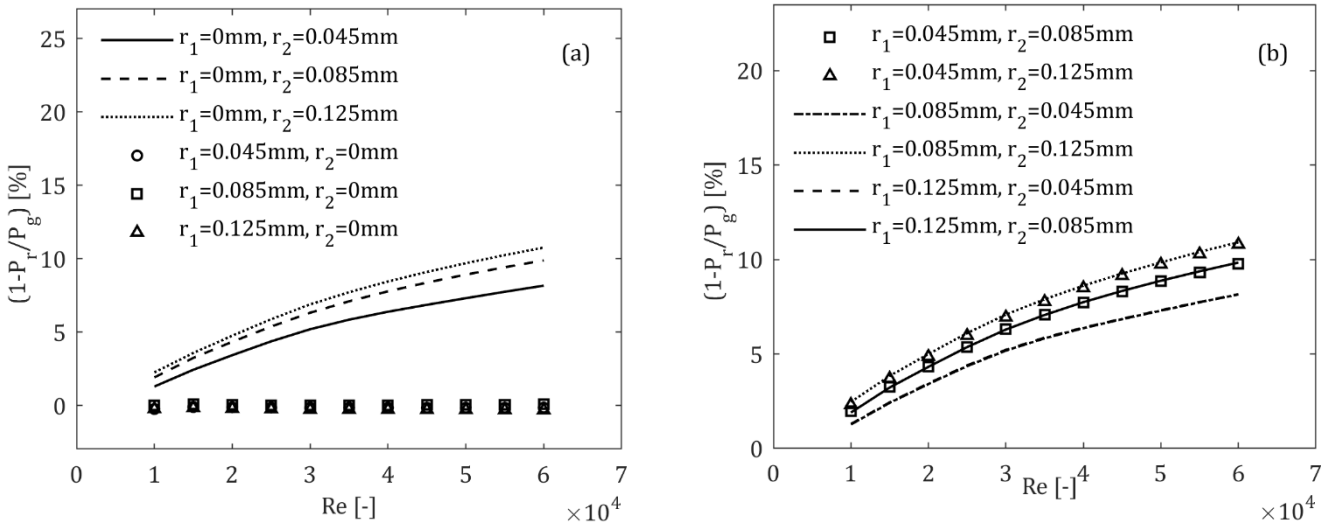

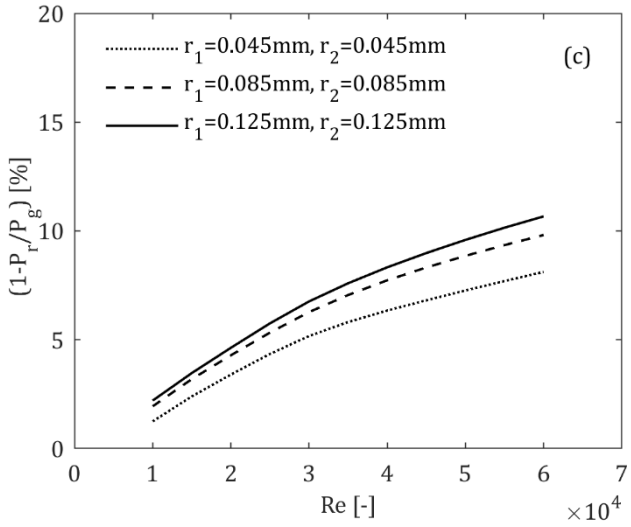

Figure 5. 5: Variation of pressure drop reductions for different groove combinations (a) sharp edges (b) different radii (c) equal radii.

Conversely, altering r_1 while keeping r_2 at 0 mm seemed to have less impact on the pressure drop despite significantly enhancing the convective heat transfer by minimising secondary flow patterns. Also, the combination of different radii resulted in significant pressure reductions, particularly at larger radii. Notably, the maximum pressure drop reduction was achieved with larger r_2 values. For instance, at r_1 = 0.045 and 0.085 mm with r_2 = 0.125 mm, the pressure drop reductions were 7.28% and 7.40%, respectively. Additionally, the highest heat transfer coefficient obtained for equal radii r_1=r_2 of 0.125 mm had a maximum average pressure reduction of 7.1%, respectively.

The impact of varying groove radii on the velocity streamline patterns within the grooved tube was explored. By examining these patterns, we can better understand how different geometric configurations influence fluid flow behaviour and ultimately affect heat transfer performance. Figure 5. 6 presents the velocity streamline patterns for various groove radii combinations. Figure 5. 6[a-c] illustrate the streamline patterns for r_1 = 0.045, 0.85, and 0.125 mm with r_2 = 0 mm near the inlet of the first groove's top edge. It is evident that increasing the r_1 significantly reduces recirculation, which impacts heat transfer. Conversely, Figure 5. 6[d-f] show the combinations of r_1 = 0 mm with r_2 = 0.045, 0.85, and 0.125 mm, respectively. It reveals that recirculation was unaffected as r_2 increased, resulting in smoother flow near the base of the rectangular groove,

which impacted the friction factor. Additionally, the combined effects of different radii and equal radii are depicted in Figure 5. 7, and Figure 5. 8 also shows the influence of flow dynamics within a corrugated tube.

This demonstrates the crucial role of both radii in turbulent flows: r_1 contributes to the increment in heat transfer, while r_2 focuses on pressure reduction. Together, combining optimal configurations of r_1 and r_2 can improve the overall efficiency of the system. Therefore, incorporating curvature into the groove design effectively minimises the pressure drop.

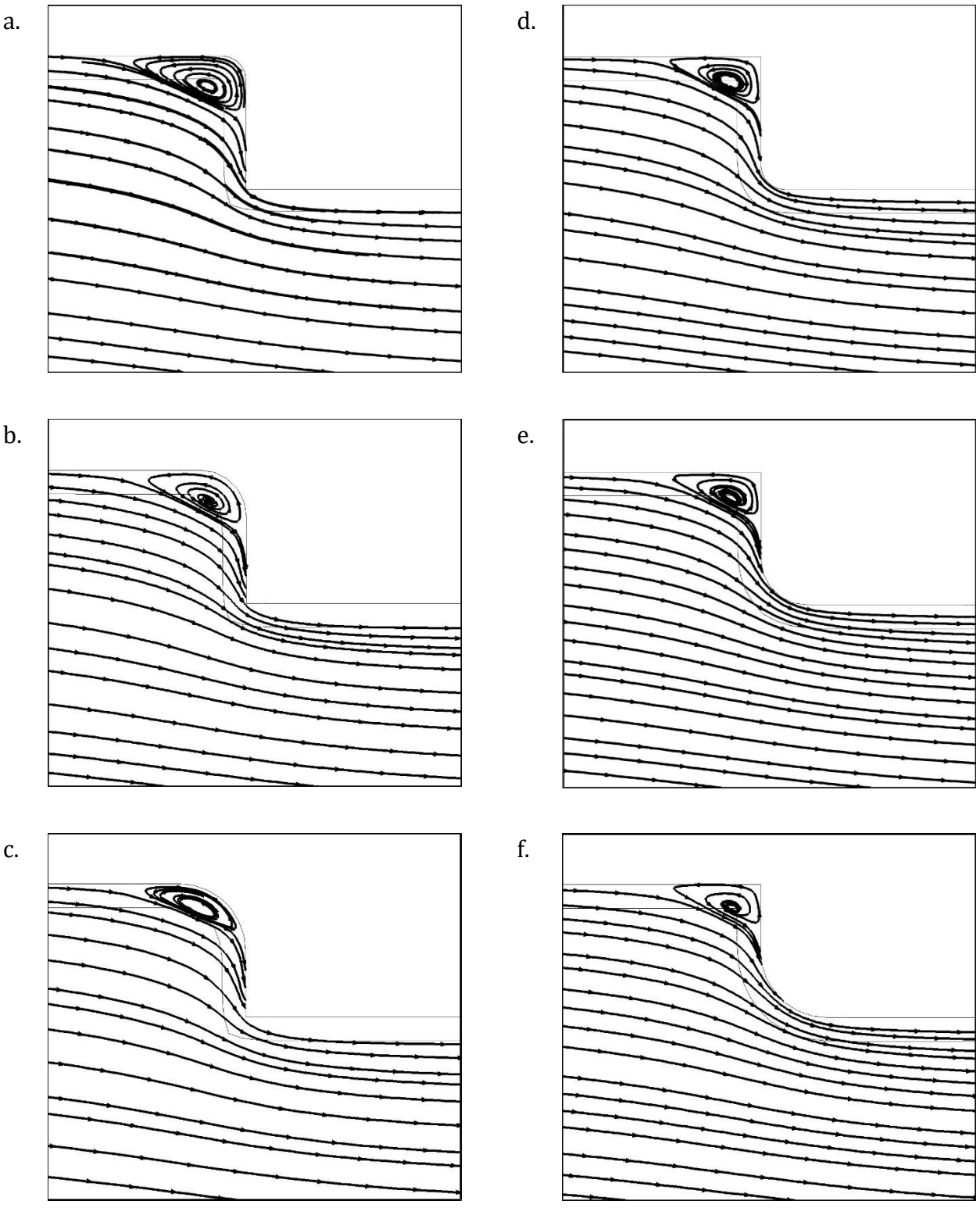

Figure 5. 6: Variation of streamlines for sharp edges groove combinations for the first groove: (a, b, c) r_1 = 0.045, 0.85, 0.125, and r_2 = 0; (d, e, f) r_1 = 0 and r_2 = 0.045, 0.85, 0.125 mm.

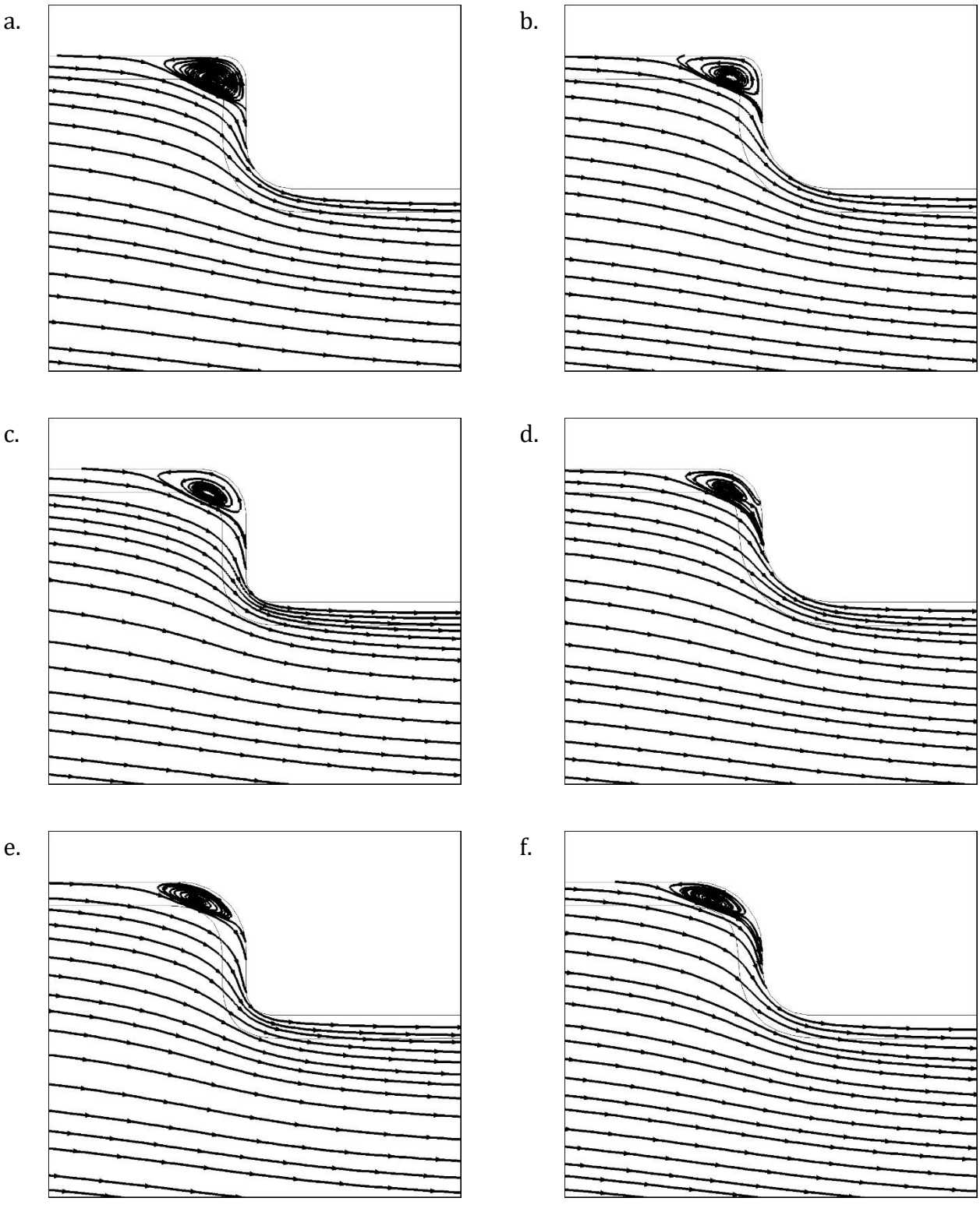

Figure 5. 7: Variation of streamlines for different radii for the first groove: (a, b) r_1 = 0.045, and r_2 = 0.045, 0.085 mm; (c, d) r_1 = 0.085 and r_2 = 0.045, 0.125 mm; (e, f) r_1 = 0.125, and r_2 = 0.045, 0.085 mm.

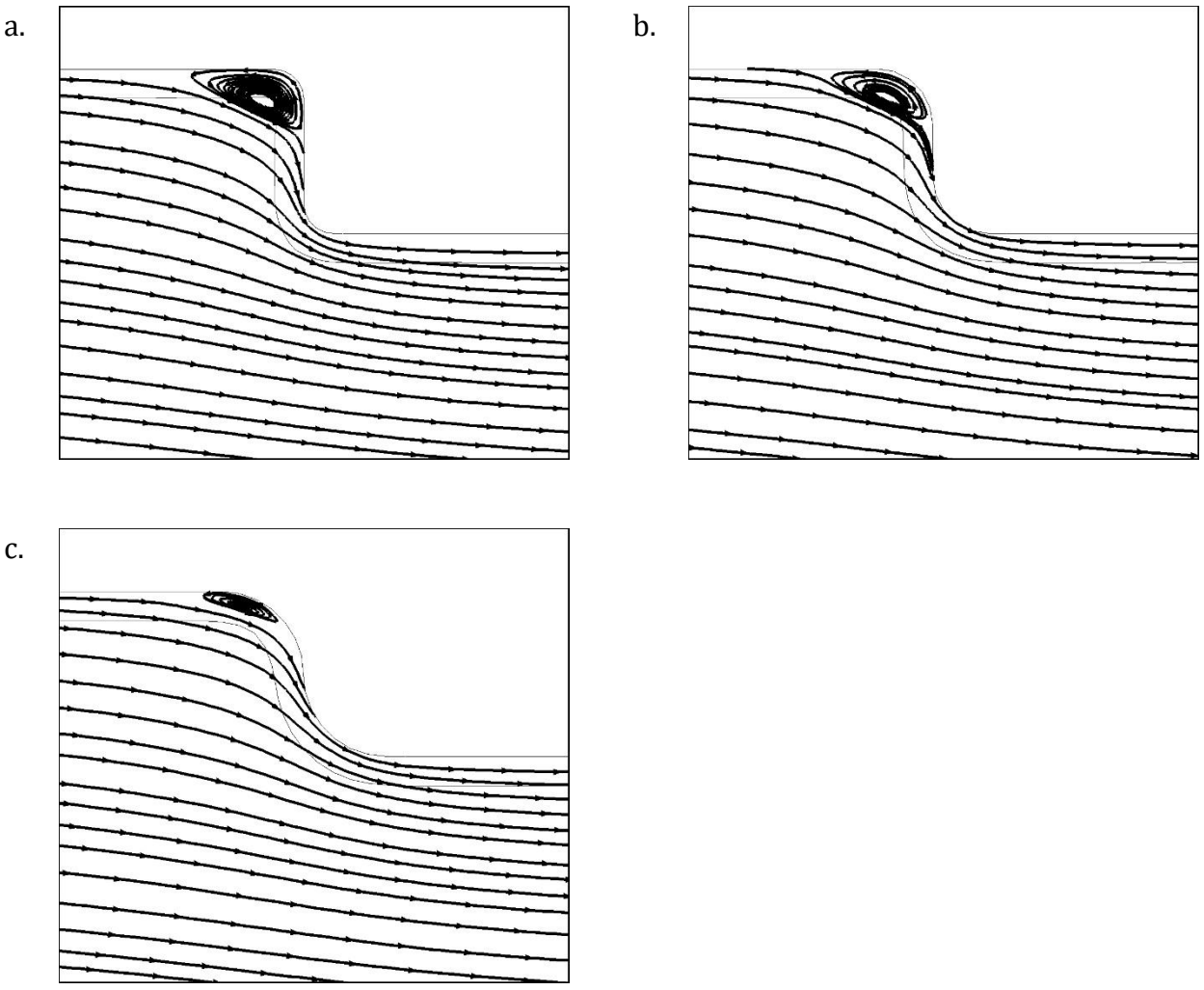

Figure 5. 8: Variation of streamlines for different groove combinations for the first groove near the tube's inlet: equal radii (a, b, c) r_1 = 0.045, 0.85, 0.125, and r_2 = 0.045, 0.85, 0.125 mm.

Figure 5. 9 illustrates the variation of the turbulent kinetic energy ratio of groove radii to the actual rectangular groove (k_r/k_g) for different groove combinations in a turbulent flow condition. The results reveal that the actual rectangular grooves exhibited higher levels of k, as k_r/k_g values were less than 1. This indicates the strong influence of the sharp groove edges on the fluid flow. Furthermore, the k ratio decreased with an increase in Reynolds number for most groove radii combinations. However, the combination with variables r_1 and r_2 = 0 mm showed a significant rise in k values, which led to enhanced heat transfer as mentioned in Figure 5. 9a. This effect was due to the variation in r_1, where a larger groove radius resulted in a smoother flow path, thereby

reducing turbulence and turbulent kinetic energy within the fluid. As a result, the flow experienced less disruption and separation around the larger groove radii compared to the small ones. In addition, the turbulent kinetic energy increased along the length of the corrugated tube due to the accumulation of the fluid's momentum, indicating increased heat transfer.

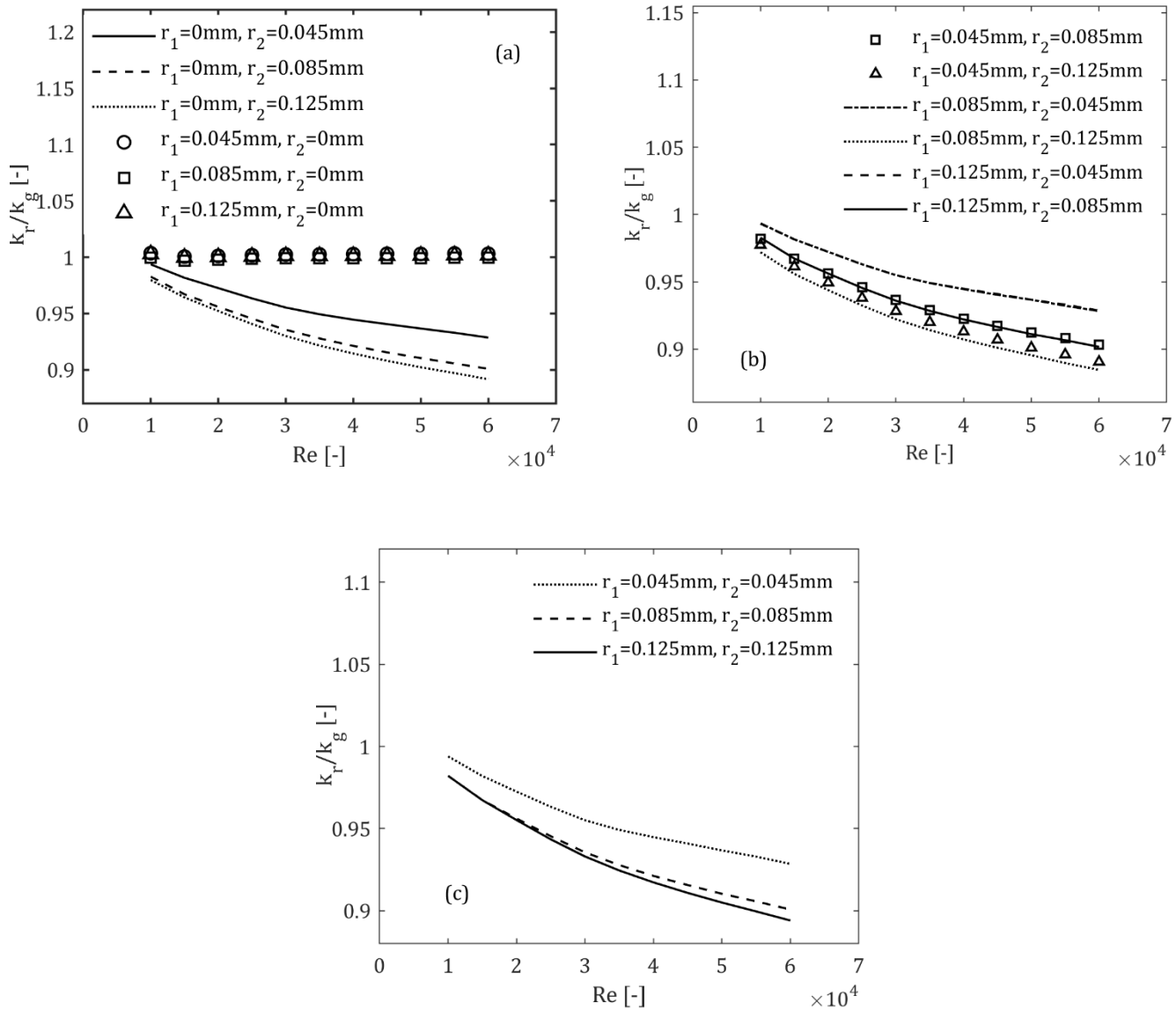

Figure 5. 9: Variation of turbulent Kinetic Energy ratio for different groove combinations (a) sharp edges (b) different radii (c) equal radii

a.

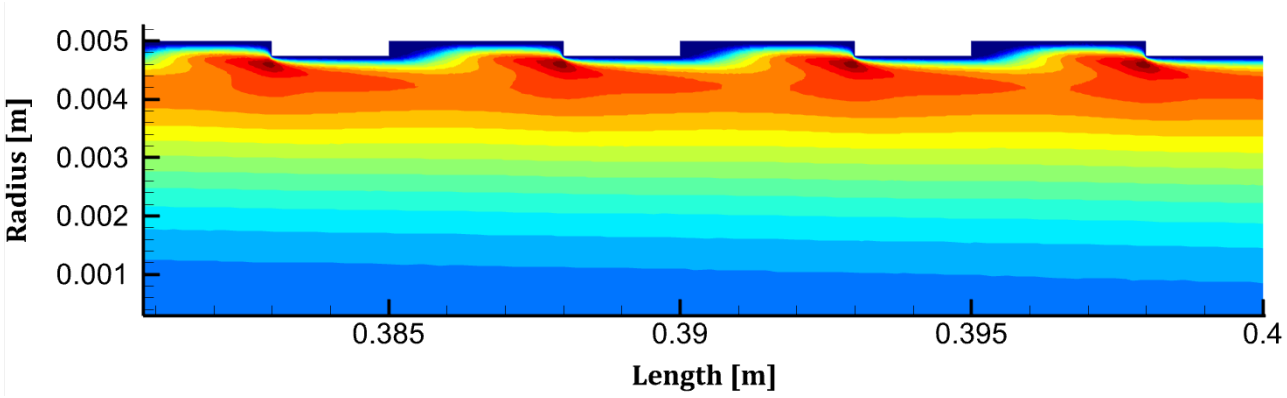

b.

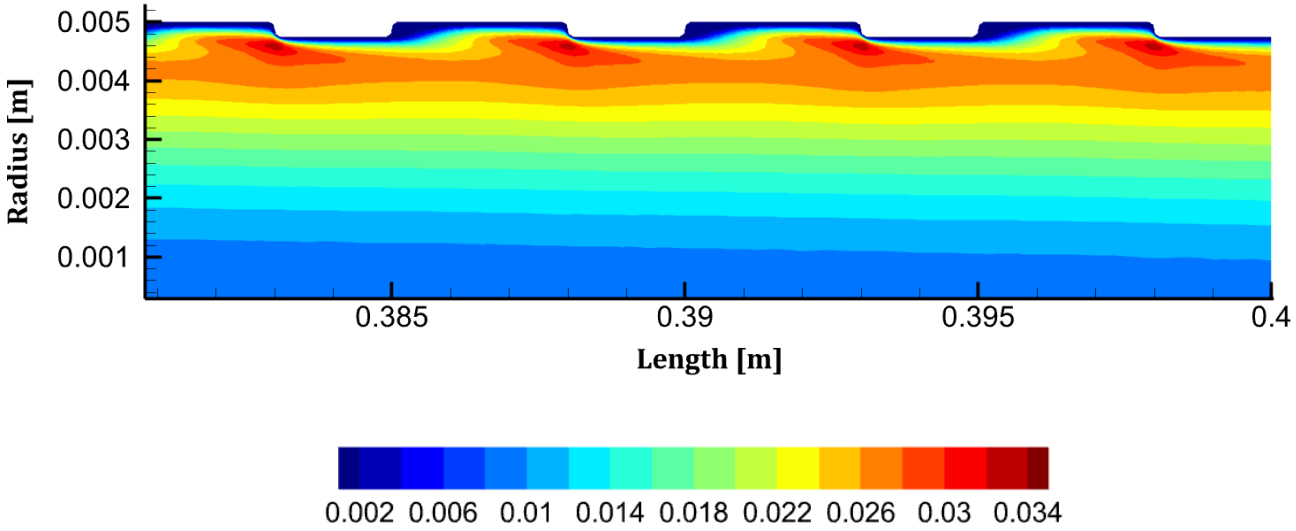

Figure 5. 10: Comparison Normalized Turbulent Kinetic Energy (TKE/u^2) for (a) original rectangular groove and (b) optimal groove combination (r_1 = r_2 = 0.125 mm) at Re = 10,000

Similarly, it was found that varying the radius r_2 (0.045, 0.085, and 0.125 mm) while maintaining r_1 at 0 mm resulted in lower normalised k levels than the reverse configuration. This is because changes in r_2 altered the flow pattern and disrupted the development of turbulent eddies, leading to a reduction in k. This reduction in k corresponds to the lower heat transfer, as shown in Figure 5. 4. Figure 5. 9b and c represent the combined effects of the radii combinations. It was evident that

the normalised *k* values were significantly lower for both different and equal radii combinations. Specifically, for the groove geometry combination (r_1 = r_2 = 0.125 mm), which provided maximum heat transfer coefficients and pressure reductions, despite having low *k* values with a reduction of k by around 20%, respectively. This clearly shows the positive aspect of the curvature grooves in reducing the overproduction of turbulence as shown in Figure 5. 10, which is a significant factor in heat transfer enhancement.

The wall shear stress ratio was susceptible to the groove radii, as shown in Figure 5. 11. Findings indicated that increasing r_2 while keeping r_1 = 0 mm combination obtained higher shear stress values than the reverse combination. This is because an increase in r_2 disrupted the flow more effectively, resulting in increased turbulence and drag coefficient, which improved the shear stress. High shear stress values promote a better mixing or blending effect, which improves convection. However, this effect was not observed for variations in r_2. Despite no augmentation in the heat transfer coefficient, the shear stress values showed a noticeable increment. As shown in Figure 5.9a, the average shear stress enhancements of r_1 = 0 mm with r_2 = 0.045, 0.085, and 0.125 mm combinations were 13.7%, 19.0%, and 22.4%, respectively, compared to the actual rectangular grooved tube. Therefore, it was evident that the shear stress increases with r_2, making these combinations less feasible for achieving high heat transfer performance.

Conversely, the modification of r_1 proved to be more effective with shear stress enhancements of 0.5%, 1.1%, and 1.5%, respectively, for r_1 = 0.045, 0.085, and 0.125 with r_2 = 0 mm combinations, respectively, resulting in a maximum increment in heat transfer performance of 7.2%. This appeared to be a reasonable scenario. In addition, it was noted that the wall shear stress continued to rise until Re = 25,000 at lower velocities. As the Reynolds number increased, the shape of the profile appeared to be constant, asymptotic, and known as a fully developed rough condition. This implies that the effect of grooves at higher velocities is independent of shear stress. The highest values were noted for equal radii (r_1=r_2 = 0.125 mm) with an average increment of 24.9%, respectively, compared to the actual rectangular grooves. This was due to the introduction of larger r_2 to the wall grooves yielding higher shear stress values. In contrast, the lowest shear stress values were detected with the lower $r_1$value groove combinations.

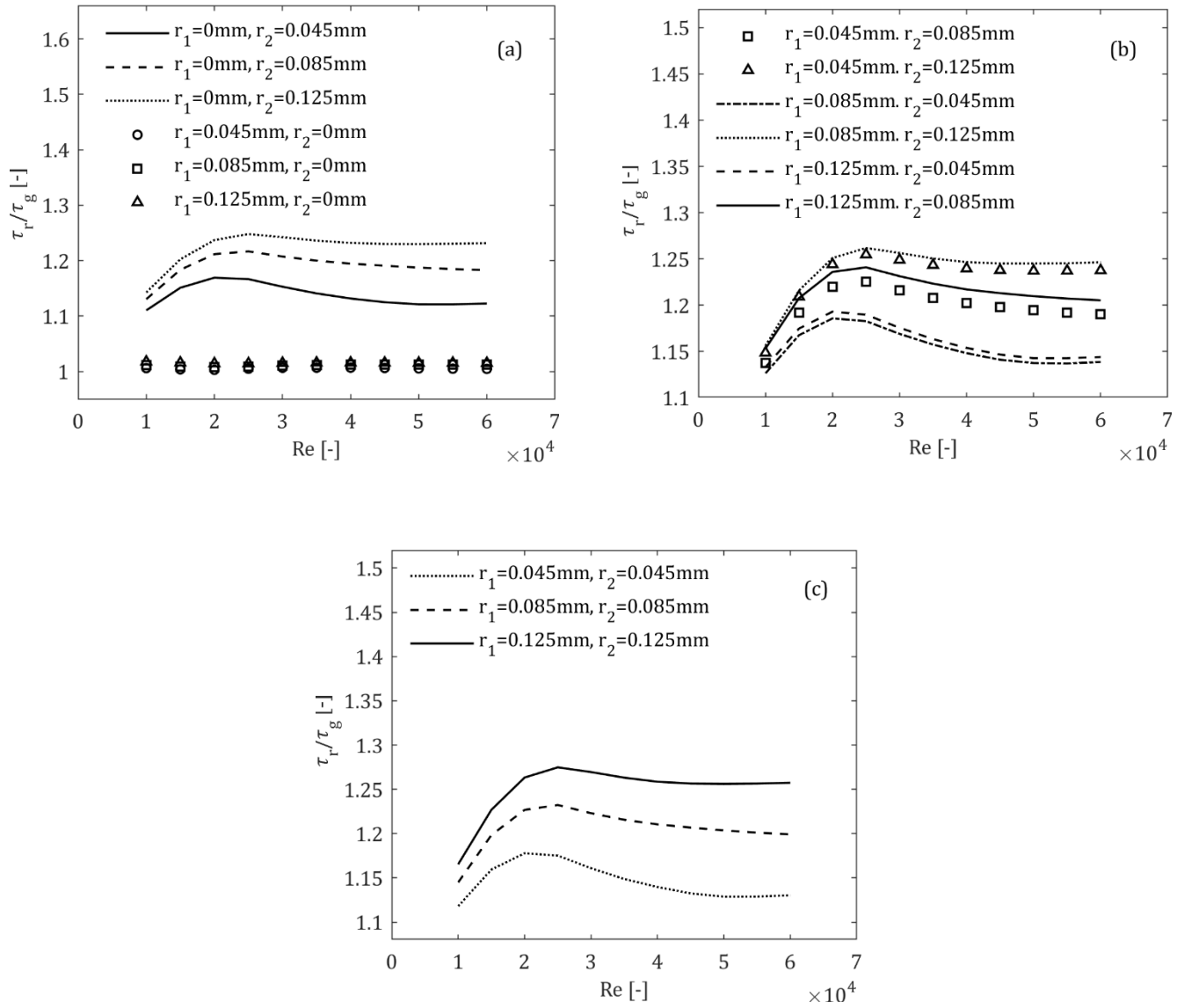

Figure 5. 11: Variation of wall shear stress ratio for different groove combinations (a) sharp edges (b) different radii (c) equal radii

Figure 5. 12 compares the PEC for varying radii through corrugated tubes to the actual rectangular groove for different Reynolds numbers ranging from 10,000 to 60,000. It can be seen that the PEC increased with an increase in the Reynolds number, reaching the highest value at Re = 45,000. This maximum PEC value corresponds to optimum Re; beyond this point, the net energy losses are high. The maximum value of PEC was obtained for the equal radii (r_1=r_2 = 0.125 mm) by 17.1%, respectively, and the average was found to be 13.2%. This is because the increased heat transfer

was more efficient than the increased friction factor, which makes this equal groove radii combination effective in terms of overall thermal and hydraulic performance. Therefore, the utilisation of this combination was thermodynamically beneficial. Additionally, Figure 5. 13 and Figure 5. 14 illustrate the flow enhancements achieved with the optimised groove geometry compared to the rectangular grooves.

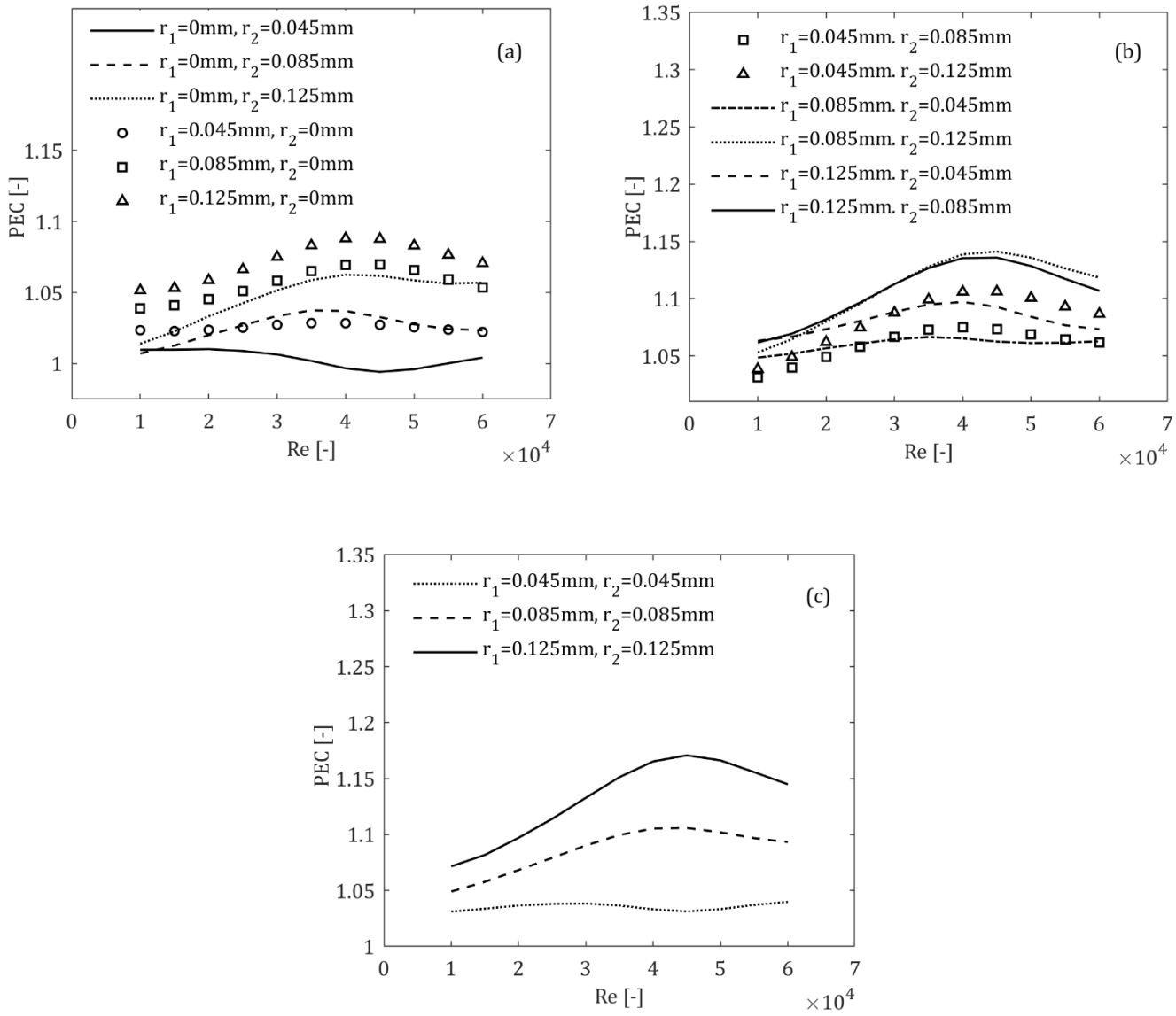

Figure 5. 12: Variation of PEC for different groove combinations (a) sharp edges (b) different radii (c) equal radii

In addition, it is evident that the PEC increased with r_1 increments. This phenomenon occurred due to the significant impact of r_1 on the fluid flow patterns and heat transfer dynamics inside the corrugated tube. The increase of r_1 led to diminishing disruptive flow behaviour, enhancing fluid mixing, and consequently improving convective heat transfer efficiency. This also led to a significant reduction in friction losses and contributed to the overall PEC augmentation. In contrast, r_2 did not affect the PEC due to its association with higher shear stress values and maintained flow stability with a minor effect on heat transfer.

a. b.

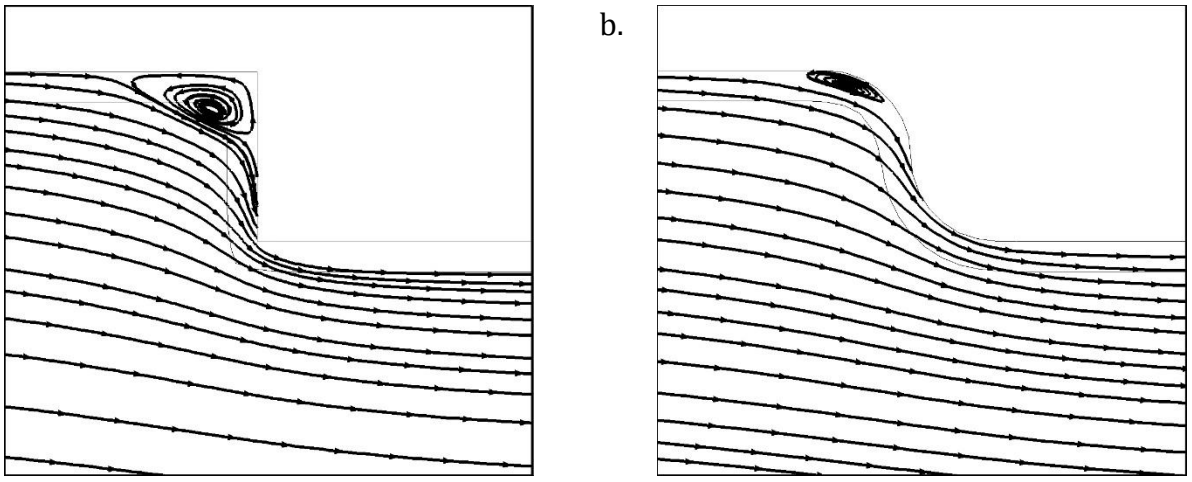

Figure 5. 13: streamlines near the first groove (a) Actual rectangular groove (b) optimized rectangular groove ($r_1 = r_2 = 0.125$ mm)

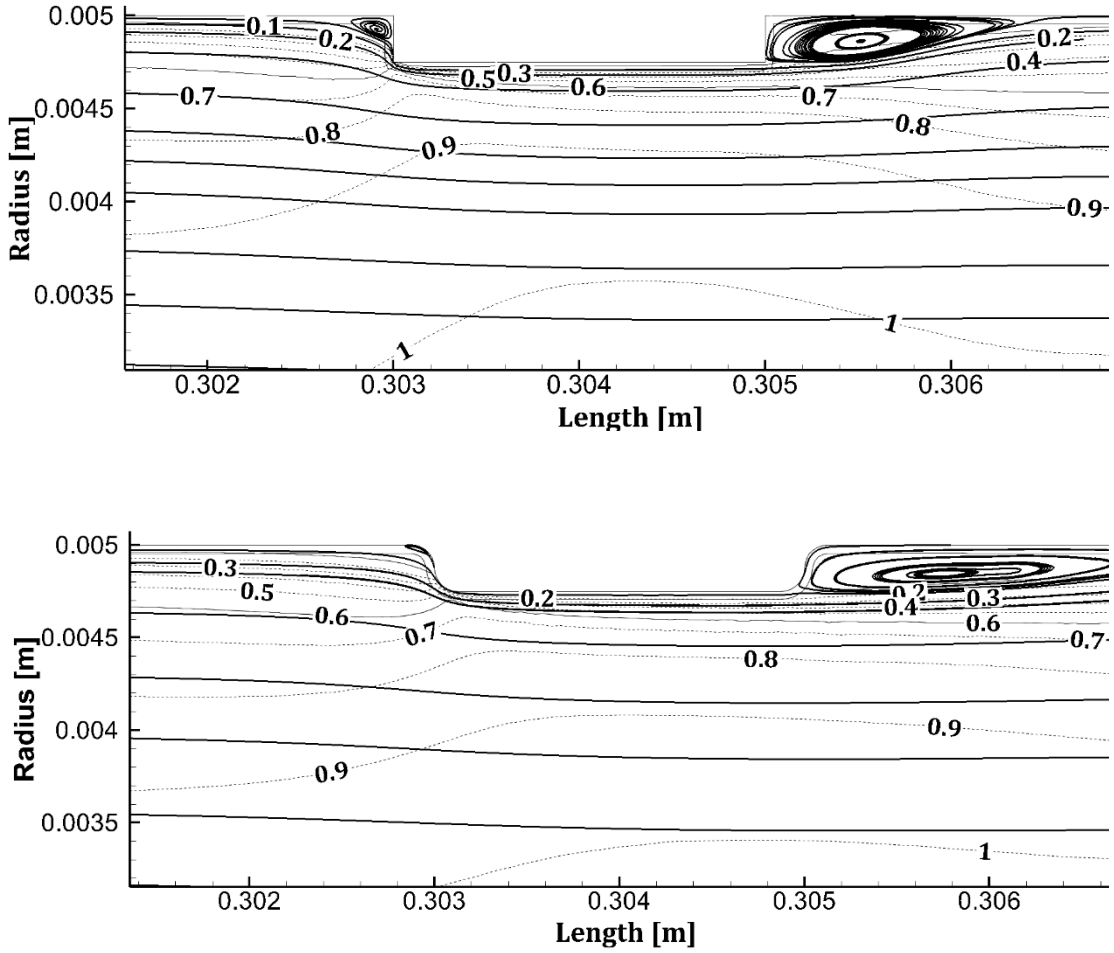

Figure 5. 14: Velocity Streamlines for Various Groove Shapes at Re=10,000

It was evident that the rectangular groove, which demonstrated the highest friction factor, was further optimised to enhance thermal performance (PEC). Figure 5. 15 compares the PEC of the optimised rectangular groove (r_1=r_2 = 0.125 mm) and the triangular groove shape combinations under turbulent conditions. The smooth tube without corrugation was used as a reference to calculate the PEC values for both groove combinations. Based on the results, it was observed that mono-triangular grooves exhibited the highest thermal performance factor (PEC) compared to the optimised groove combination for Reynolds numbers ranging from 10,000 to 60,000, respectively.

This is because of the lowest pressure drop obtained for triangular grooves. Specifically, the average PEC for triangular and optimised grooves were 8.97% and 2.06% larger than smooth tubes without corrugation, at a Reynolds number of 10,000.

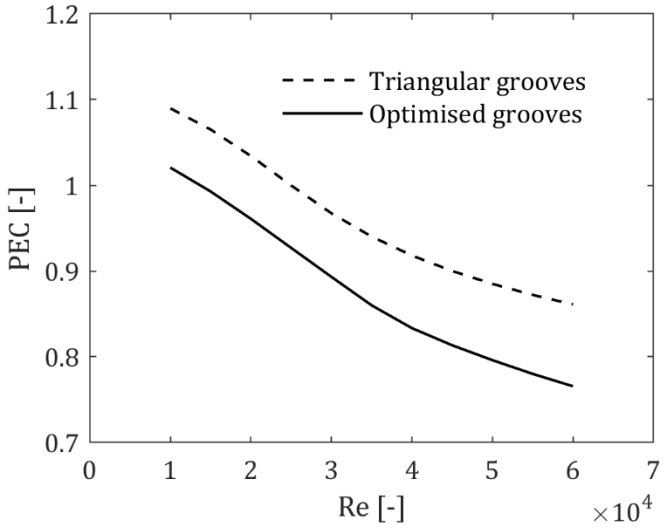

Figure 5. 15: PEC comparison of Triangular and Optimised grooved tubes

While the optimisation of rectangular grooves led to a significant reduction in pumping power and an increase in performance compared to the actual rectangular grooves, they remained less efficient than triangular grooves due to a higher friction factor. For instance, the optimised grooves showed an average friction factor 28.5% higher than that of triangular grooves for Reynolds numbers between 10,000 and 60,000. Nevertheless, the optimised grooves had an average heat transfer coefficient of 2.32% higher than the triangular grooves. As a result, the triangular grooved tube was identified as the most effective among the hybrid and optimised groove configurations. This conclusion was based on the PEC, prioritising minimal pressure drop or pumping power with an increase in Nusselt number. Additionally, the triangular groove geometry could potentially be further optimised by substituting sharp edges with curved edges in future research.

The optimisation of rectangular grooved geometry resulted in significant improvements in various aspects of convective heat transfer parameters. These optimisation strategies are extremely beneficial for most of the heat exchangers. According to the flow chart, the groove with the highest friction factor needs to be optimised to understand the maximum changes to the design. Therefore, comparing it to triangular grooves may not be reasonable, as the purpose of design optimisation is

to achieve maximum reductions in pumping power and energy savings. This implies that optimising any groove geometry can lead to significant improvements in heat transfer parameters.

5.3 Summary

In this chapter, numerical studies were carried out to understand the behaviour of fluid flow and heat transfer characteristics of various rectangular groove radii combinations within a corrugated tube using water under turbulent flow for a range of Re = 10,000 to 60,000. According to our findings, the following conclusions are:

- The optimal combination of grooves was achieved for equal radii (r_1=r_2=0.125) with a maximum increase in convective heat transfer and a substantial reduction in pressure drop. It was found that r_1 was the primary contributor to the increase in heat transfer with minimisation of recirculation. In comparison, the influence of r_2 on the reduction of the pressure drop was significant with minimal flow separations.

- It was also observed that the wall shear stress was sensitive to the variation of r_2, with average increments ranging between 10 and 25%. However, variations in r_1 had no effect. In addition, the turbulent kinetic energy decreased for almost all groove radii combinations, making the flow efficient in reducing turbulence while maintaining effective convection.

- At high Reynolds numbers, the groove radii had a weaker influence on the PEC. This highlights the importance of optimising groove shapes to achieve a balance between enhancing heat transfer and minimising pressure drop.

- The optimisation of rectangular groove geometry had a significant effect on the thermal performance factor; however, the equal groove radii (r_1=r_2=0.125 mm) were still not effective compared to the mono-triangular grooves.

Hence, it was evident that the corrugated grooves act as micro-vortex generators on walls, enhancing heat transfer.

Chapter 6: Fluid Effects – Performance Evaluation of Single- and Two-phase models Using Nanofluids

Due to the complexity and high cost of experimental research, the use of computational fluid dynamics (CFD) for simulating nanofluid heat transfer has been popular and reliable. However, the accuracy of CFD models in predicting convective heat transfer in nanofluids remains uncertain, causing difficulty to improve the thermal systems. This is because different combinations of RANS turbulent models with nanofluid numerical models (single and multiphase models) produced conflicting results from the open literature. Therefore, this numerical study examines the effect of realizable k-ε and SST k-ω models using single and two phase (Eulerian and Mixture) approaches of a circular tube using 2D turbulent forced convection over Reynolds numbers in the range of 10,000 to 60,000 using Al_2O_3-water nanofluid.

The choice of using two turbulent models, RKE and SST, is because of their robustness, accuracy, and ability to effectively capture turbulent flow phenomena. Results are reported to show the effects on the flow and thermal fields, including Nusselt number, friction factor, pressure drop, turbulent kinetic energy, wall shear stress, and turbulent viscosity. In addition, the influence of the axial and radial profiles of temperature, velocity, turbulent kinetic energy, and wall and fluid bulk temperatures on convective heat transfer and the flow characteristics are also discussed in detail. This research is beneficial in selecting an appropriate model for a related case study.

6.1 Model description

The same physical model of a 2D circular tube used in this chapter is shown in Figure 6. 1. The two-dimensional axi-symmetric model simplified the reduced computational cost and time [18, 19, 58, 213]. The circular tube is divided into two sections, with the test section placed after the hydrodynamic entry length of 0.3 m to achieve a fully developed flow condition. The tube material is assumed to be isotropic and homogeneous, with a thermal conductivity that stays constant regardless of temperature changes.

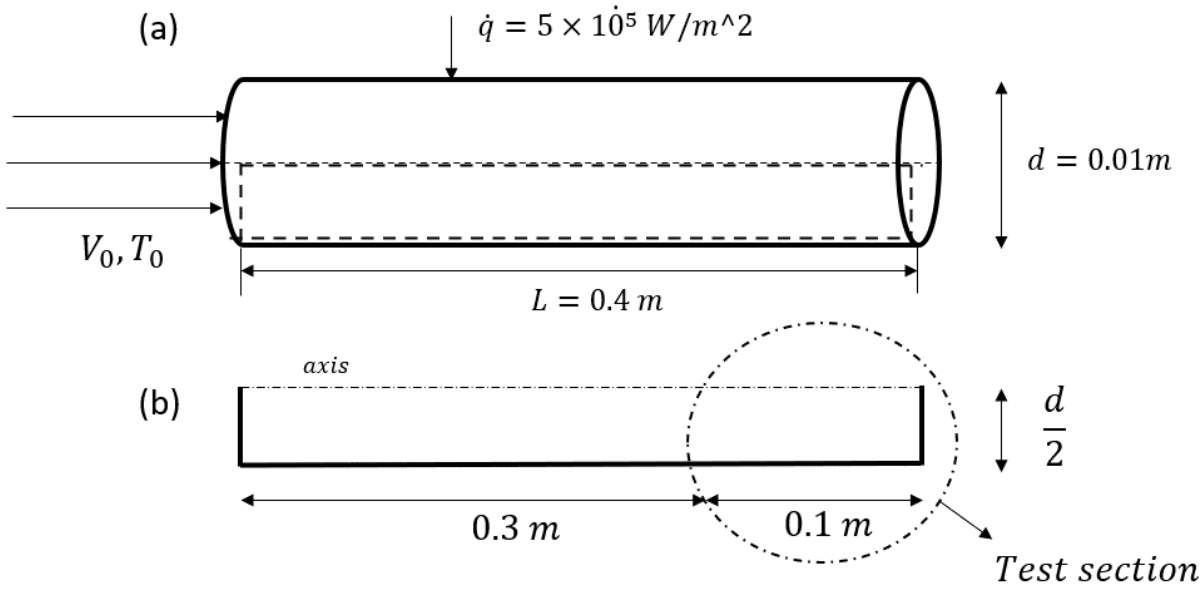

Figure 6. 1: a.) Cylindrical pipe b.) 2D pipe section.

6.1.1 Boundary conditions

Appropriate boundary conditions are used to solve the coupled and nonlinear partial differential equations. The boundary conditions used in the single-phase and two-phase models have been specified in the multi-phase mixture and dispersed model for both the fluid and solid phases. The fluid and nanoparticle temperatures at the inlet $T_{in} = 300K$, hydraulic diameter $d_h = 0.01m$, and turbulent intensity of 5% were specified at different Reynolds numbers. A constant heat flux of $q = 5 \times 10^5\ W/m^2$ and a no-slip condition were introduced on the wall pipe for both phases. At the outlet, the gauge pressure $P_{guage} = 0$ was stated. The flow and thermal fields were axisymmetric with respect to the horizontal plane. The RKE and SST turbulent models have been implemented with enhanced wall treatment to capture the viscous and thermal effects along with the single-phase model (SPM) and two-phase model (TPM). Finally, the flow was thermally and hydrodynamically fully developed at the end of the pipe.

The following assumptions were considered for steady-state governing equations:

- Flow is Newtonian, incompressible, and turbulent.

- Continuous phase (fluid) and discrete phase (nanoparticles) are in thermal equilibrium with each other and share the same local velocity, and there is no slip between them.
- The shape of nanoparticles is spherical, and they have a uniform size (13 nm).
- The Boussinesq approximation, viscous dissipation, and radiation effects are negligible.

6.1.2 Mesh sensitivity test

The mesh sensitivity test was conducted in Section 4.1 of Chapter 4 using water at $Pr = 5.83$ under a forced convection in a cylindrical tube. The unstructured grid with 380,000 cells generated the most reliable Nu and f results, at $Re = 10 \times 10^3$. Consequently, the same grid size was used for the current calculations to ensure consistency in the numerical results.

6.1.3 Validation

The computational model has been validated for hydraulically and thermally developing flow in a circular tube with constant heat flux using Al_2O_3-water. For the accuracy of this present numerical model, the existing correlations reported in equations (2.22) – (2.23) were used to validate the results for different Reynolds numbers $Re = 10 \times 10^3$ to 60×10^3 with a Prandtl number of 8.51 (φ = 1.34%) and 12.33 (φ = 2.78%) at 300K. The present numerical simulations employed the single-phase model for modelling Al_2O_3-water nanofluid along with the RKE turbulence model for turbulent flows.

Figure 6. 2 shows the numerical results of the Nusselt number were compared to the published data at both nanoparticle volume concentrations. The average deviations of the average Nusselt number were 3.6%, and -10.4%, respectively, compared to Pak and Cho [102] and Maïga, et al. [26] at φ = 1.34%. Similarly, average deviations were -2.4 and -10.7 at φ = 2.78%. It can be noted that the minus sign indicates that the numerical data underestimated the empirical data. Both RKE results showed good agreement with correlations. The maximum difference of 20% and minimum difference of 2% were observed from $Re = 10 \times 10^3$ to 60×10^3.

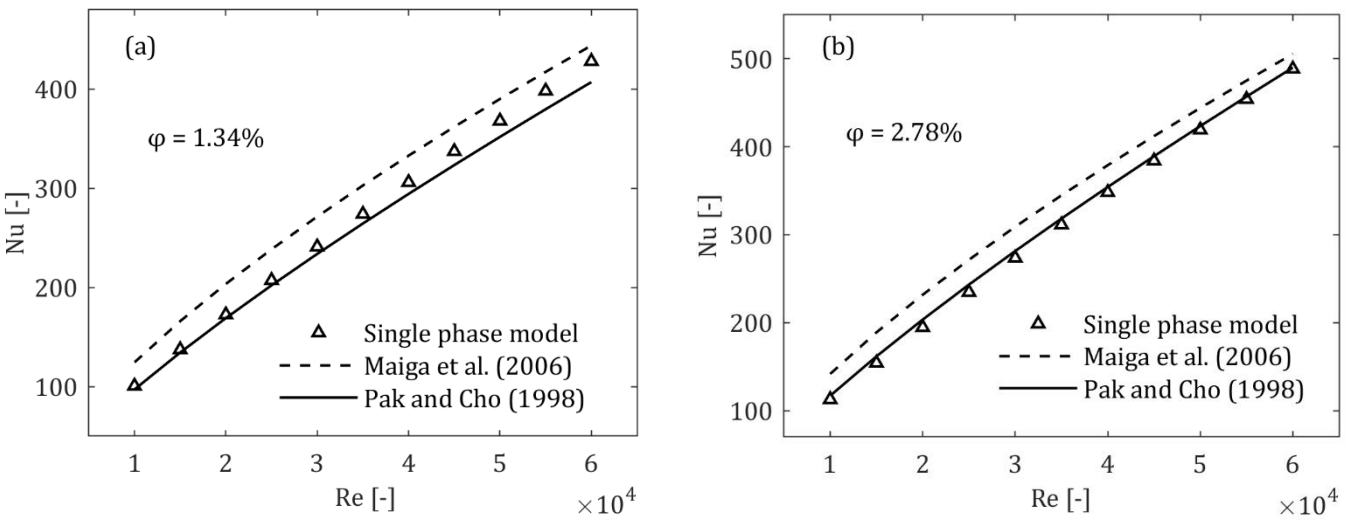

Figure 6. 2: Comparison of Nusselt number of single-phase approach using RKE turbulence model for (a) 1.34% (b) 2.78% Al_2O_3-water nanofluid with the published data

6.2 Results and Discussion

Despite extensive theoretical and practical research on multiphase flows, using various turbulent models in CFD still has challenges. In this study, the Realizable k-ε model and the SST k-ω model were compared for 1.34% and 2.78% volume concentrations of Al_2O_3-water nanofluid, respectively. These specific volume concentrations of the nanofluid were considered based on the reference thermo-physical data available from the experiment conducted by Pak and Cho [102]. For modelling the nanofluid, the Single-Phase Model (SPM) and Two-Phase Model (TPM) were used to compare the differences in convective heat transfer.

Figure 6. 3 shows the Nu comparison of single phase (SPM) and two-phase models (TPM) with the experimental data using the realizable k-ε model (RKE) and the SST k-ω model (SST). The increase of the Al_2O_3 volume concentration from 1.34% to 2.78% enhances the heat transfer coefficient by an average of between 15% and 30% compared to the water in a cylindrical tube from Re = 10,000 to 60,000. This enhancement was due to the improved thermal properties of the nanofluid due to the addition of the Al_2O_3 nanoparticles. Therefore, it was evident that Nu depends on volume

concentration and Reynolds number. In addition, the thermal conductivity of the nanofluid had a greater increment than the heat transfer coefficient, from φ = 1.34% to φ = 2.78%.

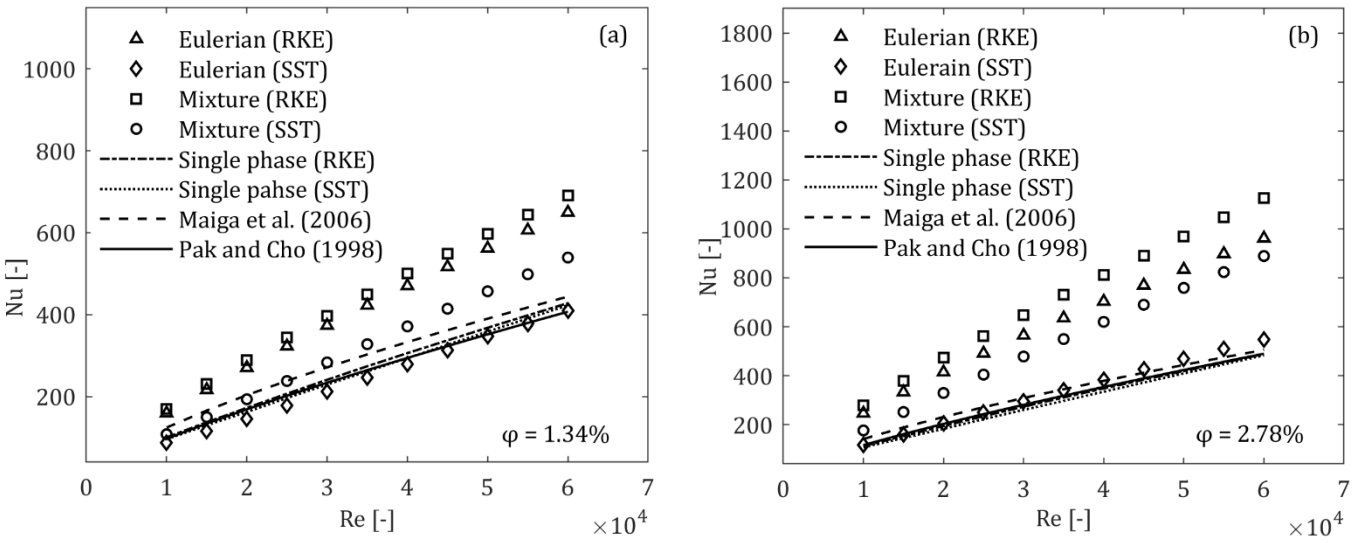

Figure 6. 3: Comparison of Nusselt number at different single- and two-phase approaches using two turbulence models at (a) 1.34% (b) 2.78% Al_2O_3-water

It was evident from Figure 6. 3 that the SPM results were closer to the experimental data for both RKE and SST turbulent models. For instance, at a lower volume concentration (φ = 1.34%), the SST model predicted more accurately, with minimal error compared to Pak and Cho [102] experimental data as shown in Figure 6. 3a. Conversely, the RKE model exhibits a closer deviation at a high-volume concentration (φ = 2.78%) as depicted in Figure 6. 3b. This demonstrates that the performance of the turbulence model in SPM is highly dependent on the nanoparticle volume concentration. Similarly, the numerical results of SPM deviate significantly from Maïga, et al. [26] correlation for both RKE and SST models, and their discrepancy (>10%) remains substantial at a higher concentration. Since there is a huge deviation of around 10%–20% between the actual experimental (eq. 2.22) and numerical (eq. 2.23) correlations, the effect of Maïga, et al. [26] correlation was neglected. Furthermore, the Maïga correlation was developed based on the numerical study and was derived from the single-phase nanofluid behaviour. Hence, it's not

reasonable to compare with TPM results. However, the SPM results have underestimated it by a maximum of 14.1%.

Results also reveal that the RKE model fails to predict the convective heat transfer coefficient in TPM for both Eulerian and mixture models at 1.34% and 2.78% nanoparticle volume concentrations. Specifically, the Eulerian model results revealed a drastic variation in predicting the convective heat transfer coefficient with an average deviation between 60.6% and 100.8% compared to the Pak and Cho [102] data. Similarly, the mixture model also exhibited errors ranging from 70.4 to 131.1%, respectively. In contrast, the SST model demonstrates better performance in TPM, closely aligning with the experimental data. For the Eulerian model, the SST model underpredicts the convective heat transfer by 6.8% at a lower volume concentration (φ = 1.34%) and overpredicts 6.2% at a high-volume concentration (φ = 2.78%). Similarly, the mixture model shows deviations of 22.5% and 70.5% at both volume concentrations.

These findings highlight two important observations. Firstly, the effect of the turbulence model was significant to see large variations or errors in Nu. This discrepancy can be attributed to the intrinsic characteristics of the Realizable k-ε model, which tends to overestimate the turbulence kinetic energy in high strain regions, leading to a marginally increased resistance to flow. Secondly, when comparing TPM, the Eulerian model exhibited closer agreement with experimental data compared to the mixture model. This indicates the inaccuracies in the mixture model, which fails to consider the appropriate drag force [133]. Moreover, the assumption of a single velocity field for both phases in the mixture model might not be valid at higher volume concentrations [123].

Table 6. 1 compares the impact of two turbulence models to better understand the deviations between SPM and TPM. In terms of the SST model, it can be seen that SPM results have relatively lower error percentages at 1.34% vol. conc. compared to the Eulerian model from Reynolds numbers 10,000 to 35,000. Beyond this range, the Eulerian model aligns more closely, with an average error of less than 3%. This suggests that SPM predicted better at Reynolds numbers below 35,000, whereas the Eulerian model was more accurate above this threshold. However, this trend is reversed at a high-volume concentration (2.78%). Overall, SPM results were closer to experimental data.

Table 6. 1: Average Nu Errors (%) of the two RANS turbulence models on nanofluid numerical approaches compared to the published data

Models	Single phase		Eulerian		Mixture	
	RKE (%)	**SST (%)**	**RKE (%)**	**SST (%)**	**RKE (%)**	**SST (%)**
1.34% Al_2O_3-water						
Pak and Cho (1998)	3.6	-0.5	60.3	-6.8	70.4	22.5
Maiga et al. (2006)	-10.4	-13.8	38.5	-19.3	47.3	6.3
2.78% Al_2O_3-water						
Pak and Cho (1998)	-2.4	-6.1	100.8	6.2	131.1	70.1
Maiga et al. (2006)	-10.7	-14.1	83.3	-2.7	111.1	55.8

Figure 6. 4 presents a numerical comparison of friction factor using both SPM and TPM with RKE and SST turbulence models at 1.34% and 2.78% vol. conc. of Al_2O_3-water nanofluid. Due to the limited availability of the experimental data, the classical Blasius equation (eq. 2.1) for water was taken as a reference. The friction factor of SPM was greater than the Blasius correlation using RKE at both volume concentrations. This observation aligns with previous literature, suggesting an increase in friction factor for Al_2O_3 nanofluid compared to water [102]. This significant increase in f can be attributed to the enhanced viscosity and density of the nanofluid due to the addition of nanoparticle concentration, which increased the flow resistance. However, SPM's SST model underpredicts the friction factor relative to the Blasius curve despite accurately predicting the convective heat transfer. This indicates that the RKE model was effective in predicting Nu and f in SPM.

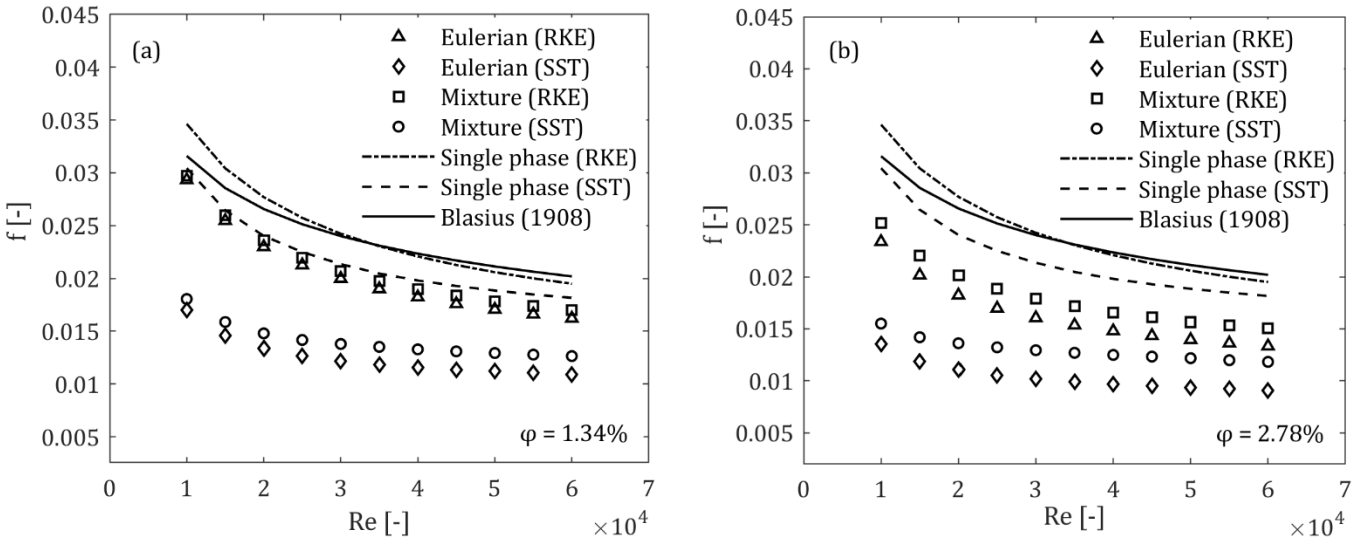

Figure 6. 4: Comparison of friction factor at different single- and two-phase approaches using two turbulence models at (a) 1.34% (b) 2.78% Al_2O_3-water

Evidently, TPM models failed to predict the friction factor at both turbulence models and volume concentrations compared to SPM. It was evident in Figure 6. 4a and 6.4b, the SST model for both Eulerian and mixture models has the least friction factor compared to RKE model combinations. For example, the average deviation of the friction factor of Eulerian (SST) was increased from 48% (φ = 1.34%) to 56% (φ = 2.78%) compared to the Blasius curve. This was due to a low pressure drop obtained in the fully developed region. A similar explanation from the numerical study of Sekrani, et al. [144] stated that the effect of the SST model, which was sensitive to the free stream, led to a reduction in pressure conditions. Conversely, the RKE model predicted a higher pressure or friction factor compared to the TPM's SST model. In addition, their discrepancy increases as the volume concentration increases. Therefore, these findings suggest that the SST model fails to predict the friction factor, despite effectively predicting Nu with the Eulerian model. In contrast, the mixture model showed relatively smaller deviations compared to the Eulerian model.

Another critical observation reveals the peculiar behaviour of the Eulerian model, which fails to predict the friction factor for both RKE and SST models. The reason lies in the fundamental assumptions of the Eulerian model. It treats each phase (solid and liquid) as continuous media with separate governing equations [194]. However, in reality, this was completely different in

determining the flow, as particle-particle, particle-fluid interactions and the dispersion effects created complex interactions leading to a non-uniform or non-continuous flow. These interactions between the phases, such as momentum and energy exchange, may not be accurately captured by this model. This indicates that the Eulerian model's assumption of local isotropy and homogeneity of turbulence does not hold due to its simplicity. Therefore, these complex multiphase phenomena resulted in larger discrepancies in predicted flow properties such as pressure drop or friction factor.

To closely examine the hydrodynamic and thermal behaviour obtained by the single- and two-phase models with two turbulent models, the axial velocity at the centre of the tube was initially compared at 1.34% Al_2O_3 volume concentration. This axial velocity profile depicted in Figure 6. 5 shows the axial evolution of the flow field along with the boundary layers. The rapid development of the boundary layer in the fully developed region causes the fluid to move from the wall towards the centre of the tube, resulting in higher axial velocity to maintain mass conservation. The overall velocity increment appears to be linear, with peak values reaching a maximum at z/L = 1, depending on turbulent closures. In addition, it can be observed that the SST turbulence model predicted higher values of axial velocity (v/v_0) than the RKE model in both SPM and TPM. This overprediction of v/v_0 signifies the weak turbulent flow leading to a low pressure drop and lower friction factor.

The radial profiles of velocity, temperature, and kinetic energy were analysed using the mean centerline at the fully developed region, which was at the mid-test section of the tube (L = 0.35 m) at Re = 10,000, as presented in Figure 6. 6. It can be seen that the boundary layer growth along the wall was consistently thinner across the RKE model compared to the SST model at both volume concentrations. This shows that the RKE model has lower values of velocities towards the center of the tube, specifically in the SPM model, leading to a high gradient of temperature and turbulent kinetic energy distributions. In addition, these gradients also increase with increasing the volume concentration of the nanoparticles. Although the non-dimensional velocity in the SPM remained nearly unchanged, there was a significant increase in TPM as the volume concentration increased from φ = 1.34% to φ = 2.78%. The TPM model exhibits the highest radial mean velocity in the fully developed region (L = 0.35m) which was 3.6% higher than SPM's RKE, which was relatively similar

to the axial velocity trends. Consequently, the temperature and TKE were lower compared to the SPM, particularly for both the RKE and SST models.

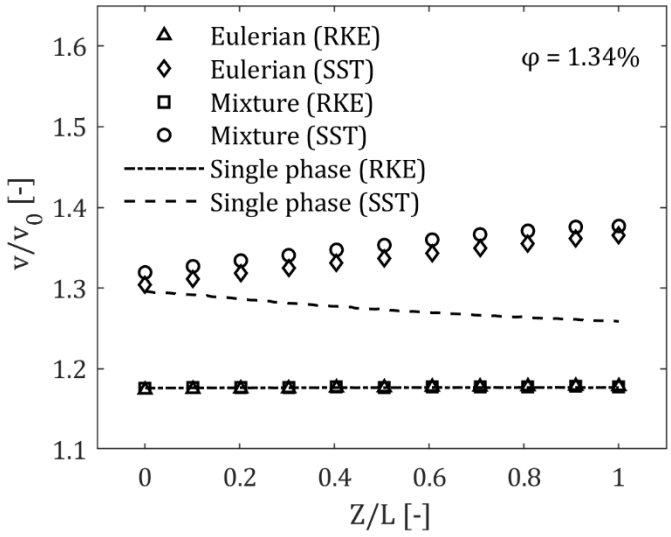

Figure 6. 5: Axial distribution of mean centre line velocity at the tube's test section at Re = 10,000

Evidently, the SST model within TPM demonstrated a notable reduction of TKE levels while accurately predicting Nu. This phenomenon can be attributed to the SST model's effective handling of turbulent transport processes, which led to more precise flow predictions. In contrast, TPM's RKE model, although closely matched the velocity and temperature profiles of SPM's RKE, exhibited higher TKE values than TPM's SST. This inconsistency in TKE values resulted in unrealistic Nu estimates by the RKE model within TPM, emphasising the importance of turbulence model selection for accurate flow behaviour prediction. This highlights the need for careful consideration when selecting turbulence models for multiphase flow simulations. However, it's important to note that despite SPM exhibiting significantly higher TKE levels, it simplified the flow by neglecting complex interactions between phases. Therefore, using SPM as a reference for evaluating TPM performance might not accurately reflect the complexities of multiphase flows. Additionally, the mixture model in TPM was found to produce higher TKE values compared to the Eulerian model using the SST formulation, resulting in larger heat transfer coefficients.

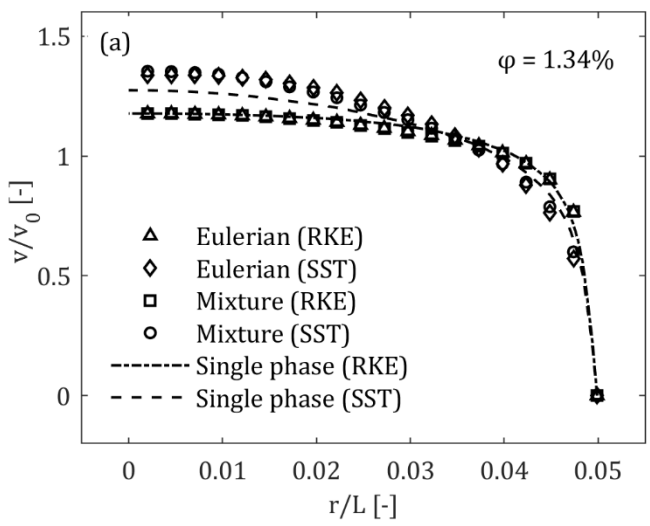
(a)
φ = 1.34%
v/v0 [-]
r/L [-]
Eulerian (RKE)
Eulerian (SST)
Mixture (RKE)
Mixture (SST)
Single phase (RKE)
Single phase (SST)

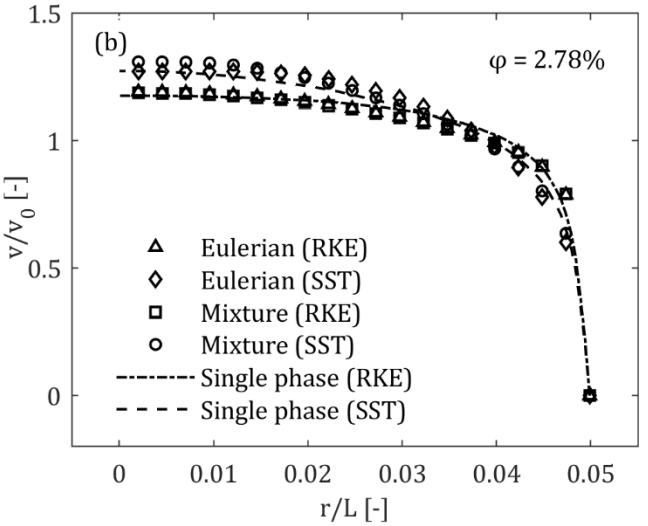
(b)
φ = 2.78%
v/v0 [-]
r/L [-]
Eulerian (RKE)
Eulerian (SST)
Mixture (RKE)
Mixture (SST)
Single phase (RKE)
Single phase (SST)

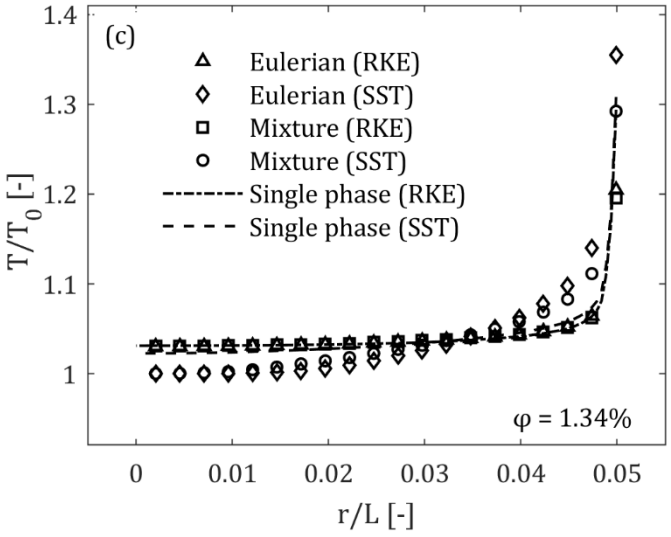
(c)
φ = 1.34%
T/T0 [-]
r/L [-]
Eulerian (RKE)
Eulerian (SST)
Mixture (RKE)
Mixture (SST)
Single phase (RKE)
Single phase (SST)

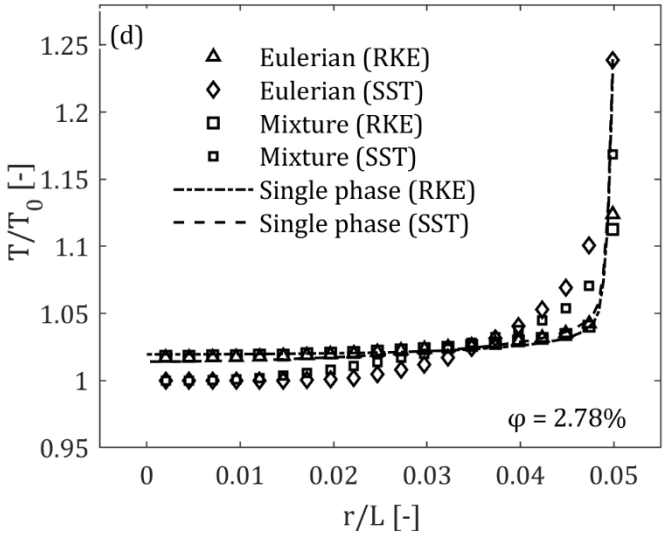
(d)
φ = 2.78%
T/T0 [-]
r/L [-]
Eulerian (RKE)
Eulerian (SST)
Mixture (RKE)
Mixture (SST)
Single phase (RKE)
Single phase (SST)

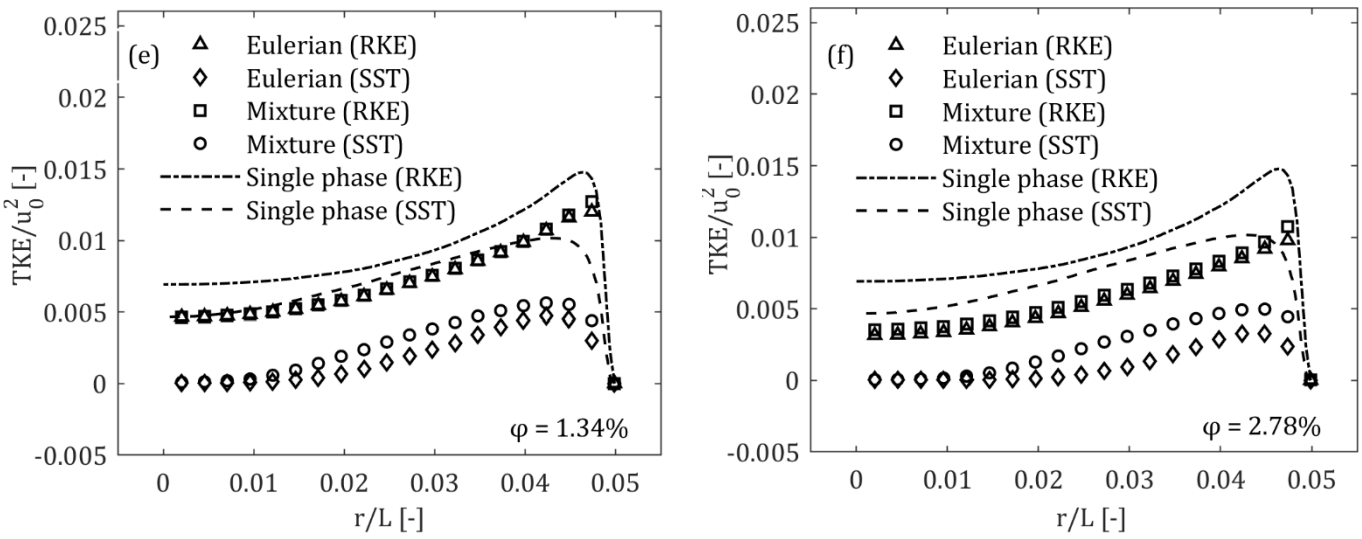

Figure 6. 6: Radial distribution of (a,b) velocity (c,d) Temperature (e,f) Turbulent kinetic energy at 1.34% and 2.78% vol. conc

Figure 6. 7 depicts the comparison of wall and bulk temperature of Al_2O_3-water nanofluid at different volume concentrations and Reynolds numbers. The results indicate that both wall and bulk temperatures decrease with an increase in Reynolds number. This suggests that higher convective heat transfer coefficients (high Re) have lower wall and bulk temperatures of the fluid. Similarly, the wall and bulk temperatures also decrease with an increase in volume concentration. For instance, the bulk temperature of Eulerian (RKE) at Re = 10,000 decreased from 315K (φ = 1.34%) to 309K (φ = 2.78%) respectively. This beneficial effect was attributed to the particle loading, which significantly improved the overall thermal properties of the nanofluid. Therefore, the impact of Tw and Tb directly affects the convective heat transfer.

The average differences in the wall and bulk temperatures between SPM and TPM for both volume concentrations were approximately less than 4.78% at φ = 1.34%. However, these differences decrease as the volume concentration increases. From the fundamental concept of Newton's law of cooling, the convective heat transfer coefficient is inversely proportional to the temperature difference between the tube's wall (T_w) and the nanofluid (T_b). This means that higher heat transfer was associated with a lower temperature difference ($T_w - T_b$). From Figure 6. 3, the combinations of Mixture and Eulerian approaches using the RKE model show significantly larger

Nu values compared to the empirical data. This is because RKE's mixture model has the smallest average temperature difference ($T_w - T_b$) of 20.11 K among all the combinations at 1.34% volume concentration. Similarly, Eulerian's RKE model temperature difference ($T_w - T_b$) was around 21.38 K. Since these temperature differences ($T_w - T_b$) were low, it was evident that they have the highest heat transfer coefficients, explaining the overestimation of Nu. In contrast, the temperature difference of the Eulerian's SST model seems to be closer to both SPM models.

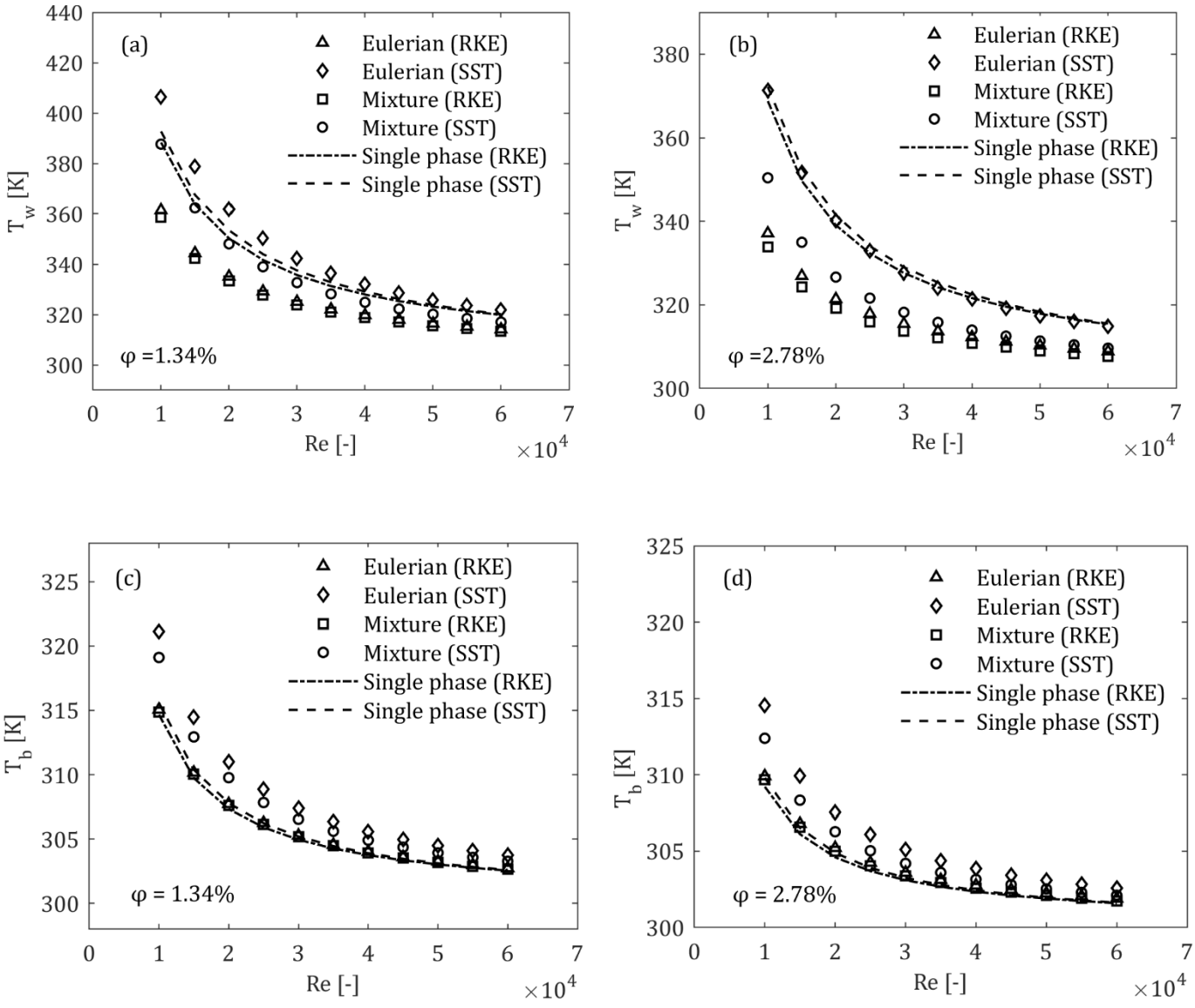

Figure 6. 7: Comparisions of (a,b) wall (c,d) bulk temperatures of different turbulent model combinations at 1.34% and 2.78% vol. conc.

The impact of turbulent kinetic energy from Re = 10,000 to 60,000 at both volume concentrations using SPM and TPM was compared in Figure 6. 8. It was evident that the production of TKE increases with the Reynolds number. This can be due to the increased vorticity and shear (velocity gradients) within the flow at higher Reynolds numbers that contributed to the enhanced mixing and energy transfer, thereby improving TKE. This improved TKE is also attributed to the developing boundary layers across the tube. In contrast, normalised turbulent kinetic energy (NTKE) decreased with an increase in Re. This signifies that the contribution of velocities to overall energy from turbulence is less significant at high Re. This scenario was reported by Akbari, et al. [39]. Moreover, the production of TKE also increases with higher nanoparticle volume concentrations.

All RKE model combinations with single- and two-phase approaches show similar profiles of TKE because they share the same transport equation for TKE. The RKE model within SPM generated the maximum values of TKE. Conversely, despite accurately predicting the Nu, the two-phase SST model exhibited the lowest values of turbulent kinetic energy among the other turbulent model combinations. This could be due to its high sensitivity to the dissipation rate at the tube inlet. The stream wise development of TKE seems to be higher and relatively identical for SST's TPM compared to the other turbulent model combinations. The SST's specific turbulence modelling approach effectively accounts for the influence of both the viscous sublayer and the outer turbulent flow region near the wall. By utilising this transitional model that smoothly shifts between two different turbulence models (the near wall (k−ω model) and the outer part (standard k−ε model), the SST model effectively captures the flow physics near the wall and in the outer turbulent region, resulting in more accurate Nu predictions despite lower TKE levels [201].

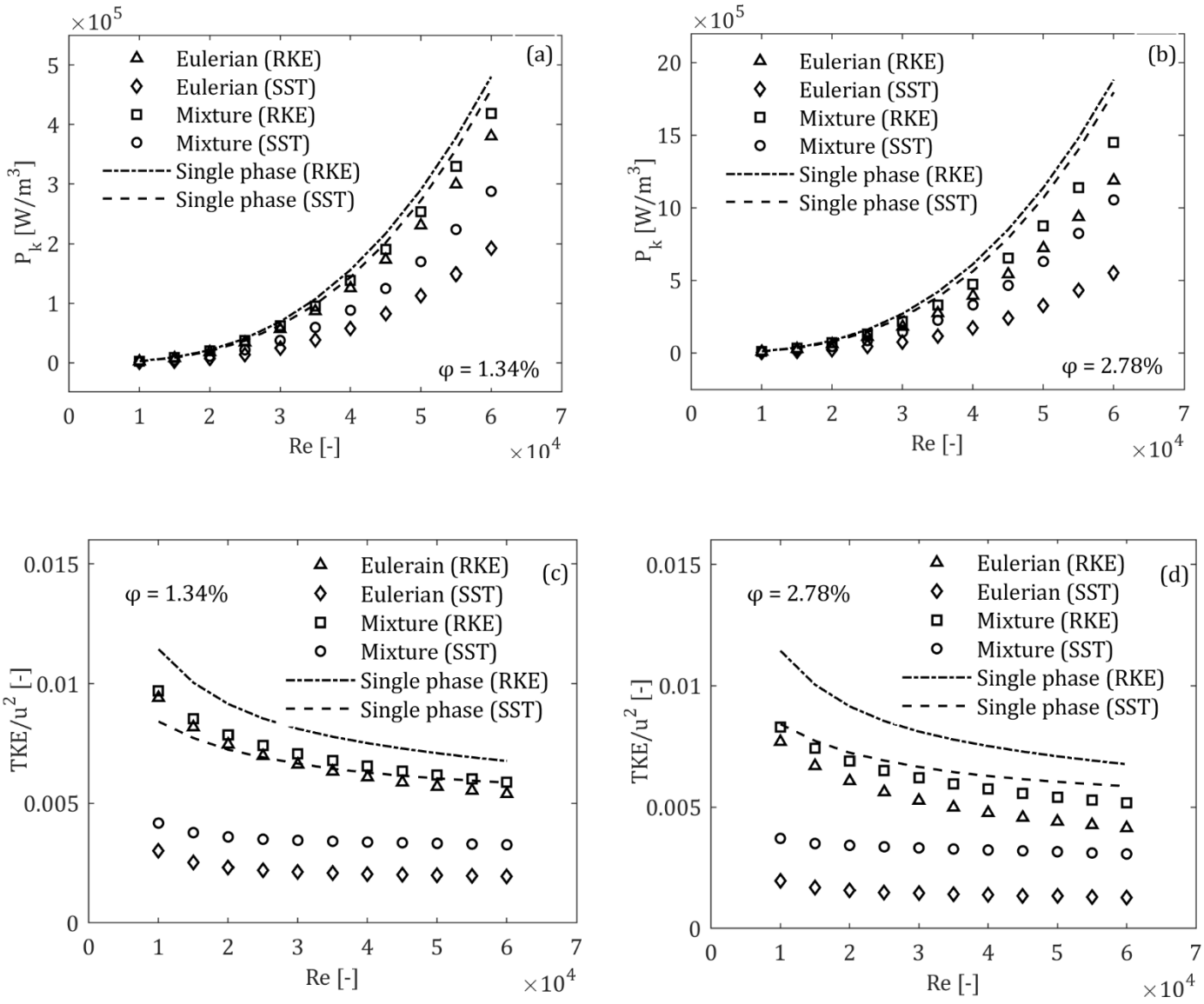

Figure 6. 8: Comparision of (a,b) Pk and (c,d) NTKE using SPM and TPM with two turbulent models at 1.34% and 2.78% vol. conc.

Figure 6. 9 illustrates the effect of turbulent viscosity in SPM and TPM for nanoparticle volume concentrations of 1.34% and 2.78%. It can be observed that the average turbulent viscosity increases with the Reynolds number. This can be due to the enhanced turbulent intensities at higher velocities. For instance, the single phase (RKE) at Re=60,000 exhibited higher levels of turbulent viscosity, signifying a larger TKE. In addition, the turbulent viscosity also increases with the nanoparticle volume concentration, indicating an improvement in the convective heat transfer.

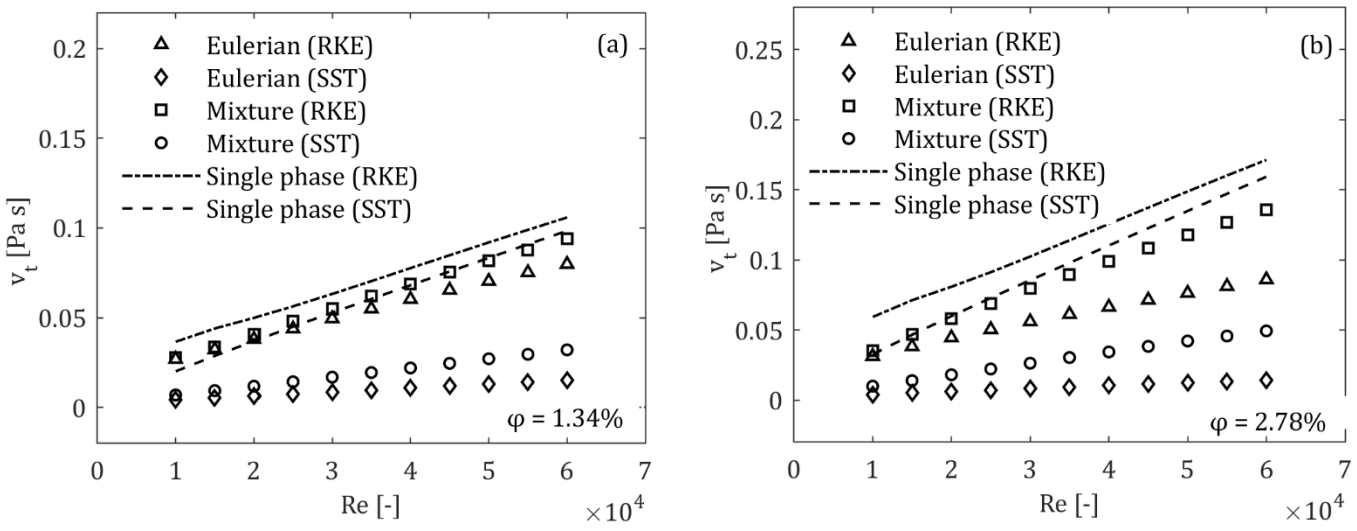

Figure 6. 9: Effect of the turbulent viscosity for different Re at (a) 1.34% (b) 2.78% vol. conc.

It was evident the RKE model exhibits higher viscosity values using SPM and TPM. This can be attributed to its turbulence modelling formulation, which was potentially more sensitive to certain flow conditions that overestimate turbulence production in the flow. The underlying reason lies in the transport equation of the dissipation rate, which was derived from the mean square vorticity fluctuation. It also includes the turbulent viscosity (C_μ) which accounts for mean and fluctuating velocity fields [199]. Due to the different transport equations and eddy viscosity formulations, the values of the dissipation term of RKE were much higher than those of the SST model. This resulted in the RKE model's overestimation of turbulent viscosity, leading to higher TKE values. Consequently, this explains large discrepancies in the Nu using Eulerian's RKE model compared to the experimental data. Moreover, the Eulerian formulation of the RKE model may introduce additional complexities such as particle-particle interactions and other phenomena such as Brownian motion, and dispersion effects, which may not fully be captured in this model. This can also be attributed to larger deviations of Nu. On the other hand, the SST's TPM models exhibit similar eddy viscosity profiles, which are higher than those predicted by SPM models along the tube axis.

Figure 6. 10 shows the effect of wall shear stress on different nanoparticle volume concentrations using SPM and TPM. It was evident from this numerical investigation that the wall shear increases

with the Reynolds number due to increased momentum transfer and shear forces near the wall. Additionally, the increase in nanoparticle volume concentrations significantly impacts the wall shear stress. For example, the wall shear stress of Mixture (RKE) increased from 146 Pa (φ = 1.34%) to 327 Pa (φ = 2.78%), respectively, at Re = 60,000. This enhancement of wall shear stress was due to the increase in thickness of the hydrodynamic boundary layer as more nanoparticles were added, thereby increasing the wall shear. This rise in wall shear stress due to the volume concentration can negatively affect the convective heat transfer because it leads to increased friction factor and pressure drop. All the wall shear stress profiles exhibited similar trends to the production term of TKE. At both volume concentrations, SPM exhibits the highest wall shear stress, specifically using the RKE turbulence model. This was due to the adverse effects of frictional forces exhibited by the fluid within the tube. In contrast, TPM's SST model obtained the lowest shear stress values for both Eulerian and mixture models. This was because of the significant impact of the lower turbulent viscosity values.

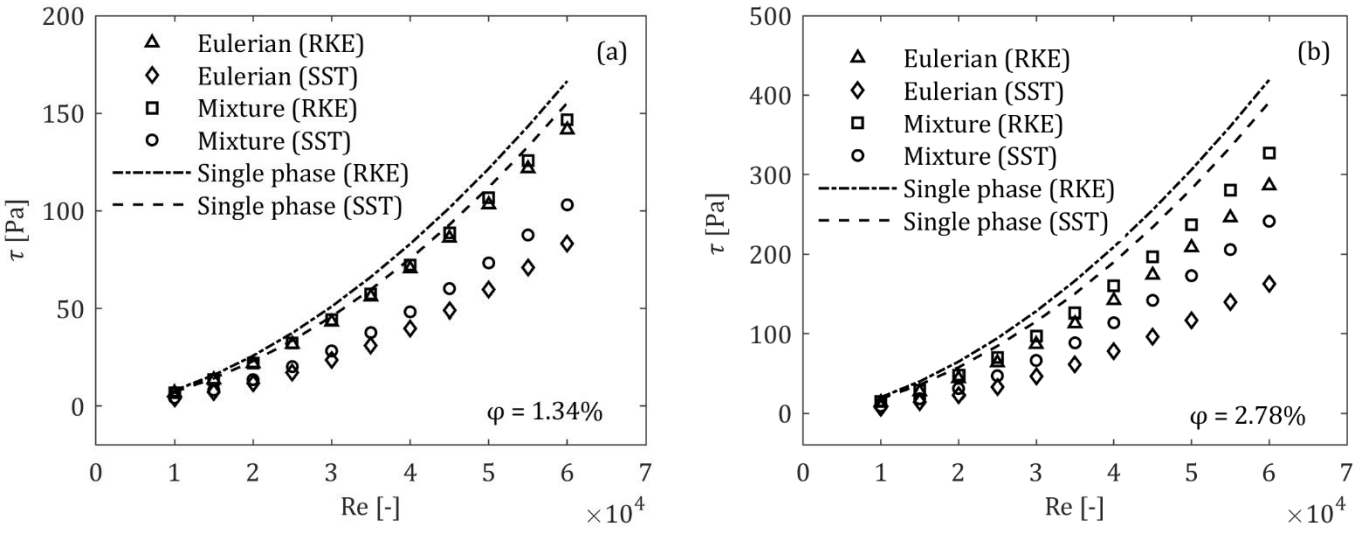

Figure 6. 10: Effect of the wall shear stress for different Re at (a) 1.34% (b) 2.78% vol. conc.

6.3 Summary

In this chapter, a numerical investigation was conducted to evaluate the accuracy of single-phase and two-phase models using the RKE and SST turbulence models for a circular tube under constant heat flux conditions with Al_2O_3-water nanofluid. Six combinations of nanofluid turbulence models were compared at 1.34% and 2.78% volume concentrations for Reynolds numbers ranging from 10,000 to 60,000. The single-phase model (SPM) showed good agreement with the experimental Nusselt number data from Pak and Cho [102], outperforming the two-phase model (TPM). Specifically, the RKE model performed better than the SST model. These numerical results were more accurate by considering the appropriate thermophysical property correlations outlined in Section 3.3. In the case of TPM, the SST model was more suitable, with the Eulerian and Mixture models showing results that were closer to the experimental data. The Eulerian model appeared to be the most appropriate within TPM. However, the RKE-Eulerian combination in TPM showed limitations, as it overestimated the Nusselt number by almost double compared to experimental values and failed to predict the friction factor accurately.

The significant deviation in the Nusselt number (Nu) of the Eulerian model using RKE can be attributed to two main factors. First, the turbulence models' impact on the numerical results was notable due to their transport equation formulations, which influenced the TKE due to higher turbulent viscosity values. Second, the TPM model has limitations in capturing particle-particle interactions, such as Brownian motion and dispersion effects. Addressing these limitations in the Eulerian RKE model may require the development of experimental validation for Al_2O_3-water nanofluid in future work, as currently, only Nusselt number data is available in the literature, limiting the accuracy of the current numerical study. Additionally, future work should also focus on advanced numerical techniques such as Large Eddy Simulation (LES) or Direct Numerical Simulation (DNS) to improve the accuracy of turbulence modelling. The discrete phase model (DPM) for nanofluid modelling could also be implemented.

Chapter 7: Fluid Effects: Impact of Hybrid Nanofluids on the Heat Transfer

Hybrid nanofluids are the combinations of hybrid nanoparticles (two or more nanoparticles) dispersed into the base fluid, such as water, ethylene glycol, etc. The hybrid nanoparticles are experimentally synthesised in the composite mixture form called hybrid nanocomposites. These hybrid nanocomposites are treated as single nanoparticles, which are then mixed with the base fluid. Therefore, it can be treated similarly to a nanofluid. This implies that one solid phase (a hybrid nanoparticle composite) and one liquid phase (base fluid) are used to model the hybrid nanofluid. Therefore, the assumption of three phases (nanoparticle 1, nanoparticle 2, and base fluid) for a hybrid nanofluid and the concept of three-phase modelling can be avoided. This assumption reduces the complexity of the numerical model and reflects the realistic approach of the experimental preparation of hybrid nanofluids.

This study focuses on Al_2O_3-based hybrid nanofluids, consisting of a combination of two nanoparticles in a base fluid. Aluminium oxide (Al_2O_3) is chosen as the primary nanoparticle due to its high thermal properties and stability, while the second nanoparticle, such as copper (Cu), copper oxide (CuO), titanium dioxide (TiO_2), silicon dioxide (SiO_2), magnesium oxide (MgO), etc., is varied to maximise the overall hybrid nanofluid's thermal characteristics. In this chapter, the single-phase model (SPM) with the Realizable k-ε approach (RKE) is used for modelling hybrid nanofluids. This chapter investigated the difference between the convective heat transfer of base fluid, nanofluid, and hybrid nanofluids in a heated circular tube. The effect of the hybrid nanoparticle composite mixture ratios was also examined. In addition, different hybrid nanofluids were also compared using the empirical correlations under turbulent flow conditions. Finally, this chapter evaluated the accuracy of classical models in predicting the Nusselt number.

7.1 Model description

The two-dimensional axi-symmetric model of a circular tube with a length of 0.4 m and a hydraulic diameter of 0.01 m, as detailed in Section 6.1, is employed in this study. Additionally, the tube material is assumed to be isotropic and homogeneous with a constant thermal conductivity, simplifying the thermal analysis.

7.1.1 Boundary conditions

The coupled and nonlinear partial differential equations were solved by using the appropriate boundary conditions. The inlet temperature of the hybrid nanofluid was 300K with a turbulent intensity of 5% for Reynolds numbers ranging from 10,000 to 60,000. A constant heat flux of $5 \times 10^5\ W/m^2$ was introduced on the wall pipe. The single-phase model (SPM) was used to model the hybrid nanofluids. The hybrid nanofluids' continuous phase (fluid) and discrete phase (nanoparticles) are in thermal equilibrium and share the same local velocity, with no slip between them. In addition, the hybrid nanoparticles were spherical, and the average size of the different nanoparticles was less than 40 nm. The Realizable k-ε approach (RKE) was implemented to model the turbulent flow with the enhanced wall treatment to capture the thermal and viscous effects near the wall region. At the outlet, the gauge pressure was maintained at $P_{guage} = 0$. The flow and thermal fields were assumed to be axisymmetric with respect to the horizontal plane. Finally, the flow was thermally and hydrodynamically fully developed at the pipe's end.

7.1.2 Mesh sensitivity test

Completed as per mesh sensitivity test in Section 4.1 of Chapter 4 using water at $Pr = 5.83$ under forced convection in a cylindrical tube. A grid size of 380,000 cells was selected for current calculations, ensuring consistency and computational efficiency.

7.1.3 Validation

The numerical validation was conducted for a smooth tube with water and Al_2O_3-water in Chapters 4 and 6, and the results were in an acceptable range. However, this section also included additional validation of 1% Al_2O_3-Cu/water hybrid nanofluid with the published data. The rationale for selecting 1% Al_2O_3-Cu/water hybrid nanofluid lies in its experimentally and numerically demonstrated superior heat transfer coefficients [38, 156, 170]. Al_2O_3 provides reliable stability, and Cu enhances thermal conductivity, providing a corresponding balance that improves heat transfer performance. Additionally, Al_2O_3-based hybrid nanofluids have been studied within limited volume concentrations (1–3%) and temperature ranges around 300 K, aligning closely with this study's heat transfer parameter range. The availability of thermophysical properties data for Al_2O_3-Cu at these specific ranges further supported its selection for this study as mentioned in Table 3.1 and Table 3.2 of Chapter 3. The selected 90:10 (Al_2O_3:Cu) ratio optimally balances conductivity and viscosity, enhancing performance without significant particle agglomeration. Therefore, Al_2O_3-Cu was selected as the ideal composition for validation in this study.

For the accuracy of this present numerical model, the simulated Nusselt number of the Al_2O_3-Cu/water hybrid nanofluid at 1% volume concentration with a nanocomposite mixture ratio of 90:10 was compared with the Takabi and Shokouhmand [38] data as shown in Figure 7. 1. The average deviation of the Nusselt number was 2.9% compared to published data, indicating a closer alignment for Reynolds numbers ranging from 10,000 to 60,000. This suggests that the effectiveness of SPM with the RKE model captured flow physics accurately. The maximum deviation of 6.2% was obtained at Re = 20,000, and the minimum difference of 0.4% was observed at Re = 50,000, respectively. This implies that average deviations of Nu decreased with increasing Reynolds number. Therefore, it was evident that this computational model is reliable in predicting the heat transfer performance of the hybrid nanofluids. In addition, Al_2O_3-Cu/water hybrid nanofluid at 1% volume concentration is specifically considered because of the limited availability of experimental data to support validation.

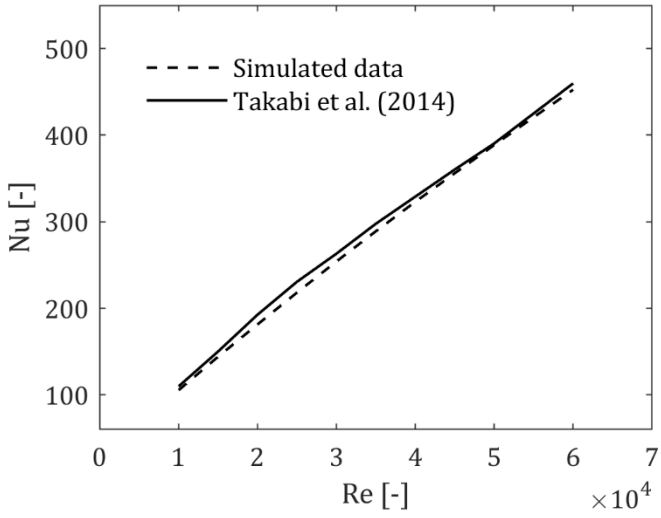

Figure 7. 1: comparison of simulated Nusselt number data with published data of Al_2O_3-Cu/water at 1% volume concentration

7.2 Results and Discussion

The numerical investigations of forced convective heat transfer were conducted for different Al_2O_3 based hybrid nanofluids and various hybrid nanoparticle composite mixture ratios with a Prandtl number ranging from 5.83 to 31.4. The results were presented in terms of Nusselt number, wall and bulk temperature, pressure drop, etc., to understand the hydrodynamic and thermal performance of the hybrid nanofluids for a fully developed flow under a turbulent regime.

7.2.1 Heat transfer comparison of base fluid, nanofluid and hybrid nanofluid

Figure 7. 2 illustrates the comparison of Nusselt numbers for water, Al_2O_3-water nanofluid, and Al_2O_3-Cu/water hybrid nanofluid with a mixture ratio of 90:10 at different Reynolds numbers and volume concentrations (φ = 1 – 2%). It can be observed that the Nusselt number increases with the increase in Reynolds number and the nanoparticle volume concentration. It was also evident that the hybrid nanofluids exhibited the highest Nusselt number compared to the nanofluid and water. For instance, the average Nusselt number of Al_2O_3-Cu/water hybrid nanofluid was increased from

23.9% to 28.4% from 1% to 2% volume concentration compared to the water. In contrast, Al_2O_3-water nanofluid's Nu increased from 11% (φ = 1%) to 21.1% (φ = 2%) for the Reynolds number ranging from 10,000 to 60,000 respectively. This implies that the hybrid nanofluid consistently showed higher heat transfer coefficients, indicating a significant improvement in overall heat transfer. In addition, the increment in heat transfer with an increase in volume concentration was attributed to the enhancement in fluid thermal properties due to the addition of nanoparticles to the base fluid.

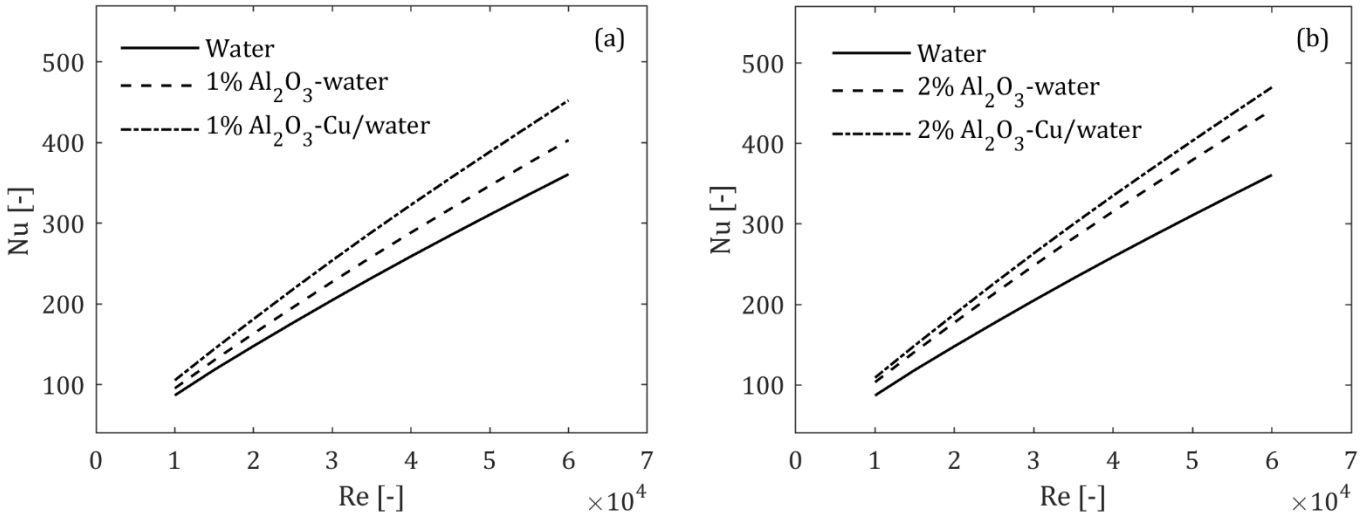

Figure 7. 2: Nusselt number comparison of water, nanofluid and hybrid nanofluid at different Reynolds numbers

It is important to note that the thermophysical properties of the fluids were obtained from the experimental data, including Al_2O_3-Cu/water hybrid nanofluid (90:10) as mentioned in Section 3.4 of Chapter 3.

The impact of wall and bulk temperatures for water, Al_2O_3-water nanofluid, and Al_2O_3-Cu/water hybrid nanofluid at different volume concentrations under turbulent flow conditions was depicted in Figure 7. 3. Results show that both wall and bulk temperature decrease with an increase in Reynolds number. This is because higher Reynolds numbers correspond to greater fluid velocities, which shortens the fluid contact time within the heated tube. This phenomenon reduces the fluid temperature. In addition, it can also be observed that the wall and bulk temperature also decrease

with increasing the Prandtl number. This indicates that the Al_2O_3-Cu/water hybrid nanofluid exhibited the lower temperature profiles compared to the Al_2O_3-water nanofluid and pure water.

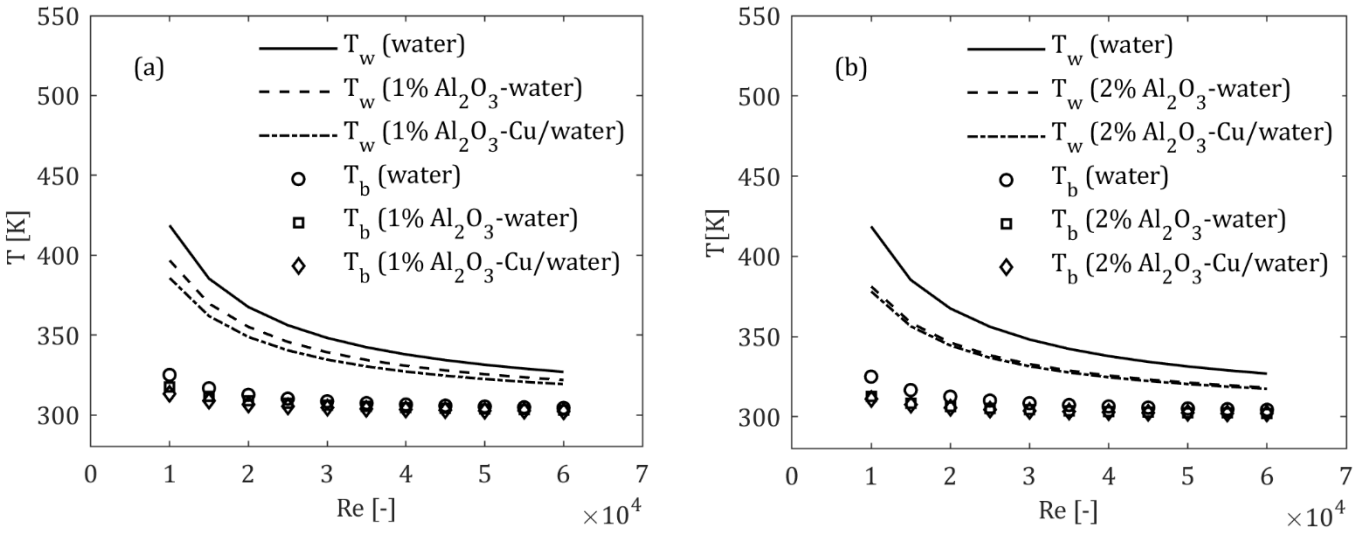

Figure 7. 3: Comparison of average wall and bulk temperatures of different fluids at various Reynolds numbers

For example, the average temperature differences ($T_w - T_b$) for water, 1% Al_2O_3-water nanofluid, and Al_2O_3-Cu/water hybrid nanofluid were 93.6 K, 79.2 K, and 72.7 K, respectively, at Re = 10,000. These lower ($T_w - T_b$) values indicate higher heat transfer coefficients. This improvement in heat transfer can be explained by the behaviour of nanoparticles in the hybrid nanofluid flow inside the tube. When the nanoparticles within the fluid come into contact with the tube's wall, they absorb thermal energy from the wall, effectively lowering the wall temperature. The absorbed thermal energy is then mixed into the bulk fluid as the nanoparticles move away from the wall. This process enhances the overall heat transfer from the wall to the fluid, contributing to a lower bulk temperature as well. Also, this effect is much higher at higher volume concentrations, with more reduction in fluid temperature values. Thus, hybrid nanofluid exhibits high convective heat transfer rates.

Figure 7. 4 shows the comparison of pressure drop for different working fluids for 1% and 2% volume concentrations for a Reynolds number ranging from 10,000 to 60,000. From both figures, the pressure drop increases with an increase in the Reynolds number due to the increase in the frictional forces. In addition, the Al_2O_3-Cu/water hybrid nanofluid exhibited a higher pressure drop

at 1% volume concentration compared to the 1% Al_2O_3-water nanofluid and pure water, as shown in Figure 7. 4a. A similar trend was observed at 2% volume concentration in Figure 7. 4b, where the hybrid nanofluid shows an even greater increase in pressure drop compared to the other fluids. For instance, the pressure drop for 2% Al_2O_3-Cu/water hybrid nanofluid was approximately 12,398 Pa, while for 2% Al_2O_3-water nanofluid and pure water it was around 8,472 Pa and 2254 Pa at Re = 60,000, respectively.

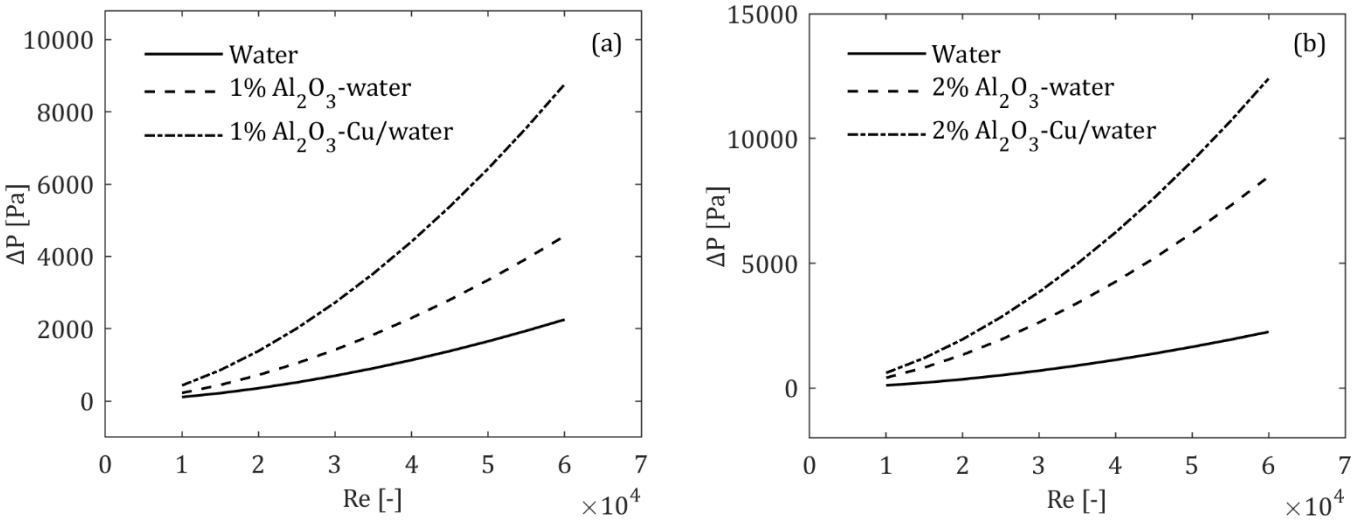

Figure 7. 4: Comparison of pressure drop of different fluids at various Reynolds numbers

Therefore, it was evident that the pressure drop increases with the increase in nanoparticle volume concentration. The reason for the higher pressure drop in hybrid nanofluids was due to the presence of nanoparticles, which improved the viscosity and density. Moreover, the interaction between Al_2O_3 and Cu nanoparticles further increases the fluid's resistance to flow, resulting in a higher pressure drop.

Figure 7. 5 compares the average turbulent kinetic energy (TKE) of water, Al_2O_3-water nanofluid (φ = 1-2%), and Al_2O_3-Cu/water hybrid nanofluid (φ = 1-2%) at various Reynolds numbers. As the Reynolds number increases, the TKE of all fluids also increases, indicating more turbulent flow at higher velocities. The hybrid nanofluid (Al_2O_3-Cu/water) consistently exhibits the highest TKE across all Reynolds numbers, followed by the Al_2O_3-water nanofluid and then pure water. This

suggests that the addition of nanoparticles, especially the combination of Al_2O_3 and Cu, enhances turbulence within the fluid, leading to improved mixing and energy transfer capabilities. Specifically, at higher volume concentrations (2%), the hybrid nanofluid demonstrates even greater TKE, further emphasising the impact of nanoparticle concentration on fluid turbulence.

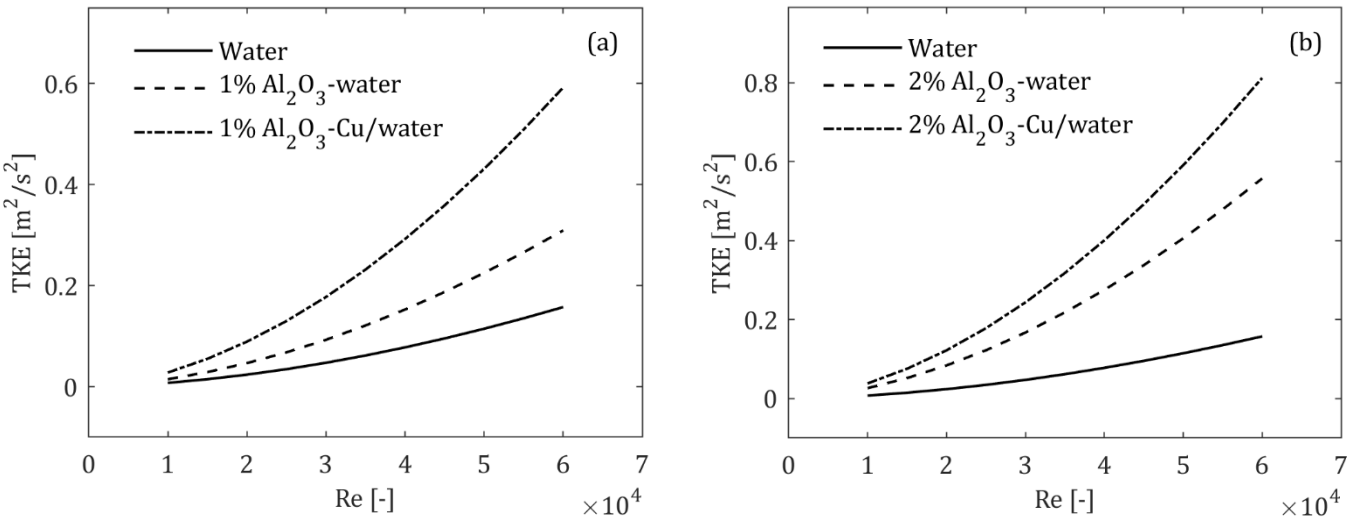

Figure 7. 5: Comparison of average turbulent kinetic energy of different fluids at various Reynolds numbers

Figure 7. 6 depicts the comparison of average wall shear stress (τ) for different fluids under turbulent flow conditions. Results reveal that the wall shear stress increases with Reynolds number for all fluids. In addition, the hybrid nanofluid (Al_2O_3-Cu/water) shows the highest wall shear stress compared to pure water and Al_2O_3-water nanofluid for both 1% and 2% volume concentrations. This is due to the larger shear forces obtained near the wall region for hybrid nanofluids. For example, the average wall shear of 2% Al_2O_3-Cu/water hybrid nanofluid was 4.49 times larger than the pure water at Re = 10,000 to 60,000, respectively.

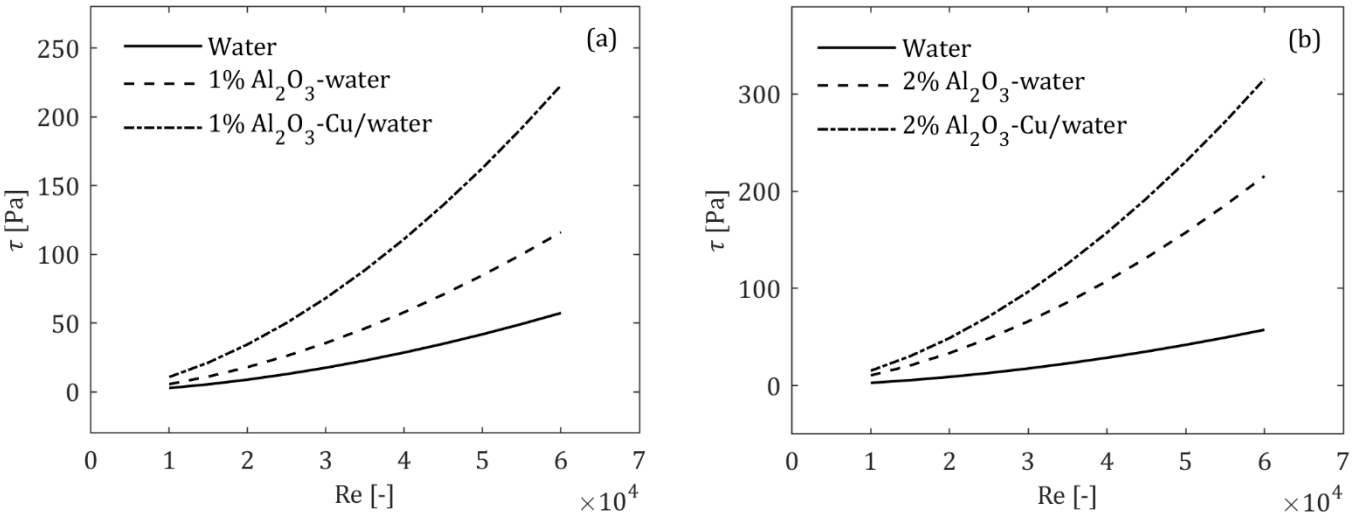

Figure 7. 6: Comparison of average wall shear stress of different fluids at various Reynolds numbers

7.2.2 Impact of hybrid nanoparticle composite mixture ratio

Due to limited experimental data of Al_2O_3-Cu/water hybrid nanofluid, this section considered the Al_2O_3-CuO/water-Ethylene Glycol (60:40) hybrid nanofluid to further investigate the impact of the hybrid composite mixture ratio on convective heat transfer. The experimental data of 1% Al_2O_3-CuO/W-EG (60:40) hybrid nanofluid was taken from the reference [155]. It can be noted that the based fluid mixture ratio (60:40) was kept constant along with the nanoparticle volume concentration (φ = 1%) for various numerical simulations. This means 60% of the base fluid concentration was treated as water and 40% to be ethylene glycol together to form a mixture.

Figure 7. 7 illustrates the effect of different nanoparticle mixture ratios (20:80, 40:60, 50:50, and 60:40) at 1% Al_2O_3-CuO/W-EG hybrid nanofluids compared to pure water using the heat transfer coefficient and the pressure drop ratios at different Reynolds numbers. It was evident that the heat transfer coefficient and the pressure drop ratios increase with higher proportions of Al_2O_3 in the hybrid nanofluid mixture. Specifically, the 60:40 (Al_2O_3: CuO) mixture exhibited the highest heat transfer coefficient of 22.7% with a pressure drop 3.7 times larger than that of the smooth tube with water for Re = 10,000 to 60,000. This improvement in heat transfer was attributed to the higher Prandtl number associated with the 60:40 (Al_2O_3) mixture. Conversely, a peculiar behaviour was

observed at the 20:80 (Al_2O_3: CuO) mixture, which showed the least heat transfer rates (h/h0<1) where the Al_2O_3 concentrations were minimal. This indicates that this combination was less effective than the base fluid (water-ethylene glycol).

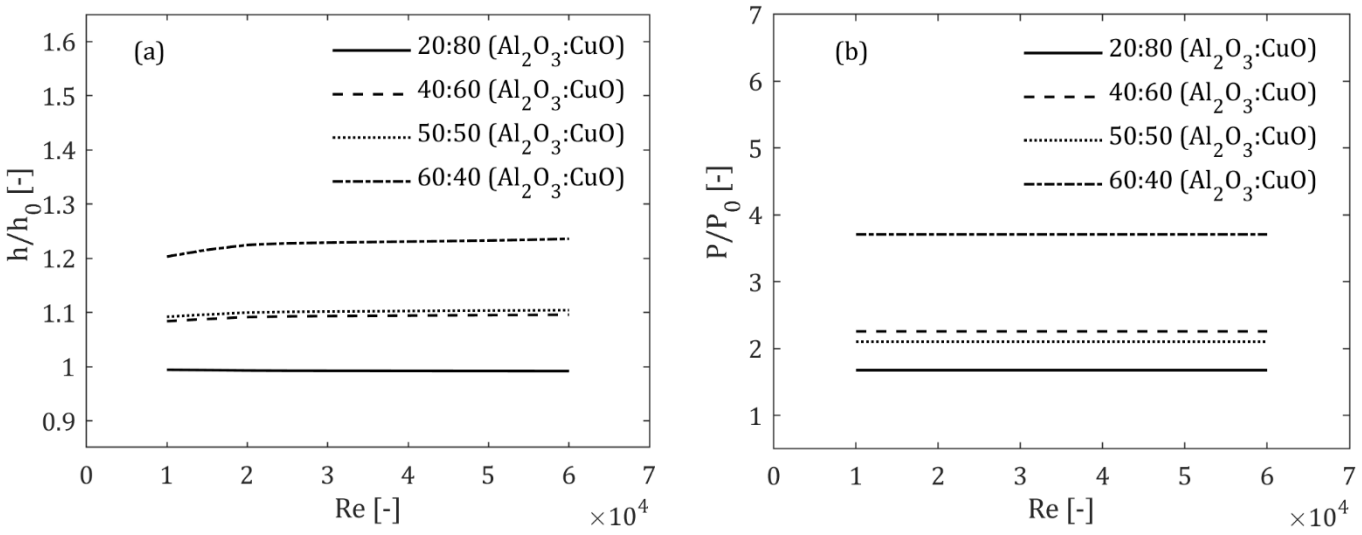

Figure 7. 7: Comparison of (a) heat transfer coefficient (b) Pressure drop at different hybrid nanocomposite mixture ratio of 1% Al_2O_3-CuO/W-EG hybrid nanofluid

Another significant observation was that despite the 40:60 (Al_2O_3: CuO) combination having a higher pressure drop than the 50:50 (Al_2O_3: CuO) combination, it exhibited lower heat transfer rates. In addition, for almost all cases, the pressure drop remained constant with increasing Reynolds number and mixture ratio. Furthermore, it can also be noted that the 1% Al_2O_3-CuO/W-EG hybrid nanofluid (60:40) has a higher Nusselt number compared to the 1 and 2% Al_2O_3-Cu/water hybrid nanofluid due to its superior thermal properties.

7.2.3 Comparison of different hybrid fluids using empirical models

This section examines only a few hybrid nanofluids because the experimental data based on the available range of temperature, volume concentration, nanoparticle size, and hybrid nanocomposite mixture ratio were limited. This numerical analysis was conducted to identify the effective hybrid

nanofluid combination that has maximum heat transfer performance. The thermo-physical properties of different hybrid nanofluids were mentioned in Table 3.1 of Chapter 3.

The effect of different hybrid nanofluids with various mixture ratios on convective heat transfer was compared at 1% volume concentration under turbulent flow conditions, as shown in Figure 7. 8. It was evident that all hybrid nanofluids exhibited increasing trends of the Nusselt number. Specifically, 1% Al_2O_3-CuO/W-EG (60:40) exhibited the highest Nusselt number compared to the other combinations. This heat transfer enhancement was due to the combined effect of base fluid (water-ethylene glycol mixture) and nanoparticles (Al_2O_3-CuO mixture) with superior thermal properties.

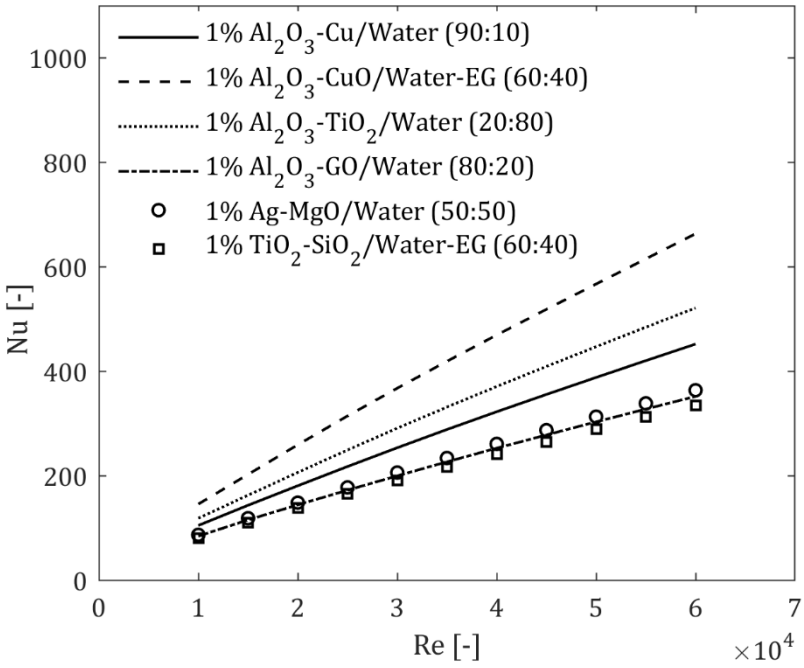

Figure 7. 8: Comparison of Nusselt number for different hybrid nanofluids at 1% volume concentration

For instance, the average increment in Nusselt number of 1% Al_2O_3-CuO/W-EG (60:40) was 78.8% higher than the pure water. This was followed by Al_2O_3-TiO2/water (60:40) and Al_2O_3-Cu-water (90:10) with average enhancements of 41.9% and 23.9%, respectively, for Re = 10,000 to 60,000. However, Al_2O_3-GO/water (80:20), Ag-MgO/water (50:50), and TiO2-SiO2/W-EG (60:40) did not show any significant improvements in Nu compared to the pure water.

Figure 7. 9 presents the performance evaluation criteria (PEC) for different hybrid nanofluids at 1% volume concentration across various Reynolds numbers. The findings show that the 1% Al_2O_3-CuO/W-EG (60:40) hybrid nanofluid demonstrated the highest PEC, reaching above 1.78, indicating superior performance in terms of heat transfer enhancement and pressure drop. Consequently, this hybrid nanofluid was identified as the optimal working fluid. The maximum enhancement of heat transfer of 83.8% was observed at Re = 60,000 compared to the pure water. Hence, this optimal Reynolds number can be employed as a standard case for developing efficient thermal systems.

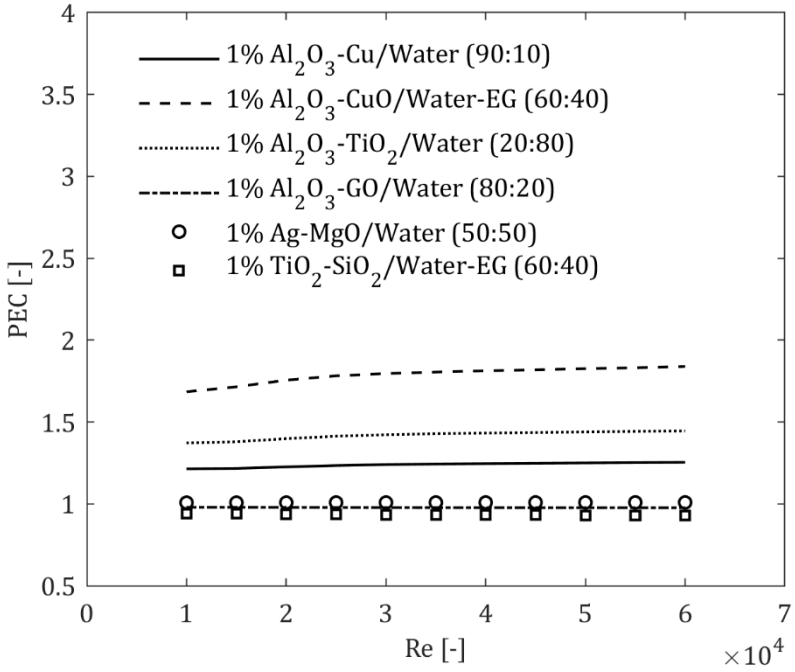

Figure 7. 9: Comparison of PEC for different hybrid nanofluids at 1% volume concentration

An exceptional finding was also observed for the two hybrid nanofluids (Al_2O_3-GO/water (80:20) and TiO2-SiO2/W-EG (60:40), where the average PEC was less than 1, which suggests the heat transfer was less than water for different Reynolds numbers. This implies the reduction in convective heat transfer. Typically, the addition of nanoparticles to the based fluid should improve the heat transfer, according to the open literature. This discrepancy indicates the inaccurate values of the empirical data or correlations obtained.

7.2.4 Impact of the classical model's accuracy

Due to the limited experimental research conducted on hybrid nanofluids, most researchers rely on classical models for calculating the thermophysical properties of different hybrid nanofluids. The density and specific heat equations, as mentioned in Section 3.4.2 of Chapter 3, were based on the linear equation due to their simplicity and reliability; they provided accurate values. However, calculating the thermal conductivity and viscosity of nanofluids and hybrid nanofluids raises the issue due to consideration of a wide range of parameters such as temperature, volume fraction, nanoparticle size, mixture ratio, etc. Therefore, the accuracy of the classical models remains uncertain and not explored widely. This section compares the experimental data of Al_2O_3-Cu/water (90:10) hybrid nanofluid as a reference to compare the classical models.

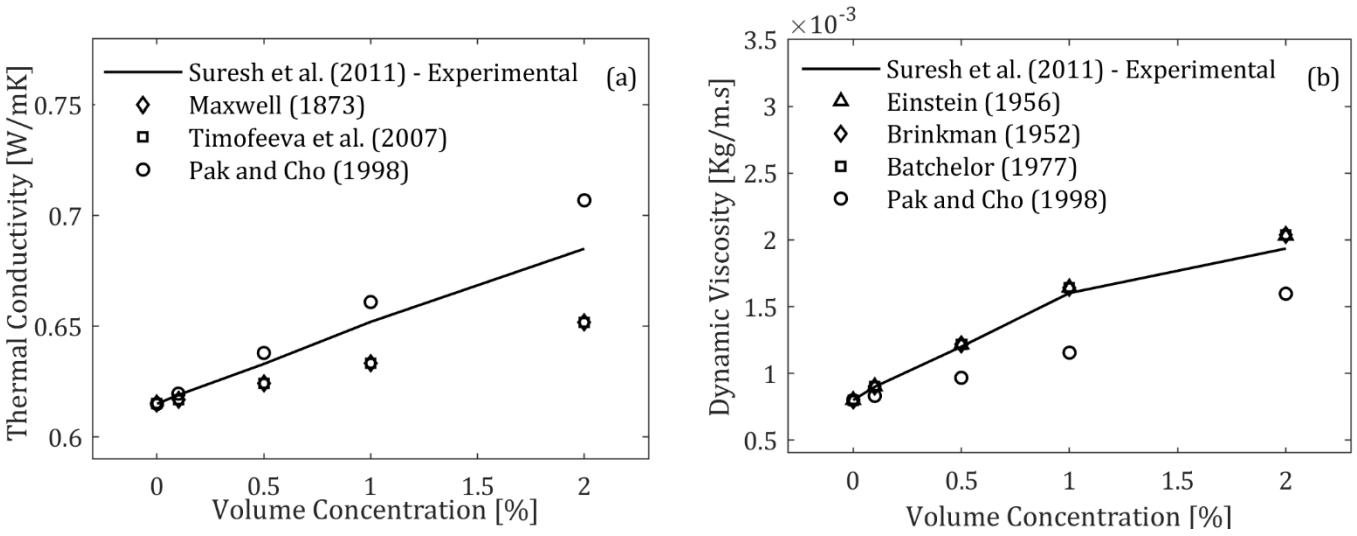

Figure 7. 10: Comparison of thermal conductivity and viscosity of Al203/Cu-water hybrid nanofluid using classical models at 300K

Figure 7. 10 compares the thermal conductivity and viscosity of Al_2O_3-Cu/water hybrid nanofluid with the classical models for different volume concentrations. Results reveal that the thermal conductivity and viscosity values increase almost linearly with the nanoparticle volume concentration. This indicates the presence of nanoparticles enhanced the thermal properties of

hybrid nanofluid. From Figure 7. 10a, the experimental data of Suresh, et al. [215] are closely aligned by the thermal conductivity trend predicted by the Pak and Cho [102] model, where the average error between them was around 1%, approximately for φ = 1-2%. In contrast, other classical models such as Maxwell [87] and Timofeeva, et al. [206] underestimated the experimental data.

Similarly, the dynamic viscosity of Al_2O_3-Cu/water hybrid nanofluid predicted by the Einstein [207] model also showed closer agreement with the empirical data followed by the Brinkman [108], Batch - Batchelor [208] models, as shown in Figure 7. 10b. However, the Pak and Cho [102] viscosity model exhibited larger deviations.

Since the Pak and Cho [102] thermal conductivity model and Einstein [207] viscosity model predicted accurate thermo-physical properties of hybrid nanofluid. The impact of different mixture ratios using these classical models at 1% Al_2O_3-Cu/water was investigated to understand the thermal and hydrodynamic behaviour accuracy of the single tube heat exchanger.

Figure 7. 11 depicts the comparison of Nusselt numbers for different hybrid nanocomposite mixture ratios (20:80, 40:60, 50:50, and 60:40) at 1% Al_2O_3-Cu/water hybrid nanofluid under turbulent flow conditions. For all mixture ratios, the Nusselt number increases with Reynolds number, showing that heat transfer improves with higher flow rates. However, it can be observed that the Nusselt number did not vary for different mixture ratios; in fact, Nu values are almost the same for all Reynolds numbers ranging from 10,000 to 60,000. This implies that the classical models failed to predict the convective heat transfer coefficients. This is because the thermal conductivity and viscosity predicted by the classical models were the same, which led to fewer fluctuations in the Prandtl number as mentioned in Table 7. 1.

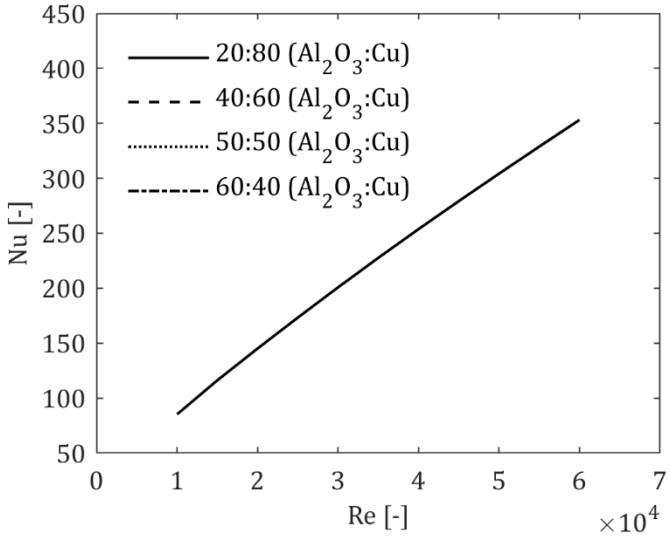

Figure 7. 11: Nusselt number comparison of different mixture ratio at 1% volume concentration for various Reynolds numbers

Table 7. 1: Thermo-physical properties of different mixture ratio at 1% Al_2O_3-Cu/water hybrid nanofluid

Mixture ratio	$\boldsymbol{\rho[kg/m^3]}$	$\boldsymbol{c_p[J/kgK]}$	$\boldsymbol{k\ [w/mK]}$	$\boldsymbol{\mu\ [Kg/m\ s]}$	$\boldsymbol{Pr}$
20:80	1065.203	4140.898	**0.6609**	**0.00082**	5.137747
40:60	1055.263	4141.677	**0.6609**	**0.00082**	5.138712
50:50	1050.293	4142.066	**0.6609**	**0.00082**	5.139195
60:40	1045.323	4142.455	**0.6609**	**0.00082**	5.139678

The impact of different Al_2O_3-based hybrid nanofluids was also evaluated to test the accuracy of the classical models using the Pak and Cho [102] thermal conductivity model and Einstein [207] viscosity at 1% volume concentration.

Figure 7. 12 illustrates the comparison of Nusselt numbers for different hybrid nanofluids with a mixture ratio of 60:40 at 1% nanoparticle volume concentration. Results show that the Nusselt number increases with the Reynolds number, indicating improved heat transfer performance at higher Reynolds numbers for all hybrid nanofluids. It can also be observed that the trend of the Nusselt number was almost identical for all combinations of hybrid nanofluids. Again, this points

out the inaccuracy of the classical models' predictions of the same thermal conductivity and viscosity values as highlighted in Table 7. 2. Therefore, the classical models are ineffective in predicting heat transfer because they fail to consider the fluid parameters such as nanoparticle diameter, volume concentration, mixture ratio, etc.

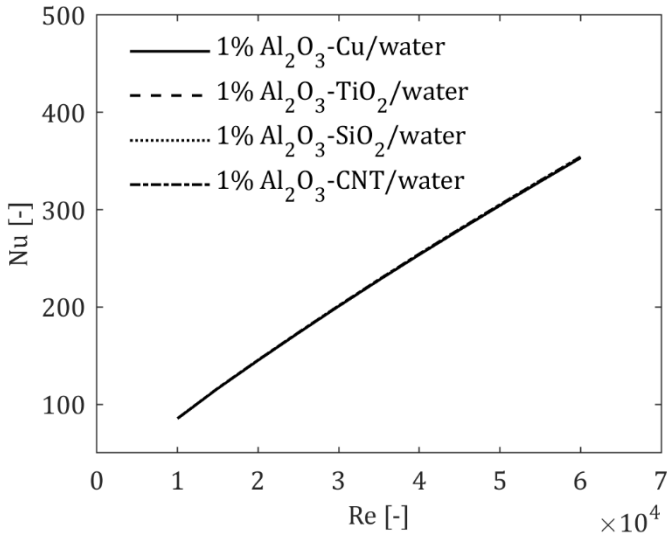

Figure 7. 12: Nusselt number comparison of different hybrid nanofluids at 1% volume concentration for various Reynolds numbers

Table 7. 2: Thermo-physical properties of different hybrid nanofluids at 1% volume concentration

Hybrid nanofluids	$\boldsymbol{\rho[kg/m^3]}$	$\boldsymbol{c_p[J/kgK]}$	$\boldsymbol{k\ [w/mK]}$	$\boldsymbol{\mu\ [Kg/m\ s]}$	***Pr***
Al_2O_3-Cu/water	1045.323	4142.455	**0.6609**	**0.00082**	5.139678
Al_2O_3-TiO2/water	1007.338	4143.663	**0.6609**	**0.00082**	5.141177
Al_2O_3-SiO2/water	999.2182	4143.707	**0.6609**	**0.00082**	5.141232
Al_2O_3-CNT/water	1017.963	4177.391	**0.6609**	**0.00082**	5.183024

Hence, it is important to rely on empirical correlations or data because classical methods clearly failed to predict the heat transfer for different mixture ratios and different hybrid nanofluids because of their incorrect thermophysical properties that do not replicate the experimental data.

7.3 Summary

In this chapter, the numerical study focused on exploring different hybrid nanofluids to study the thermal and hydrodynamic behaviour under a turbulent regime. The impact of hybrid nanocomposite mixture ratios and different types of hybrid nanoparticle combinations was also examined to determine the optimal nanofluid combination with enhanced heat transfer in a single tube heat exchanger.

The following conclusions can be summarised as:

- The hybrid nanofluids demonstrated superior heat transfer properties, such as Nusselt number, pressure drop, turbulent kinetic energy, and wall shear stress, compared to both nanofluids and pure water. Specifically, a hybrid nanofluid with a nanoparticle mixture ratio of 90:10 (Al_2O_3: Cu) exhibited the highest heat transfer coefficients.

- The Al_2O_3-CuO/W-EG (60:40) hybrid nanofluid exhibited higher PEC values due to its maximum Prandtl number and was identified as the optimal working fluid compared to other combinations. This indicates the potential of hybrid nanofluids for various heat transfer applications, providing high thermal performance with minimal pressure drop.

- The classical models failed to accurately predict the Nusselt number for different nanoparticle mixture ratios and Al_2O_3-based hybrid nanofluids. This was primarily due to inaccurate thermal conductivity and viscosity values.

Therefore, the implementation of different hybrid nanofluids in any thermal system can improve the overall convective heat transfer performance. While this study focused particularly on Al_2O_3-based hybrid nanofluids, exploring other alternatives such as TiO_2, SiO_2, graphene, and carbon nanotubes could improve its industrial relevance. TiO_2 and SiO_2 stand out for their cost-effectiveness and durability [216, 217], while graphene and carbon nanotubes provide exceptional thermal conductivity [218, 219], ideal for high-performance heat transfer systems in electronics and aerospace. Future research contrasting these with Al_2O_3-CuO nanofluids could enhance

understanding of hybrid nanofluid efficiency, making the findings more applicable across diverse fields of heat transfer.

Chapter 8: Geometry and Fluid effects - Impact of Groove and Nanofluids

This chapter focuses on enhancing heat transfer by integrating effective grooves in a corrugated tube with nanofluids and hybrid nanofluids. The triangular grooves, which showed the highest thermal performance factor (PEC), are considered the optimal groove combination. These grooves are then combined with nanofluids and hybrid nanofluids to achieve maximum heat transfer. Although higher volume concentrations of nanofluids exhibit the highest heat transfer coefficients from the open literature, they come with challenges such as agglomeration, etc. For modelling nanofluids, hybrid nanofluids, and turbulent flows, the single-phase model combined with the Realizable k-ε (RKE) turbulence model was employed due to its proven accuracy in capturing the flow and heat transfer characteristics. The same boundary conditions were applied to the circular tube with corrugation under constant heat flux in a turbulent flow. Numerical results were assessed in terms of Nusselt number, turbulent kinetic energy, and PEC at various volume concentrations. Finally, numerical correlations were then developed to predict the Nusselt number for triangular grooves using nanofluids with different volume fractions.

8.1 Results and discussion

8.1.1 Triangular Groove with Al_2O_3-water nanofluid

This section combines the effects of triangular grooves with Al_2O_3 -water nanofluid at different volume concentrations to examine the thermal behaviour of the single tube heat exchanger. Figure 8. 1 illustrates the ratio of the Nusselt number of grooved tubes (Nu_g) to the Nusselt number of the smooth tube (Nu_s) across various Reynolds numbers and different volume concentrations. The results show that the ratio of Nusselt number increases with the nanoparticle volume concentrations from 1.34% to 2.78%. This is because the enhanced thermal conductivity of the nanofluid at higher volume concentrations. For instance, the average increments in Nusselt

numbers were 35.45%, 58.18%, and 83.22% for triangular grooves at particle volume concentrations of 0%, 1.34%, and 2.78%, respectively, compared to the smooth tube with water for Re = 10,000 to 60,000. This indicates that the presence of triangular grooves along with nanofluid enhances the overall convection rate by almost double compared to a smooth tube without corrugation.

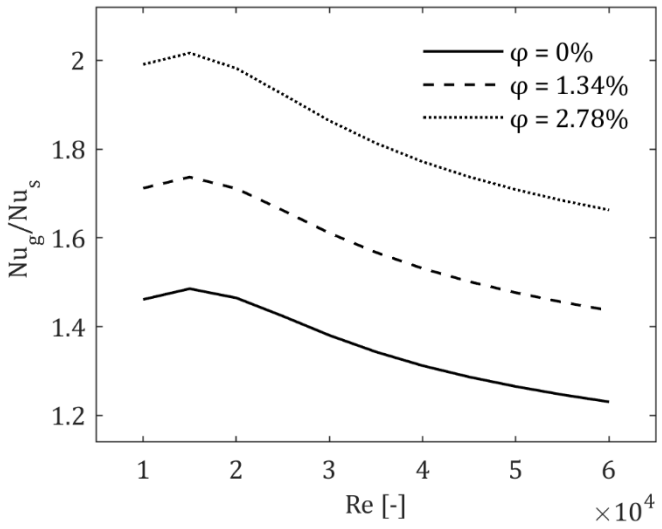

Figure 8. 1: Nusselt number ratio of triangular groove at different nanoparticle volume concentrations

It was evident that the influence of the Reynolds number was also significant for convective heat transfer. At lower Reynolds numbers, the Nu_g/Nu_s ratio is higher, indicating that the enhancement in heat transfer due to grooves and nanoparticles is more significant at lower flow rates. Specifically, the highest ratio of Nusselt number (φ = 2.78%) was observed at a Reynolds number of 15,000, which was almost 2.02 times higher than the smooth tube with water. As the Reynolds number increases, the Nu_g/Nu_s ratio decreases for all volume concentrations. This suggests that the relative benefit of using grooves and nanoparticles diminishes at higher flow rates.

The effect of turbulent kinetic energy ratio for a triangular groove (TKE_g) to that of a smooth tube (TKE_s) at different nanoparticle volume concentrations (0%, 1.34%, and 2.78%) across various Reynolds numbers was depicted in Figure 8. 2. As the volume concentration of Al_2O_3 nanoparticles increased from 0% to 2.78%, the TKE ratio experienced a drastic improvement. For example, the

average TKE ratio of the triangular groove increases from 1.92 to 11.39 times higher than the smooth tube for 0% to 2.78% volume concentration. This huge enhancement was because of the combined effect of nanofluid properties and the triangular groove shape. This implies that the increase in TKE is significantly reflected in the turbulence generation and heat transfer coefficient enhancements as mentioned in Figure 8. 1. In addition, the increment in TKE ratio was more pronounced at high volume concentrations. This suggests that the effect of nanoparticles on turbulence is more dominant than the effect of increasing Reynolds number. In contrast, the TKE ratio of water (φ = 0%) remains stable and almost constant, indicating that the increase in Reynolds number does not significantly impact the flow behaviour due to the absence of nanoparticles.

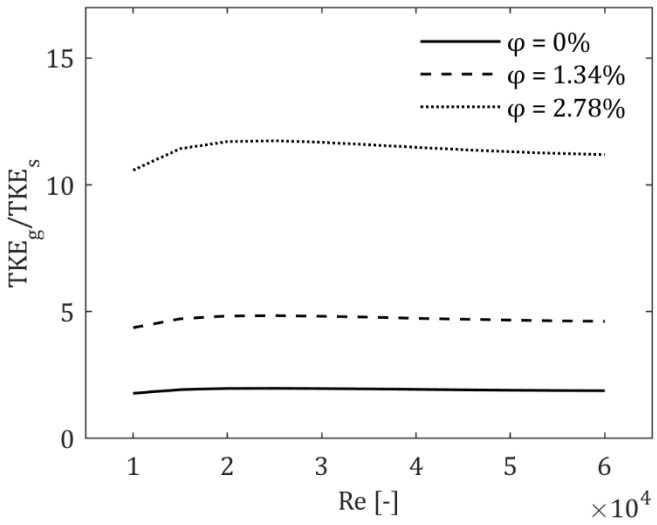

Figure 8. 2: TKE ratio of triangular groove at different nanoparticle volume concentrations

Figure 8. 3 shows the Performance Evaluation Criterion (PEC) of triangular grooves at different nanoparticle volume concentrations across various Reynolds numbers (10,000 to 60,000). It can be observed that the PEC significantly increases as the Al_2O_3 nanoparticle volume concentration increases from 0% to 2.78%, respectively. At a nanoparticle concentration of 2.78%, the triangular groove PEC was consistently higher than at 0% and 1.34%, with an average increment of 35.26% compared to the smooth tube with water at different Reynolds numbers. However, the optimal PEC was achieved at the Reynolds number of 10,000, where the PEC has the highest value of 1.48 at a particle volume concentration of 2.78%. This indicates the maximum performance obtained by combining the triangular grooves and Al_2O_3-water nanofluid at high volume concentration.

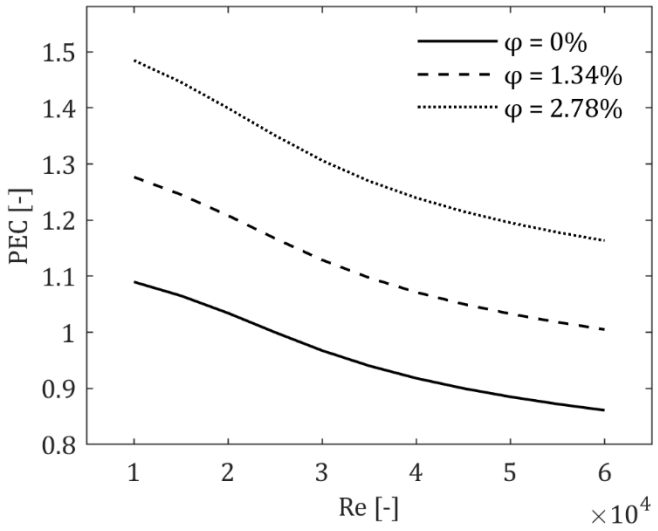

Figure 8. 3: PEC of triangular groove at different nanoparticle volume concentrations

This study also developed a new correlation using non-linear regression analysis to accurately calculate the Nusselt number (*Nu*), which is a function of Reynolds number (*Re*) and Prandtl number (*Pr*). The numerical tests are conducted with different volume concentrations ranging from 0% to 2.78%, where the Prandtl numbers are between 5.83 and 12.33. This correlation provides the combined effect of the Al_2O_3 -water nanofluid and the triangular grooves and covers a wide range of values. The following correlation was obtained from the single-phase model results and expressed as follows:

$$Nu = 0.1127\ Re^{0.5091}\ Pr^{0.6706} \tag{8.1}$$

The above equation is applicable for the following ranges of parameters:

$$1 \times 10^5 \leq Re \leq\ 6 \times 10^5;\ 5.83 \leq\ Pr\ \leq 12.33;\ 0 \leq\ \varphi\ (\%) \leq 2.78$$

The correlation exhibits a maximum, mean, and standard deviation of relative error less than 1%, which appears far more reasonable. It is important to consider that the numerical results were based on Pak and Cho [102] empirical thermo-physical property correlations. Furthermore, the

maximum values of the Nusselt number can be obtained at low Reynolds numbers and high-volume concentrations.

Hence, the combination of the triangular groove and Al_2O_3 -water nanofluid had a significant impact on overall convective heat transfer, while the pumping power had a minimal effect.

8.1.2 Triangular Groove with Al_2O_3 based Hybrid nanofluids

Since 1% Al_2O_3-CuO/W-EG (60:40) hybrid nanofluid exhibited the highest heat transfer compared to the other hybrid nanofluids. Therefore, it is considered the optimum nanofluid. According to the flow chart mentioned in Section 2.5 of Chapter 2, the optimum groove (triangular grooves) is combined with the optimum nanofluid to obtain the maximum heat transfer. It is important to note that the volume concentration of the hybrid nanofluid was limited to 1% due to the unavailability of empirical data. This section compares the triangular grooved tube with Al_2O_3-water nanofluid and 1% Al_2O_3-CuO/W-EG (60:40) hybrid nanofluid at different Reynolds numbers.

Figure 8. 4 compares the Nusselt number ratio of the corrugated tube with nanofluids to the smooth tube with water at 1% volume concentration for different Reynolds numbers. The results indicated that the Nusselt number ratio for the Al_2O_3-CuO/Water-EG hybrid nanofluid is consistently higher than that for the Al_2O_3-Water nanofluid across all Reynolds numbers. For instance, the average increment in Nusselt number for 1% Al_2O_3-CuO/Water-EG hybrid nanofluid was 2.6 times larger than the Al_2O_3-water nanofluid in a corrugated tube for Reynolds numbers ranging from 10,000 to 60,000, respectively. This suggests that the hybrid nanofluid provides a more effective heat transfer performance in a corrugated tube than the single nanoparticle nanofluid. Additionally, the Nusselt number ratio for both nanofluids slightly decreases as the Reynolds number increases, implying that the relative enhancement in heat transfer diminishes at higher flow rates. However, the Al_2O_3-CuO/Water-EG nanofluid still maintains a significant advantage over the Al_2O_3-Water nanofluid in terms of heat transfer efficiency throughout the tested Reynolds number range.

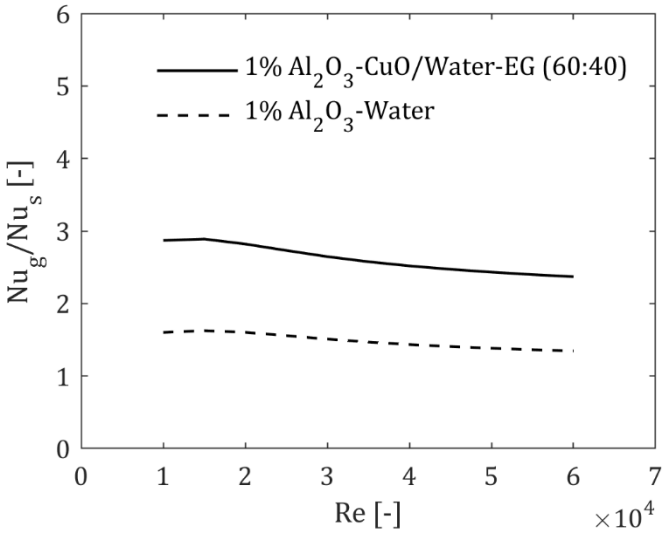

Figure 8. 4: Comparison of Nusselt number ratio in a corrugated tube using different nanofluids

The effect of turbulent kinetic energy (TKE) ratio in a corrugated tube with two different nanofluids (1% Al_2O_3-CuO/Water-EG (60:40) and 1% Al_2O_3-Water) was compared in Figure 8. 5. It can be seen that the TKE ratio was significantly higher for 1% Al_2O_3-CuO/Water-EG (60:40) hybrid nanofluid. Specifically, the TKE of the 1% Al_2O_3-CuO/Water-EG (60:40) hybrid nanofluid was approximately 45 times larger than the 1% Al_2O_3-Water. This drastic enhancement in TKE was attributed to a significant increment in viscosity values of the hybrid nanofluid, with a 310% increment compared to the nanofluid. This implies that the higher viscosity led to a higher velocity gradient that caused more turbulence, thereby increasing the turbulent kinetic energy levels of the hybrid nanofluid. In contrast, the TKE ratio of 1% Al_2O_3-Water remains relatively stable across different Reynolds numbers and still exhibited enhancement compared to a smooth tube with water.

Figure 8. 6 illustrates the Performance Evaluation Criteria (PEC) for 1% Al_2O_3-CuO/Water-EG (60:40) and 1% Al_2O_3-Water in a corrugated tube for various Reynolds numbers. Results indicate that the overall heat transfer performance relative to the pressure drop for 1% Al_2O_3-CuO/Water-EG hybrid nanofluids was almost two times larger than the 1% Al_2O_3-Water nanofluid for Re = 10,000 to 60,000, respectively. The maximum PEC values were obtained at Reynolds number of 10,000 for both nanofluids. For instance, the optimum value of a PEC corrugated tube with hybrid

nanofluids was 214% higher than a smooth tube with pure water at Re = 10,000. This suggests that the hybrid nanofluids were much more efficient than nanofluids and water. In addition, it was also observed that the PEC decreases with the Reynolds number, indicating PEC values were not effective at high Re. Furthermore, the development of correlation for calculating PEC and Nusselt number of a hybrid nanofluid was avoided due to volume concentration constraints limited to 1%, indicating a small data set.

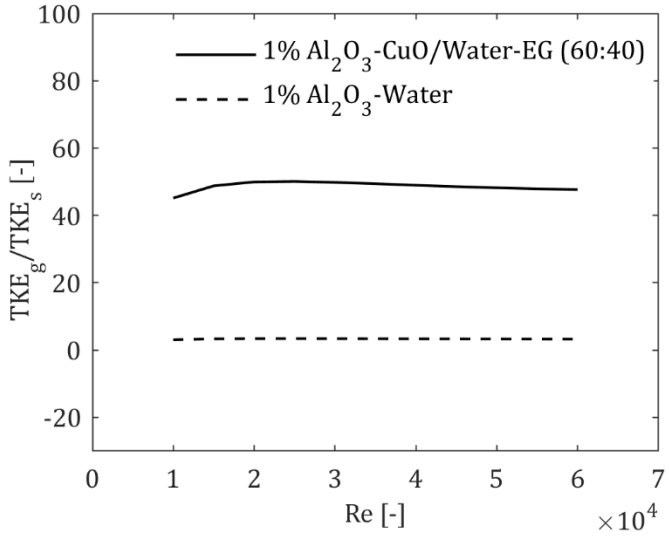

Figure 8. 5: Comparison of turbulent kinetic energy ratio in a corrugated tube using different nanofluids

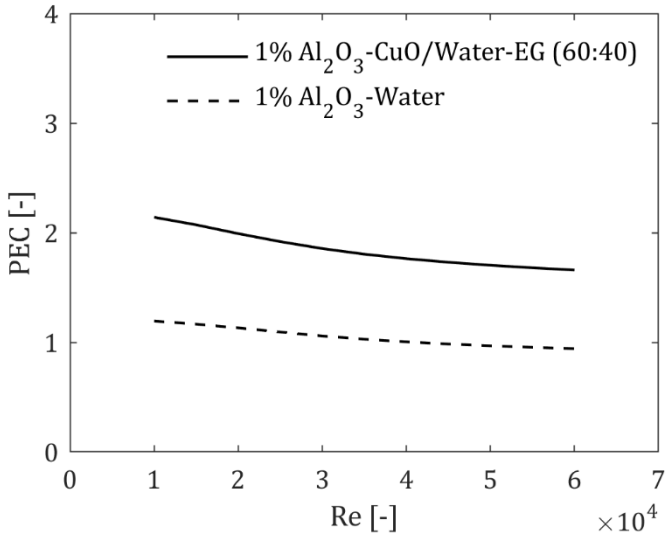

Figure 8. 6: Comparison of PEC in a corrugated tube using different nanofluids

8.2 Summary

In this study, the combined effects of optimised grooves (triangular grooves) and nanofluids along with hybrid nanofluids were investigated in a heated circular tube under a turbulent regime. The single-phase model (SPM) with the RKE turbulence model was implemented to understand the thermohydraulic behaviour of the single tube heat exchanger. The comparison of numerical results was performed at different volume concentrations and Reynolds numbers ($Re = 10 \times 10^3 - 60 \times 10^3$).

The following conclusions are summarised:

- The Al_2O_3-water nanofluid in a corrugated tube demonstrated a significant improvement in convective heat transfer compared to a smooth tube with pure water under turbulent flow. However, an increase in nanoparticle volume concentration resulted in a higher pressure drop and pumping power. Therefore, finding a balance between the Nusselt number and pumping power is crucial in nanofluid applications.

- The Al_2O_3-CuO/Water-EG (60:40) hybrid nanofluid in a corrugated tube provided superior performance (PEC) values compared to the Al_2O_3-water nanofluid. This improvement was due to the combined effects of the two nanoparticles and two base fluids, enhancing the thermophysical properties of the hybrid nanofluid. However, hybrid nanofluids showed higher pressure coefficients, with the heat transfer coefficient improvements providing an effective balance. Therefore, both nanofluids and hybrid nanofluids in various heat exchangers can be more efficient and a better choice to improve the overall thermal performance.

Chapter 9: Conclusions and Future Recommendations

9.1 Conclusions

This research investigated the optimisation of heat transfer inside a corrugated tube using nanofluids using turbulent forced convection. Initially, numerical simulations were conducted to study the thermal and hydrodynamic performance of various groove shapes, including the hybrid groove combinations. Later, optimisation of rectangular grooves was performed to further examine the impact of pressure drop on heat transfer coefficients. This study also evaluated the accuracy of single-phase and two-phase models with different turbulence models (RKE and SST) to predict the heat transfer parameters. In addition, different hybrid nanofluids were also explored to study the thermal performance of the single tube heat exchanger. The findings indicate the significant impact of hybrid grooves, groove geometry optimisation, nanofluid numerical model accuracy, and hybrid nanofluids on the overall heat transfer performance.

Based on the comprehensive analysis, the following conclusions can be drawn:

- The mono-triangular grooves demonstrated the highest thermal performance factor (PEC) compared to other groove geometries such as circular, trapezoidal, and rectangular grooves. This can be attributed to the lowest pressure drop and relatively high heat transfer coefficients observed under turbulent flow conditions. Furthermore, the six different combinations of hybrid grooves did not significantly improve heat transfer performance compared to the individual mono-groove shapes.

- The optimisation of grooves focused on rectangular grooves due to their higher friction factor and pressure drop compared to other mono-groove shapes. The equal radii combination ($r_1 = r_2 = 0.125$ mm) resulted in substantial improvements in convective heat transfer and reduced pumping power among fifteen transverse corrugated tubes. However, mono-triangular grooves outperformed in achieving higher thermal performance factors

(PEC) while maintaining a balance with pressure drop. As a result, mono-triangular grooves were identified as the most effective combination. Future research could further optimise triangular grooves to reduce energy losses from friction and turbulence.

- The single-phase model (SPM) with the Realizable k-ε (RKE) turbulence model provided results that were closer to experimental data in predicting the Nusselt number compared to the two-phase model (TPM). The influence of turbulent models on SPM and TPM was significant. The RKE model in TPM (Eulerian and Mixture models) overpredicted turbulent kinetic energy, viscosity, and heat transfer coefficients, leading to inaccuracies. In contrast, the SST k-ω model obtained reasonable results in both SPM and TPM. Specifically, the SST-Eulerian combination was more accurate than the mixture model, as the lower turbulent viscosity values of the SST model improved predictions of wall shear stress, Nusselt number, and heat transfer performance.

- The Al_2O_3-based hybrid nanofluids in a smooth tube demonstrated a significant improvement in heat transfer compared to pure water. Specifically, the 1% Al_2O_3-CuO/Water-EG (60:40) hybrid nanofluid outperformed other hybrid nanofluids, showing a maximum heat transfer enhancement of 83.8% compared to pure water at Re = 60,000. As a result, it was identified as the optimal working fluid. Additionally, the hybrid nanofluid with a nanoparticle ratio of 60:40 (Al_2O_3: Cu) exhibited the highest heat transfer coefficients. However, the classical models failed to accurately predict convective heat transfer.

- The combination of a triangular grooved tube with nanofluids and hybrid nanofluids significantly enhanced heat transfer rates. Specifically, higher volume concentrations resulted in substantial improvements in Nusselt number and turbulent kinetic energy, leading to a notable increase in the thermal performance factor. Additionally, the optimal Reynolds number was found to be 10,000, at which the single-tube heat exchanger exhibited the highest heat transfer coefficients.

9.2 Practical Implications

The results of the study show that the combination of triangular grooves with Al_2O_3-based hybrid nanofluids in a forced convection single tube has improved thermal performance by more than 2 times compared to a smooth tube without corrugation using water. These findings have profound implications for advancing energy-efficient thermal systems across various full-scale heat exchangers in industrial sectors. Some examples are shell and tube heat exchangers (used in power plants, refineries, chemical processing, etc.); plate heat exchangers (used in HVAC systems, food processing, etc.); double tube heat exchangers (used in cooling systems); air-cooled heat exchangers (automotive cooling and HVAC systems); and spiral heat exchangers (used in chemical industries, wastewater treatment, etc.). By incorporating the optimised groove design and effective hybrid nanofluids, heat exchangers can achieve superior thermal performance, leading to a drastic reduction in energy consumption. This not only results in smaller, more cost-effective equipment but could also reduce the operational costs of industries.

Furthermore, these advancements contribute to environmental sustainability by lowering greenhouse gas emissions, minimising reliance on non-renewable energy sources, and reducing household and industrial energy bills. The combined improvements in heat transfer and the reduction in pumping power requirements translate to significant energy savings, aligning with global efforts to achieve more sustainable and eco-friendly industrial operations. As a result, these improvements lead to more effective, reliable, and environmentally sustainable thermal systems, contributing to the ongoing transition toward greener energy solutions.

9.3 Recommendations for future research

The current numerical study of geometrical and fluid effects provided a significant improvement in the convective heat transfer performance of a single-tube heat exchanger. Based on the numerical findings, the following points are recommended for future work:

- Since the numerical models, such as Eulerian-Mixture and Eulerian-Eulerian with Realizable k-ε and SST k-ω models, failed to predict the friction factor and pressure drop accurately due to their limitations (e.g., idealised boundary conditions and simplified flow assumptions, etc.) as detailed in Chapter 3. These models simplify complex flow behaviours and may not fully capture particle-fluid interactions and the effects of extreme operating conditions. Future work should focus on the experimental validation of the optimised designs, such as triangular grooves combined with hybrid nanofluids, which is essential to verify numerical findings and assess their feasibility in a single-tube heat exchanger. Such validation could address concerns about the limitations of numerical models and strengthen the study's conclusions.

- To further overcome the limitations of the current numerical models, future research should explore advanced turbulence models such as Large Eddy Simulation (LES) and Direct Numerical Simulation (DNS), which are better suited for capturing detailed flow dynamics in grooved and complex geometries. Additionally, incorporating Eulerian-Lagrangian methods, such as the Discrete Phase Model (DPM), would enable a more precise representation of particle-fluid and particle-particle interactions, particularly for hybrid nanofluids.

- The study could be expanded by exploring additional parameters to understand broader thermal and fluid dynamic behaviours. Investigating transient thermal responses under extreme conditions, such as varying Reynolds number, pressure, and wall heat flux, could extend the applicability of the optimised designs. Additionally, assessing alternative working fluids, such as bio-based or advanced hybrid nanofluids, could improve thermal performance and sustainability. Furthermore, testing flow non-uniformity, fouling effects, and integrating optimised designs into multi-tube heat exchangers would enhance the scalability and applicability of the findings across diverse industrial heat transfer applications (e.g., HVAC systems, chemical processing, power plants, etc.).

- The optimised groove designs and fluid choices could significantly improve industrial heat exchangers by enhancing heat transfer efficiency, reducing size, and cutting material costs. In specific applications such as automotive, energy, or aerospace systems, the minimised pumping power and pressure drop directly translate to reduced energy consumption and operational costs. Future research should prioritise precise cost-benefit analyses for these industries to quantify the economic and efficiency gains, ensuring the practical value of these advancements in real-world heat exchanger applications is fully realised.

References

[1] R. Du, D. Jiang, Y. Wang, and K. W. Shah, "An experimental investigation of CuO/water nanofluid heat transfer in geothermal heat exchanger," *Energy and Buildings,* vol. 227, p. 110402, 2020, doi: https://doi.org/10.1016/j.enbuild.2020.110402.

[2] B. Saleh and L. S. Sundar, "Experimental study on heat transfer, friction factor, entropy and exergy efficiency analyses of a corrugated plate heat exchanger using Ni/water nanofluids," *International Journal of Thermal Sciences,* vol. 165, p. 106935, 2021, doi: https://doi.org/10.1016/j.ijthermalsci.2021.106935.

[3] A. Moradi, D. Toghraie, A. H. M. Isfahani, and A. Hosseinian, "An experimental study on MWCNT–water nanofluids flow and heat transfer in double-pipe heat exchanger using porous media," *Journal of Thermal Analysis and Calorimetry,* vol. 137, no. 5, pp. 1797-1807, 2019, doi: https://doi.org/10.1007/s10973-019-08076-0.

[4] M. Basit Shafiq *et al.*, "Thermal performance enhancement of shell and helical coil heat exchanger using MWCNTs/water nanofluid," *Journal of Thermal Analysis and Calorimetry,* vol. 147, no. 21, pp. 12111-12126, 2022, doi: https://doi.org/10.1007/s10973-022-11405-5.

[5] R. K. Ajeel, W. Saiful-Islam, K. Sopian, and M. Yusoff, "Analysis of thermal-hydraulic performance and flow structures of nanofluids across various corrugated channels: An experimental and numerical study," *Thermal Science and Engineering Progress,* vol. 19, p. 100604, 2020, doi: https://doi.org/10.1016/j.tsep.2020.100604.

[6] E. Tavousi, N. Perera, D. Flynn, and R. Hasan, "Numerical investigation of laminar heat transfer and fluid flow characteristics of Al2O3 nanofluid in a double tube heat exchanger," *International Journal of Numerical Methods for Heat & Fluid Flow,* 2023, doi: https://doi.org/10.1108/HFF-03-2023-0114.

[7] E. Tavousi, N. Perera, D. Flynn, and R. Hasan, "Heat transfer and fluid flow characteristics of the passive method in double tube heat exchangers: a critical review," *International Journal of Thermofluids,* p. 100282, 2023, doi: https://doi.org/10.1016/j.ijft.2023.100282.

[8] W.-C. Huang, C.-A. Chen, C. Shen, and J.-Y. San, "Effects of characteristic parameters on heat transfer enhancement of repeated ring-type ribs in circular tubes," *Experimental Thermal and Fluid Science,* vol. 68, pp. 371-380, 2015, doi: https://doi.org/10.1016/j.expthermflusci.2015.06.007.

[9] J. Liu, G. Xie, and T. W. Simon, "Turbulent flow and heat transfer enhancement in rectangular channels with novel cylindrical grooves," *International Journal of Heat and Mass Transfer,* vol. 81, pp. 563-577, 2015, doi: https://doi.org/10.1016/j.ijheatmasstransfer.2014.10.021.

[10] Z. Hernádi and G. Kristóf, "Prediction of pressure drop and heat transfer coefficient in helically grooved heat exchanger tubes using large eddy simulation," *Proceedings of the Institution of Mechanical Engineers, Part A: Journal of Power and Energy,* vol. 228, no. 3, pp. 317-327, 2014, doi: https://doi.org/10.1177/0957650913515669.

[11] C. Kang and K.-S. Yang, "Heat transfer enhancement in turbulent ribbed-pipe flow," *Journal of Heat Transfer,* vol. 139, no. 7, p. 071901, 2017, doi: https://doi.org/10.1115/1.4035712.

[12] P. Selvaraj, J. Sarangan, and S. Suresh, "Computational fluid dynamics analysis on heat transfer and friction factor characteristics of a turbulent flow for internally grooved tubes," *Thermal Science,* vol. 17, no. 4, pp. 1125-1137, 2013, doi: https://doi.org/10.2298/TSCI110404010S.

[13] H. Zontul, H. Hamzah, N. Kurtulmuş, and B. Şahin, "Investigation of convective heat transfer and flow hydrodynamics in rectangular grooved channels," *International Communications in Heat and Mass Transfer,* vol. 126, p. 105366, 2021, doi: https://doi.org/10.1016/j.icheatmasstransfer.2021.105366.

[14] P. Xu, T. Zhou, J. Xing, J. Chen, and Z. Fu, "Numerical investigation of heat-transfer enhancement in helically coiled spiral grooved tube heat exchanger," *Progress in Nuclear Energy,* vol. 145, p. 104132, 2022, doi: https://doi.org/10.1016/j.pnucene.2022.104132.

[15] N. A. Fadhila, A. M. Al-dabaghb, and F. F. Hatemb, "Experimental study of the double pipe heat exchanger for heat transfer and pressure drop characteristics of the grooved tube," *Engineering and Technology Journal,* vol. 42, no. 01, pp. 78-89, 2024, doi: http://doi.org/10.30684/etj.2023.140948.1477.

[16] F. N. Elwekeel, Q. Zheng, and A. M. Abdala, "Effects of Circumferential and Longitudinal Ribs and Grooves in Swirl Cooling on Characteristics of Pressure Drop and Heat Transfer," *Iranian Journal of Science and Technology, Transactions of Mechanical Engineering,* pp. 1-15, 2023, doi: https://doi.org/10.1007/s40997-023-00707-0.

[17] A. Afzal, A. Mohammed Samee, R. Abdul Razak, S. A. Khan, and H. Khan, "Optimum spacing between grooved tubes: An experimental study," *Journal of Mechanical Science and Technology,* vol. 34, pp. 469-475, 2020, doi: https://doi.org/10.1007/s12206-019-1244-7.

[18] H. Mohammed, A. K. Abbas, and J. Sheriff, "Influence of geometrical parameters and forced convective heat transfer in transversely corrugated circular tubes," *International Communications in Heat and Mass Transfer,* vol. 44, pp. 116-126, 2013, doi: https://doi.org/10.1016/j.icheatmasstransfer.2013.02.005.

[19] A. Kaood, T. Abou-Deif, H. Eltahan, M. Yehia, and E. Khalil, "Numerical investigation of heat transfer and friction characteristics for turbulent flow in various corrugated tubes,"

Proceedings of the Institution of Mechanical Engineers, Part A: Journal of Power and Energy, vol. 233, no. 4, pp. 457-475, 2018, doi: https://doi.org/10.1177/0957650918806407.

[20] X. Chen, Z. Yu, W. Chen, F. Wang, Y. Zhao, and Z. Lin, "Study on generating rolling method for manufacturing cylindrical parts with external cross ribs," *Journal of Manufacturing Processes,* vol. 111, pp. 1-20, 2024, doi: https://doi.org/10.1016/j.jmapro.2024.01.009.

[21] R. Kocurek and J. Adamiec, "Manufacturing technologies of finned tubes," *Advances in materials science,* vol. 13, no. 3, pp. 26-35, 2013.

[22] K. Bilen, M. Cetin, H. Gul, and T. Balta, "The investigation of groove geometry effect on heat transfer for internally grooved tubes," *Applied Thermal Engineering,* vol. 29, no. 4, pp. 753-761, 2009, doi: https://doi.org/10.1016/j.applthermaleng.2008.04.008.

[23] G. Lauriat, "On the uses of classical or improved heat transfer correlations for the predictions of convective thermal performances of water-Al2O3 nanofluids," *Applied Thermal Engineering,* vol. 129, pp. 1039-1057, 2018, doi: https://doi.org/10.1016/j.applthermaleng.2017.10.033.

[24] N. A. C. Sidik, M. N. A. W. M. Yazid, S. Samion, M. N. Musa, and R. Mamat, "Latest development on computational approaches for nanofluid flow modeling: Navier–Stokes based multiphase models," *International Communications in Heat and Mass Transfer,* vol. 74, pp. 114-124, 2016, doi: http://dx.doi.org/10.1016/j.icheatmasstransfer.2016.03.007.

[25] S. K. Das, S. U. Choi, and H. E. Patel, "Heat transfer in nanofluids—a review," *Heat transfer engineering,* vol. 27, no. 10, pp. 3-19, 2006, doi: https://doi.org/10.1080/01457630600904593.

[26] S. Maïga, C. Tam Nguyen, N. Galanis, G. Roy, T. Maré, and M. Coqueux, "Heat transfer enhancement in turbulent tube flow using Al2O3 nanoparticle suspension," *International Journal of Numerical Methods for Heat & Fluid Flow,* vol. 16, no. 3, pp. 275-292, 2006, doi: https://doi.org/10.1108/09615530610649717.

[27] P. Kumar and R. Ganesan, "A CFD study of turbulent convective heat transfer enhancement in circular pipeflow," *International Journal of Physical and Mathematical Sciences,* vol. 6, no. 8, pp. 909-916, 2012.

[28] H. M. Ali, M. U. Sajid, and A. Arshad, *Heat transfer applications of TiO2 nanofluids* (Application of titanium dioxide). 2017.

[29] S. P. Manikandan and R. Baskar, "Heat transfer studies in compact heat exchanger using Zno and TiO2 nanofluids in ethylene glycol/water," *Chemical Industry and Chemical Engineering Quarterly,* vol. 24, no. 4, pp. 309-318, 2018, doi: https://doi.org/10.2298/CICEQ170720003M.

[30] S. Z. Heris, M. N. Esfahany, and S. G. Etemad, "Experimental investigation of convective heat transfer of Al2O3/water nanofluid in circular tube," *International journal of heat and fluid flow,* vol. 28, no. 2, pp. 203-210, 2007, doi: https://doi.org/10.1016/j.ijheatfluidflow.2006.05.001.

[31] J. T. Cieslinski and T. Z. Kaczmarczyk, "Pool boiling of water-Al2O3 and water-Cu nanofluids on horizontal smooth tubes," *Nanoscale research letters,* vol. 6, pp. 1-9, 2011, doi: http://dx.doi.org/10.1186/1556-276X-6-220.

[32] C. Ho, C. Chang, W.-M. Yan, and P. Amani, "A combined numerical and experimental study on the forced convection of Al2O3-water nanofluid in a circular tube," *International Journal of Heat and Mass Transfer,* vol. 120, pp. 66-75, 2018, doi: https://doi.org/10.1016/j.ijheatmasstransfer.2017.12.031.

[33] C. Ho, C. Chang, and W.-M. Yan, "An experimental study of forced convection effectiveness of Al2O3-water nanofluid flowing in circular tubes," *International Communications in Heat and Mass Transfer,* vol. 83, pp. 23-29, 2017, doi: https://doi.org/10.1016/j.icheatmasstransfer.2017.03.002.

[34] C. Ho *et al.*, "Laminar forced convection effectiveness of Al2O3–water nanofluid flow in a circular tube at various operation temperatures: Effects of temperature-dependent properties," *International Journal of Heat and Mass Transfer,* vol. 100, pp. 464-481, 2016, doi: https://doi.org/10.1016/j.ijheatmasstransfer.2016.04.105.

[35] A. Mwesigye and Z. Huan, "Thermodynamic analysis and optimization of fully developed turbulent forced convection in a circular tube with water–Al2O3 nanofluid," *International Journal of Heat and Mass Transfer,* vol. 89, pp. 694-706, 2015, doi: https://doi.org/10.1016/j.ijheatmasstransfer.2015.05.099.

[36] G. Huminic and A. Huminic, "Hybrid nanofluids for heat transfer applications–a state-of-the-art review," *International Journal of Heat and Mass Transfer,* vol. 125, pp. 82-103, 2018, doi: https://doi.org/10.1016/j.ijheatmasstransfer.2018.04.059.

[37] T. L. Ba, G. Gróf, V. O. Odhiambo, S. Wongwises, and I. M. Szilágyi, "A CFD study on heat transfer performance of SiO2-TiO2 nanofluids under turbulent flow," *Nanomaterials,* vol. 12, no. 3, p. 299, 2022, doi: https://doi.org/10.3390/nano12030299.

[38] B. Takabi and H. Shokouhmand, "Effects of Al2O3–Cu/water hybrid nanofluid on heat transfer and flow characteristics in turbulent regime," *International Journal of Modern Physics C,* vol. 26, no. 04, p. 1550047, 2015, doi: https://doi.org/10.1142/S0129183115500473.

[39] M. Akbari, N. Galanis, and A. Behzadmehr, "Comparative assessment of single and two-phase models for numerical studies of nanofluid turbulent forced convection," *International Journal*

of Heat and Fluid Flow, vol. 37, pp. 136-146, 2012, doi: http://dx.doi.org/10.1016/j.ijheatfluidflow.2012.05.005.

[40] W. Peng, B. Minli, L. Jizu, H. Chengzhi, and W. Yuyan, "Numerical investigation on the turbulent flow characteristic of nanofluids in a horizontal circular tube," *Numerical Heat Transfer, Part A: Applications,* vol. 66, no. 6, pp. 646-668, 2014, doi: https://doi.org/10.1080/10407782.2014.894389.

[41] M. Kalteh, A. Abbassi, M. Saffar-Avval, A. Frijns, A. Darhuber, and J. Harting, "Experimental and numerical investigation of nanofluid forced convection inside a wide microchannel heat sink," *Applied Thermal Engineering,* vol. 36, pp. 260-268, 2012, doi: https://doi.org/10.1016/j.applthermaleng.2011.10.023.

[42] A. Behzadmehr, M. Saffar-Avval, and N. Galanis, "Prediction of turbulent forced convection of a nanofluid in a tube with uniform heat flux using a two phase approach," *International journal of heat and fluid flow,* vol. 28, no. 2, pp. 211-219, 2007, doi: https://doi.org/10.1016/j.ijheatfluidflow.2006.04.006.

[43] M. Hejazian and M. K. Moraveji, "A comparative analysis of single and two-phase models of turbulent convective heat transfer in a tube for TiO2 nanofluid with CFD," *Numerical Heat Transfer, Part A: Applications,* vol. 63, no. 10, pp. 795-806, 2013, doi: https://doi.org/10.1080/10407782.2013.756759.

[44] A. Beheshti, M. K. Moraveji, and M. Hejazian, "Comparative numerical study of nanofluid heat transfer through an annular channel," *Numerical Heat Transfer, Part A: Applications,* vol. 67, no. 1, pp. 100-117, 2015, doi: https://doi.org/10.1080/10407782.2014.894359.

[45] F. Karami, A. A. A. Arani, O. A. Akbari, F. Pourfattah, and D. Toghraie, "Numerical study of location and depth of rectangular grooves on the turbulent heat transfer performance and characteristics of CuO-water nanofluid flow," *Heliyon,* vol. 9, no. 3, 2023, doi: https://doi.org/10.1016/j.heliyon.2023.e14239.

[46] S. D. Salman, "Comparative study on heat transfer enhancement of nanofluids flow in ribs tube using CFD simulation," *Heat Transfer—Asian Research,* vol. 48, no. 1, pp. 148-163, 2019, doi: https://doi.org/10.1002/htj.21376.

[47] A. A. Alkumait, T. K. Ibrahim, M. H. Zaidan, and A. T. Al-Sammarraie, "Thermal and hydraulic characteristics of TiO 2/water nanofluid flow in tubes possessing internal trapezoidal and triangular rib shapes," *Journal of Thermal Analysis and Calorimetry,* pp. 1-14, 2020, doi: https://doi.org/10.1007/s10973-020-10289-7.

[48] R. Ekiciler and M. S. A. Çetinkaya, "A comparative heat transfer study between monotype and hybrid nanofluid in a duct with various shapes of ribs," *Thermal Science and Engineering Progress,* vol. 23, p. 100913, 2021, doi: https://doi.org/10.1016/j.tsep.2021.100913.

[49] A. A. Varzaneh, D. Toghraie, and A. Karimipour, "Comprehensive simulation of nanofluid flow and heat transfer in straight ribbed microtube using single-phase and two-phase models for choosing the best conditions," *Journal of Thermal Analysis and Calorimetry,* vol. 139, pp. 701-720, 2020, doi: https://doi.org/10.1007/s10973-019-08381-8.

[50] E. Tavousi, N. Perera, D. Flynn, and R. Hasan, "Numerical Investigation of Heat Transfer and Fluid Flow Characteristics of Al2O3 Nanofluid In A Double Tube Heat Exchanger With Turbulator Insertion," presented at the Proceedings of the 9th World Congress on Mechanical, Chemical, and Material Engineering (MCM'23), Brunel University, London, United Kingdom, August 06-08, 2023, HTFF 218.

[51] S. Z. Dizjeh and J. Brinkerhoff, "Numerical investigations of turbulent heat transfer enhancement in circular tubes via modified internal profiles," *International Journal of Thermofluids,* vol. 16, p. 100237, 2022, doi: https://doi.org/10.1016/j.ijft.2022.100237.

[52] K.-B. Hong, D.-W. Kim, J. Kwark, J.-S. Nam, and H.-S. Ryou, "Numerical Study on the Effect of the Pipe Groove Height and Pitch on the Flow Characteristics of Corrugated Pipe," *Energies,* vol. 14, no. 9, p. 2614, 2021, doi: https://doi.org/10.3390/en14092614.

[53] H. Hajabdollahi, M. Salarmofrad, S. Shamsi, and M. Rezaeian, "Numerical study of heat transfer and friction factor in a tube with groove and rib on the wall," *Heat Transfer,* vol. 49, no. 3, pp. 1214-1236, 2020, doi: https://doi.org/10.1002/htj.21659.

[54] N. S. Dhaidan and A. K. Abbas, "Turbulent forced convection flow inside inward-outward rib corrugated tubes with different rib-shapes," *Heat Transfer—Asian Research,* vol. 47, no. 8, pp. 1048-1060, 2018, doi: https://doi.org/10.1002/htj.21365.

[55] W. Wang, Y. Zhang, J. Liu, B. Li, and B. Sundén, "Large eddy simulation of turbulent flow and heat transfer in outward transverse and helically corrugated tubes," *Numerical Heat Transfer, Part A: Applications,* vol. 75, no. 7, pp. 456-468, 2019, doi: https://doi.org/10.1080/10407782.2019.1608763.

[56] A. M. Abed, D. F. Kareem, H. S. Majdi, and A. Abdulkadhim, "Experimental and CFD Analysis of two-phase forced convection flow in channels of various rib shapes," *Journal of Advanced Research in Fluid Mechanics and Thermal Sciences,* vol. 77, no. 1, pp. 36-50, 2021, doi: https://doi.org/10.37934/arfmts.77.1.3650.

[57] K. Mohebbi, R. Rafee, and F. Talebi, "Effects of rib shapes on heat transfer characteristics of turbulent flow of Al2O3-water nanofluid inside ribbed tubes," *Iranian Journal of Chemistry and Chemical Engineering (IJCCE),* vol. 34, no. 3, pp. 61-77, 2015, doi: https://doi.org/10.30492/ijcce.2015.14753.

[58] A. A. Ramadhan and Y. T. Al Anii, "Groove geometry effects on turbulent heat transfer and fluid flow," *Heat and Mass Transfer,* vol. 49, pp. 185-195, 2013, doi: https://doi.org/10.1007/s00231-012-1076-9.

[59] W. Wang, Y. Zhang, B. Li, H. Han, and X. Gao, "Influence of geometrical parameters on turbulent flow and heat transfer characteristics in outward helically corrugated tubes," *Energy Conversion and Management,* vol. 136, pp. 294-306, 2017, doi: https://doi.org/10.1016/j.enconman.2017.01.029.

[60] F. Pourfattah, M. Motamedian, G. Sheikhzadeh, D. Toghraie, and O. A. Akbari, "The numerical investigation of angle of attack of inclined rectangular rib on the turbulent heat transfer of Water-Al2O3 nanofluid in a tube," *International Journal of Mechanical Sciences,* vol. 131, pp. 1106-1116, 2017, doi: https://doi.org/10.1016/j.ijmecsci.2017.07.049.

[61] S. Wang, S. To, X. Chen, H. Wang, and H. Xia, "A study of the fabrication of v-groove structure in ultra-precision milling," *International Journal of Computer Integrated Manufacturing,* vol. 27, no. 11, pp. 986-996, 2014, doi: https://doi.org/10.1080/0951192X.2013.869835.

[62] N. Zheng, P. Liu, F. Shan, Z. Liu, and W. Liu, "Turbulent flow and heat transfer enhancement in a heat exchanger tube fitted with novel discrete inclined grooves," *International Journal of Thermal Sciences,* vol. 111, pp. 289-300, 2017, doi: https://doi.org/10.1016/j.ijthermalsci.2016.09.010.

[63] S. T. Firoozeh, N. Pourmahmoud, and M. Khalilian, "Two-tube heat exchanger with variable groove angle on the inner pipe surface: Experimental study," *Applied Thermal Engineering,* vol. 234, p. 121274, 2023, doi: https://doi.org/10.1016/j.applthermaleng.2023.121274.

[64] P. G. Vicente, A. Garcıa, and A. Viedma, "Experimental investigation on heat transfer and frictional characteristics of spirally corrugated tubes in turbulent flow at different Prandtl numbers," *International journal of heat and mass transfer,* vol. 47, no. 4, pp. 671-681, 2004, doi: https://doi.org/10.1016/j.ijheatmasstransfer.2003.08.005.

[65] T. S. Mogaji, A. O. Olapojoye, E. T. Idowu, and B. Saleh, "CFD study of heat transfer augmentation and fluid flow characteristics of turbulent flow inside helically grooved tubes," *Journal of the Brazilian Society of Mechanical Sciences and Engineering,* vol. 44, no. 3, p. 90, 2022, doi: https://doi.org/10.1007/s40430-021-03299-5.

[66] M. Miansari, M. R. Darvishi, D. Toghraie, P. Barnoon, M. Shirzad, and A. a. Alizadeh, "Numerical investigation of grooves effects on the thermal performance of helically grooved shell and coil tube heat exchanger," *Chinese Journal of Chemical Engineering,* vol. 44, pp. 424-434, 2022, doi: https://doi.org/10.1016/j.cjche.2021.05.038.

[67] Z. Wu, C. Qian, G. Liu, Z. Liu, and P. Sheng, "Mechanical properties and heat transfer performance of conically corrugated tube," *Materials,* vol. 14, no. 17, p. 4902, 2021, doi: https://doi.org/10.3390/ma14174902.

[68] J.-A. Meng, X.-G. Liang, Z.-J. Chen, and Z.-X. Li, "Experimental study on convective heat transfer in alternating elliptical axis tubes," *Experimental Thermal and Fluid Science,* vol. 29, no. 4, pp. 457-465, 2005, doi: https://doi.org/10.1016/j.expthermflusci.2004.04.006.

[69] H. S. Dizaji, S. Jafarmadar, and F. Mobadersani, "Experimental studies on heat transfer and pressure drop characteristics for new arrangements of corrugated tubes in a double pipe heat exchanger," *International Journal of Thermal Sciences,* vol. 96, pp. 211-220, 2015, doi: https://doi.org/10.1016/j.ijthermalsci.2015.05.009.

[70] Z. Xu and Z.-B. Zhang, "Experimental investigation of the applied performance of several typical enhanced tubes," *Journal of Enhanced Heat Transfer,* vol. 17, no. 4, 2010, doi: http://dx.doi.org/10.1615/JEnhHeatTransf.v17.i4.40.

[71] X.-w. Li, J.-a. Meng, and Z.-x. Li, "Roughness enhanced mechanism for turbulent convective heat transfer," *International Journal of Heat and Mass Transfer,* vol. 54, no. 9-10, pp. 1775-1781, 2011, doi: https://doi.org/10.1016/j.ijheatmasstransfer.2010.12.039.

[72] S. Rozzi, R. Massini, G. Paciello, G. Pagliarini, S. Rainieri, and A. Trifiro, "Heat treatment of fluid foods in a shell and tube heat exchanger: Comparison between smooth and helically corrugated wall tubes," *Journal of food engineering,* vol. 79, no. 1, pp. 249-254, 2007, doi: https://doi.org/10.1016/j.jfoodeng.2006.01.050.

[73] B. S. Petukhov, "Heat transfer and friction in turbulent pipe flow with variable physical properties," in *Advances in heat transfer*, vol. 6: Elsevier, 1970, pp. 503-564.

[74] R. Notter and C. Sleicher, "A solution to the turbulent Graetz problem—III Fully developed and entry region heat transfer rates," *Chemical Engineering Science,* vol. 27, no. 11, pp. 2073-2093, 1972, doi: https://doi.org/10.1016/0009-2509(72)87065-9.

[75] V. Gnielinski, "New equations for heat and mass transfer in turbulent pipe and channel flow," *International chemical engineering,* vol. 16, no. 2, pp. 359-367, 1976.

[76] H. Blasius, *Grenzschichten in Flüssigkeiten mit kleiner Reibung*. Druck von BG Teubner, 1908.

[77] W. Wang, Y. Shuai, L. Ding, B. Li, and B. Sundén, "Investigation of complex flow and heat transfer mechanism in multi-tube heat exchanger with different arrangement corrugated tube," *International Journal of Thermal Sciences,* vol. 167, p. 107010, 2021, doi: https://doi.org/10.1016/j.ijthermalsci.2021.107010.

[78] N. Kurtulmuş and B. Sahin, "A review of hydrodynamics and heat transfer through corrugated channels," *International communications in heat and mass transfer,* vol. 108, p. 104307, 2019, doi: https://doi.org/10.1016/j.icheatmasstransfer.2019.104307.

[79] P. Chakraborty, T. Ma, L. Cao, and Y. Wang, "Significantly enhanced convective heat transfer through surface modification in nanochannels," *International Journal of Heat and Mass Transfer,* vol. 136, pp. 702-708, 2019, doi: https://doi.org/10.1016/j.ijheatmasstransfer.2019.03.053.

[80] L. Zhang and D. Che, "Turbulence models for fluid flow and heat transfer between cross-corrugated plates," *Numerical Heat Transfer, Part A: Applications,* vol. 60, no. 5, pp. 410-440, 2011, doi: https://doi.org/10.1080/10407782.2011.600583.

[81] S. M. Vanaki, P. Ganesan, and H. A. Mohammed, "Numerical study of convective heat transfer of nanofluids: A review," *Renewable and Sustainable Energy Reviews,* vol. 54, pp. 1212-1239, 2016, doi: https://doi.org/10.1016/j.rser.2015.10.042.

[82] H. Chiam, W. Azmi, N. Adam, and M. Ariffin, "Numerical study of nanofluid heat transfer for different tube geometries–A comprehensive review on performance," *International Communications in Heat and Mass Transfer,* vol. 86, pp. 60-70, 2017, doi: http://dx.doi.org/10.1016/j.icheatmasstransfer.2017.05.019.

[83] M. Kong and S. Lee, "Performance evaluation of Al2O3 nanofluid as an enhanced heat transfer fluid," *Advances in Mechanical Engineering,* vol. 12, no. 8, p. 1687814020952277, 2020, doi: https://doi.org/10.1177/1687814020952277.

[84] G. Saha and M. C. Paul, "Numerical analysis of the heat transfer behaviour of water based Al2O3 and TiO2 nanofluids in a circular pipe under the turbulent flow condition," *International Communications in Heat and Mass Transfer,* vol. 56, pp. 96-108, 2014, doi: https://doi.org/10.1016/j.icheatmasstransfer.2014.06.008.

[85] A. R. Sajadi, S. S. Sadati, M. Nourimotlagh, O. Pakbaz, D. Ashtiani, and F. Kowsari, "EXPERIMENTAL STUDY ON TURBULENT HEAT TRANSFER, PRESSURE DROP, AND THERMAL PERFORMANCE OF ZnO/WATER NANOFLUID FLOW IN A CIRCULAR TUBE," *Thermal Science,* vol. 18, no. 4, 2014, doi: https://doi.org/10.2298/TSCI131114022S.

[86] E. Ebrahimnia-Bajestan, H. Niazmand, W. Duangthongsuk, and S. Wongwises, "Numerical investigation of effective parameters in convective heat transfer of nanofluids flowing under a laminar flow regime," *International journal of heat and mass transfer,* vol. 54, no. 19-20, pp. 4376-4388, 2011, doi: http://dx.doi.org/10.1016/j.ijheatmasstransfer.2011.05.006.

[87] J. C. Maxwell, *A treatise on electricity and magnetism*. Oxford: Clarendon Press, 1873.

[88] A. Meriläinen *et al.*, "Influence of particle size and shape on turbulent heat transfer characteristics and pressure losses in water-based nanofluids," *International journal of heat and mass transfer,* vol. 61, pp. 439-448, 2013, doi: http://dx.doi.org/10.1016/j.ijheatmasstransfer.2013.02.032.

[89] R. K. Tiwari and M. K. Das, "Heat transfer augmentation in a two-sided lid-driven differentially heated square cavity utilizing nanofluids," *International Journal of heat and Mass transfer,* vol. 50, no. 9-10, pp. 2002-2018, 2007, doi: https://doi.org/10.1016/j.ijheatmasstransfer.2006.09.034.

[90] H. F. Oztop and E. Abu-Nada, "Numerical study of natural convection in partially heated rectangular enclosures filled with nanofluids," *International journal of heat and fluid flow,* vol. 29, no. 5, pp. 1326-1336, 2008, doi: https://doi.org/10.1016/j.ijheatfluidflow.2008.04.009.

[91] C.-J. Ho, M. Chen, and Z. Li, "Numerical simulation of natural convection of nanofluid in a square enclosure: effects due to uncertainties of viscosity and thermal conductivity," *International Journal of Heat and Mass Transfer,* vol. 51, no. 17-18, pp. 4506-4516, 2008, doi: https://doi.org/10.1016/j.ijheatmasstransfer.2007.12.019.

[92] S. Aminossadati and B. Ghasemi, "Natural convection cooling of a localised heat source at the bottom of a nanofluid-filled enclosure," *European Journal of Mechanics-B/Fluids,* vol. 28, no. 5, pp. 630-640, 2009, doi: https://doi.org/10.1016/j.euromechflu.2009.05.006.

[93] E. V. Timofeeva, J. L. Routbort, and D. Singh, "Particle shape effects on thermophysical properties of alumina nanofluids," *Journal of applied physics,* vol. 106, no. 1, 2009, doi: https://doi.org/10.1063/1.3155999.

[94] S. Murshed, K. Leong, and C. Yang, "Enhanced thermal conductivity of TiO2-water based nanofluids," *International Journal of thermal sciences,* vol. 44, no. 4, pp. 367-373, 2005, doi: https://doi.org/10.1016/j.ijthermalsci.2004.12.005.

[95] P. Keblinski, S. Phillpot, S. Choi, and J. Eastman, "Mechanisms of heat flow in suspensions of nano-sized particles (nanofluids)," *International journal of heat and mass transfer,* vol. 45, no. 4, pp. 855-863, 2002, doi: https://doi.org/10.1016/S0017-9310(01)00175-2.

[96] L. Zhang, A. Zhang, Y. Jing, P. Qu, and Z. Wu, "Effect of particle size on the heat transfer performance of SiO2–water nanofluids," *The Journal of Physical Chemistry C,* vol. 125, no. 24, pp. 13590-13600, 2021, doi: https://doi.org/10.1021/acs.jpcc.1c02014.

[97] R. Davarnejad, S. Barati, and M. Kooshki, "CFD simulation of the effect of particle size on the nanofluids convective heat transfer in the developed region in a circular tube," *SpringerPlus,* vol. 2, pp. 1-6, 2013, doi: https://doi.org/10.1186/2193-1801-2-192.

[98] K. Anoop, T. Sundararajan, and S. K. Das, "Effect of particle size on the convective heat transfer in nanofluid in the developing region," *International journal of heat and mass transfer,* vol. 52, no. 9-10, pp. 2189-2195, 2009, doi: https://doi.org/10.1016/j.ijheatmasstransfer.2007.11.063.

[99] T. Ambreen and M.-H. Kim, "Influence of particle size on the effective thermal conductivity of nanofluids: A critical review," *Applied Energy,* vol. 264, p. 114684, 2020, doi: https://doi.org/10.1016/j.apenergy.2020.114684.

[100] N. Dukhan, "Forced convection of nanofluids in metal foam: an essential review," *International Journal of Thermal Sciences,* vol. 187, p. 108156, 2023, doi: https://doi.org/10.1016/j.ijthermalsci.2023.108156.

[101] S. Chakraborty and P. K. Panigrahi, "Stability of nanofluid: A review," *Applied Thermal Engineering,* vol. 174, p. 115259, 2020, doi: https://doi.org/10.1016/j.applthermaleng.2020.115259.

[102] B. C. Pak and Y. I. Cho, "Hydrodynamic and heat transfer study of dispersed fluids with submicron metallic oxide particles," *Experimental Heat Transfer an International Journal,* vol. 11, no. 2, pp. 151-170, 1998, doi: https://doi.org/10.1080/08916159808946559.

[103] S. E. B. Maiga, S. J. Palm, C. T. Nguyen, G. Roy, and N. Galanis, "Heat transfer enhancement by using nanofluids in forced convection flows," *International journal of heat and fluid flow,* vol. 26, no. 4, pp. 530-546, 2005, doi: https://doi.org/10.1016/j.ijheatfluidflow.2005.02.004.

[104] B.-S. Chen and C.-C. Liu, "Heat transfer and entropy generation in fully-developed mixed convection nanofluid flow in vertical channel," *International Journal of Heat and Mass Transfer,* vol. 79, pp. 750-758, 2014, doi: https://doi.org/10.1016/j.ijheatmasstransfer.2014.08.078.

[105] C. Ho, W. Liu, Y. Chang, and C. Lin, "Natural convection heat transfer of alumina-water nanofluid in vertical square enclosures: An experimental study," *International Journal of Thermal Sciences,* vol. 49, no. 8, pp. 1345-1353, 2010, doi: https://doi.org/10.1016/j.ijthermalsci.2010.02.013.

[106] U. Rea, T. McKrell, L.-w. Hu, and J. Buongiorno, "Laminar convective heat transfer and viscous pressure loss of alumina–water and zirconia–water nanofluids," *International Journal of Heat and Mass Transfer,* vol. 52, no. 7-8, pp. 2042-2048, 2009, doi: https://doi.org/10.1016/j.ijheatmasstransfer.2008.10.025.

[107] W. Azmi, K. Sharma, R. Mamat, A. Alias, and I. I. Misnon, "Correlations for thermal conductivity and viscosity of water based nanofluids," in *IOP Conference Series: Materials Science and Engineering*, 2012, vol. 36, no. 1: IOP Publishing, p. 012029, doi: https://doi.org/10.1088/1757-899X/36/1/012029.

[108] H. C. Brinkman, *The viscosity of concentrated suspensions and solutions* (The Journal of chemical physics, no. 4). 1952, pp. 571-571.

[109] S. El Bécaye Maïga, C. Tam Nguyen, N. Galanis, G. Roy, T. Maré, and M. Coqueux, "Heat transfer enhancement in turbulent tube flow using Al2O3 nanoparticle suspension," *International Journal of Numerical Methods for Heat & Fluid Flow,* vol. 16, no. 3, pp. 275-292, 2006, doi: https://doi.org/10.1108/09615530610649717.

[110] K. Veeramanikandan, S. Vignesh, B. P. Krishnan, M. Mathanbabu, and M. Ashokkumar, "Investigation of Al2O3-water nano fluid flow through the circular tube," *Materials Today: Proceedings,* vol. 46, pp. 8288-8295, 2021, doi: https://doi.org/10.1016/j.matpr.2021.03.253.

[111] H. Eshgarf, A. A. Nadooshan, and A. Raisi, "A review of multi-phase and single-phase models in the numerical simulation of nanofluid flow in heat exchangers," *Engineering Analysis with Boundary Elements,* vol. 146, pp. 910-927, 2023, doi: https://doi.org/10.1016/j.enganabound.2022.10.013.

[112] S. Zhang, L. Lu, T. Wen, and C. Dong, "Turbulent heat transfer and flow analysis of hybrid Al2O3-CuO/water nanofluid: An experiment and CFD simulation study," *Applied Thermal Engineering,* vol. 188, p. 116589, 2021, doi: https://doi.org/10.1016/j.applthermaleng.2021.116589.

[113] N. Kumar and B. Puranik, "Numerical study of convective heat transfer with nanofluids in turbulent flow using a Lagrangian-Eulerian approach," *Applied Thermal Engineering,* vol. 111, pp. 1674-1681, 2017, doi: http://dx.doi.org/10.1016/j.applthermaleng.2016.08.038.

[114] G. Saha and M. C. Paul, "Investigation of the characteristics of nanofluids flow and heat transfer in a pipe using a single phase model," *International Communications in Heat and Mass Transfer,* vol. 93, pp. 48-59, 2018, doi: https://doi.org/10.1016/j.icheatmasstransfer.2018.03.001.

[115] M. Z. Saghir, A. Ahadi, T. Yousefi, and B. Farahbakhsh, "Two-phase and single phase models of flow of nanofluid in a square cavity: comparison with experimental results," *International Journal of Thermal Sciences,* vol. 100, pp. 372-380, 2016, doi: https://doi.org/10.1016/j.ijthermalsci.2015.10.005.

[116] A. Alshare, W. Al-Kouz, and W. Khan, "Cu-Al2O3 water hybrid nanofluid transport in a periodic structure," *Processes,* vol. 8, no. 3, p. 285, 2020, doi: http://dx.doi.org/10.3390/pr8030285.

[117] G. Liang and I. Mudawar, "Review of single-phase and two-phase nanofluid heat transfer in macro-channels and micro-channels," *International Journal of Heat and Mass Transfer,* vol. 136, pp. 324-354, 2019, doi: https://doi.org/10.1016/j.ijheatmasstransfer.2019.02.086.

[118] W. Jamshed, K. S. Nisar, R. P. Gowda, R. N. Kumar, and B. Prasannakumara, "Radiative heat transfer of second grade nanofluid flow past a porous flat surface: a single-phase mathematical model," *Physica Scripta,* vol. 96, no. 6, p. 064006, 2021, doi: https://doi.org/10.1088/1402-4896/abf57d.

[119] Z. Ding, C. Qi, T. Luo, Y. Wang, J. Tu, and C. Wang, "Numerical simulation of nanofluids forced convection in a corrugated double-pipe heat exchanger," *The Canadian Journal of Chemical Engineering,* vol. 100, no. 8, pp. 1954-1964, 2022, doi: https://doi.org/10.1002/cjce.24267.

[120] K. R. Akbari, R. M. Abbasalizadeh, S. PESTEII, and S. M. Esmaeilei, "simulation of Single-phase and two-phase flow of water-titanium oxide nanofluids in a double-tube counter flow heat exchanger and Investigation of heat transfer and pressure drop," 2021.

[121] A. M. Hussein, K. Sharma, R. Bakar, and K. Kadirgama, "The effect of cross sectional area of tube on friction factor and heat transfer nanofluid turbulent flow," *International Communications in Heat and Mass Transfer,* vol. 47, pp. 49-55, 2013, doi: http://dx.doi.org/10.1016/j.icheatmasstransfer.2013.06.007.

[122] M. Akhtari, M. Haghshenasfard, and M. Talaie, "Numerical and experimental investigation of heat transfer of α-Al2O3/water nanofluid in double pipe and shell and tube heat exchangers," *Numerical Heat Transfer, Part A: Applications,* vol. 63, no. 12, pp. 941-958, 2013, doi: https://doi.org/10.1080/10407782.2013.772855.

[123] M. Amani, P. Amani, A. Kasaeian, O. Mahian, and W.-M. Yan, "Two-phase mixture model for nanofluid turbulent flow and heat transfer: Effect of heterogeneous distribution of nanoparticles," *Chemical Engineering Science,* vol. 167, pp. 135-144, 2017, doi: https://doi.org/10.1016/j.ces.2017.03.065.

[124] A. Albojamal and K. Vafai, "Analysis of single phase, discrete and mixture models, in predicting nanofluid transport," *International Journal of Heat and Mass Transfer,* vol. 114, pp. 225-237, 2017, doi: https://doi.org/10.1016/j.ijheatmasstransfer.2017.06.030.

[125] M. Manninen, V. Taivassalo, and S. Kallio, "On the mixture model for multiphase flow," 1996.

[126] Y. Xuan and Q. Li, "Investigation on convective heat transfer and flow features of nanofluids," *J. Heat transfer,* vol. 125, no. 1, pp. 151-155, 2003, doi: https://doi.org/10.1115/1.1532008.

[127] S. Mirmasoumi and A. Behzadmehr, "Numerical study of laminar mixed convection of a nanofluid in a horizontal tube using two-phase mixture model," *Applied Thermal Engineering,* vol. 28, no. 7, pp. 717-727, 2008, doi: https://doi.org/10.1016/j.applthermaleng.2007.06.019.

[128] A. Akbarinia and R. Laur, "Investigating the diameter of solid particles effects on a laminar nanofluid flow in a curved tube using a two phase approach," *International Journal of Heat*

and Fluid Flow, vol. 30, no. 4, pp. 706-714, 2009, doi: https://doi.org/10.1016/j.ijheatfluidflow.2009.03.002.

[129] R. Lotfi, Y. Saboohi, and A. Rashidi, "Numerical study of forced convective heat transfer of nanofluids: comparison of different approaches," *International Communications in Heat and Mass Transfer,* vol. 37, no. 1, pp. 74-78, 2010, doi: https://doi.org/10.1016/j.icheatmasstransfer.2009.07.013.

[130] A. Moghadassi, E. Ghomi, and F. Parvizian, "A numerical study of water based Al2O3 and Al2O3–Cu hybrid nanofluid effect on forced convective heat transfer," *International Journal of Thermal Sciences,* vol. 92, pp. 50-57, 2015, doi: https://doi.org/10.1016/j.ijthermalsci.2015.01.025.

[131] O. A. Beg, M. Rashidi, M. Akbari, and A. Hosseini, "Comparative numerical study of single-phase and two-phase models for bio-nanofluid transport phenomena," *Journal of Mechanics in Medicine and Biology,* vol. 14, no. 01, p. 1450011, 2014, doi: https://doi.org/10.1142/S0219519414500110.

[132] N. Hazeri-Mahmel, Y. Shekari, and A. Tayebi, "Three-dimensional analysis of forced convection of Newtonian and non-Newtonian nanofluids through a horizontal pipe using single-and two-phase models," *International Communications in Heat and Mass Transfer,* vol. 121, p. 105119, 2021, doi: https://doi.org/10.1016/j.icheatmasstransfer.2021.105119.

[133] S. Al Mahmud, A. F. Ismail, J. H. Bappy, and W. I. Noor, "A Study on Accuracy Range of Multiphase Mixture Model for Turbulent Convective Heat Transfer Enhancement Simulation of Water-Al2O3 Nanofluid," *Journal of Nanofluids,* vol. 12, no. 2, pp. 438-447, 2023, doi: https://doi.org/10.1166/jon.2023.1972.

[134] S. Göktepe, K. Atalık, and H. Ertürk, "Comparison of single and two-phase models for nanofluid convection at the entrance of a uniformly heated tube," *International Journal of Thermal Sciences,* vol. 80, pp. 83-92, 2014, doi: https://doi.org/10.1016/j.ijthermalsci.2014.01.014.

[135] H. El-Batsh, M. Doheim, and A. Hassan, "On the application of mixture model for two-phase flow induced corrosion in a complex pipeline configuration," *Applied Mathematical Modelling,* vol. 36, no. 11, pp. 5686-5699, 2012, doi: https://doi.org/10.1016/j.apm.2012.01.017.

[136] A. Rezaei Gorjaei and R. Rahmani, "Numerical simulation of nanofluid flow in a channel using eulerian–eulerian two-phase model," *International Journal of Thermophysics,* vol. 42, pp. 1-16, 2021, doi: https://doi.org/10.1007/s10765-021-02821-0.

[137] M. Hejazian, M. K. Moraveji, and A. Beheshti, "Comparative study of Euler and mixture models for turbulent flow of Al2O3 nanofluid inside a horizontal tube," *International*

Communications in Heat and Mass Transfer, vol. 52, pp. 152-158, 2014, doi: http://dx.doi.org/10.1016/j.icheatmasstransfer.2014.01.022.

[138] I. Behroyan, P. Ganesan, S. He, and S. Sivasankaran, "Turbulent forced convection of Cu–water nanofluid: CFD model comparison," *International Communications in Heat and Mass Transfer,* vol. 67, pp. 163-172, 2015, doi: http://dx.doi.org/10.1016/j.icheatmasstransfer.2015.07.014.

[139] M. Kalteh, A. Abbassi, M. Saffar-Avval, and J. Harting, "Eulerian–Eulerian two-phase numerical simulation of nanofluid laminar forced convection in a microchannel," *International journal of heat and fluid flow,* vol. 32, no. 1, pp. 107-116, 2011, doi: https://doi.org/10.1016/j.ijheatfluidflow.2010.08.001.

[140] I. Behroyan, S. M. Vanaki, P. Ganesan, and R. Saidur, "A comprehensive comparison of various CFD models for convective heat transfer of Al2O3 nanofluid inside a heated tube," *International Communications in Heat and Mass Transfer,* vol. 70, pp. 27-37, 2016, doi: https://doi.org/10.1016/j.icheatmasstransfer.2015.11.001.

[141] E. Ebrahimnia-Bajestan, M. C. Moghadam, H. Niazmand, W. Daungthongsuk, and S. Wongwises, "Experimental and numerical investigation of nanofluids heat transfer characteristics for application in solar heat exchangers," *International Journal of Heat and Mass Transfer,* vol. 92, pp. 1041-1052, 2016, doi: https://doi.org/10.1016/j.ijheatmasstransfer.2015.08.107.

[142] M. Bahiraei, "A numerical study of heat transfer characteristics of CuO–water nanofluid by Euler–Lagrange approach," *Journal of Thermal Analysis and Calorimetry,* vol. 123, pp. 1591-1599, 2016, doi: https://doi.org/10.1007/s10973-015-5031-0.

[143] A. Shynybayeva and L. R. Rojas-Solórzano, "Eulerian–Eulerian modeling of multiphase flow in horizontal annuli: Current limitations and challenges," *Processes,* vol. 8, no. 11, p. 1426, 2020, doi: https://doi.org/10.3390/pr8111426.

[144] G. Sekrani, S. Poncet, and P. Proulx, "Modeling of convective turbulent heat transfer of water-based Al2O3 nanofluids in an uniformly heated pipe," *Chemical Engineering Science,* vol. 176, pp. 205-219, 2018, doi: https://doi.org/10.1016/j.ces.2017.10.044.

[145] M. K. Isman, "Numerical studies on convective heat transfer of Al2O3 nanofluid in circular pipe," *Heat and Mass Transfer,* vol. 56, no. 5, pp. 1421-1428, 2020, doi: https://doi.org/10.1007/s00231-019-02800-0.

[146] M. U. Sajid and H. M. Ali, "Thermal conductivity of hybrid nanofluids: a critical review," *International Journal of Heat and Mass Transfer,* vol. 126, pp. 211-234, 2018, doi: https://doi.org/10.1016/j.ijheatmasstransfer.2018.05.021.

[147] N. A. C. Sidik, M. M. Jamil, W. M. A. A. Japar, and I. M. Adamu, "A review on preparation methods, stability and applications of hybrid nanofluids," *Renewable and Sustainable Energy Reviews,* vol. 80, pp. 1112-1122, 2017, doi: http://dx.doi.org/10.1016/j.rser.2017.05.221.

[148] A. Ramadhan, W. Azmi, R. Mamat, and K. Hamid, "Experimental and numerical study of heat transfer and friction factor of plain tube with hybrid nanofluids," *Case Studies in Thermal Engineering,* vol. 22, p. 100782, 2020, doi: https://doi.org/10.1016/j.csite.2020.100782.

[149] M. Nabil, W. Azmi, K. Hamid, and R. Mamat, "Heat transfer and friction factor of composite TiO2–SiO2 nanofluids in water-ethylene glycol (60: 40) mixture," in *IOP Conference Series: Materials Science and Engineering*, 2017, vol. 257, no. 1: IOP Publishing, p. 012066, doi: https://doi.org/10.1088/1757-899X/257/1/012066.

[150] A. Zareie and M. Akbari, "Hybrid nanoparticles effects on rheological behavior of water-EG coolant under different temperatures: An experimental study," *Journal of Molecular Liquids,* vol. 230, pp. 408-414, 2017, doi: http://dx.doi.org/10.1016/j.molliq.2017.01.043.

[151] O. Soltani and M. Akbari, "Effects of temperature and particles concentration on the dynamic viscosity of MgO-MWCNT/ethylene glycol hybrid nanofluid: experimental study," *Physica E: Low-dimensional Systems and Nanostructures,* vol. 84, pp. 564-570, 2016, doi: http://dx.doi.org/10.1016/j.physe.2016.06.015.

[152] E. Bellos and C. Tzivanidis, "Thermal analysis of parabolic trough collector operating with mono and hybrid nanofluids," *Sustainable Energy Technologies and Assessments,* vol. 26, pp. 105-115, 2018, doi: http://dx.doi.org/10.1016/j.seta.2017.10.005.

[153] H. Yarmand *et al.*, "Graphene nanoplatelets–silver hybrid nanofluids for enhanced heat transfer," *Energy conversion and management,* vol. 100, pp. 419-428, 2015, doi: http://dx.doi.org/10.1016/j.enconman.2015.05.023.

[154] K. A. Hamid, W. Azmi, M. Nabil, and R. Mamat, "Experimental investigation of nanoparticle mixture ratios on TiO2–SiO2 nanofluids heat transfer performance under turbulent flow," *International Journal of Heat and Mass Transfer,* vol. 118, pp. 617-627, 2018, doi: https://doi.org/10.1016/j.ijheatmasstransfer.2017.11.036.

[155] V. V. Wanatasanappan, M. Abdullah, and P. Gunnasegaran, "Thermophysical properties of Al2O3-CuO hybrid nanofluid at different nanoparticle mixture ratio: An experimental approach," *Journal of Molecular Liquids,* vol. 313, p. 113458, 2020, doi: https://doi.org/10.1016/j.molliq.2020.113458.

[156] M. Tekir, R. Ekiciler, and K. Arslan, "Numerical simulation of hybrid nanofluid flow in a square cross-sectioned horizontal duct," in *18th Symposium on Thermal Science and Engineering of Serbia, Sokobanja, Serbia*, Sokobanja, Serbia, 2017: Society of thermal engineers of serbia, 2017.

[157] I. J. K. Wong and N. T. A. Tiong, "Simulation approach on turbulent thermal performance factor of Al2O3-Cu/water hybrid nanofluid in circular and non-circular ducts," *SN Applied Sciences,* vol. 3, no. 3, p. 329, 2021, doi: https://doi.org/10.1007/s42452-021-04317-w.

[158] A. Bhattad, J. Sarkar, and P. Ghosh, "Discrete phase numerical model and experimental study of hybrid nanofluid heat transfer and pressure drop in plate heat exchanger," *International Communications in Heat and Mass Transfer,* vol. 91, pp. 262-273, 2018, doi: https://doi.org/10.1016/j.icheatmasstransfer.2017.12.020.

[159] A. Parsian and M. Akbari, "New experimental correlation for the thermal conductivity of ethylene glycol containing Al 2 O 3–Cu hybrid nanoparticles," *Journal of Thermal Analysis and Calorimetry,* vol. 131, pp. 1605-1613, 2018, doi: https://doi.org/10.1007/s10973-017-6694-5.

[160] D. Toghraie, V. A. Chaharsoghi, and M. Afrand, "Measurement of thermal conductivity of ZnO–TiO 2/EG hybrid nanofluid: effects of temperature and nanoparticles concentration," *Journal of Thermal Analysis and Calorimetry,* vol. 125, pp. 527-535, 2016, doi: https://doi.org/10.1007/s10973-016-5436-4.

[161] K. Hamid, W. Azmi, M. Nabil, and R. Mamat, "Improved thermal conductivity of TiO2–SiO2 hybrid nanofluid in ethylene glycol and water mixture," in *IOP Conference series: materials science and engineering*, 2017, vol. 257, no. 1: IOP Publishing, p. 012067, doi: https://doi.org/10.1088/1757-899X/257/1/012067.

[162] K. A. Hamid, W. Azmi, M. Nabil, R. Mamat, and K. Sharma, "Experimental investigation of thermal conductivity and dynamic viscosity on nanoparticle mixture ratios of TiO2-SiO2 nanofluids," *International Journal of Heat and Mass Transfer,* vol. 116, pp. 1143-1152, 2018, doi: https://doi.org/10.1016/j.ijheatmasstransfer.2017.09.087.

[163] N. N. Esfahani, D. Toghraie, and M. Afrand, "A new correlation for predicting the thermal conductivity of ZnO–Ag (50%–50%)/water hybrid nanofluid: an experimental study," *Powder Technology,* vol. 323, pp. 367-373, 2018, doi: https://doi.org/10.1016/j.powtec.2017.10.025.

[164] S. Akilu, A. T. Baheta, and K. Sharma, "Experimental measurements of thermal conductivity and viscosity of ethylene glycol-based hybrid nanofluid with TiO2-CuO/C inclusions," *Journal of Molecular Liquids,* vol. 246, pp. 396-405, 2017, doi: https://doi.org/10.1016/j.molliq.2017.09.017.

[165] M. Vafaei, M. Afrand, N. Sina, R. Kalbasi, F. Sourani, and H. Teimouri, "Evaluation of thermal conductivity of MgO-MWCNTs/EG hybrid nanofluids based on experimental data by selecting optimal artificial neural networks," *Physica E: Low-dimensional Systems and Nanostructures,* vol. 85, pp. 90-96, 2017, doi: http://dx.doi.org/10.1016/j.physe.2016.08.020.

[166] M. H. Esfe, A. A. A. Arani, M. Rezaie, W.-M. Yan, and A. Karimipour, "Experimental determination of thermal conductivity and dynamic viscosity of Ag–MgO/water hybrid nanofluid," *International Communications in Heat and Mass Transfer,* vol. 66, pp. 189-195, 2015, doi: http://dx.doi.org/10.1016/j.icheatmasstransfer.2015.06.003.

[167] M. Nabil, W. Azmi, K. A. Hamid, R. Mamat, and F. Y. Hagos, "An experimental study on the thermal conductivity and dynamic viscosity of TiO2-SiO2 nanofluids in water: ethylene glycol mixture," *International Communications in Heat and Mass Transfer,* vol. 86, pp. 181-189, 2017, doi: http://dx.doi.org/10.1016/j.icheatmasstransfer.2017.05.024.

[168] A. S. Dalkılıç *et al.*, "Experimental investigation on the viscosity characteristics of water based SiO2-graphite hybrid nanofluids," *International Communications in Heat and Mass Transfer,* vol. 97, pp. 30-38, 2018, doi: https://doi.org/10.1016/j.icheatmasstransfer.2018.07.007.

[169] S. Akilu, A. T. Baheta, M. A. M. Said, A. A. Minea, and K. Sharma, "Properties of glycerol and ethylene glycol mixture based SiO2-CuO/C hybrid nanofluid for enhanced solar energy transport," *Solar Energy Materials and Solar Cells,* vol. 179, pp. 118-128, 2018, doi: https://doi.org/10.1016/j.solmat.2017.10.027.

[170] S. Suresh, K. Venkitaraj, M. S. Hameed, and J. Sarangan, "Turbulent heat transfer and pressure drop characteristics of dilute water based Al2O3–Cu hybrid nanofluids," *Journal of nanoscience and nanotechnology,* vol. 14, no. 3, pp. 2563-2572, 2014, doi: https://doi.org/10.1166/jnn.2014.8467.

[171] L. S. Sundar, M. K. Singh, and A. C. Sousa, "Enhanced heat transfer and friction factor of MWCNT–Fe3O4/water hybrid nanofluids," *International Communications in Heat and Mass Transfer,* vol. 52, pp. 73-83, 2014, doi: http://dx.doi.org/10.1016/j.icheatmasstransfer.2014.01.012.

[172] G. Huminic and A. Huminic, "Application of nanofluids in heat exchangers: A review," *Renewable and Sustainable Energy Reviews,* vol. 16, no. 8, pp. 5625-5638, 2012, doi: https://doi.org/10.1016/j.rser.2012.05.023.

[173] A. Turgut and E. Elbasan, "Nanofluids for electronics cooling," in *2014 IEEE 20th International Symposium for Design and Technology in Electronic Packaging (SIITME)*, 2014: IEEE, pp. 35-37, doi: https://doi.org/10.1109/SIITME.2014.6966989.

[174] O. Mahian, A. Kianifar, S. A. Kalogirou, I. Pop, and S. Wongwises, "A review of the applications of nanofluids in solar energy," *International Journal of Heat and Mass Transfer,* vol. 57, no. 2, pp. 582-594, 2013, doi: https://doi.org/10.1016/j.ijheatmasstransfer.2012.10.037.

[175] J. Buongiorno, L.-W. Hu, S. J. Kim, R. Hannink, B. Truong, and E. Forrest, "Nanofluids for enhanced economics and safety of nuclear reactors: an evaluation of the potential features,

issues, and research gaps," *Nuclear Technology,* vol. 162, no. 1, pp. 80-91, 2008, doi: https://doi.org/10.13182/NT08-A3934.

[176] T. Jia, R. Wang, and R. Xu, "Performance of MoFe2O4–NiFe2O4/Fullerene-added nano-oil applied in the domestic refrigerator compressors," *International journal of refrigeration,* vol. 45, pp. 120-127, 2014, doi: https://doi.org/10.1016/j.ijrefrig.2014.06.001.

[177] M. Raja, R. Vijayan, S. Suresh, and R. Vivekananthan, "Effect of heat transfer enhancement and NO x emission using AL 2 O 3/water nanofluid as coolant in CI engine," 2013.

[178] D. P. Kulkarni, D. K. Das, and R. S. Vajjha, "Application of nanofluids in heating buildings and reducing pollution," *Applied Energy,* vol. 86, no. 12, pp. 2566-2573, 2009, doi: https://doi.org/10.1016/j.apenergy.2009.03.021.

[179] D. P. Kulkarni, R. S. Vajjha, D. K. Das, and D. Oliva, "Application of aluminum oxide nanofluids in diesel electric generator as jacket water coolant," *Applied Thermal Engineering,* vol. 28, no. 14-15, pp. 1774-1781, 2008, doi: https://doi.org/10.1016/j.applthermaleng.2007.11.017.

[180] J. S. Basha and R. Anand, "An experimental study in a CI engine using nanoadditive blended water–diesel emulsion fuel," *International journal of green energy,* vol. 8, no. 3, pp. 332-348, 2011, doi: https://doi.org/10.1080/15435075.2011.557844.

[181] E. Tombácz, D. Bica, A. Hajdú, E. Illés, A. Majzik, and L. Vékás, "Surfactant double layer stabilized magnetic nanofluids for biomedical application," *Journal of Physics: Condensed Matter,* vol. 20, no. 20, p. 204103, 2008, doi: https://doi.org/10.1088/0953-8984/20/20/204103.

[182] T. Sharma, A. L. M. Reddy, T. Chandra, and S. Ramaprabhu, "Development of carbon nanotubes and nanofluids based microbial fuel cell," *International journal of hydrogen energy,* vol. 33, no. 22, pp. 6749-6754, 2008, doi: https://doi.org/10.1016/j.ijhydene.2008.05.112.

[183] A. Vatani and H. Mohammed, "Turbulent nanofluid flow over periodic rib-grooved channels," *Engineering applications of computational fluid mechanics,* vol. 7, no. 3, pp. 369-381, 2013, doi: https://doi.org/10.1080/19942060.2013.11015478.

[184] O. A. Akbari, D. Toghraie, and A. Karimipour, "Numerical simulation of heat transfer and turbulent flow of water nanofluids copper oxide in rectangular microchannel with semi-attached rib," *Advances in Mechanical Engineering,* vol. 8, no. 4, p. 1687814016641016, 2016, doi: https://doi.org/10.1177/1687814016641016.

[185] Q. Gravndyan *et al.*, "The effect of aspect ratios of rib on the heat transfer and laminar water/TiO2 nanofluid flow in a two-dimensional rectangular microchannel," *Journal of Molecular Liquids,* vol. 236, pp. 254-265, 2017, doi: https://doi.org/10.1016/j.molliq.2017.04.030.

[186] M. Khoshvaght-Aliabadi, S. Hassani, and S. H. Mazloumi, "Enhancement of laminar forced convection cooling in wavy heat sink with rectangular ribs and Al2O3/water nanofluids," *Experimental Thermal and Fluid Science,* vol. 89, pp. 199-210, 2017, doi: https://doi.org/10.1016/j.expthermflusci.2017.08.017.

[187] L. Syam Sundar, A. C. Sousa, and M. K. Singh, "Heat transfer enhancement of low volume concentration of carbon nanotube-Fe3O4/water hybrid nanofluids in a tube with twisted tape inserts under turbulent flow," *Journal of Thermal Science and Engineering Applications,* vol. 7, no. 2, p. 021015, 2015, doi: https://doi.org/10.1115/1.4029622.

[188] U. Arunachalam and M. Edwin, "Experimental studies on laminar flow heat transfer in nanofluids flowing through a straight circular tube with and without V-cut twisted tape insert," *Heat and Mass Transfer,* vol. 54, no. 3, pp. 673-683, 2018, doi: https://doi.org/10.1007/s00231-017-2162-9.

[189] H. Togun *et al.*, "Efficient heat transfer augmentation in channels with semicircle ribs and hybrid Al2O3-Cu/water nanofluids," *Nanomaterials,* vol. 12, no. 15, p. 2720, 2022, doi: https://doi.org/10.3390/nano12152720.

[190] *ANSYS Fluent 2023*. (2023). ANSYS, Inc. [Online]. Available: https://www.ansys.com

[191] L. Godson, B. Raja, D. M. Lal, and S. Wongwises, "Enhancement of heat transfer using nanofluids—an overview," *Renewable and sustainable energy reviews,* vol. 14, no. 2, pp. 629-641, 2010, doi: https://doi.org/10.1016/j.rser.2009.10.004.

[192] L. Schiller, "A drag coefficient correlation," *Zeit. Ver. Deutsch. Ing.,* vol. 77, pp. 318-320, 1933.

[193] M. Syamlal and D. Gidaspow, "Hydrodynamics of fluidization: prediction of wall to bed heat transfer coefficients," *AIChE Journal,* vol. 31, no. 1, pp. 127-135, 1985, doi: https://doi.org/10.1002/aic.690310115.

[194] M. Akbari, N. Galanis, and A. Behzadmehr, "Comparative analysis of single and two-phase models for CFD studies of nanofluid heat transfer," *International Journal of Thermal Sciences,* vol. 50, no. 8, pp. 1343-1354, 2011, doi: http://dx.doi.org/10.1016/j.ijthermalsci.2011.03.008.

[195] S. Kakaç and A. Pramuanjaroenkij, "Single-phase and two-phase treatments of convective heat transfer enhancement with nanofluids–A state-of-the-art review," *International journal of thermal sciences,* vol. 100, pp. 75-97, 2016, doi: http://dx.doi.org/10.1016/j.ijthermalsci.2015.09.021.

[196] M. Syamlal and T. J. O'Brien, "Computer simulation of bubbles in a fluidized bed," in *AIChE Symp. Ser*, 1989, vol. 85, no. 270: Publ by AIChE, pp. 22-31.

[197] M. Roco, *Particulate two-phase flow* (Chemical Engineering Progress). Boston, 1952.

[198] R. a. Marshall, *Evaporation from Drops* (Chemical Engineering Progress). 1952, pp. 141-146.

[199] T.-H. Shih, W. W. Liou, A. Shabbir, Z. Yang, and J. Zhu, "A new k-ϵ eddy viscosity model for high reynolds number turbulent flows," *Computers & fluids,* vol. 24, no. 3, pp. 227-238, 1995, doi: https://doi.org/10.1016/0045-7930(94)00032-T.

[200] V. Ghazanfari, M. Imani, M. M. Shadman, Y. Amini, and F. Zahakifar, "Numerical study on the thermal performance of the shell and tube heat exchanger using twisted tubes and Al2O3 nanoparticles," *Progress in nuclear energy,* vol. 155, p. 104526, 2023, doi: https://doi.org/10.1016/j.pnucene.2022.104526.

[201] F. R. Menter, "Two-equation eddy-viscosity turbulence models for engineering applications," *AIAA journal,* vol. 32, no. 8, pp. 1598-1605, 1994, doi: https://doi.org/10.2514/3.12149.

[202] M. Akbarzadeh, S. Rashidi, N. Karimi, and R. Ellahi, "Convection of heat and thermodynamic irreversibilities in two-phase, turbulent nanofluid flows in solar heaters by corrugated absorber plates," *Advanced Powder Technology,* vol. 29, no. 9, pp. 2243-2254, 2018, doi: https://doi.org/10.1016/j.apt.2018.06.009.

[203] O. Manca, S. Nardini, and D. Ricci, "A numerical study of nanofluid forced convection in ribbed channels," *Applied Thermal Engineering,* vol. 37, pp. 280-292, 2012, doi: http://dx.doi.org/10.1016/j.applthermaleng.2011.11.030.

[204] K. Khanafer and K. Vafai, "A critical synthesis of thermophysical characteristics of nanofluids," *International journal of heat and mass transfer,* vol. 54, no. 19-20, pp. 4410-4428, 2011, doi: http://dx.doi.org/10.1016/j.ijheatmasstransfer.2011.04.048.

[205] M. Gupta, V. Singh, S. Kumar, S. Kumar, N. Dilbaghi, and Z. Said, "Up to date review on the synthesis and thermophysical properties of hybrid nanofluids," *Journal of cleaner production,* vol. 190, pp. 169-192, 2018, doi: https://doi.org/10.1016/j.jclepro.2018.04.146.

[206] E. V. Timofeeva *et al.*, "Thermal conductivity and particle agglomeration in alumina nanofluids: experiment and theory," *Physical Review E—Statistical, Nonlinear, and Soft Matter Physics,* vol. 76, no. 6, p. 061203, 2007, doi: https://doi.org/10.1103/PhysRevE.76.061203.

[207] A. Einstein, *Investigations on the Theory of the Brownian Movement*. Courier Corporation, 1956.

[208] G. K. Batchelor, "The effect of Brownian motion on the bulk stress in a suspension of spherical particles," *Journal of fluid mechanics,* vol. 83, no. 1, pp. 97-117, 1977, doi: https://doi.org/10.1017/S0022112077001062.

[209] V. V. Wanatasanapan, M. Abdullah, and P. Gunnasegaran, "Effect of TiO2-Al2O3 nanoparticle mixing ratio on the thermal conductivity, rheological properties, and dynamic viscosity of water-based hybrid nanofluid," *Journal of Materials Research and Technology,* vol. 9, no. 6, pp. 13781-13792, 2020, doi: https://doi.org/10.1016/j.jmrt.2020.09.127.

[210] K. Selvarajoo, V. V. Wanatasanappan, and N. Y. Luon, "Experimental measurement of thermal conductivity and viscosity of Al2O3-GO (80: 20) hybrid and mono nanofluids: A new correlation," *Diamond and Related Materials,* vol. 144, p. 111018, 2024, doi: https://doi.org/10.1016/j.diamond.2024.111018.

[211] V. Ozceyhan, S. Gunes, O. Buyukalaca, and N. Altuntop, "Heat transfer enhancement in a tube using circular cross sectional rings separated from wall," *Applied energy,* vol. 85, no. 10, pp. 988-1001, 2008, doi: https://doi.org/10.1016/j.apenergy.2008.02.007.

[212] P. Naphon, M. Nuchjapo, and J. Kurujareon, "Tube side heat transfer coefficient and friction factor characteristics of horizontal tubes with helical rib," *Energy Conversion and Management,* vol. 47, no. 18-19, pp. 3031-3044, 2006, doi: https://doi.org/10.1016/j.enconman.2006.03.023.

[213] T. E. Conder and S. A. Solovitz, "Computational optimization of a groove-enhanced minichannel," *Heat transfer engineering,* vol. 32, no. 10, pp. 876-890, 2011, doi: https://doi.org/10.1080/01457632.2011.548632.

[214] O. Aydin, "Effects of viscous dissipation on the heat transfer in a forced pipe flow. Part 2: Thermally developing flow," *Energy Conversion and management,* vol. 46, no. 18-19, pp. 3091-3102, 2005, doi: https://doi.org/10.1016/j.enconman.2005.03.011.

[215] S. Suresh, K. Venkitaraj, P. Selvakumar, and M. Chandrasekar, "Synthesis of Al2O3–Cu/water hybrid nanofluids using two step method and its thermo physical properties," *Colloids and Surfaces A: Physicochemical and Engineering Aspects,* vol. 388, no. 1-3, pp. 41-48, 2011, doi: https://doi.org/10.1016/j.colsurfa.2011.08.005.

[216] H. M. Ali, H. Babar, T. R. Shah, M. U. Sajid, M. A. Qasim, and S. Javed, "Preparation techniques of TiO2 nanofluids and challenges: a review," *Applied Sciences,* vol. 8, no. 4, p. 587, 2018, doi: https://doi.org/10.3390/app8040587.

[217] W. Azmi, K. Sharma, P. Sarma, R. Mamat, S. Anuar, and V. D. Rao, "Experimental determination of turbulent forced convection heat transfer and friction factor with SiO2 nanofluid," *Experimental Thermal and Fluid Science,* vol. 51, pp. 103-111, 2013, doi: https://doi.org/10.1016/j.expthermflusci.2013.07.006.

[218] E. Sadeghinezhad *et al.*, "A comprehensive review on graphene nanofluids: Recent research, development and applications," *Energy Conversion and Management,* vol. 111, pp. 466-487, 2016, doi: https://doi.org/10.1016/j.enconman.2016.01.004.

[219] S. S. Murshed and C. N. De Castro, "Superior thermal features of carbon nanotubes-based nanofluids–A review," *Renewable and Sustainable Energy Reviews,* vol. 37, pp. 155-167, 2014, doi: https://doi.org/10.1016/j.rser.2014.05.017.

Appendix

Chapter 4

Figure 1 to Figure 4 display the differences between the 2D and 3D contours of heat transfer parameters, such as velocity, temperature, turbulent kinetic energy, and pressure, complementing Figure 4. 7 of Chapter 4.

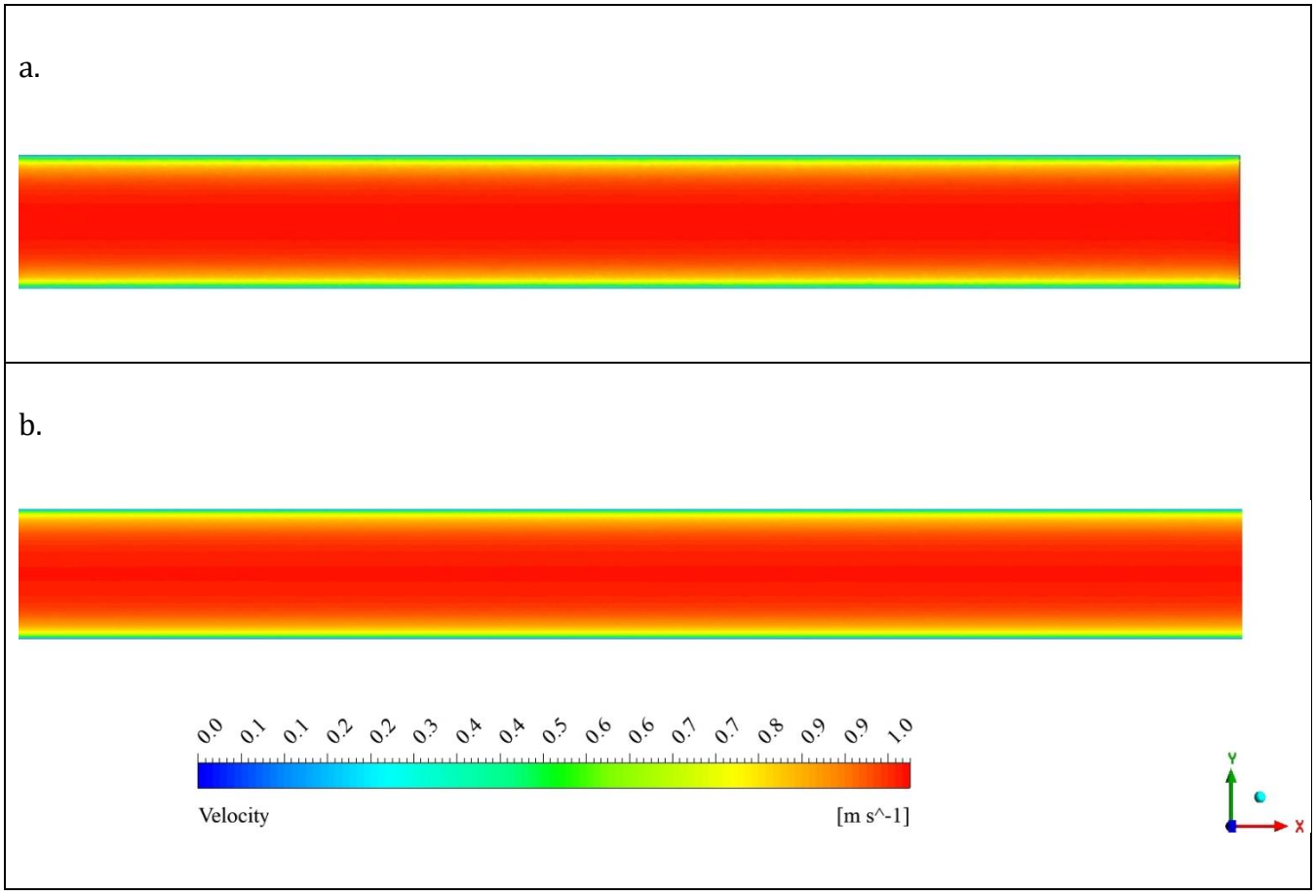

Figure 1: Comparison of (a) 3D and (b) 2D Contours of Velocity in the Smooth Tube's Test Section at Re = 10,000

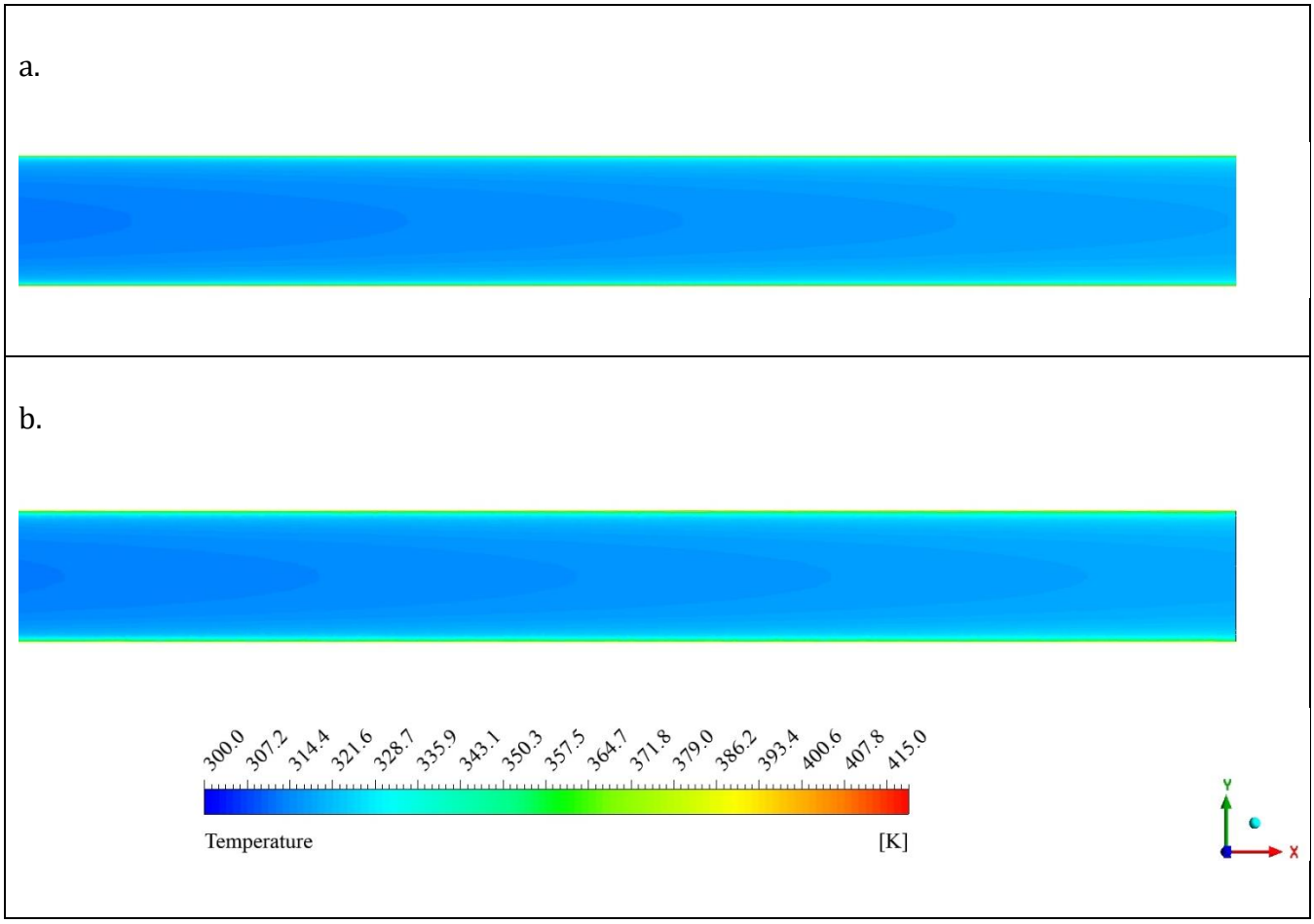

Figure 2: Comparison of (a) 3D and (b) 2D Contours of Temperature in the Smooth Tube's Test Section at Re = 10,000

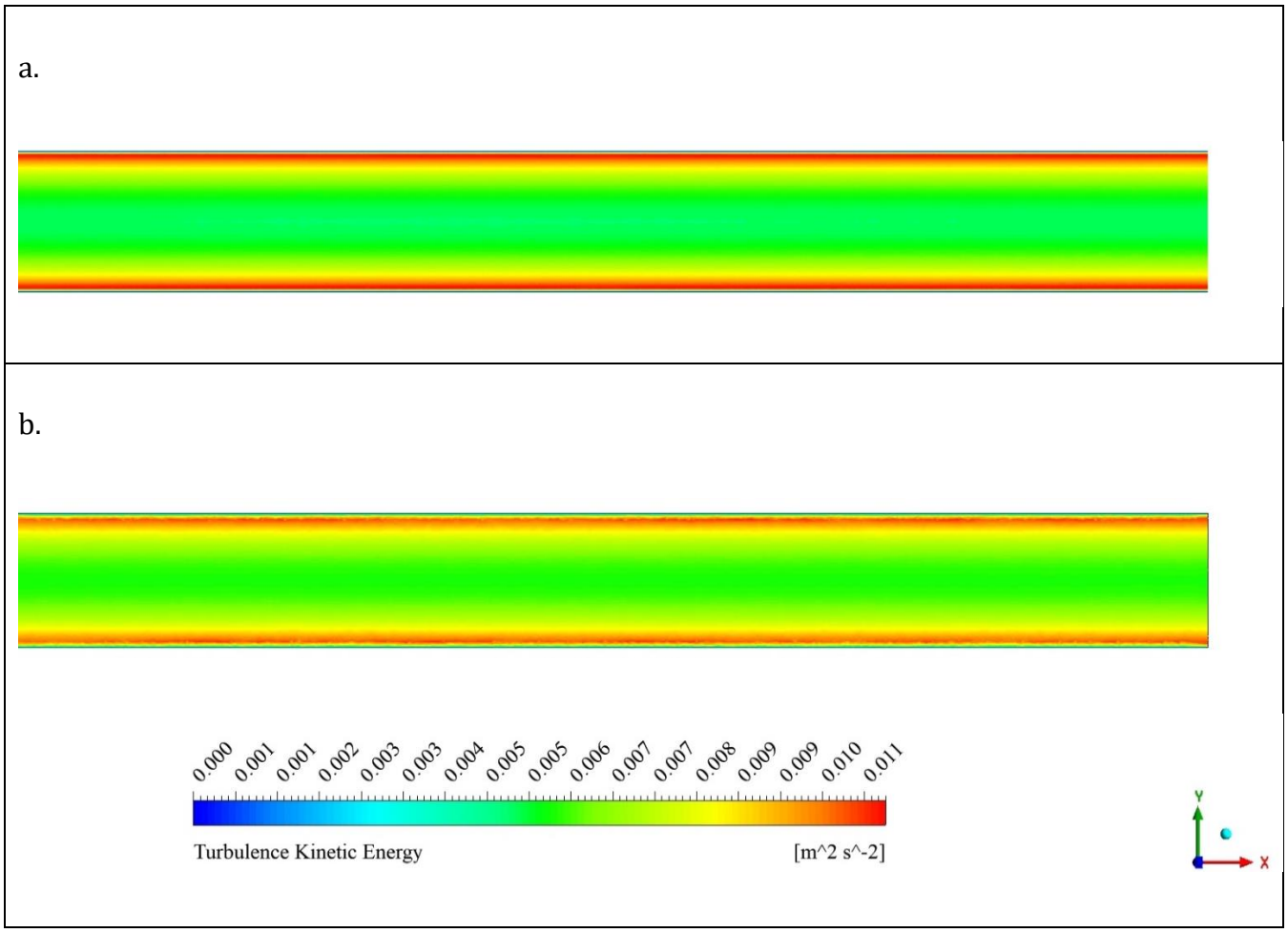

Figure 3: Comparison of (a) 3D and (b) 2D Contours of Turbulent Kinetic Energy in the Smooth Tube's Test Section at Re = 10,000

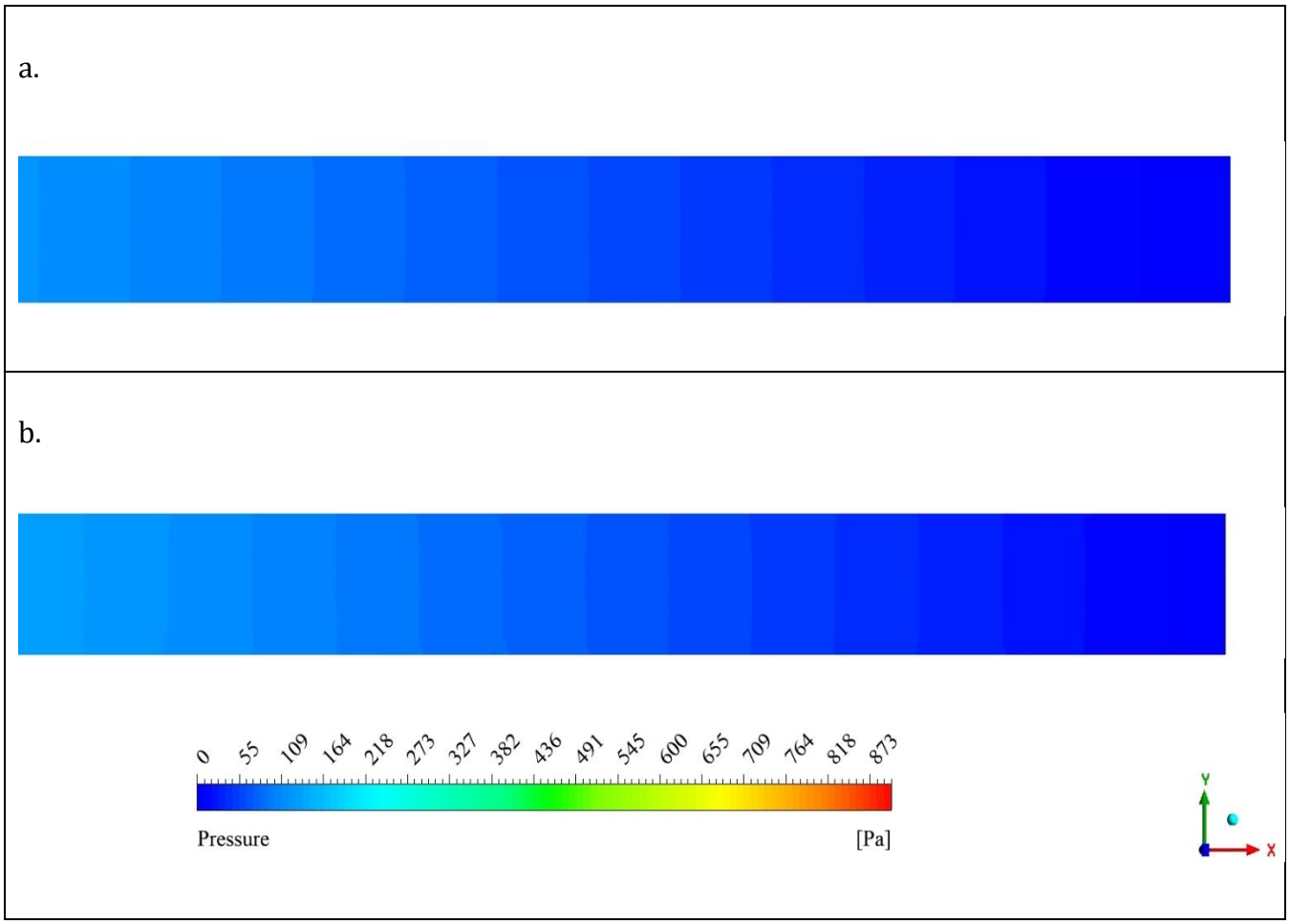

Figure 4: Comparison of (a) 3D and (b) 2D Contours of Pressure in the Smooth Tube's Test Section at Re = 10,000